

Palacký University Olomouc
Faculty of Science
Department of Cell Biology and Genetics



and

Institute of Experimental Botany AS CR
Centre of Plant Structural and Functional Genomics



**Analysis of dynamics and 3D organization of the
nuclear genome in barley (*Hordeum vulgare*)**

Ph.D. Thesis

Mgr. Kateřina Kaduchová

Olomouc 2023

Supervisor: Assoc. prof. Aleš Pečinka, Ph.D.

Acknowledgments

I want to express my profound gratitude to my supervisor Assoc. Prof. Aleš Pečinka, Ph.D. for his guidance, assistance, and unwavering encouragement. I am truly thankful that he entrusted me with this extremely interesting and challenging project, which thought me far more than I initially anticipated.

I extend my heartfelt thanks to all my lab colleagues and group members who always gave me valuable advices and feedback during our discussions and created an amazing working atmosphere.

Additionally, I want to acknowledge the former and current heads of the laboratory, Prof. Ing. Jaroslav Doležel, DrSc., and Mgr. Jan Bartoš, Ph.D., for providing me with the opportunity to work in the Centre of Plant Structural and Functional Genomics.

Finally, my heartfelt appreciation goes to my family for their tireless support throughout my studies, and especially to my husband Ondra, who patiently listened to my complaints while encouraging me to overcome challenges. And, of course, to our cat Kamui, because I am sure that she made this thesis one hair better.

Declaration

I hereby declare that I wrote the Ph.D. thesis independently under the supervision of Assoc. Prof. Aleš Pečinka, Ph.D., using the information sources listed in the References.

In Olomouc

.....

This work was supported by the European Regional Development Fund (ERDF) project 'Plants as a tool for sustainable global development' (no. CZ.02.1.01/0.0/0.0/16_019/0000827), the Ministry of Education, Youth and Sports of the Czech Republic (MEYS) INTER-COST grant LTC18026 and The Czech Science Foundation (GACR) grant 21-02929S.

Bibliographical identification

Author's first name and surname	Kateřina Kaduchov
Title	Analysis of dynamics and 3D organization of the nuclear genome in barley (<i>Hordeum vulgare</i>)
Type of thesis	Ph.D. Thesis
Department	Department of Cell Biology and Genetics, Palack University Olomouc and Centre of Plant Structural and Functional Genomics, Institute of Experimental Botany of the Czech Academy of Sciences
Supervisor	Assoc. prof. Aleř Peinka, Ph.D.
The year of presentation	2024

Abstract

The organization of the nuclear genome changes dynamically during the cell cycle. Primarily, it is defined by the cell and tissue types and organism developmental needs. In response to environmental conditions and stress stimuli, cells alter genome organization to adjust gene transcription levels, modify accessibility for DNA binding proteins, or allow repair processes. The most notable alterations in the nuclear and cellular organization occur during mitotic division, a dynamic process that ensures the even distribution of genetic information into emerging daughter cells.

The majority of knowledge about plant nuclear and cellular dynamics is based on the relatively small and repeat-poor genome of the model plant *Arabidopsis thaliana* ($2n = 2x = 10$; 119 Mbp/1C). However, there is noticeably less information about the dynamics of large plant genomes found in certain representatives with an extensive agronomic impact. Expanding the knowledge about how their genome organization changes could help to select cultivars adapted to changing climatic conditions.

To shed light on the organization and dynamics of large plant genomes, a series of stable translational fusion fluorescent marker lines of barley (*Hordeum vulgare*) were developed within this thesis. Barley is a temperate cereal crop with a diploid genome ($2n = 2x = 14$; 4.88 Gbp/1C) organized in Rab1 conformation with centromeres and telomeres positioned on the opposite nuclear poles. Analyzing chromatin, nucleolar, and microtubular fluorescent marker lines, we characterized the progress of mitosis in barley root cells and uncovered its features typical for barley. Simultaneously, we developed the *in vivo* microscopy setup for time-lapse analysis of cells in living cereal crop roots. These findings will help the plant community to broaden the knowledge about the cereal crops genome organization dynamics and provide valuable material for future studies.

Keywords	barley, mitosis, genome organization, fluorescent marker line, confocal <i>in vivo</i> microscopy, chromosome
Number of pages	113
Number of appendices	VI
Language	English

Bibliografická identifikace

Jméno a příjmení autora	Kateřina Kaduchová
Název práce	Analýza dynamiky a 3D organizace jaderného genomu u ječmene setého (<i>Hordeum vulgare</i>)
Typ práce	Dizertační práce
Pracoviště	Katedra buněčné biologie a genetiky, Univerzita Palackého v Olomouci a Centrum strukturní a funkční genomiky rostlin, Ústav experimentální botaniky Akademie věd České republiky
Vedoucí práce	doc. Aleš Pečinka, Ph.D.
Rok obhajoby práce	2024

Abstrakt

Organizace jaderného genomu se v průběhu buněčného cyklu dynamicky mění. Primárně je definována typem buňky, pletiva a vývojovými potřebami organismu. Nicméně se dynamicky mění v reakci buněk na měnící se podmínky životního prostředí a stresové podněty, čímž pomáhá upravit úroveň transkripce genů, přístupnost DNA pro vazbu specifických proteinů, nebo umožňuje DNA opravné procesy. K nejrozsáhlejším změnám jaderné a buněčné organizace dochází v průběhu mitotického dělení, které zajišťuje rovnoměrné rozdělení genetické informace do vznikajících dceřiných buněk.

Většina znalostí o jaderné a buněčné dynamice rostlin je založena na modelové rostlině huseníčku rolním (*Arabidopsis thaliana*), majícím malý kompaktní genom s malým počtem repetitivních sekvencí ($2n = 2x = 10$; 119 Mbp/1C). Nicméně existuje jen omezené množství informací o dynamice velkých rostlinných genomů, které nalzáme u významné části rostlin s hospodářským významem. Rozšířením znalostí o tom, jak se mění organizace jejich genomu, by mohlo napomoci vyselektovat odrůdy přizpůsobené změnám klimatických podmínek.

Pro porozumění organizaci a dynamice velkých rostlinných genomů byla v rámci této dizertační práce vyvinuta série stabilních translačně-fúzních fluorescenčních markerových linií ječmene setého (*Hordeum vulgare*). Ječmen je obilovina mírného podnebného pásma mající diploidní genom ($2n = 2x = 14$; 4,88 Gbp/1C) organizovaný v Rablově konformaci, v rámci které jsou centromery a telomery chromozomů lokalizovány na opačných jaderných pólech. Analýzou chromatinových, jadérkových a mikrotubulárních markerových linií byl v rámci této práce charakterizován průběh mitózy v buňkách kořenové špičky ječmene a odhaleny znaky typické pro mitózu ječmene. Souběžně byl v rámci této práce vyvinut systém pro *in vivo* časosběrnou mikroskopickou analýzu buněk v živých kořenech obilovin. Poznatky a zdroje získané v rámci této práce mohou pomoci vědecké rostlinné komunitě rozšířit znalosti o dynamice genomů obilovin a poskytnou jedinečný materiál pro budoucí vědecké studie.

Klíčová slova	ječmen, mitóza, organizace genomu, markerová linie, konfokální <i>in vivo</i> mikroskopie, chromozóm
Počet stran	113
Počet příloh	VI
Jazyk	Anglický

CONTENT

1	LITERATURE OVERVIEW	12
1.1	Evolution and taxonomy of cultivated barley	12
1.2	Barley as a temperate cereal genetic model	13
1.3	General principles of plant nucleus organization	14
1.3.1	Spatial chromosome configuration in the nucleus	16
1.3.2	Mitotic chromosome organization	18
1.3.3	Organization of the nuclear envelope and the nuclear lamina	20
1.3.4	Organization of the nucleolus	22
1.3.5	Organization of microtubules	23
1.4	Mitotic division in higher plants: an overview	24
1.4.1	Regulation of cell cycle and mitosis in plants	25
1.4.2	Dynamics of nuclear components and microtubules in plant mitosis	26
1.4.2.1	Chromosomes in plant mitosis	26
1.4.2.2	Nucleolus in plant mitosis	27
1.4.2.3	Nuclear envelope and nuclear lamina in plant mitosis	27
1.4.2.4	Microtubules in plant mitosis	28
1.5	Methodological approaches to study cell organization and dynamics in crops	29
1.5.1	<i>In vitro</i> methodological approaches	29
1.5.2	<i>In vivo</i> methodological approaches to localize specific DNA sequences	31
1.5.3	<i>In vivo</i> methodological approaches for protein localization studies	32
1.6	Confocal microscopy	34
1.7	Image analysis software tools for microscopy data post-processing	36
1.8	<i>Agrobacterium tumefaciens</i> -mediated transformation of plants	38
2	AIMS OF THE THESIS	40
2.1	Development of translational fusion fluorescent marker lines for <i>in vivo</i> nuclear and cell dynamics studies in barley	40
2.2	Optimization of the time-lapse <i>in planta</i> microscopy analysis of fluorescent marker lines	40
2.3	Understanding the spatial organization and dynamics of chromosomes and microtubules during barley mitosis	41
3	SUMMARY OF THE RESULTS	42
3.1	Development and characterization of fluorescent marker lines for <i>in vivo</i> nuclear organization studies in barley	42

3.2	Development and optimization of ‘EasyClick’ sample holder for <i>in vivo</i> time-lapse microscopy of cereal roots	47
3.3	Spatial organization and dynamics of mitosis in barley root cells.....	51
3.4	Determination of <i>in vivo</i> duration of mitosis in barley root cells	57
4	PUBLICATIONS	60
4.1	FIRST AUTHOR PUBLICATIONS	60
4.1.1	Image analysis workflows to reveal the spatial organization of cell nuclei and chromosomes	60
4.1.2	Spatial organization and dynamics of chromosomes during barley mitosis.	60
4.1.3	EasyClick: An improved system for confocal microscopy of live roots with a user-optimized sample holder.....	60
4.2	CO-AUTHORSHIP PUBLICATIONS.....	64
4.2.1	Proteome analysis of condensed barley mitotic chromosomes	64
5	CONTRIBUTION TO THE PUBLICATIONS	66
5.1	Image analysis workflows to reveal the spatial organization of cell nuclei and chromosomes.....	66
5.2	Spatial organization and dynamics of chromosomes during barley mitosis	67
5.3	EasyClick: An improved system for confocal microscopy of live roots with a user-optimized sample holder	68
5.4	Proteome analysis of condensed barley mitotic chromosomes.....	69
6	PUBLISHED CONFERENCE ABSTRACTS	70
6.1	Towards <i>in vivo</i> analysis of chromatin dynamics in barley	70
6.2	<i>In planta</i> microscopy of barley fluorescent marker lines.....	70
6.3	Developing system for tracking <i>in planta</i> chromatin dynamics in barley (<i>Hordeum vulgare</i>).....	70
6.4	Developing system for <i>in planta</i> tracking of chromatin dynamics in barley (<i>Hordeum vulgare</i>).....	70
6.5	Analysis of <i>in vivo</i> chromatin dynamics during mitotic division in barley (<i>Hordeum vulgare</i>).....	70
6.6	Live analysis of barley nuclei and chromosomes using fluorescent marker lines	71
6.7	Towards understanding of spatial <i>in vivo</i> dynamics of mitotic division in barley (<i>Hordeum vulgare</i>).....	71
6.8	Towards understanding of spatial <i>in vivo</i> dynamics of mitotic division in barley (<i>Hordeum vulgare</i>).....	71
7	DISCUSSION	80

7.1	Development of the fluorescent marker lines for <i>in vivo</i> nuclear and cellular organization and dynamics studies in barley	80
7.2	Live imaging uncovers unique features of barley genome dynamics	82
7.3	<i>In planta</i> microscopy brings challenges in mounting of living samples.....	83
8	CONCLUSIONS	86
9	REFERENCES	87
10	LIST OF ABBREVIATIONS	107
11	SUPPLEMENTARY MATERIAL	112
11.1	Supplementary video 1.....	112
11.2	Supplementary video 2.....	112
11.3	Supplementary video 3.....	112
12	LIST OF APPENDICES	113

1 LITERATURE OVERVIEW

1.1 Evolution and taxonomy of cultivated barley

Cultivated barley (*Hordeum vulgare* L. subsp. *vulgare*) belongs to the evolutionary successful worldwide distributed tribe *Triticae* of the grass family *Poaceae* (von Bothmer *et al.*, 2003, Ullrich, 2014). The diversity of the *Triticae* is a consequence of a diverse variety of speciation mechanisms, including interspecific and intergeneric hybridizations of diploid and polyploid taxa (Badr *et al.*, 2000, von Bothmer *et al.*, 2003, Mascher *et al.*, 2017).

Based on archaeological research, the domestication of wild progenitor of cultivated barley *Hordeum vulgare* L. subsp. *spontaneum* (K. Koch) Thell. started about 8,000 – 10,000 years ago in the current Israel-Jordan area of the Fertile Crescent (Badr *et al.*, 2000, Zeder, 2008). This was proved by analysis of 317 wild and 57 cultivated barley genotypes using 400 amplified fragment length polymorphism (AFLP) markers which uncovered a monophyletic origin of cultivated barleys. Due to the gradually increasing colonization, barley spread from its original area in the Middle East to become one of the most successful crops worldwide, primarily thanks to its agronomical value and efficient adaptation to variable environmental conditions (Badr *et al.*, 2000, Ullrich, 2014).

The genus *Hordeum* L. consists of approximately 32 species. It can be arbitrarily divided into five main groups based on a decreasing hybridization self-compatibility. These groups include: 1) cultivated barley breeding lines or cultivars, 2) landraces (adapted and non-adapted), 3) *H. vulgare* subsp. *spontaneum* (with agronomic potential or with *wild-type* genes), 4) “*Hordeum bulbosum*” (crosses result in chromosome elimination and sterility), and 5) other wild *Hordeum* species (theoretical agronomic potential). Groups 1-3 are considered as the primary breeding gene pools, *H. bulbosum* as the secondary gene pool, and the other wild *Hordeum* species as the tertiary gene pool (von Bothmer *et al.*, 1995, von Bothmer *et al.*, 2003). The majority of barley species, including cultivars and landraces, are diploids ($2n = 2x = 14$). However, wild species encompass also tetraploids ($2n = 4x = 28$) and hexaploids ($2n = 6x = 42$). Barley species with increased ploidy levels are mainly segmental allopolyploids; nevertheless, true autopolyploids (*H. bulbosum*, *H. brevisubulatum*) are known likewise (von Bothmer *et al.*, 2003, Brassac and Blattner, 2015). These polyploid species are occasionally used to

introduce new (mainly resistance) genes into the cultivated barley (Ullrich, 2014, Kumar *et al.*, 2020).

Since the onset of agriculture, barley was established as one of the most essential crops initially in Eurasia and later also worldwide. Currently, barley yearly production reaches 141 million tons in a total area of 55 million hectares, making it the fifth highest after wheat, rice, maize, and soybean (Ullrich, 2014, FAO, 2022 - October). Barley finds the greatest use as an animal feed (grains, malt) and in the brewing (beer) and distilling (whiskey) industry, nevertheless it has been used also in the biotechnology for the molecular pharming and in the cosmetic industry (reviewed in Mrizova *et al.*, 2014, Swanston *et al.*, 2014, Ullrich, 2014).

1.2 Barley as a temperate cereal genetic model

The barley genomic resources have been developed continuously since the late 1990s (Sato, 2020). Until now, they include mutant collections and information about plant phenotypes, or genomic sequence with annotated genes supplemented by genes' structure and their corresponding functions (CGIAR, 2023, GrainGenes, 2023, IPK_Genbank, 2023, NordGen, 2023, USDA, 2023).

The pioneering research focused on barley expressed sequence tags (EST) which helped to set the basis for single nucleotide polymorphisms (SNPs) collections (HarvEST:Barley, 2015). Moreover, barley full-length cDNA sequence with annotated genes and contigs (Carninci *et al.*, 1996, Sato *et al.*, 2009, Matsumoto *et al.*, 2011, Sato *et al.*, 2016), the same as a high-quality genetic map and bacterial artificial chromosome (BAC) libraries (Yu *et al.*, 2000, Stein *et al.*, 2007, Close *et al.*, 2009, Munoz-Amatriain *et al.*, 2011) were produced.

The efforts to expand barley genomic resources resulted in the establishment of the International Barley Sequencing Consortium (IBSC, 2012), which developed a barley physical map of 4.88 Gbp with more than 3.90 Gbp anchored to a high-resolution genetic map of the reference cultivar Morex. Almost 40,000 high-confidence and an additional 42,000 low-confidence genes were predicted (Mascher *et al.*, 2017). The physical map is gradually supplemented by improved sequencing datasets, whole-genome assemblies, and annotations (Mayer *et al.*, 2012, Mascher *et al.*, 2013, Mascher *et al.*, 2017, Mascher, 2021, Mascher *et al.*, 2021). Organelle genomes (Middleton *et al.*, 2014, Hisano *et al.*,

2016, Mascher *et al.*, 2017) and a variety of transcriptomes (Tanaka *et al.*, 2019, Liew *et al.*, 2020, Vinje *et al.*, 2021, Peirats-Llobet *et al.*, 2023) are also available. The analysis of the barley genome revealed, similar to several other cereals with large genomes, that the majority of the genome consists of repetitive sequences, including RNA and DNA transposons and rDNA genes (Gerlach and Bedbrook, 1979, Singh *et al.*, 2017, Wicker *et al.*, 2017).

Genes and transposons are unequally distributed in the barley genome. Genes show a high density at the ends of chromosome arms, while repetitive elements cover telomere-distal and centromere-proximal parts of the arms (Mascher *et al.*, 2017). This profoundly affects the distribution of meiotic crossovers to the gene-rich parts of chromosomes and significantly decreases recombination efficiency at the repeat-rich regions. In practical terms, this makes large parts of barley chromosomes depleted of meiotic recombination events and thus hard to use for breeding programs (Dreissig *et al.*, 2019, Casale *et al.*, 2022).

1.3 General principles of plant nucleus organization

DNA molecule is folded hierarchically and non-randomly in the nucleus. Despite the differences between individual higher organisms, the basic organization of the chromatin in the nuclear space preserves similarities.

At the first level, double stranded DNA spirals around the octamer of HISTONE proteins (two molecules of H2A, H2B, H3, and H4 each) to form nucleosomes. The stability of the nucleosome structure is secured by the addition of HISTONE H1 variant (Figure 1). The fiber comprising nucleosome structure is known as the nucleosome fiber and is assumed the fundamental structural subunit of chromosomes (Manuelidis and Chen, 1990, Wolffe and Hayes, 1999). It forms extensive chromatin loops often present between gene islands and closely associating transcriptionally active genes (Dong *et al.*, 2017) (Figure 1). These loops are actively formed by the activity of CONDENSIN and COHESIN proteins (described in more detail in Chapter 1.3.2.).

In plants, chromatin loops form topologically associated domain-like (TAD-like) structures, which are the alternative of TADs typically present in Animalia genomes. However, the formation of plant TAD-like structures is not conserved between all plant species. They were not observed in *Arabidopsis* ($2n=2x=10$; 125 Mbp/1C) (AGI, 2000,

Wang *et al.*, 2015) compact genome but were found in the large genome of wheat ($2n=6x=42$; 17 Gbp/1C) (Brenchley *et al.*, 2012, Concia *et al.*, 2020). TAD-like structures are also difficult to define as plants lack CCCTC-BINDING FACTOR (CTCF) present in Mammalian cells where it separates distinct chromatin loops and also defines chromatin expression state (Dong *et al.*, 2017).

In plant large genomes, individual TAD-like structures can be organized into mammalian-like A/B compartments defined by the preferential presence of either transcriptionally active or inactive chromatin. Finally, domains and compartments form distinct chromosome territories comprise individual chromosomes organized in chromosome territories (reviewed in Dogan and Liu, 2018).

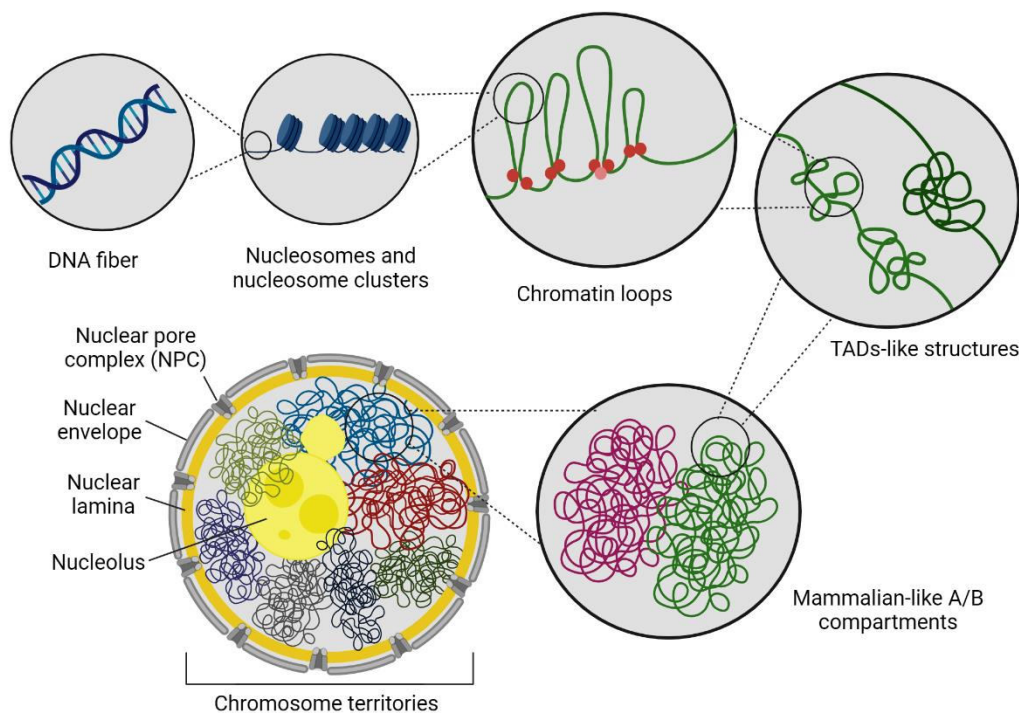


Figure 1. Hierarchical organization of chromatin of large plant genomes. The DNA fiber is coiled around the histone proteins to form nucleosomes and nucleosome fiber. Nucleosome fiber forms chromatin loops organized into TAD-like structures based on their expression state. TAD-like structures organize into mammalian-like A/B compartments differing in their transcriptionally active or inactive status. A/B compartments of distinct chromosomes form chromosome territories that interact with NPCs, nuclear lamina, and nucleolus based on their transcription activity. Modified from (Dogan and Liu, 2018).

Within the chromosome territories, transcriptionally inactive genes (e.g., silenced protein-coding genes, transposable elements, and other repetitive non-coding sequences) cluster to the nuclear periphery and interact with a nuclear lamina (NL) (van Steensel and Belmont, 2017, Sakamoto, 2020). After the transcriptional activation, genes are moved into the nucleoplasm to the proximity of transcription factories containing RNA-

polymerase II, which initiates their transcription (Egecioglu and Brickner, 2011, Concia *et al.*, 2020). Repetitive ribosomal RNA (rRNA) genes preferentially localize to the periphery of the nucleolus, nevertheless their localization is also dependent on their transcriptional status (Pontvianne *et al.*, 2013).

Organization of the chromatin can be strongly modified by changing environmental conditions or in the response to stress (Pecinka and Mittelsten Scheid, 2012, Rosa *et al.*, 2013, Probst and Mittelsten Scheid, 2015). These changes also often cause alterations in cell epigenetic profile (histone-specific variants or specific histone modifications), which lead to modifications in genes transcription or to gene silencing (reviewed in Pecinka and Mittelsten Scheid, 2012, Baurle and Trindade, 2020).

1.3.1 Spatial chromosome configuration in the nucleus

Despite the generic organization of eukaryotic chromosomes into the chromosome territories, interphase chromosomes can arrange themselves specifically based on the strict positioning of centromeres and telomeres.

In some plants with large genomes, interphase chromosomes adopt the so-called Rabl configuration (Figure 2A), where centromeres and telomeres cluster at opposite nuclear poles (Rabl, 1885, Cowan *et al.*, 2001). This chromosome configuration is typical for wheat (17 Gbp/1C) or barley (4.88 Gbp/1C) nuclei but was found only tissue-specifically in some other cereal crops. For example in rice (466 Mbp/1C) root xylem and undifferentiated anther cells (Prieto *et al.*, 2004).

Based on these findings, the formation of Rabl is not only dependent on organism genome size (Santos and Shaw, 2004). It was shown that *Arabidopsis* mutants in CONDENSIN II frequently resemble Rabl-like chromosome organization with clustered centromeres and abolished formation of chromosome territories (Sakamoto *et al.*, 2019). Moreover, the role of CONDENSIN II in Rabl formation was supported by an evolutionary study where organisms lacking some of CONDENSIN II subunits presumably showed higher frequencies of non-homologous chromosome contacts and Rabl-like centromere clustering (Hoencamp *et al.*, 2021).

Additionally, a recent study in barley showed that the Rabl configuration of chromosomes is reinforced by an anaphase chromosome positioning and subsequently seems to be actively maintained (Nowicka *et al.*, 2023). It was hypothesized that Rabl is

present primarily in the fast-cycling mitotically active cells and loosened when cells pass into a differentiation pathway (Santos and Shaw, 2004, Nowicka *et al.*, 2023). In barley endosperm cells, loss of Rab1 was observed with increasing endoreduplication levels and lowered division rate. Establishment of Rab1 configuration can be possibly influenced also by changed cell epigenetic status because decreased DNA methylation levels induced Rab1 in rice cells where it is not usually maintained (Santos *et al.*, 2011). However, this trend was not observed in *Arabidopsis* DNA demethylation mutants *decrease in DNA methylation 1 (ddm1)* or *methyltransferase 1 (met1)* (Soppe *et al.*, 2002).

In recent years, the non-Rab1 chromosome configuration also got into the research focus (reviewed in Oko *et al.*, 2020). In this configuration (Figure 2B), chromosome arms are dispersed through the nucleoplasm, centromeres are arranged at the nuclear periphery, and telomeres are primarily present in the nuclear interior. (Zhou *et al.*, 2019, Shan *et al.*, 2021).

Alternatively, interphase chromosomes can be organized in the nucleus in a rosette-like organization (Figure 2C). A typical example are *Arabidopsis* nuclei (125 Mbp/1C), where telomeres and nucleolus organizing region (NOR) cluster to nucleolar proximity, while centromeres localize randomly to the nuclear periphery. Centromeric heterochromatin, consisting of repetitive DNA, forms distinct dense chromocenters characteristic by inactive epigenetic marks. From the chromocenters, individual chromosome arms emanate (Fransz *et al.*, 2002, Pecinka *et al.*, 2004). Despite the apparent differences between the rosette-like and Rab1 chromosome organizations, the similarity can be found in the clustering of the chromosome ends at the nuclear (Rab1) or nucleolar (rosette-like) periphery. This leads to the closer non-homologous chromosome association and increases the probability of inter-chromosome interactions emergence probability (Ashley, 1979).

Chromosomes adopt characteristic configurations not only in interphase but also during meiosis. In the meiotic prophase (leptotene to pachytene), they resemble telomere bouquet organization where telomeres of homologous chromosomes pair together and attach to the nuclear envelope (NE) (Harper *et al.*, 2004) (Figure 2D). It has been observed in various plant, animal, and fungi species. In plant cells a bouquet is formed opposite to the microtubule band (Thomas and Kaltsikes, 1976). Centromeres localization is not strict in the telomere bouquet. Before and after the leptotene-pachytene telomere bouquet formation, telomeres are not entirely attached to the nuclear envelope and frequently

move alongside its inner layer, resulting in the formation of pre-bouquet or post-bouquet configurations respectively (Figure 2E) (Harper *et al.*, 2004).

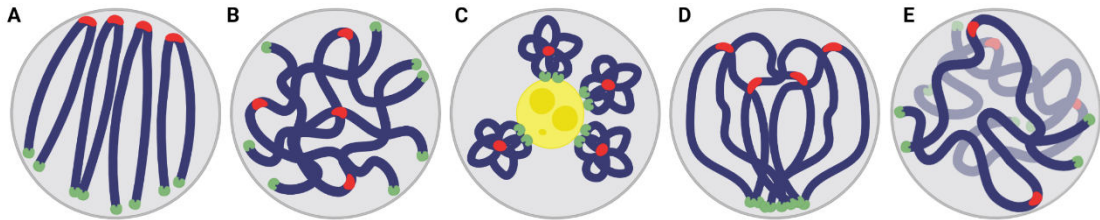


Figure 2. Patterns of chromosome arrangement in the nucleus. (A) Rabl configuration. (B) Non-Rabl configuration. (C) Rosette-like configuration. (D) Telomere bouquet. (E) Pre-bouquet and post-bouquet organization. Centromeres and telomeres are marked in red and green, nucleolus in yellow, and chromosomes in blue. Modified from (Lysak, 2022)

1.3.2 Mitotic chromosome organization

In maximal mitotic spiralization, chromosomes shape into rod-like structures, compacting chromatin up to 1,000 fold, to decondense again when the mitosis is finished (Bajer, 1959, Kuznetsova *et al.*, 2017, Kubalova *et al.*, 2023) (Figure 3).

The fundamental principles of condensed chromosome structure formation can be described by helical and non-helical models (Kubalova *et al.*, 2023). Helical models postulate that the chromatin of each sister chromatid is organized into the helix structure (Ohnuki, 1965, Gibcus *et al.*, 2018, Schloissnig *et al.*, 2021), whereas in non-helical models, coiled chromatin folds “side-by-side” (Rodley *et al.*, 1976, Kireeva *et al.*, 2004, Naumova *et al.*, 2013). Recent data from barley support the helical model (Kubalova *et al.*, 2023) (Figure 3). Hi-C data and super-resolution microscopy of fluorescence *in situ* hybridization using oligonucleotide probes (oligo-FISH) revealed that barley mitotic chromosome is formed by a 400 nm thick helically-wound chromatin fiber (i.e., chromonema). In chromonema, adjacent turns of the chromatin helixes frequently

intermingle. Interestingly, it was shown that the helical turns vary in size due to the differences in chromatin density (Kubalova *et al.*, 2023) (Figure 3).

Chromosome spiralization and its maintenance are regulated by various proteins including previously mentioned STRUCTURAL MAINTENANCE OF CHROMOSOMES (SMC) complexes CONDENSIN I and CONDENSIN II, and TOPOISOMERASE II (Maeshima and Laemmli, 2003, Sun *et al.*, 2018, Kim *et al.*,

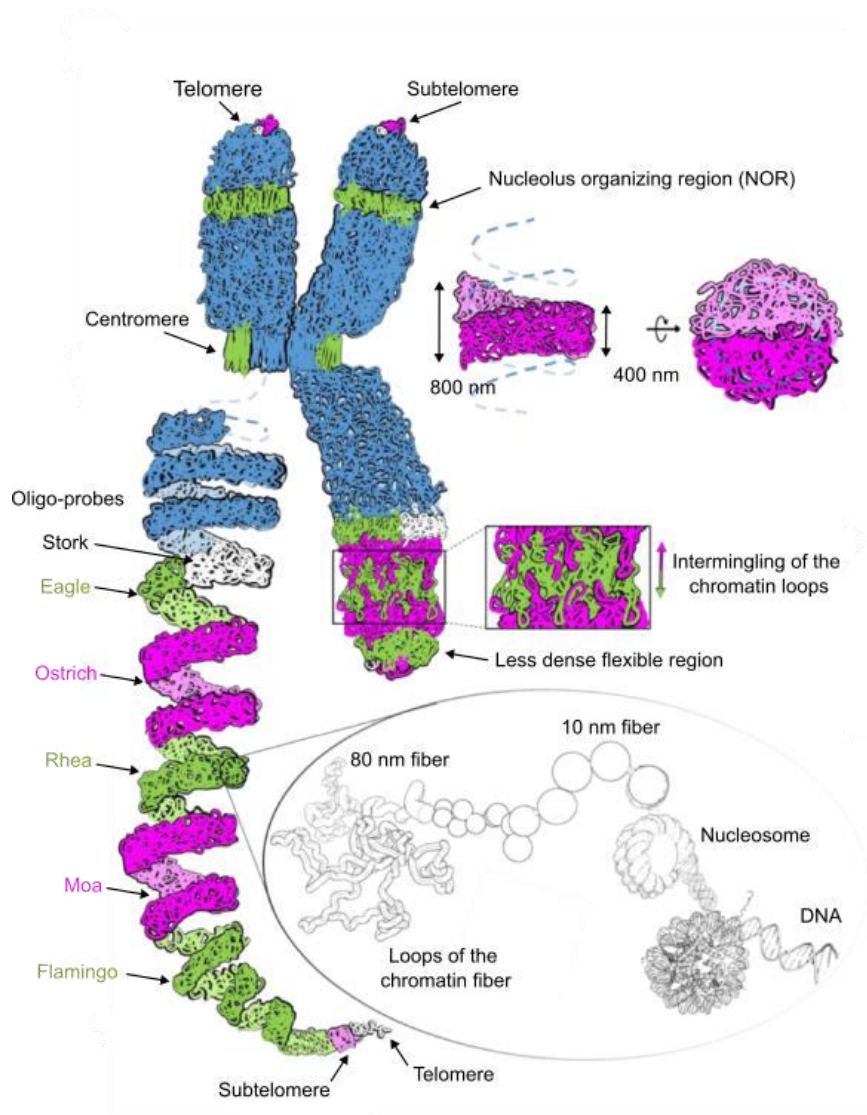


Figure 3. Model of the helical coiling organization in barley metaphase chromosomes.

Bottom right: loops of the 80 nm lower-order chromatin fibers, formed of consecutive nucleosomes. Differently colored consecutive loops correspond to oligo-probes used for the chromatin loop width and length measurement (Stork, Eagle, Ostrich, Rhea, Moa, Flamingo). The coils fill completely the chromatin without large cavities. Adjacent chromonema turns intermingle at their edges due to the flexibility of the smaller 80 nm chromatin fibers. The chromosomal termini contain less condensed, more flexible chromatin. Due to the flexibility, the telomeres may be embedded into the subtelomeric chromatin and not appear at the very end of the chromatid. Modified from (Kubalova *et al.*, 2023).

2022). CONDENSIN I and CONDENSIN II control chromatin organization and loop formation by wrapping around the DNA strand, which they extrude through the SMC-molecule central ring (Alipour and Marko, 2012). The main role of COHESIN is to secure the maintenance of sister chromatids replicated during the cell cycle S phase. However, it is significantly involved also in DNA condensation and gene expression regulation (Anderson *et al.*, 2002). Finally, TOPOISOMERASE II activity arranging recurrent DNA cutting and rejoining helps to untangle and tangle complex chromatin fiber structures (Goto and Wang, 1982).

CONDENSIN I and II have divergent roles in chromatin condensation in higher plants. They differ in the cell-localization pattern and the timing of loading onto the DNA. Nucleoplasma-localized CONDENSIN II loads to chromosomes already in the S phase. It shortens chromosomes axially by forming ~400 kbp loops and establishes sister chromatids resolution (reviewed in Shintomi and Hirano, 2010). Cytoplasm-localized CONDENSIN I targets DNA after the nuclear envelope breakdown in prometaphase and secures lateral chromosome compaction via forming nested ~80 kbp loops that substantially aggregate (Green *et al.*, 2012). Moreover, CONDENSIN II plays a role in chromosome and centromere compaction (Fujimoto *et al.*, 2005, Sakamoto *et al.*, 2019).

The surface structure of the condensed mitotic chromosomes has been thoroughly examined since high- and super-resolution microscopy establishment. Approaches involving scanning electron microscopy or stimulated emission depletion (STED) microscopy revealed the formation of chromosome cavities from prophase to telophase (Wanner *et al.*, 1991, Schaper *et al.*, 2000, Hamano *et al.*, 2014, Kuznetsova *et al.*, 2017, Kubalova *et al.*, 2021). These cavities serve as docking stations for proteins mediating transcription on compact mitotic chromosomes (Palozola *et al.*, 2017). In Animalia cells, the layer of proteins coating mitotic chromosomes known as the perichromosomal layer can be found (Gautier *et al.*, 1992, Gautier *et al.*, 1994, Hernandez-Verdun and Gautier, 1994). However, this structure has not been described in plants yet.

1.3.3 Organization of the nuclear envelope and the nuclear lamina

Plant nuclear envelope (NE) and nuclear lamina (NL) serve as a physical barrier separating the content of the cell nucleus from the cytoplasmic protein synthesis apparatus and thus ensure the maintenance of unreplaceable functions in the cell. Besides these

roles, there is growing evidence that they are involved in chromatin organization and gene expression regulation (Tiang *et al.*, 2012, Bishop *et al.*, 2021). Moreover, they maintain gradients of molecules. For instance, of cytoplasmic Ras-related nuclear protein guanosine 5'-diphosphate (RanGDP) and nucleic Ras-related nuclear protein guanosine 5'-triphosphate (RanGTP) which mediate plant cell responses and lead mitotic spindle localization and NE assembly, respectively (Guttinger *et al.*, 2009).

NE consists of a double layer of phospholipids forming the outer nuclear membrane (ONM) extending into the endoplasmic reticulum membrane with attached ribosomes and the inner nuclear membrane (INM) linking NE with NL. The distinctive representative protein of the ONM are membrane KLARSICHT ANC-1 SYNE HOMOLOGY (KASH) interacting with a cytoskeleton. For the INM, transmembrane C-terminal SUNs and NUCLEAR ENVELOPE ASSOCIATED PROTEIN (NEAP) providing NE-NL linkage are typical. Together, they are part of the LINKER OF NUCLEOSKELETON (LINC) complex (Tatout *et al.*, 2014). The transverse connection between the ONM and INM, the same as the nucleus and cytoplasmic molecular communication, are mediated by NUCLEAR PORE COMPLEX (NPC) proteins represented by PLANT NUCLEAR ENVELOPE TRANSMEMBRANE 1 (PNET1) or a variety of NUCLEOPORIN proteins (e.g., NUP358, NUP188, NUP153, etc.) (Tamura *et al.*, 2010, Parry, 2014, Tang *et al.*, 2020).

The role of plant lamina in chromatin organization and nuclear border shaping shares the essential characteristics with NL in animal or human cells, even though it has distinct specifics (Ciska and de la Espina, 2014). In plants, NL is not constituted by lamin proteins but by their plant functional homologs. So far, proteins such as PLANT NUCLEAR ENVELOPE TRANSMEMBRANE 2 (PNET2), CROWDED NUCLEI (CRWN), or JAPANESE FOR NUCLEUS 4 (KAKU4) are considered the main components of the plant NL (Wang *et al.*, 2013, Goto *et al.*, 2014, Tang *et al.*, 2022). CRWN1 and CRWN4 secure direct interaction between NL and nuclear periphery by associating with SUN proteins and help to shape the nucleus surface. Consequently, *crwn1* and *crwn4* mutants show a significant reduction in nuclear volume, altered nuclear shape, and significantly lower number of centromeric chromocenters (Sakamoto and Takagi, 2013). The same situation applies also to *kaku4* (Goto *et al.*, 2014). These results suggest that both NL and NE proteins are essential not only for the stabilization of the nuclear membrane but also for proper chromosome organization and their attachment to

NL, as indicated by proven interactions of CRWN1/4 with CONDENSIN II (Sakamoto *et al.*, 2022).

1.3.4 Organization of the nucleolus

Nucleolus is a large sub-nuclear compartment assembling around the active 45S rDNA loci (nucleolus organizers, NORs) localized on some chromosomes. The rDNA transcription, rRNA post-processing, and ribosome biogenesis occur there. 45S rDNAs are formed by 5.8S, 18S, and 28S genes separated by internal transcribed spacers (ITSs). Their transcription products are processed by snoRNPs (small nucleolar ribonucleoproteins) (reviewed in Shaw and Brown, 2012). The transcriptional activity of NORs is epigenetically regulated.

The separation of the nucleolus from the nucleoplasm is based on the liquid-liquid phase character of the interactions between RNA and protein cell constituents (reviewed in Lafontaine, 2019). The nucleolus internal architecture comprises fibrillar centers, dense fibrillar components, granular components, nucleolar chromatin, and nucleolar vacuoles (Stepinski, 2014). Fibrillar centers and dense fibrillar components can be interwoven into the so-called nucleolomena. This structure is characterized by the presence of RNA polymerase I transcribed rDNA genes, pre-rRNA processing machinery accomplished by small nucleolar RNAs/proteins (snoRNAs/snoRNPs), spliceosomal small nuclear RNAs/proteins (snRNAs/snRNPs), NUCLEOLAR PROTEIN52 (NOP52) involved in ribosome biosynthesis, and rRNA methyltransferase FIBRILLARIN (FIB) arranging post-transcriptional modifications (Hernandez-Verdun, 2011). In the granular component, ribosomal small (40S) and large (60S) subunits assemble into functional ribosomes. After the assembly, ribosomes are transported through the nucleoplasm into the cytoplasm, where they arrange protein synthesis (reviewed in Fromont-Racine *et al.*, 2003).

Nucleoli structure substantially changes during the cell cycle. It increases its volume if higher protein synthesis is required in the G1 phase of the cell cycle and is reduced if cells persist in an already differentiated state (Hernandez-Verdun, 2011, Lockhead *et al.*, 2020). The substantial changes in nucleolar structure happen before every mitotic division when the nucleolus disassembles during the prometaphase to reassemble again in the telophase around the early-emerging prenucleolar bodies (PNBs) (Hernandez-Verdun, 2011). Despite this, changes in nucleolar structures are prominent

under abiotic or biotic stress conditions and reflect alterations in cell and organism transcription needs (reviewed in Kalinina *et al.*, 2018). The exposure of plants to cold or heat stress leads to the formation of nucleolar speckles or nucleolar cavities (Hayashi and Matsunaga, 2019). Cavities and the nucleolar vacuole temporarily store accumulated biochemical factors involved in the ubiquitin-proteasome system (e.g., snoRNAs, snoRNPs, snRNAs, or snRNPs). Their stress-induced release into the nucleoplasm frequently initiates complex biochemical stress-dependent reactions (reviewed in Stepinski, 2014).

1.3.5 Organization of microtubules

Microtubules are essential for many biological processes in living cells, such as molecular transport, cell space reinforcement, and cell division. These cytoskeleton components consist of heterodimers of α/β -TUBULIN polymerizing into typically 13 parallel protofilaments via guanosine 5'-triphosphate (GTP) hydrolysis. They form spiral-like head-to-tail organized microtubule tubes, which dynamically grow or shrink on the plus ends unless they are fixed via GTP-cap addition (reviewed in Hashimoto, 2015). The transitional state between microtubule growth and shortening is known as microtubule catastrophe. If the switch is from shortening to growing, it is referred to as microtubule rescue. These processes result from stochastic fluctuations in the microtubule length, shape, and GTP-cap attachment (Margolin *et al.*, 2012). In contrast with animals, plant microtubules can moderately depolymerase on the minus ends during the process of polymer treadmilling typical for cortical microtubules (Shaw *et al.*, 2003). Based on the *in vitro* experiments, this process is controlled by plant-specific microtubule-associated proteins (MAPs) localized at microtubule plus and minus ends (Hotta *et al.*, 2016).

In eukaryotes, microtubule nucleation is initiated by the activity of γ -TUBULIN, arranging the formation of γ -TUBULIN RING COMPLEXES (γ -TuRCs) (Zheng *et al.*, 1995, Binarova *et al.*, 2006). The nucleation activity of γ -TUBULIN is crucial in plant cells that do not contain microtubule-organizing center (MTOC) and centrosomes, which nucleate microtubules and secure the formation of the mitotic spindle in non-plant species (reviewed in Hashimoto, 2015). In interphase plant cells, nucleation of cortical microtubules predominantly occurs at the plasma membrane alongside already present mother microtubules or in a branching pattern (Jacobs *et al.*, 2022). The resulting cortical

microtubule network is connects kinesin motor proteins at the plus ends of microtubules. These proteins are involved in the unidirectional transport of vesicles, organelles, and morphogenesis or also in cytokinesis by associating with CELLULOSE SYNTHASES (CESAs) and CELLULOSE SYNTHASE COMPLEX (CSC) (reviewed in McFarlane *et al.*, 2014). Additionally, microtubules, kinesin motor proteins, and MAPs organize the separation of chromosomes, organelles, and other cellular components in mitotic and meiotic division, including the cell plate formation (reviewed in Li *et al.*, 2012).

1.4 Mitotic division in higher plants: an overview

Mitosis is the main process that allows higher organisms to increase cell numbers and control their growth and development. During the cell cycle, cellular components and genetic material are duplicated and then evenly distributed into the newly emerging cells by the mitotic apparatus (Figure 4). In contrast to Animalia, plant cells lack centrosomes, typically organizing microtubules into the mitotic spindle. Moreover, they deal with the presence of cell walls, which need to be rebuilt during cytokinesis (reviewed in Gutierrez, 2009, Smertenko *et al.*, 2017). Despite the growing knowledge about plant mitosis progress and regulation, there is still much worth investigating in this process.

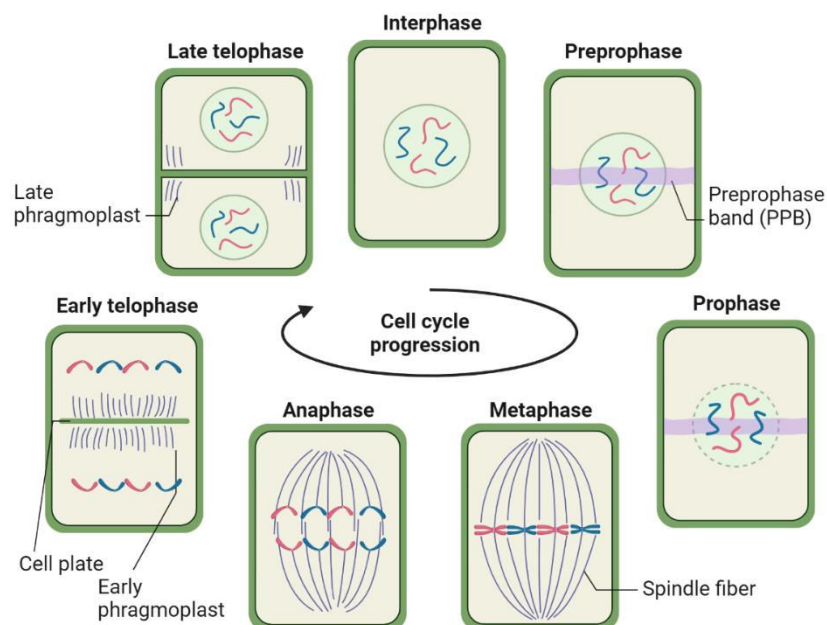


Figure 4. Mitotic division in higher plants. Schematic overview of plant mitosis. Chromosomes are visualized in red and blue. Modified from Biorender template (Rasmussen *et al.*, 2011, Smertenko *et al.*, 2017).

1.4.1 Regulation of cell cycle and mitosis in plants

The regulation of mitosis is inseparably synchronized with the cell cycle progression. The main regulators of plant cell cycle and mitosis are periodically activated CYCLIN-DEPENDENT KINASES (CDKs), which interact with different CYCLINS (CYCs) or CYCLIN-DEPENDENT KINASE INHIBITORS (CKIs), and together direct the progression of cell cycle from G1 to S phase, and G2 to M phase (reviewed in Inze and De Veylder, 2006, Komaki and Sugimoto, 2012). The cell cycle regulation is highly complex and not yet profoundly studied and understood in plants.

In contrast to yeast and animals, plants encode significantly more CDKs and interacting CYCs, probably owing to the whole genome duplication events (Jiao *et al.*, 2014). Apart from the CDKA class, the plant-specific CDKB class, subdividing into CDKB1 and CDKB2 subclasses, regulates the cell cycle and potential transition into the endoreduplication cycle. Endoreduplication is initiated in the absence of CDKB2, while its presence leads to cytokinesis (Menges *et al.*, 2005). In Arabidopsis, 10 A-type CYCs (CYCAs), 11 B-type CYCs (CYCBs), and 10 D-type CYCs (CYCDs) can be found. CYCAs and CYCBs comprise three subgroups (CYCA1-CYCA3 or CYCB1-CYCB3) and CYCDs of seven subgroups CYCD1-CYCD7 (reviewed in Inze and De Veylder, 2006, Komaki and Sugimoto, 2012).

The transition from the G1 to the S phase, as well as the progression of the S phase, is triggered by the binding of CDKA1 with CYCDs or CYCA3 in plants (Boruc *et al.*, 2010, Van Leene *et al.*, 2011). The switch from G2 to M phase, along with the M phase progression, is caused by the interaction between CDKA1 and CYCD3 or by CDKBs with CYCA2 and CYCBs (Boudolf *et al.*, 2009).

The progression of the plant cell cycle can be controlled on different levels by diverse mechanisms. On the first level, the amount of CYCs available in the nucleoplasm is regulated transcriptionally (reviewed in Berckmans and De Veylder, 2009). On the second level, when CYCs are already present in cells, their number is reduced by ubiquitin-mediated proteolysis (reviewed in Vodermaier, 2004). CYCs polyubiquitination promotes the transition from G1 to S phases, which is realized by SKP-CULLIN1-F-BOX E3 LIGASE (SCF) (Zheng *et al.*, 2011). On the other hand, middle M phase (anaphase) CYCs are polyubiquitinated by another E3 ligase known as ANAPHASE-PROMOTING COMPLEX/CYCLOSOME (APC/C complex; CULLIN-

RING FINGER E3 LIGASE). These events lead to the escape of the cell from mitosis to cytokinesis (Zheng *et al.*, 2011).

1.4.2 Dynamics of nuclear components and microtubules in plant mitosis

During the mitotic division, substantial dynamic changes occur in the cellular components' localization. These changes happen in both the cytoplasm and the nucleolus. In the cytoplasm, the cytoskeleton reorganizes itself to prepare for mitotic spindle formation. In the nucleus, changes in chromatin and nucleolus structure follow.

1.4.2.1 Chromosomes in plant mitosis

Interphase chromosomes undergo striking changes during the mitotic compaction, where they form metaphase-visible rod-like structures (Figure 2). The first steps of chromosome compaction are initiated already during the prophase by the activity of CONDENSIN II. Afterward, the process is accelerated by loading of CONDENSIN I after the prometaphase nuclear envelope breakdown. Chromosome compaction reaches the maximum around the metaphase (Sun *et al.*, 2018).

During the mitosis, prometaphase chromosomes move into the cell center, forming a metaphase band comprising lined chromosomes. The position of the metaphase band is given by the preprophase band (PPB), a ring-like structure formed by cortical microtubules. Moreover, PPB regulates the localization of the mitotic spindle and a future-formed phragmoplast, which serves as the basis for the newly formed cell wall assembly (Ambrose and Cyr, 2008). In metaphase, individual sister chromatids are detached after the SEPARASE cleaves the kleisin SISTER CHROMATID COHESION1 (SCC1) COHESIN's subunit on the onset of anaphase (reviewed in Nasmyth and Haering, 2005). After chromosomes are pulled to the opposite cell poles, CONDENSIN I and II are removed gradually from the DNA by interacting PRECOCIOUS DISSOCIATION OF SISTERS 5 (PDS5) and WINGS APART-LIKE (WAPL) proteins. This leads to the chromosome decondensation and the formation of emerging daughter cells (Pradillo *et al.*, 2015, Hernandez *et al.*, 2018).

1.4.2.2 Nucleolus in plant mitosis

The nucleolus disassembles synchronously with the nuclear envelope breakdown at the onset of mitotic prometaphase. Firstly, granular component disintegrates and disperses throughout the cytoplasm. Afterward, dense fibrillar component dissipates between the condensed chromosomes; thereby, the nucleolus disassembly is finished. It was proposed that some components of the RNA POLYMERASE I (POL I) COMPLEX and pre-rRNA processing complex as FIB1, NUCLEOLIN 1, or NOP52 associate with condensed metaphase and anaphase chromosomes, becoming the components of the perichromosomal layer typical for Animalia and yeast cells (Risueno *et al.*, 1982, Saez-Vasquez and Medina, 2008). During the telophase, these proteins form prenucleolar bodies (PNBs) near the surface of chromosomes.

The newly forming nucleoli reassemble around chromosome NORs to where PNB components are actively transported (Savino *et al.*, 2001). The early-forming PNBs contain mainly FIB1 protein, whereas NOP52 is preferentially present in the late-forming PNBs. During the CYCB degradation and CDKA activity decrease, the transcription of rDNA is restored (Sirri *et al.*, 2002).

1.4.2.3 Nuclear envelope and nuclear lamina in plant mitosis

The nuclear envelope and nuclear lamina disintegrate during the mitotic preprophase to be reconstituted around the newly formed daughter nuclei in telophase. In plants, the nuclear envelope breakdown is initiated by the phosphorylation of LINC complex proteins by CDKA, which afterward relocalizes to the mitotic spindle, PPB, and phragmoplast. Nuclear lamina proteins CRWNs migrate to the mitotic spindle (CRWN1) and cytoplasm (CRWN4) (reviewed in Evans *et al.*, 2009, Kimura *et al.*, 2010). On the contrary, C-terminal SUN (SUN1) presence was detected in both mitotic spindle poles and around condensed metaphase-anaphase chromosomes, the same as the presence of NUCLEOPORIN88 (NUP88) (van Damme *et al.*, 2004, Xu *et al.*, 2007, Graumann and Evans, 2011). The SUN2 preferentially localizes with membrane vesicles throughout the mitotic division (Masuda *et al.*, 1999, Graumann and Evans, 2011).

In the process of nuclear envelope/lamina reconstruction, SUNs and CRWNs attach to chromosomes and mitotic spindle poles periphery and then gradually move into the spindle central part where phragmoplast emerges. The separation of daughter cells is initiated by centrifugal formation of the cell plate at the position given by RanGTPase

gradient and PPB (Xu *et al.*, 2007) by incorporation of the cell wall components, SUNs, and nuclear pore complexes (van Damme *et al.*, 2004).

1.4.2.4 Microtubules in plant mitosis

The rearrangement of interphase cortical microtubules attached laterally to the nuclear envelope is initiated by the accumulation of the RanGTP, which allows the release of the mitotic spindle assembly factors (Haizel *et al.*, 1997, Caudron *et al.*, 2005). During the late prophase, cortical microtubules (i.e., bridging microtubules) radiate from PPB to contact with the nuclear envelope and to set the future division plane together with GTPase ACTIVATING PROTEIN (RanGAP) (Ambrose and Cyr, 2008, Xu *et al.*, 2008). The association of the PPB with RanGTP initiates enrichment of cortical microtubules around nuclei and their association with TARGETING PROTEIN FOR XKLP2 (TPX2) (spindle assembly promotion), NUCLEAR MITOTIC APPARATHUS PROTEIN (NuMA) (localization of microtubules into the poles) and RIBONUCLEIC ACID EXPORT1 (RAE1) (bipolar spindle formation after forming RAE1/NuMA complex). The association process leads to the formation of the bipolar mitotic spindle (Stoppin *et al.*, 1994, Binarova *et al.*, 2006, Vos *et al.*, 2008).

In plants, three functionally diverse AURORA kinases can be found (Demidov *et al.*, 2005). AURORA 1 and 2 (α -type AURORA kinases) secure the formation of bipolar spindle, asymmetric cell divisions, and function also during cytokinesis (reviewed in Weimer *et al.*, 2016). Moreover, AURORA 1 can interact and phosphorylate microtubule-localized TPX2 (Tomastikova *et al.*, 2015). AURORA 3 (β -type AURORA kinase), localized in the inner-kinetochore part, leads nucleation and growth of kinetochore microtubules by regulating interactions between kinetochores, NUCLEAR FILAMENT-CONTAINING PROTEIN 2 (NUF2) subunit of FOUR-PROTEIN NUCLEAR DIVISION CYCLE80 (NDC80) and TONNEAU/FASS (TON2) (Kirik *et al.*, 2012, Weimer *et al.*, 2016, Li *et al.*, 2021). It is involved in mediating interaction between microtubules and outer-kinetochore localized NDC80 complex.

In a correctly polarized mitotic spindle, fully stretched kinetochore microtubules shield NDC80 from the AURORA 1 phosphorylation activity, which increases NDC80-microtubules binding affinity (Cowley *et al.*, 2009). After spindle assembly, kinetochore microtubules direct condensed chromosomes into the metaphase band and then pull them to the opposite spindle poles during the anaphase (reviewed in Weimer *et al.*, 2016).

The mitotic spindle breakage is initiated in telophase by the ubiquitination activity of the APC/C complex. During cytokinesis, microtubules participate in the formation of the cell plate and phragmoplast by organizing the transport of vesicles, components of the cell wall and membranes, and by the distribution of organelles. Finally, they lead to daughter cell separation (reviewed in Vodermaier, 2004).

1.5 Methodological approaches to study cell organization and dynamics in crops

The analysis of cereal plant's cell organization and dynamics is a challenging process. First insights into the cereal tissue and cell architecture focused primarily on *in vitro* staining of seed storage products (e.g., starch, β -glucans, lipids, etc.) (Yiu, 1993). With improving microscopy resolution, specific *in vitro* analysis of cellular and nuclear organization were done firstly in 2D and afterward also in 3D space in plants (reviewed in Dumur *et al.*, 2019). The evolution of *in vitro* microscopy was also significantly accelerated by the involvement of molecular techniques. In parallel, progress in *in vivo* microscopy enabled visualization of living structures not only in the bright field or by detection of autofluorescence but also by using *in vivo* fluorescent labeling (reviewed in Fricker *et al.*, 2006, Meschichi *et al.*, 2021). Together, these techniques have substantially helped to increase the knowledge about the cellular and molecular dynamics of cereals.

1.5.1 *In vitro* methodological approaches

Various molecular and cytogenetic techniques are used for investigations of chromatin arrangement. The increasing capacity of sequencing technology enabled the expansion of approaches uncovering complex interactions within chromatin units on different functional and structural levels. These methods comprise techniques like chromosome conformation capture (3C), circular chromosome conformation capture (4C), 3C-carbon copy (5C), Hi-C or micro-C (reviewed in Simonis *et al.*, 2007, Dogan and Liu, 2018).

In the 3C approach, interaction frequency between two chosen loci (e.g., promoter and enhancer) is investigated (Dekker *et al.*, 2002). This technique was, for example, used for mapping the linear order of sequences across the pericentromeric regions and to

investigate the 3D organization of chromatin in the nucleus at megabase resolution level in barley (Mascher *et al.*, 2017).

Complex interactions within the whole genome and one specific loci are uncovered using the 4C technique, which is the extension of the 3C (Zhao *et al.*, 2006).

Interactions between thousands of selected loci are studied by the 5C approach (Dostie *et al.*, 2006) or, eventually, by Hi-C, which extends the capacity of the 3C method to the genome-wide interaction network on both short-range and long-range (Lieberman-Aiden *et al.*, 2009).

In recent years, Hi-C significantly helped to uncover specific features of crops' genome organization and regulation, same as to improve genome assemblies. It was used in the modeling of barley metaphase chromosomes' spiralization (Kubalova *et al.*, 2023), telomere-to-telomere assembly of barley MorexV3 reference genome (Navratilova *et al.*, 2022), the study of wheat chromatin architecture where it uncovered formation of genome territories and transcriptional factories (Concia *et al.*, 2020), and for analysis of inter-chromosomal interactions (Jia *et al.*, 2021). Afterward, Hi-C was optimized for use on the single-cell level. This helped to investigate the chromosome structure and or cell variability between different cell types, like 3D genome structures of rice gametes and unicellular zygotes (Nagano *et al.*, 2013, Zhou *et al.*, 2019).

The strength of the 3C techniques is even more prominent when combined with other approaches unfolding chromatin interactions, such as chromatin immunoprecipitation (ChIP, ChIP-seq, ChiA-PET, HiChIP or others) (Li *et al.*, 2010, Nagano *et al.*, 2013, Mumbach *et al.*, 2016). There, specific interactions between the DNA and proteins in their native or translational fusion-tagged form are investigated. As for the 3C techniques, decreased sequencing price allowed the comprehensive analysis of gene regulation sequences (e.g., transcription factors and enhancers). It was used for association analysis of active and heterochromatin genes in rice (Zhao *et al.*, 2019) and also helped with sequences' annotations (Li *et al.*, 2010, Mumbach *et al.*, 2016).

The specific chromatin regions can be afterward directly visualized by commonly used *in vitro* microscopy techniques. For instance, by fluorescence *in situ* hybridization (FISH) or by its three-dimensional extension (3D-FISH), where hybridization is done on fixed samples with preserved 3D structure. Alternatively, multicolor FISH and oligo-painting broaden the microscopy range by using differentially labeled hybridization probes (Solovei *et al.*, 2002, Beliveau *et al.*, 2015, Fudenberg and Imakaev, 2017).

Especially after the rise of super-resolution microscopy techniques, represented by confocal microscopy, stimulated emission depletion (STED), photo-activated localization microscopy (PALM), or structured illumination microscopy (SIM), *in vitro* microscopy techniques have become a powerful tool for cell and chromatin organization studies (reviewed in Komis *et al.*, 2015, Schubert, 2017, Huang *et al.*, 2020). Moreover, their application potential has even grown after tuning them for *in vivo* live microscopy in live-STED on live-confocal microscopy setups. However, these techniques have not been fully optimized for use in plants (reviewed in Guo *et al.*, 2021).

1.5.2 *In vivo* methodological approaches to localize specific DNA sequences

The dynamic nature of cell organization encourages the study of mobility using *in vivo* microscopy, which enables direct visualization and tracking of living objects during a defined time period. Techniques used for the *in vivo* studies are primarily based on the fusion of marker proteins with a fluorescent tag (described in more detail in Chapter 1.5.3.) or on the recognition of specific sequences integrated into the DNA/RNA by fluorescently tagged proteins. Since these techniques often differ in their capacity, they need to be well-chosen and optimized based on the exact application.

Several techniques were developed for chromatin mobility studies. The pioneering approach, known as the *lacO*-LacI system, uses fluorescently tagged bacterial transcription factor LacI, which binds to the *lacO* repeat motif integrated into the organism genome (Kato and Lam, 2003, Matzke *et al.*, 2005, Leland and King, 2014). The positional change of the *lacO* locus in the nucleus is tracked in time and gives information about the chromatin mobility, especially when two differently labeled LacI fusion proteins are used (allowing to score two genomic regions simultaneously). Obtained data are even more complex if the exact position of the *lacO* integration site is known (e.g., same or different chromosomes, same or different chromosome arms, heterochromatinic/euchromatinic regions) (Matzke *et al.*, 2005, Rosa *et al.*, 2013). The disadvantage of the *lacO*-LacI system lies mainly in the length of the *lacO* repetitive locus (more than 5 kbp), which can alter local chromatin structure or lead to transcriptional inactivation caused by its repetitive-like character (Pecinka *et al.*, 2005, Watanabe *et al.*, 2005, Rosa *et al.*, 2013).

The ANCHOR system has a significant advantage over the *lacO*-LacI system. Only short low-copy *parS* locus (1 kbp) integrates into the genome and is specifically recognized by fluorescently tagged ParB proteins that oligomerize around the *parS*. This enables fluorescence signal intensity amplification (Meschichi *et al.*, 2021). If *parS*-ParB from different bacteria species are used and tagged by diverse fluorescent proteins, the ANCHOR system can serve for simultaneous visualization of more genomic loci (Saad *et al.*, 2014).

The specifically chosen genomic loci can be preferentially tracked by advanced approaches using tagged TALENs, zinc-fingers (ZFs), or CRISPR with nucleolytically dead Cas9 (dCas9) (Ishii *et al.*, 2019, Khosravi *et al.*, 2020). In these systems, specific DNA sequence-recognizing proteins are translationally fused with fluorescent proteins and guided to the exact genomic position either based on their DNA binding properties (TALEN, ZFs) or based on the sequence complementarity with a guide RNA molecule (CRISPR). In recent years, dCas9 was adapted for a specific single-locus visualization. For example, it was successfully used for *in vivo* visualization of telomeric sequences in *Nicotiana benthamiana* (Dreissig *et al.*, 2017) but has not been fully developed for *in vivo* visualizations in living plants to date.

The approaches mentioned above are mainly used for tracking specific genomic loci or evaluating chromatin mobility. However, to analyze entire cellular structures and compartments, systems that use a translational fusion of specifically localizing fluorescently labelled marker proteins have taken the lead (Wu *et al.*, 2013).

1.5.3 *In vivo* methodological approaches for protein localization studies

Despite the visualization of specific DNA sequences, there is a need to localize and track specific proteins. This is predominantly done by the creation of fluorescent marker lines. The fluorescent marker lines, also known as fluorescent reporter lines, are created by translational fusion between the gene of interest and coding sequences of a fluorescent protein (Figure 5) (Kirienko *et al.*, 2012). These marker lines find application in various *in vivo* imaging setups and localization studies at the molecular, cellular, tissue, or organism levels. Their significance has grown even further after the implementation of plant transformation protocols generating stable transgenic plants (see more in Chapter 1.7).

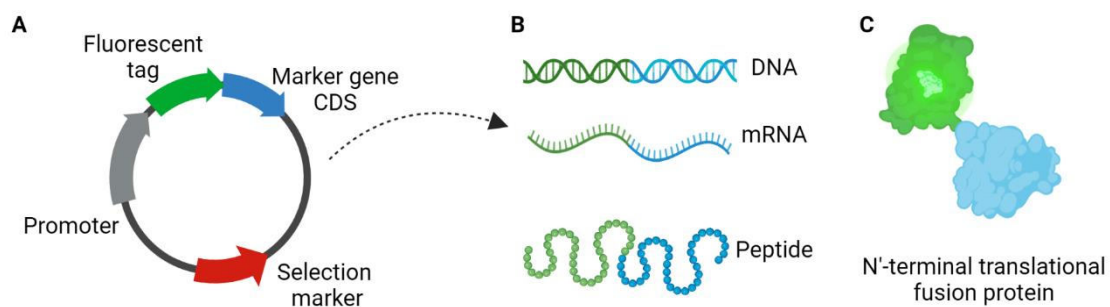


Figure 5. The principle of translational fusion protein assembly. (A) Translational fusion construct. (B) Transcription and translation of fusion protein coding sequence. (C) Folded translational fusion fluorescent marker protein.

Fluorescent marker lines enable tracking of the fluorescent signal emitted by a fluorescently tagged protein in real-time, providing insights into the protein 3D dynamics, subcellular localization, interactions between neighboring cells, and protein mobility in living cells and tissues. Several fluorescence spectro-microscopy techniques, such as Fluorescence Recovery After Photobleaching (FRAP), Fluorescence Loss In Photobleaching (FLIP), or Fluorescence Correlation Spectroscopy (FCS) are commonly used for protein-dynamic's studies in plants (reviewed in Fricker *et al.*, 2006, Reddy *et al.*, 2007). These techniques are based on the quantitative measurement of the fluorescence signal gain or loss.

In FRAP, the recovery of a fluorescence signal in a specific cell area irreversibly photobleached by a high-energy laser pulse gives information about a tagged protein cell mobility. FRAP is mainly used to investigate organelle-protein dynamics, such as the flow of proteins from the endoplasmic reticulum to the Golgi apparatus (DaSilva *et al.*, 2004).

In FLIP, the drain of the signal from connected compartments is measured after the continuous photobleaching of the specific cell region (reviewed in Fricker *et al.*, 2006).

In the FCS approach, parameters such as protein diffusion, cell protein concentration changes, or binding ability are studied (Hink *et al.*, 2002).

Specific quantitative interactions between two molecules are uncovered by techniques as Fluorescence Cross-Correlation Spectroscopy (FCCS), Förster Resonance Energy Transfer (FRET), or Fluorescence-Lifetime Imaging Microscopy (FLIM). These methods compare changes in fluorescence intensities using two differently tagged

candidate proteins (FCCS) or energy donor and acceptor molecules (FRET, FLIM) (Schwille *et al.*, 1997, Zelazny *et al.*, 2007, reviewed in Miyawaki, 2011).

FRET and FLIM are widely used in plant *in vivo* applications because they are independent of the donor and acceptor molecule concentrations. The FRET-FLIM combination helped to understand cell-type-specific protein interactions in *A. thaliana* root and embryo development (Bücherl *et al.*, 2010, Long *et al.*, 2017).

Alternatively, fluorescently tagged proteins can be used in Fluorescence Activated Cell Sorting (FACS) to isolate specific cells expressing these proteins (Afonso *et al.*, 1985).

Overall, the amount of comprehensive knowledge gained from the techniques mentioned above is outstanding. Nevertheless, it would not be possible without a high-quality microscopy data and data post-processing techniques.

1.6 Confocal microscopy

Confocal microscopy is a high-resolution light microscopy technique used for the analysis of fixed and live samples emitting fluorescence (reviewed in Elliott, 2020). Compared to other fluorescence microscopy techniques, illumination and detection optics are focused on the same spot (in the focal plane). During scanning, the spot is moved through the sample focal plane to provide a complete section image captured by the detector. The individual optical section can then be used for the 3D object reconstruction. As any light emitted outside of the focal plane is filtered out, the final image is sharp and not blurred. Due to this, confocal microscopy is frequently used for deep analysis of thicker samples (Callamaras and Parker, 1999).

In the principle of confocal microscopy (Figure 6), illumination light refracts on the dichromatic mirror to pass through the scanning mirror, sweeping the light beam across the sample. Then it goes through the objective lens, which focuses the beam on a single sample point. Emitted fluorescence passes back through the objective lens and dichromatic mirror to be detected by a sensitive detector. Before the detection, emitted out-of-focus light is filtered out by a pinhole placed before the detector (Callamaras and Parker, 1999).

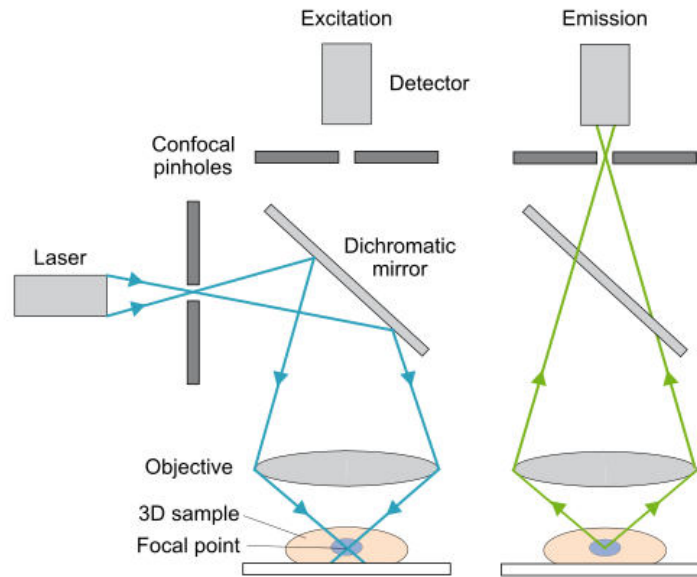


Figure 6. Principle of confocal microscopy. Light from a laser source is reflected by the dichromatic mirror and reflects the objective lens, which focuses the beam on a point in the sample. Emitted fluorescence passes back through the optics into the detector. Out-of-focus light is filtered out by a confocal pinhole placed before the detector. Modified from (Elliott, 2020, Ibidi, 2023)

The sample resolution value obtained by confocal microscopy can reach approximately 180 nm in the lateral and 500 μm in the axial axis (Fouquet *et al.*, 2015). However, this resolution is more of a theoretical number due to the specific sample properties decreasing a resolution potential.

The main advantage of confocal microscopy lies in the high-resolution of obtained images. It can be further increased by a pinhole width adjustment or selection of objectives with high numerical aperture (NA) and sensitive detectors (reviewed in Elliott, 2020). Except for the classical photomultiplier tubes (PMTs), more sensitive hybrid detectors (HyDs) have become a favored detector option (reviewed in Jonkman and Brown, 2015). The main confocal microscopy limitations are considered low scanning speed and higher phototoxicity and photobleaching. Nevertheless, some of these limitations have already been overcome by advanced confocal microscopy setups.

The most common confocal microscope type is a Laser Scanning Confocal Microscope (LSCM), which uses a laser beam sweeping over the sample by scanning mirrors (reviewed in Paddock, 1999, and Elliott, 2020). The z-stack image is obtained by moving the focal plane through the sample. It can provide multi-color images in 3D (x, y, z), 4D (x, y, z, t; t = time), or 5D (x, y, z, t, λ ; λ = wavelength). The main advantages of LSCM are its axial resolution and light penetration, the disadvantages are lower

imaging speed and photodamage. Nevertheless, scanning speed can be improved by the addition of highly efficient resonant scanners (Wu *et al.*, 2015). Compared to the LSCM, a spinning disk confocal microscope enables fast image scanning by using metal discs with high numbers of small holes serving as individual pinholes (reviewed in Paddock, 1999, and Elliott, 2020). The emitted light is detected by a sensitive charged-coupled device (CCD) camera. Spinning disk microscopes cause less damage to the sample as only a small sample part is illuminated at a particular moment. However, the obtained sample resolution is lower and frequently leads to artifacts if the camera and spinning disk speeds are not synchronized.

Except for LSCMs and spinning disks, there are also other confocal microscope types combining the advantages of these microscopes. For example, a hybrid scanning confocal microscope where a round pinhole is replaced by a rectangular slit rejecting out-of-focus light, which increases scanning speed and light collection efficiency (reviewed in Paddock, 1999). Additionally, a re-scan confocal microscope improves lateral resolution by 1.4 ($\sqrt{2}$) (De Luca *et al.*, 2013), or the Airyscan technology (Zeiss) provides 1.7x higher resolution in x, y, and z by improving the signal-to-noise ratio (Huff, 2015).

1.7 Image analysis software tools for microscopy data post-processing

Raw digitalized microscopy data undergo several post-processing transformations before they are quantitatively and qualitatively analyzed. In the initial post-processing steps, parameters like noise reduction, contrast enhancement, convolution, and background subtraction are adjusted to improve the quality of the raw microscopy images (reviewed in Cardullo and Hinchcliffe, 2013). These mathematical operations help to increase the raw microscopy image quality affected by the nature of the sample (e.g., unequal staining or high background intensity).

General image post-processing is done in microscope-integrated software such as LAS X Life Science Microscope Software (Leica Microsystems), ZEISS ZEN Microscopy Software (ZEISS), or Celleste Image Analysis Software (Olympus LS). Nevertheless, these software programs are continuously superseded by more advanced post-processing approaches integrated into specialized programs equipped with user-optimized tools and plugins. These tools are available either as separate tools or as part of comprehensive software platforms like ImageJ/FIJI (Schindelin *et al.*, 2012) or Imaris

bitplane (Imaris). In Imaris, advanced features allowing surface extraction and rendering, object segmentation, quantitative localization analysis, or time-lapse object tracking are processed in both 3D and 4D workspaces. Moreover, software can process them automatically or with some user guidance for threshold adjustments.

Quantitative measurements of cell growth anisotropy and cytoskeleton organization can be efficiently tracked using the ImageJ plugin FibrilTool (Boudaoud *et al.*, 2014). This plugin automatically subtracts individual fibrillar structures from the background based on differences in signal intensity, creating a complex fibrillar network. FibrilTool has been integrated into the MorphographX platform, allowing computer-assisted analysis of cell segmentation and microtubule organization (de Reuille *et al.*, 2015).

For cell segmentation, staining the cell walls with a contrasting dye is a common approach. Frequently, propidium iodide is used for short-time live imaging. Nevertheless, it is not recommended for a long-period time-lapse analysis due to its partial toxicity (Kierzkowski *et al.*, 2019). Instead, non-toxic vital dyes like FM4-64, which label plasma membranes or specific fluorescent marker lines can be used (Grandjean *et al.*, 2004, de Reuille *et al.*, 2015, Kiss *et al.*, 2017). Stained cell walls can be detected by several semi-automatic or automatic segmentation programs, such as MorphographX, MARS/ALT, PlantSeq, or ImageJ plugin SurfCut (Fernandez *et al.*, 2010, de Reuille *et al.*, 2015, Erguvan *et al.*, 2019, Wolny *et al.*, 2020). Some of these programs even allow segmentation in 3D, like PlantSeq 3D segmentation (Proj3D) (Wolny *et al.*, 2020) or previously mentioned Imaris bitplane (Imaris).

Nowadays, deep learning and machine learning approaches, especially with the involvement of artificial intelligence softwares, are increasingly used for the routine analysis of complex datasets (reviewed in von Chamier *et al.*, 2019). These approaches are particularly beneficial for the detection of actively dividing cells in mitosis and identification of individual mitotic phases, as well as for improving standardized object segmentations and related analyses (Aivia AI Analysis Software, Leica Microsystems; Amira Software for Life and Biomedical Sciences, ThermoFisher Scientific) (Nagaki *et al.*, 2021).

1.8 *Agrobacterium tumefaciens*-mediated transformation of plants

Agrobacterium tumefaciens-mediated plant transformation has become an essential method for generating transgenic plants. Compared to other plant transformation techniques like particle bombardment or microinjection, *Agrobacterium* significantly increased transformation efficiency by up to tens of percent (Thomas *et al.*, 2011).

In natural conditions, *Agrobacterium* carries a tumor-inducing (Ti) plasmid that integrates a part of its DNA (known as transferred DNA or T-DNA) into the host nuclear genome and causes a tumor-like structure formation (Chilton *et al.*, 1977). Mutated *Agrobacterium* used for transformation poses the ability to integrate engineered T-DNA into the host genome but does not lead to tumorigenesis (Bevan *et al.*, 1983, Fraley *et al.*, 1983, Herreraestrella *et al.*, 1983, reviewed in De Saeger *et al.*, 2021).

To meet specific application needs (such as transformation efficiency, number of T-DNA copies integrated into a genome, or host specificity), various *Agrobacterium* strains like AGL1, GW3101, EHA105, and LBA4404 have been engineered (reviewed in De Saeger *et al.*, 2021). Among these strains, AGL1 is primarily used for cereal crop transformation (Chabaud *et al.*, 2003).

Agrobacterium-mediated transformation of immature embryos is the primary method used for cereal crops like barley. It is much more efficient compared to other *Agrobacterium* barley transformation techniques using shoot apical meristems and apices, shoot base segments (Sharma *et al.*, 2004), embryonic pollen cultures, or embryos from mature seeds (Hua *et al.*, 2013). It results in a significantly higher number of regenerated transgenic plants, which are mostly not chimeric, unlike if using embryos from mature seeds (Ye *et al.*, 2023).

Transformation efficiency was greatly improved by using optimized binary vectors, hyper-virulent *Agrobacterium* strains (e.g., AGL1), and adjusting the transformation protocols and growth media (Marthe *et al.*, 2015). Further improvement in plant regeneration was achieved by modifying binary vectors overexpressing the regeneration-supportive genes, such as *GROWTH-REGULATING FACTOR 4-GRF-INTERACTING FACTOR 1* fusion (*GRF4-GIF1*) (Debernardi *et al.*, 2020), *BABY BOOM* (*BBM*), or *WUSCHEL 2* (*WUS2*) (Jones *et al.*, 2019).

Despite the existence of various *Agrobacterium* immature embryo transformation protocols, the underlying process remains similar (Figure 7). Immature embryos at the

appropriate developmental stage are co-cultivated with *Agrobacterium* of an optimized optical density and then transferred to callus induction media containing selective antibiotics. In the case of monocots like barley, hygromycin is primarily used (Marthe *et al.*, 2015). The calli grown in the dark are afterward transferred to callus regeneration media and exposed to light, which induces the emergence of regenerated plantlets. These plantlets are usually genotyped for the presence of an antibiotic resistance gene (such as *hygromycin phosphotransferase* gene, *hpt*) to select positive transgenic plants and avoid potential selection escapes (Harwood, 2009, Marthe *et al.*, 2015, Hinchliffe and Harwood, 2019). The selected transgenic plants are then further genotyped for the presence of the desired trait (e.g., a fluorescent signal, mutation, or others).

As *Agrobacterium* can cause multiple T-DNA insertions, their exact number is estimated via segregation analysis, Southern blot (Southern, 1975), or molecular methods like thermal asymmetric interlaced (TAIL-)PCR (Liu *et al.*, 1995), quantitative PCR (qPCR) (Higuchi *et al.*, 1992), or digital droplet PCR (ddPCR) (Hindson *et al.*, 2011).

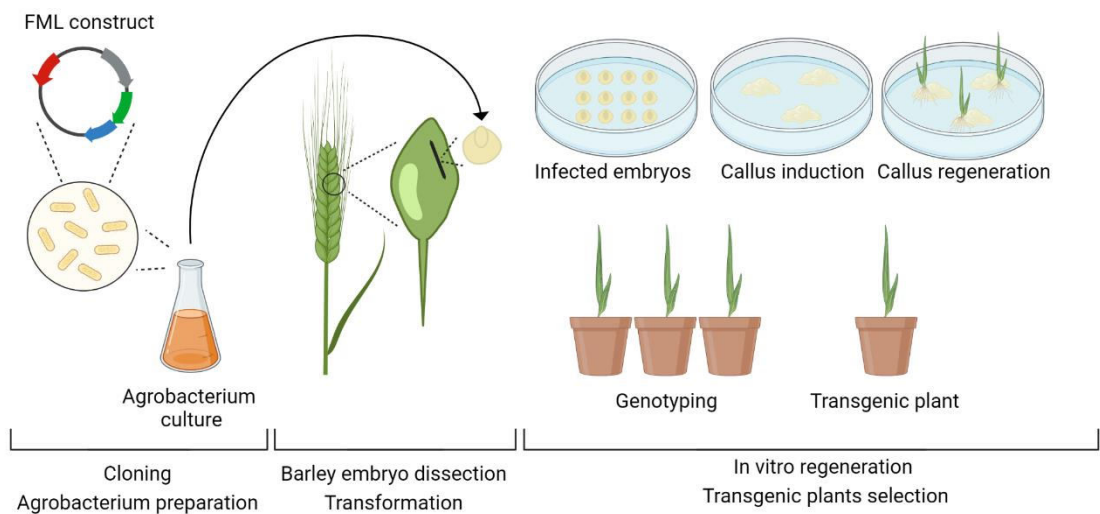


Figure 7. Agrobacterium-mediated transformation of immature barley embryos with a translational fusion line construct. The transformation process consists of the cloning of the FML construct and its transformation into the selected *Agrobacterium* strain, dissection and *Agrobacterium* transformation of the immature barley embryos, induction of callus and in vitro plant regeneration, and the selection and genotyping of the transgenic plants.

2 AIMS OF THE THESIS

2.1 Development of translational fusion fluorescent marker lines for *in vivo* nuclear and cell dynamics studies in barley

The first aim of the thesis was to develop a collection of translational fusion fluorescent marker lines (FMLs) of barley, which could be used for studying *in vivo* nuclear and cellular processes in living plants with large genomes. The initial step was to select marker genes with an indicative localization of the protein products within specific nuclear and cellular compartments. We aimed to design and clone marker gene expression constructs differing in the marker protein, fluorescent protein tag, and tag N' or C'-terminal translational fusion variant. Afterward, to transform these constructs into immature barley embryos by *Agrobacterium tumefaciens*-mediated transformation, select transgenic lines with specific fusion proteins and characterize these marker lines. Moreover, we aimed to create multi-marker fluorescent lines by crossing the single lines differing in expressed fusion protein, and finally to use these lines for nuclear and cellular dynamics studies.

2.2 Optimization of the time-lapse *in planta* microscopy analysis of fluorescent marker lines

The thesis' second aim was to improve and optimize the *in planta* time-lapse analysis of cell dynamics in growing barley roots. Plant roots are favorable model tissue for *in vivo* cellular dynamics analysis thanks to the high frequency of cell divisions and the absence of chlorophyll. Due to the thickness and higher growth rate of barley roots, we aimed to design and optimize a microscopy holder for *in vivo* analysis of cereal crop roots.

2.3 Understanding the spatial organization and dynamics of chromosomes and microtubules during barley mitosis

The thesis' third aim was to analyze the mitotic division in barley roots using the developed EYFP-FIBRILLARIN1 (EYFP-FIB1), CFP-HISTONE 2B (CFP-H2B) or EYFP-HISTONE 2B (EYFP-H2B) and mCHERRY-TUBULIN ALPHA3 (mCHERRY-TUA3) in double and triple FML combinations, focusing on the characterization of trends typical for plant mitosis and the ones unique for mitosis in barley root cells. Finally, we aimed to measure the duration of individual mitotic phases and the entire mitotic division in barley root cells.

3 SUMMARY OF THE RESULTS

3.1 Development and characterization of fluorescent marker lines for *in vivo* nuclear organization studies in barley

The first goal of the thesis was to create a set of stable translational fusion fluorescent marker lines (FMLs) for tracking *in vivo* nuclear and cellular dynamics in barley. Based on the protein-localization specificity, we selected marker proteins (Table 1) for visualization of chromatin (HISTONE 2B; H2B), nucleolus (FIBRILLARIN 1; FIB1), centromeres (CENTROMERIC HISTONE 3; CENH3), telomeres (TELOMERIC REPEAT BINDING FACTOR 1; TRB1), nuclear envelope (SAD1/UNC-84 DOMAIN PROTEIN 2; SUN2) of DNA condensation process (CONDENSIN-1 COMPLEX SUBUNIT H; CAP-H; CONDENSIN-2 COMPLEX SUBUNIT H2; CAP-H2). We cloned the marker gene CDS sequence upstream or downstream with CDS of different fluorescent proteins (CFP, EYFP, RFP, or GFP). To ensure that the fluorescent tag does not affect the fusion protein behaviour, we tested both N'-terminal and C'-terminal fusion variants. Afterward, we transformed the final constructs by *Agrobacterium tumefaciens*-mediated transformation into immature barley embryos. The list of verified translational fusion marker lines (FMLs) is provided in Table 1.

Afterward, we examined plant growth phenotype, fluorescent signal localization and intensity, and the number of T-DNA copies. The goal was to select homozygous plants with a single T-DNA copy, normal growth phenotype and fluorescent signal localization in the expected cellular domain. For some of the FMLs, the process is still ongoing. For the RFP-CENH3 line, we successfully mapped the T-DNA insertion site using inverse PCR (Križňanská, 2022). However, this process was tedious and failed with several other lines (not shown).

We made reciprocal crosses between the FMLs expressing different marker protein variants. Additionally, we used a microtubular marker line mCHERRY-TUBULIN ALPHA CHAIN 3 (mCHERRY-TUA3), which was developed and characterized jointly by the laboratories of Mgr. Petr Galuszka Ph.D. and Prof. Jozef Šamaj (Palacký University, Olomouc, Czech Republic). After several rounds of subsequent crosses and selection steps, we selected different double, triple, and tetra FML combinations (Table 2). As an example, single, double and triple FMLs, which were used

for the *in vivo* characterization of mitotic division in barley root cells (Kaduchová *et al.*, 2023) are visible in Figure 8.

We conclude that the aim to develop FMLs for studying nuclear and cellular dynamics in barley was fulfilled. We created single and multi-FMLs for chromatin, nucleolus, centromeres and microtubules and used them for *in vivo* analysis of barley cells.

Table 1. List of developed FMLs

FML line name	Marker gene	Marker gene ID number (HORVU.MOREX.r3.)	Expected localization	Tag	Fusion (terminus)	Construct composition	State-of-the-art	Independent transformants (n)	Selected FML		
									T-DNA copies (n)	Zygoty	Seeds generation
EYFP-FIB1	<i>FIBRILLARIN 1</i>	6HG0630670	Nucleolus	EYFP	N	<i>ZmUBI1:EYFP-HvFIB1:T35S</i>	characterized	4	1*	homozygous	T4
CFP-H2B	<i>HISTONE 2B</i>	3HG0252240	Chromatin	CFP	N	<i>ZmUBI1:CFP-H2B:T35S</i>	characterized	3	1	heterozygous	T4
EYFP-H2B	<i>HISTONE 2B</i>	3HG0252240	Chromatin	EYFP	N	<i>ZmUBI1:EYFP-H2B:T35S</i>	characterized	3	1*	homozygous	T3
GFP-H2B	<i>HISTONE 2B</i>	3HG0252240	Chromatin	GFP	N	<i>ZmUBI1:EGFP-H2B:T35S</i>	characterized	10	in progress	in progress	T2
H2B-CFP	<i>HISTONE 2B</i>	3HG0252240	Chromatin	CFP	C	<i>ZmUBI1:H2B-CFP:Tnos</i>	no signal	9	n.a.	n.a.	T2
TRB1-GFP	<i>TELOMERIC REPEAT BINDING FACTOR 1</i>	1HG0019730	Telomere	GFP	C	<i>ZmUBI1:TRB-GFP:T35S</i>	no signal	4	n.a.	n.a.	T2
RFP-CENH3	<i>CENTROMERIC HISTONE 3 BETA</i>	6HG0573870	Centromere	RFP	N	<i>ZmUBI1:RFP-CENH3:T35S</i>	characterized	10	in progress	in progress	T3
CENH3-RFP	<i>CENTROMERIC HISTONE 3 BETA</i>	6HG0573870	Centromere	RFP	C	<i>ZmUBI1:CENH3-RFP:T35S</i>	no signal	5	n.a.	n.a.	T2
SUN2-CFP	<i>SAD1/UNC-84 DOMAIN PROTEIN 2</i>	1HG0020270	Nuclear envelope	CFP	C	<i>ZmUBI1:SUN2-CFP:Tnos</i>	characterization in progress	21	n.a.	n.a.	T2
CFP-SUN2	<i>SAD1/UNC-84 DOMAIN PROTEIN 2</i>	1HG0020270	Nuclear envelope	CFP	N	<i>ZmUBI1:CFP-SUN2:T35S</i>	characterization in progress	4	n.a.	n.a.	T2
CAP-H-RFP	<i>CONDENSIN-1 COMPLEX SUBUNIT H</i>	3HG0264440	Chromosomes / cytoplasm	RFP	C	<i>HvCAP-Hpro:HvCAP-H-RFP:T35S</i>	characterization in progress	2	n.a.	n.a.	T2
GFP-CAP-H2	<i>CONDENSIN-2 COMPLEX SUBUNIT H2</i>	2HG0140960	Chromosomes /nucleoplasm	GFP	N	<i>HvCAP-H2pro:GFP-CAP-H2:T35S</i>	characterization in progress	2	n.a.	n.a.	T2
mCHERRY-TUA3	<i>TUBULIN ALPHA 3 **</i>	4HG0338800	Microtubules	mCHERRY	N	<i>ZmUBI1:mCHERRY-TUA3:Tnos</i>	characterized	-	1	homozygous	T5

* verified by ddPCR

** developed and characterized by Galuszka's and Šamaj's group (Palacký University Olomouc, CZE)

Table 2. Generated single, and crossed double and triple FMLs

FML line	Type	Publication	Generation
EYFP-FIB1 ^{+/+}	single marker line	Perutka et al. (2021); Kaduchová et al. (2023)	T4
CFP-H2B ^{+/-}	single marker line	Kaduchová et al. (2023)	T4
EYFP-H2B ^{+/+}	single marker line	Kaduchová et al. (2023)	T3
RFP-CENH3 [?]	single marker line	Randall et al. (2022)	T3
mCHERRY-TUA3 ^{+/+}	single marker line	Kaduchová et al. (2023)	T5
EYFP-FIB1 ^{+/+} CFP-H2B ^{+/-}	double marker line	Kaduchová et al. (2023)	F4
EYFP-FIB1 ^{+/+} mCHERRY-TUA3 ^{+/+}	double marker line	Kaduchová et al. (2023)	F3
CFP-H2B ^{+/-} mCHERRY-TUA3 ^{+/+}	double marker line	Kaduchová et al. (2023)	F2
EYFP-H2B ^{+/+} mCHERRY-TUA3 ^{+/+}	double marker line	Kaduchová et al. (2023)	F2
EYFP-FIB1 ^{+/+} CFP-H2B ^{+/-} mCHERRY-TUA3 ^{+/+}	triple marker line	Kaduchová et al. (2023)	F3
EYFP-FIB1 ^{+/+} RFP-CENH3 [?]	double marker line	Unpublished	F2
CFP-H2B ^{+/-} RFP-CENH3 [?]	double marker line	Randall et al. (2022)	F2
EYFP-H2B ^{+/+} RFP-CENH3 [?]	double marker line	Unpublished	F2
GFP-H2B [?] RFP-CENH3 [?]	double marker line	Unpublished	F2
EYFP-FIB1 ^{+/+} CFP-H2B ^{+/-} RFP-CENH3 [?]	triple marker line	Unpublished	F3
EYFP-H2B ^{+/-} mCHERRY-TUA3 ^{+/+} RFP-CENH3 [?]	triple marker line	Unpublished	F2
EYFP-FIB1 ^{+/+} CFP-H2B ^{+/-} mCHERRY-TUA3 ^{+/+} RFP-CENH3 [?]	tetra marker line	Unpublished	F2

[?] unknown zygosity under characterization

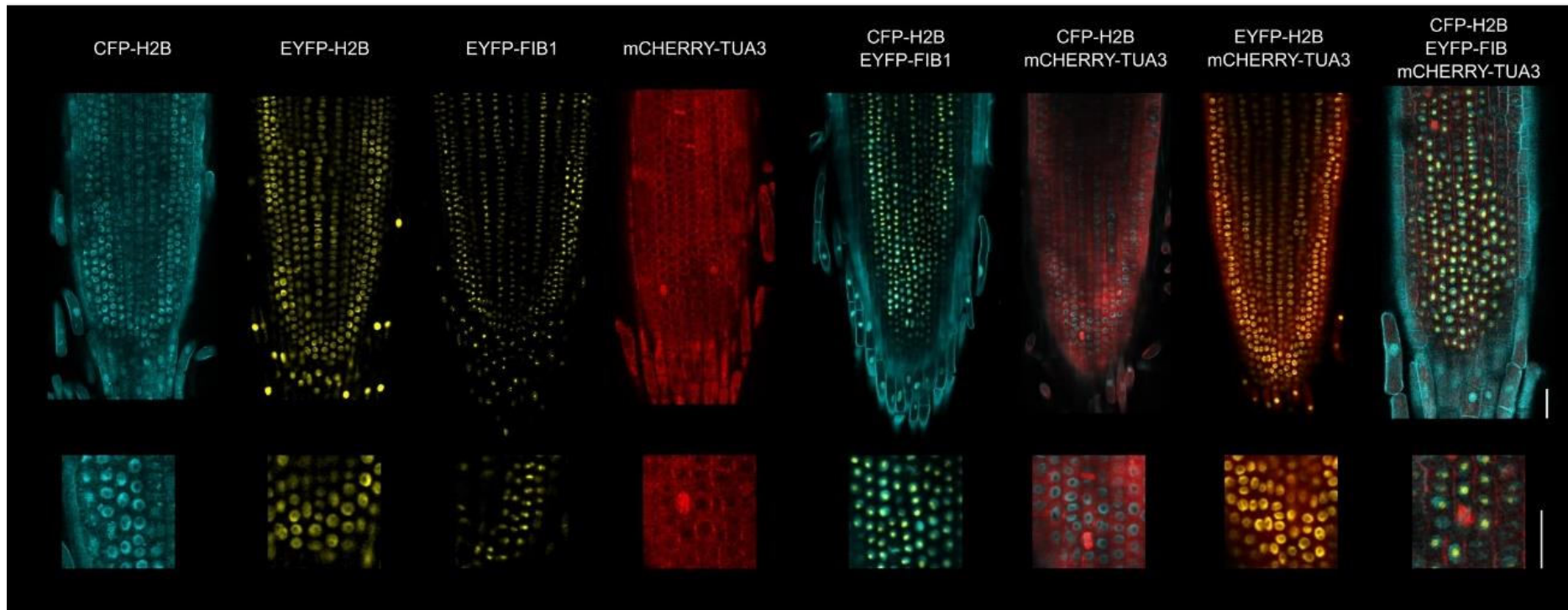


Figure 8. Overview of barley FMLs used for in vivo characterization of mitotic division in barley root cells. Representative confocal microscopy optical longitudinal sections of roots from single, double, and triple FMLs. Multi-marker lines were generated by crossing single lines. Squares indicate selected magnified regions that are shown below each root. Scale bars = 20 μ m.

3.2 Development and optimization of ‘EasyClick’ sample holder for *in vivo* time-lapse microscopy of cereal roots

The second aim of the thesis was to develop a system for live *in vivo* microscopy analysis of nuclear and cellular dynamics in fast-growing barley roots. Unfortunately, the high growth rate of barley primary roots at approximately $500 \mu\text{m}\cdot\text{h}^{-1}$ (Higuchi *et al.*, 2017), along with their side movements, makes it challenging to conduct detailed cell-level microscopy analysis.

After the first trials of time-lapse root analysis, we observed that the centered sample either grew out of the vision field or moved from the focus plane (Figure 9). We tested various approaches to control root growth direction, like placing the root between two nylon strings or weighing the sample with an agarose block (Rahni and Birnbaum, 2019). Nevertheless, these methods were difficult to set and did not lead to high-quality microscopy data we were aiming for.

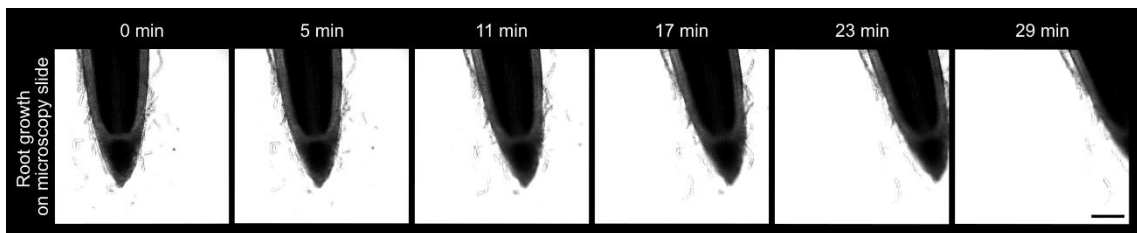


Figure 9. Barley root movements during time-lapse scanning. Movement of free barley root placed on the microscopy slide documented by bright-field microscopy. Total scanning time 29 min. Scale bar = $200 \mu\text{m}$.

To address these challenges, we initiated the development of the “EasyClick” sample holder by Pragolab s.r.o company and took part in its optimization and testing. Individual prototypes of the EasyClick differing in the holder assembly mechanism and used materials are visible on Figure 10. The final version of EasyClick (Figure 11) is specifically designed for microscopy of fast-growing roots of greater thickness, like those of cereal crops. It is easy to assemble and allows long-time imaging.

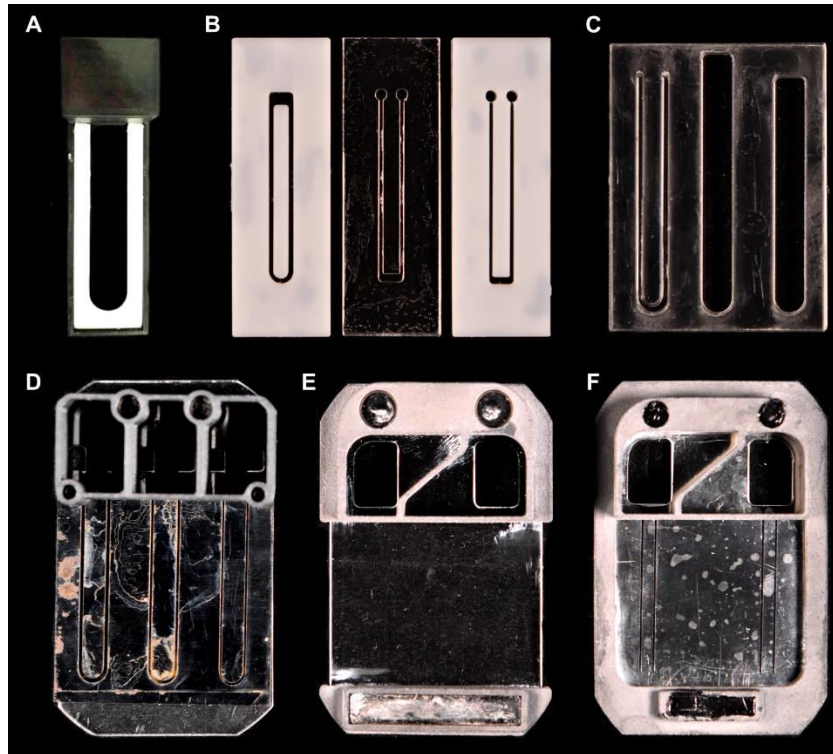


Figure 10. Prototypes of the EasyClick microscopy sample holder. (A) Plastic holder matrix with container for single root sample. (B) Different designs of inserts for single plant sample with root growth channels. Inserts differ in plastic material type (non-transparent, transparent). (C) Transparent plastic insert for three plant samples combining three different growth channel designs. (D) Assembled holder prototype for three plant samples with magnetically attached 3D-printed sample container and metal plate with three growth channels. Metal insert is from rusting material. (E) Assembled holder prototype with 3D printed half-frame and container for two plant samples. Metal plate with growth channels is not attached. (F) Pre-final version of holder prototype with 3D-printed full-frame and containers for two plant samples. Metal plate with growth channels made from non-rusting material is attached.

The EasyClick comprises several components: a 3D-printed holder matrix that fits into a universal microscope holder, a stainless-steel metal plate with growth channels of varying widths, a plastic seal, series of magnets, and a large cover glass (Figure 11A, B). All these parts are permanently fixed together except for the metal plate and large cover glass, which are removable and can be fixed using two free magnets.

In EasyClick assembly, the plantlet is placed into 3D-printed matrix containers, and then roots are gently pushed into the metal plate channels of the pre-assembled holder (Figure 11C, D). In the end, containers are filled with water or growth media and covered by wet tissue paper to ensure proper hydration and prevent drying out.

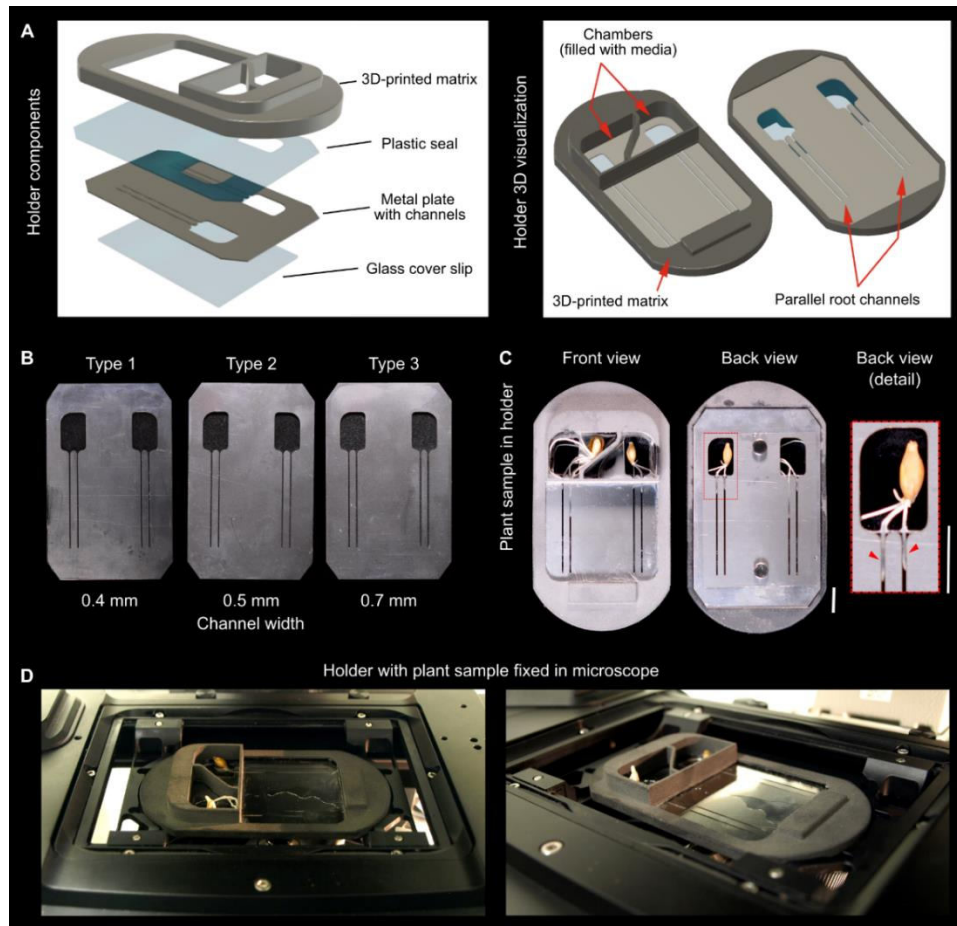


Figure 11. Description and assembly of the microscopy EasyClick sample holder. (A) 3D model of individual EasyClick parts. (B) Three types of the metal plate differ in the growth channel widths (0.4, 0.5, and 0.7 mm). (C) Detailed view of germinated barley seedling in the holder. (D) Installation of the EasyClick holder in the inverted microscope.

EasyClick was primarily designed for detailed time-lapse analysis of fast-growing roots of greater thickness. We observed that when grown in the EasyClick, there was a positive reduction in the root side movements (Figure 12A, B). However, we were not able to completely eliminate the shift of the root in the Z-axis (focus plane) due to the conical shape of a barley root meristematic zone, where cells originally set in a focus plane are pushed into higher scanning layers as new cells emerge (Figure 12C, D). To overcome this issue, we focused on cells in flatter parts of the root meristematic zone. This situation was also observed in other cereal crop species' roots tested in the holder, such as wheat, oat, and rye.

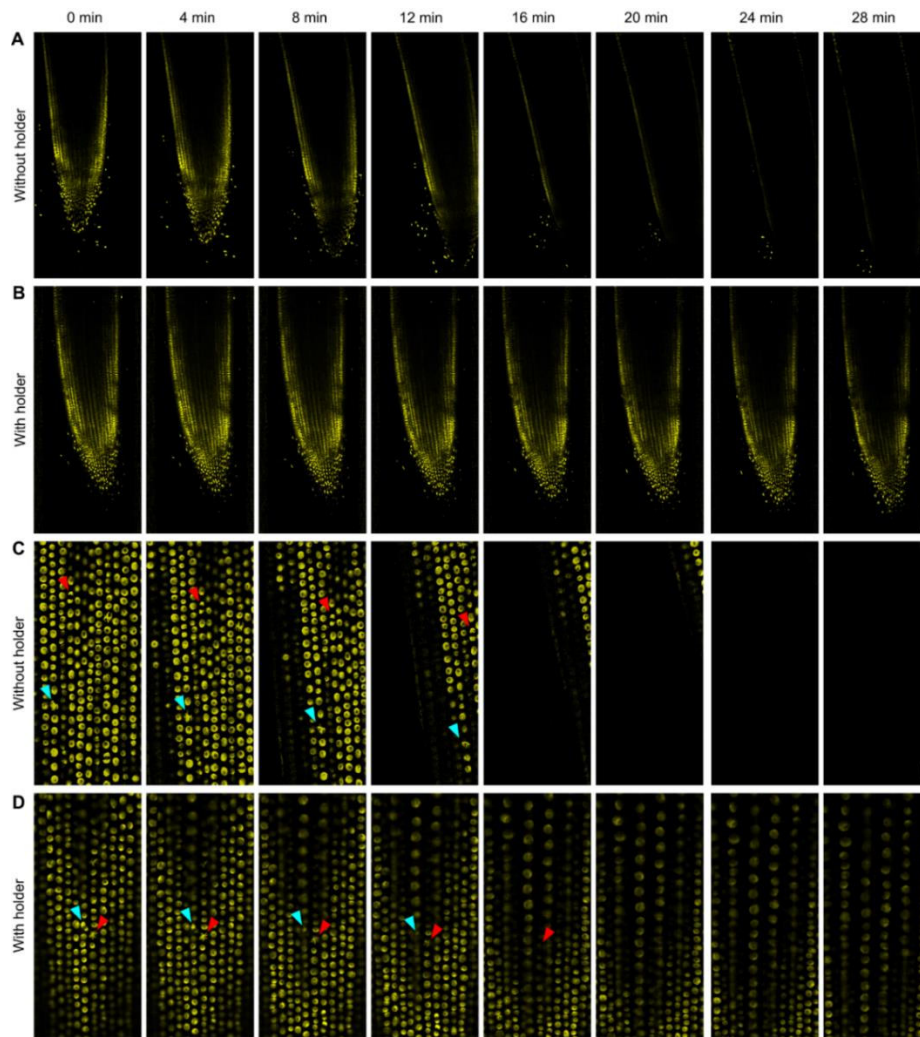


Figure 12. Live cell confocal microscopy imaging of barley root apical meristem without and with EasyClick holder. Nuclei and chromosomes were visualized with the chromatin EYFP-H2B FML. (A) Example of rapid root movements during microscopy without holder. (B) Channel-directed root movement with EasyClick holder. (C) Detailed time-lapse single-cell layer scanning of root on microscopy slide without holder. This series of images demonstrates shifts in the horizontal (red arrow) and vertical (cyan) directions. (D) The situation as in (C) but with improved parameters due to EasyClick holder use.

We also assessed whether the EasyClick holder affects barley root growth along its main growth axis (Figure 13). We compared the growth rate of roots grown in the holder and freely on a microscopy slide after 1 h and 24 h from mounting. We observed greater variability as to the root growth rate in unrestricted conditions after 1 h on the microscopy slide, but the median growth rate was almost the same for both conditions at this time-point. Although the samples after 24 h differed 1.8-fold in their median, this difference was not significant, possibly due to a relatively large variation in the growth speeds between individual roots (Figure 13). When comparing the growth rate between 1 h and 24 h setups, the reduction was not significant for the free growing roots, but

opposite was true for the roots in holder, speculatively due to the interaction between the root and the channel surface.

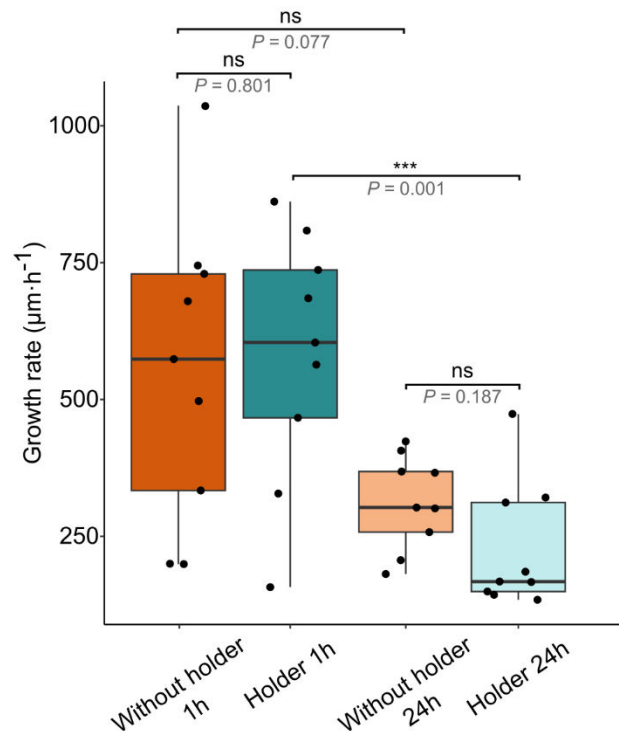


Figure 13. Root growth rate without and using EasyClick sample holder. Speed of growth of roots from two days old barley plants grown freely on a microscopic slide (Without holder 1 h), shortly after introduction into the EasyClick (Holder 1 h), after 24 h of freely growing on a microscopy slide (Without holder), and after 24 h in the EasyClick (Holder 24 h). Significance level ($P \leq 0.001$), samples are not significantly different by Kruskal-Wallis and post-hoc Dunn's test.

We conclude that the aim to develop a setup for live cell imaging of cellular dynamics in growing barley roots was fulfilled. We designed and created the EasyClick microscopy sample holder and optimized it for the analysis of growing cereal crops roots.

3.3 Spatial organization and dynamics of mitosis in barley root cells

Mitosis is the primary cell division process by which organisms increase the number of cells and regulate their growth and development. We used developed FMLs for the *in vivo* analysis of mitotic division in barley root cells.

Firstly, we defined individual mitotic phases based on cell and nucleus size, chromatin structure, nucleoli number, nucleoli volume, and microtubule organization (Figure 14; Supplementary videos 1-3).

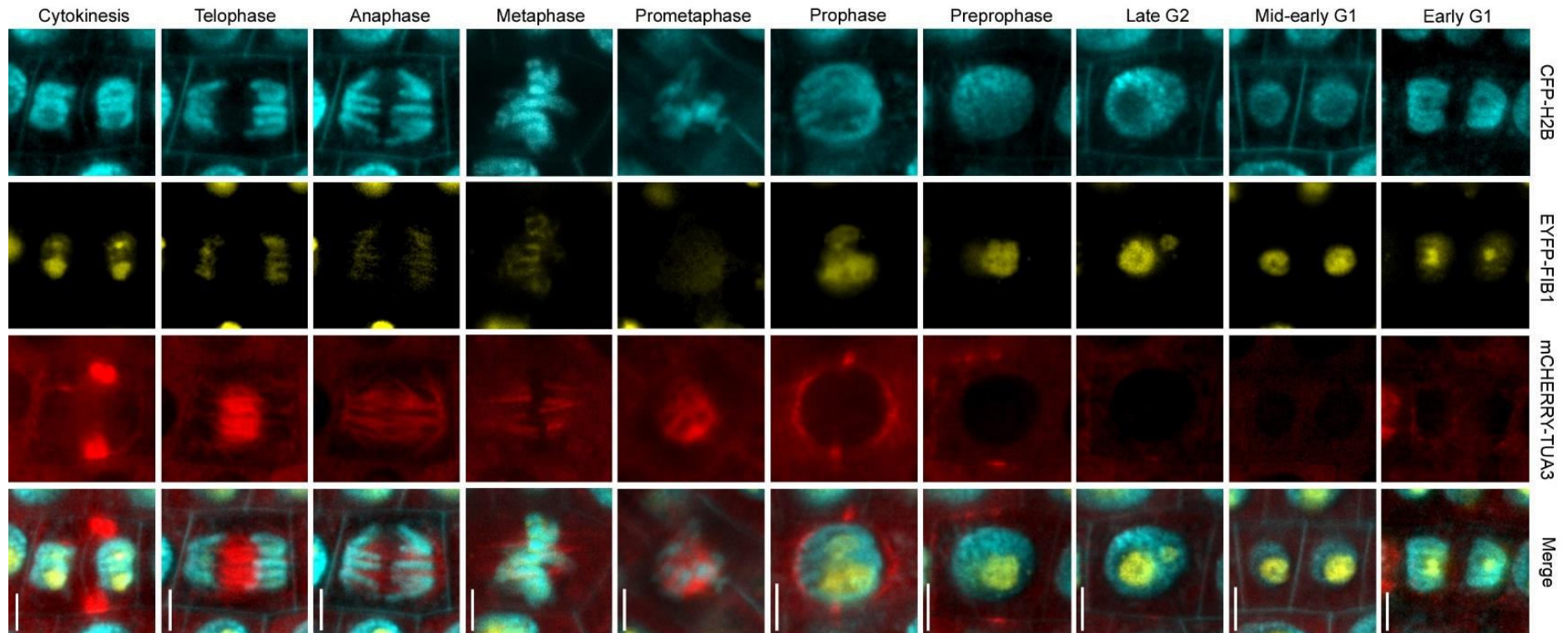


Figure 14. Localization of fluorescent marker proteins in different cell cycle phases. The rows represent images of typical barley epidermal cells corresponding to individual cell cycle phases. The columns show signals of individual marker proteins: CFP-H2B for chromosomes (cyan), mCHERRY-TUA3 for microtubules (red), EYFP-FIB1 for nucleolus (yellow), and their combination (merge). Non-nuclear/chromosomal signals in the first column correspond to cell walls that are visible due to cell wall autofluorescence in the CFP emission spectrum. Scale bars = 5 μ m

We observed a significant difference between early G1 and late G2 cells in terms of increased ratio of cell wall lengths (the ones parallel with a root growth axis and perpendicular ones) (Figure 15A, B), nucleolar (Figure 15C-D) and nuclear volume (Figure 15F) and nuclear area (Figure 15G). By tracking nucleolar dynamics, we were able to distinguish early G1 and late G2 cells based on the number of nucleoli (Supplementary video 1). Early G1 cells, formed shortly after the mitosis, contained 3-4 nucleoli, whereas late G2 cells entering mitosis only had 1-2 prominently large nucleoli (Figure 15E).

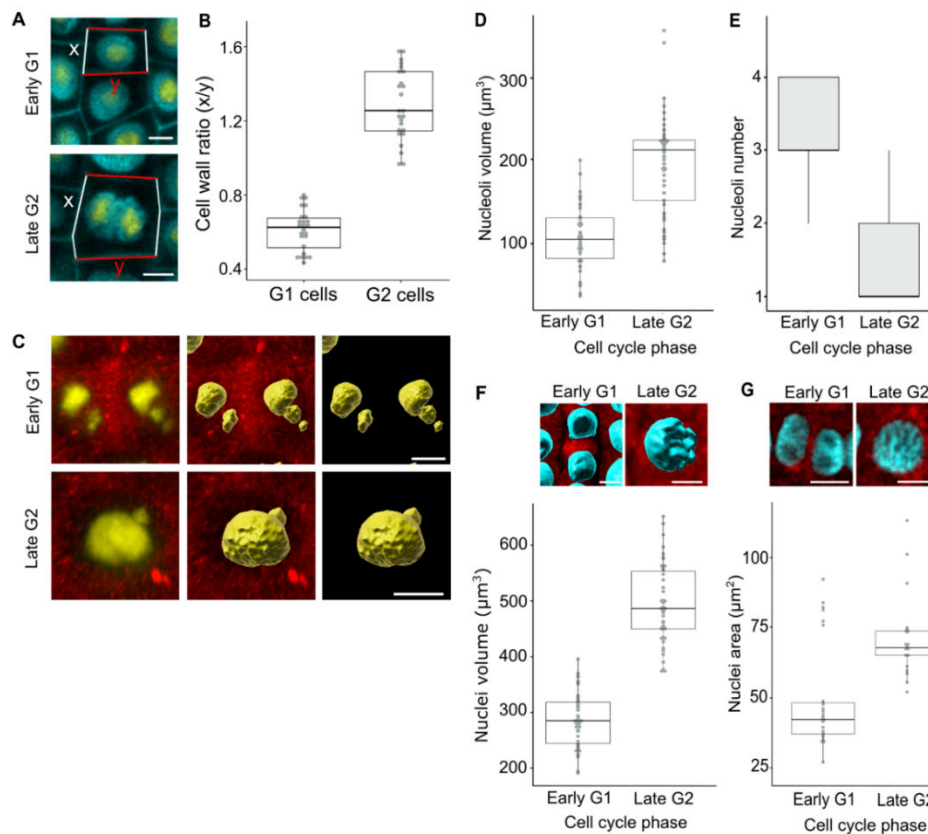


Figure 15. Nuclear and nucleolar parameters of barley G1 and G2 cells. Cells express nucleolar (EYFP-FIB1; yellow) and nuclear (CFP-H2B; cyan) fluorescent markers, and autofluorescent cell walls are visible in the cyan channel. Values marked with an identical letter did not differ in Tukey's and Fisher's exact methods ($P \leq 0.05$). (A) Representative images of early G1 and late G2 cells. The white lines (x) show cell walls linear, and red lines (y) show cell walls perpendicular to the main root growth axis. (B) The box plots show the cumulative cell wall ratio of x/y. Scale bars = 5 μm . (C) 3D projection of cells in early G1 and late G2 expressing nucleolar and microtubular fluorescent markers before and after 3D surface rendering made in Imaris bitplane software. Scale bars = 5 μm . (D) Number of nucleoli per cell in early G1 and late G2 phases. (E) Nucleoli total volume per cell in early G1 and late G2 phases. (F) Nuclei volume per cell in early G1 and late G2 phases. (G) Nuclei area per cell in early G1 and late G2 phases.

We observed that chromatin condensation was not uniform during preprophase. Around 40 % of preprophase cells exhibited already condensed chromatin, suggesting that chromatin condensation is initiated already during late G2/early preprophase or persists from the previous mitotic division in the process of speeding chromatin compaction (Figure 16A, B; Supplementary video 2).

Moreover, we tracked mitotic chromosomes condensation level and found that they progressively increased the arm-length compaction from 8.05 μm in prophase to 5.76 μm in metaphase, 4.71 μm in anaphase, reaching the minimal length of 4.25 μm in telophase, which corresponds to a 47% reduction from the karyokinesis onset (Figure 16C).

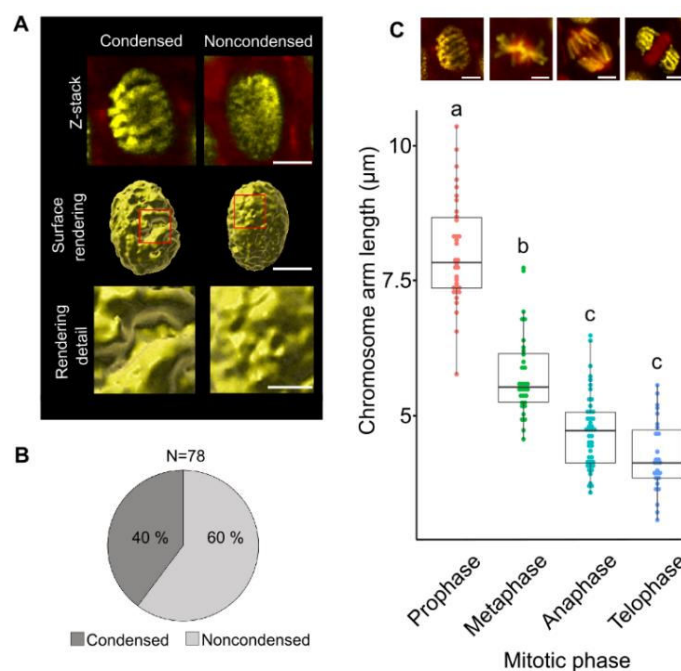


Figure 16. Chromosome condensation in barley root cells. (A) Confocal microscopy-based 3D projection of preprophase nuclei (Z-stack) with condensed (left) and non-condensed (right) chromatin visualized by EYFP-H2B (yellow) and microtubules with mCHERRY-TUA3 (red). The next rows show a surface rendering of whole nuclei, and detail of a region indicated by a red square, in Imaris bitplane. Scale bars of whole nuclei = 5 μm and insets = 2 μm . (B) Percentage of preprophase cells with condensed and non-condensed chromosomes. (C) Average chromosome arm length in different mitotic phases. Values marked with an identical letter did not differ in Tukey's and Fisher's exact methods ($P \leq 0.05$). Scale bars = 5 μm .

Surprisingly, we found that in most cases, the mitotic chromosomes lined in the metaphase band were not pulled into centers of opposite cell walls during anaphase, as is typical for model plant *Arabidopsis*, but in a tilted division angle oriented into the opposite cell wall corners. To measure the division angle diversion, we developed an

image post-processing pipeline in Imaris bitplane software and used it on Z-stack scans of CFP-H2B RFP-CENH double FML anaphase cells (Figure 17). After the initial steps of volume adjustment, centromeres segmentation, rendering of chromosomes, and cell walls 3D space reduction, we were able to define the cell elongation axis, reference axis, and chromosomes pulling axis from set coordinates, which allowed us to measure a chromosome division angle in 3D.

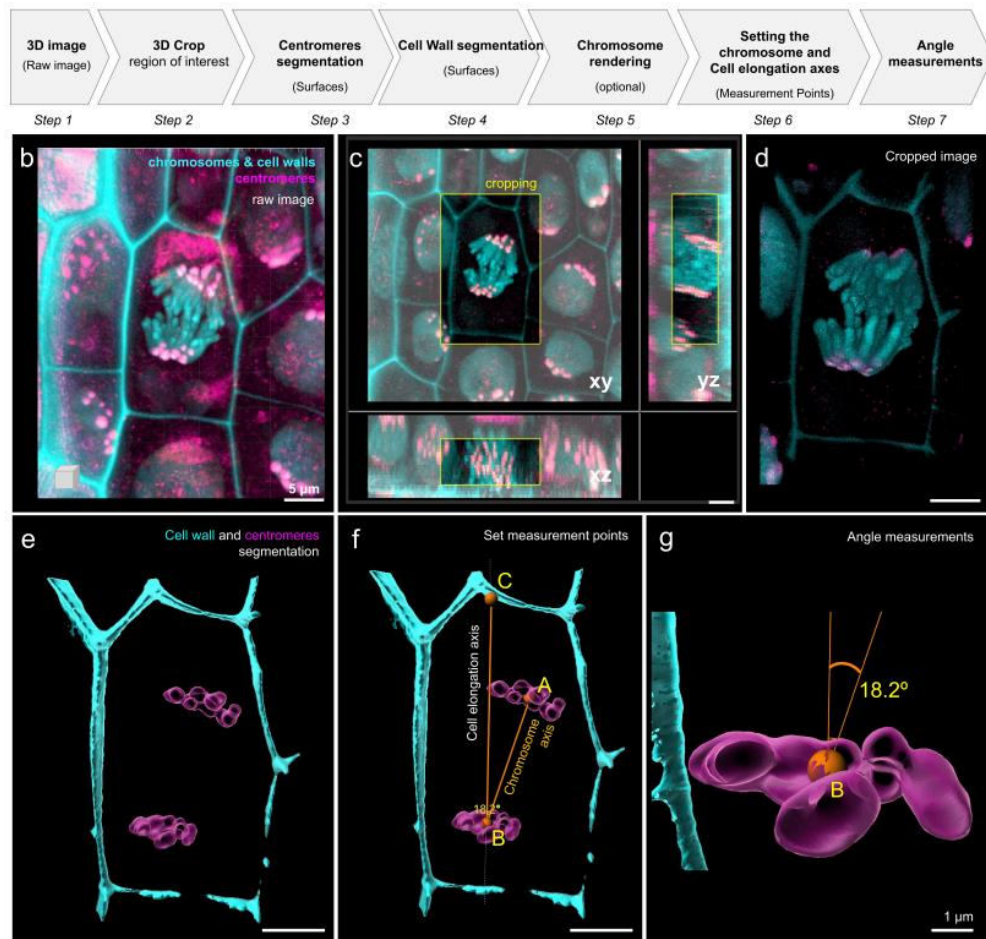


Figure 17. Division angle measurement using surface-rendered cellular structures in living barley root cells. (A) Workflow overview showing the sequence of tasks to process a raw picture and set measurement lines within the 3D cell space. (B) Confocal image of barley root tissue from FML visualizing chromatin (CFP-H2B; cyan) and centromeric (RFP-CENH3; magenta). Cell walls are visible (cyan) due to their autofluorescence in CFP emission spectra. The image is a partial projection from a z-stack. (C) Selection of a region of interest (anaphase cell) by 3D cropping of the image (yellow frame). Orthogonal projections are shown in xy, yz, and xz. (D) Rendered image in 3D ('blend' mode). (E) 'Surface' rendering of segmented centromeres (magenta) and the cell wall (cyan). (F) The setting of 'Measurement points' and their connective lines. Chromosome division axis (AB), cell elongation axis (BC). (G) Detailed visualization of the angle formed between both axes defined by AB and BC measurement lines. The angle is measured in 3D by Imaris. Scale bars: B-F, 5 μm ; G, 1 μm .

During tracking mitotic chromosome dynamics, we observed that the EYFP-FIB1 signal localized on the condensing chromosomes after the prometaphase nucleolus disorganization (Figure 14, 18). This localization persisted until telophase when newly formed nuclei emerged from prenucleolar bodies. We confirmed the results from *in vivo* observations by immunodetection of both FIB1 and EYFP to obtain the same chromosome localization pattern. The distinct signal was also visible on some of the chromosomes in the kinetochore region (Figure 18C). As FIB1 is an RNA methyltransferase that functions in complex with RNAs and other proteins, we hypothesized that the protein localizes on chromosomes together with RNA molecules. We confirmed this by immunodetection of FIB1 on flow-sorted chromosomes from both WT and EYFP-FIB1, where we observed loss of the FIB1 signal (Figure 18B, D).

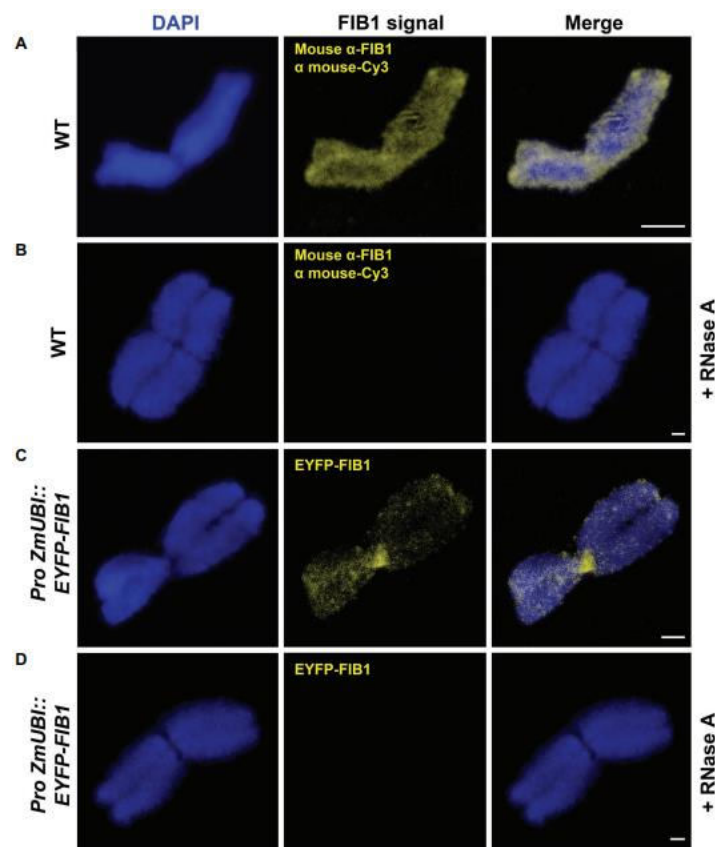


Figure 18. FIB1 is removed from chromosomes by RNase A treatment. All chromosomes were counterstained with DAPI. (A) WT flow-sorted chromosome with immunolocalized FIB1. (B) Representative chromosomes prepared in the same way with additional RNase A treatment. (C) Chromosome from FML expressing EYFP-FIB1 (yellow) fusion protein. (D) Chromosome from the same material as in (C) with additional RNase A treatment. Scale bars = 2 μm

We conclude that the aim to use our FMLs for live cell imaging of nuclear and cellular dynamics was fulfilled. We used these lines for analysis of the mitotic division in barley root cells and uncovered new features of this process.

3.4 Determination of *in vivo* duration of mitosis in barley root cells

The duration of the mitotic division defines the speed of the cell cycle. Therefore, after characterizing all mitotic phases, we measured the duration of the mitosis and its phases based on the *in vivo* time-lapse analysis. We measured the median duration of almost all mitotic phases except for prophase, where we set a minimal duration due to a problematic determination of prophase onset (Figure 19; Supplementary videos 1-3).

Our findings show that the median duration of prophase in barley root cells is 32.6 min but can vary considerably. Prometaphase lasts 7.2 min in the median, metaphase 9 min, anaphase only 6 min, telophase 10.3 min, and cytokinesis 13 min, though this phase also showed some variability in length (Figure 19).

Using these individual measurements, we calculated the approximate total duration of the mitotic division in barley root cells. However, we were able to measure only up to three divisions, starting from prophase and ending with telophase. In most cases, the live imaging either started during or ended before the end of the given phase. To compensate for this limitation, we based the mitosis duration calculation on the median duration of each mitotic phase.

Based on our analysis, we concluded that a typical mitosis in barley root cells takes about 65.2 min from prophase to telophase, or approximately 78.2 min until the end of cytokinesis (Figure 19), and created an atlas of barley cell cycle including mitosis dynamics (Figure 20).

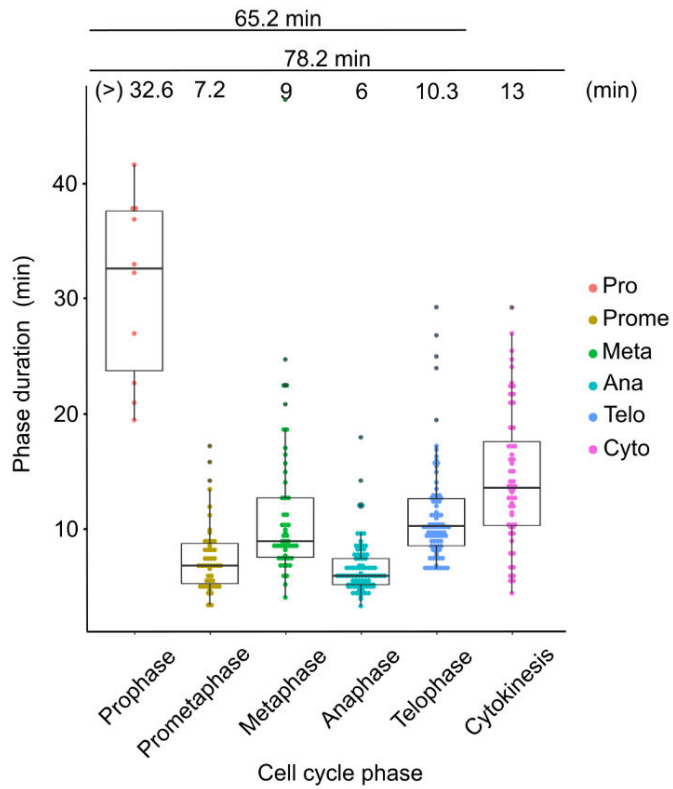


Figure 19. Duration of mitosis in barley root cells. Numbers above the boxplot graphs indicate the durations of individual mitotic phases and the median duration of mitotic division in barley root cells.

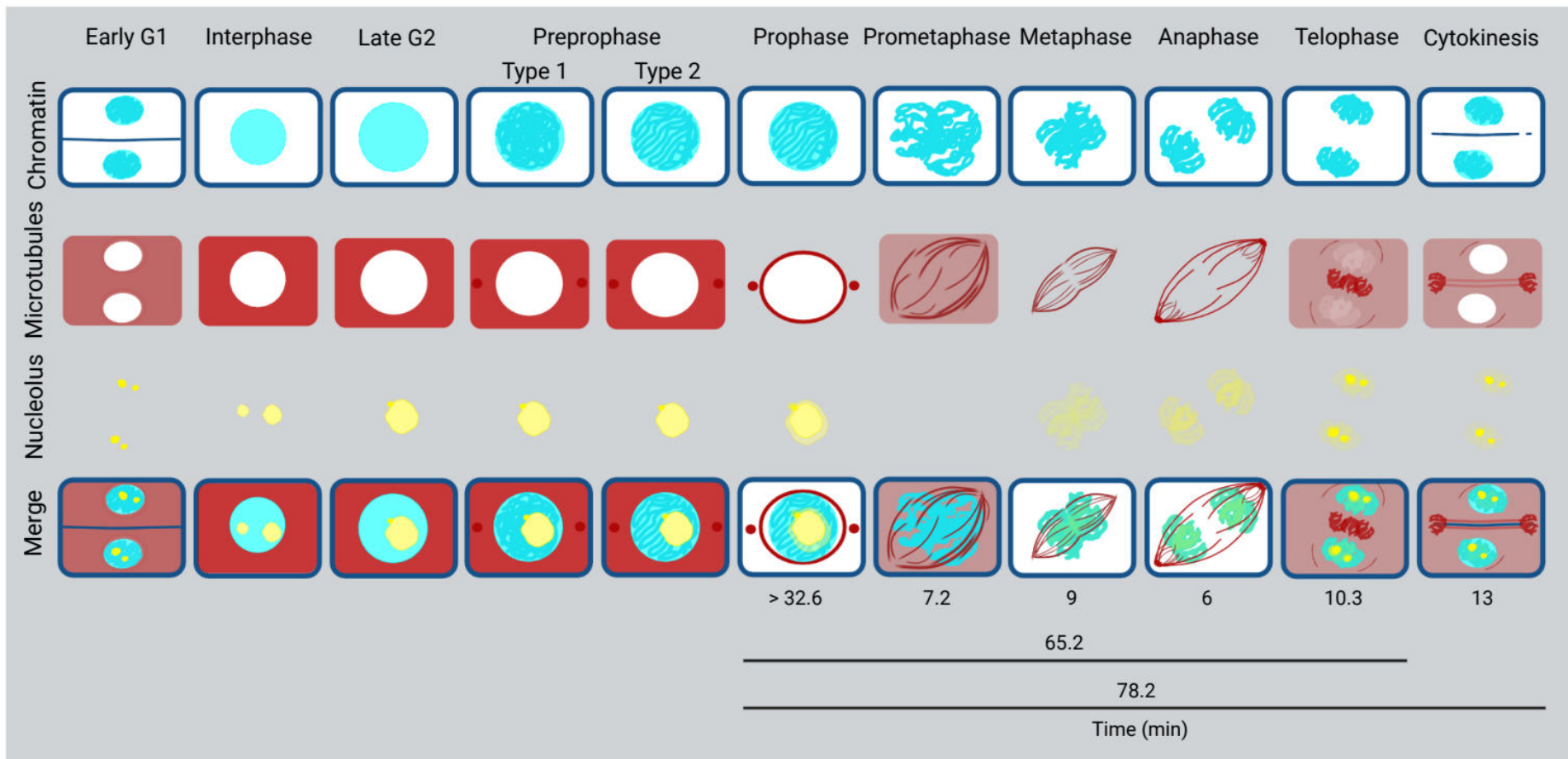


Figure 20. An atlas of barley cell cycle as visualized using fluorescent marker lines described in this study. Chromatin and cell walls = light blue, microtubules = red, and nucleolus = yellow. The time indicates the median duration of individual mitotic stages and whole mitosis, > symbol indicates the non-defined start of prophase.

4 PUBLICATIONS

4.1 FIRST AUTHOR PUBLICATIONS

4.1.1 Image analysis workflows to reveal the spatial organization of cell nuclei and chromosomes

(Appendix I)

4.1.2 Spatial organization and dynamics of chromosomes during barley mitosis

(Appendix II)

4.1.3 EasyClick: An improved system for confocal microscopy of live roots with a user-optimized sample holder

(Appendix III)

4.1.1. Image analysis workflows to reveal the spatial organization of cell nuclei and chromosomes

Randall, R.S.[†], Jourdain, C.[†], Nowicka, A.[†], **Kaduchová, K.**[†], Kubová, M.[†], Ayoub, M.A.[†], Schubert, V.[†], Tatout, Ch.[†], Colas, I.[†], Kalyanikrishna, Dasset, S., Mermet, S., Stevens, A., Kubalova, I., Mandáková, T., Heckmann, S., Lysak, M.A., Panatta, M., Santoro, R., Schubert, D., Pecinka, A., Routh, D., and Baroux, C.

[†]Authors contributed equally

Nucleus

DOI: <https://doi.org/10.1080/19491034.2022.2144013>

IF (2022): 3.45

Abstract:

Nucleus, chromatin, and chromosome organization studies heavily rely on fluorescence microscopy imaging to elucidate the distribution and abundance of structural and regulatory components. Three-dimensional (3D) image stacks are a source of quantitative data on signal intensity level and distribution and on the type and shape of distribution patterns in space. Their analysis can lead to novel insights that are otherwise missed in qualitative-only analyses. Quantitative image analysis requires specific software and workflows for image rendering, processing, segmentation, setting measurement points and reference frames and exporting target data before further numerical processing and plotting. These tasks often call for the development of customized computational scripts and require an expertise which is not broadly available in the community of experimental biologists. Yet, the increasing accessibility of high- and super-resolution imaging methods fuel the demand for user-friendly image analysis workflows. Here, we provide a compendium of strategies developed by participants of a training school from the COST action INDEPTH to analyze the spatial distribution of nuclear and chromosomal signals from 3D image stacks, acquired by diffraction-limited confocal microscopy and super-resolution microscopy methods (SIM and STED). While the examples make use of one specific commercial software package, the workflows can easily be adapted to concurrent commercial and open-source software. The aim is to encourage biologists lacking custom-script-based expertise to venture into quantitative image analysis and to better exploit the discovery potential of their images.

4.1.2. Spatial organization and dynamics of chromosomes during barley mitosis

Kaduchová, K., Marchetti, C., Ovečka, M., Galuszka, M., Bergougnoux, V., Šamaj, J., and Pecinka, A.

The Plant Journal

DOI: <https://doi.org/10.1111/tpj.16355>

IF (2022): 7.2

Abstract:

Mitosis and cytokinesis are fundamental processes through which somatic cells increase their numbers and allow plant growth and development. Here, we analyzed the organization and dynamics of mitotic chromosomes, nucleoli, and microtubules in living cells of barley root primary meristems using a series of newly developed stable translational-fusion lines and time-lapse confocal microscopy. The median duration of mitosis from prophase until the end of telophase was 65.2 and 78.2 minutes until the end of cytokinesis. We showed that barley chromosomes frequently start condensation before mitotic prophase, as defined by the organization of microtubules, and maintain it even after entering into the new interphase. Furthermore, we found that the process of chromosome condensation does not finish at metaphase but gradually continues until the end of mitosis. These basic characteristics of barley mitosis can be used as a reference in future genetic and physiological studies of this model crop.

This publication was chosen as the “Research Highlight” article and was used for the issue “Cover Art”.

4.1.3. EasyClick: An improved system for confocal microscopy of live roots with a user-optimized sample holder

Kaduchová, K., Čmiel, V., Koláčková, V., and Pecinka, A.

Planta

in press

IF (2021): 4.45

Abstract:

Preparation and mounting of the samples are key factors for successful live cell microscopy. To acquire biologically relevant data, it is necessary to minimize stress and avoid physical damage to plant tissues during the installation of the sample into the microscope. This is challenging, particularly when the whole plant is mounted as the living sample needs to be properly anchored in the microscopic system to obtain high-quality and high-resolution data. Here, we present a user-optimized sample holder EasyClick for live cell inverted confocal microscopic analysis of plant roots with diameters from 0.3 to 0.7 mm. The EasyClick holder was tested on an inverted confocal microscope using germinating plants of several cereals. Nevertheless, it can be directly used on other types of inverted microscopes from various producers and on different plant species. The EasyClick holder effectively restricts root lateral and vertical movements. This greatly improves the conditions for time-lapse microscopy of the samples of interest.

4.2 CO-AUTHORSHIP PUBLICATIONS

The cooperation within the following publication was based on the topic's relationship to the 3D organization of the nucleus.

4.2.1 Proteome analysis of condensed barley mitotic chromosomes

(Appendix IV)

4.2.1. Proteome analysis of condensed barley mitotic chromosomes

Perutka, Z., Kaduchová, K., Chamrád, I., Beinhauer, J., Lenobel, R., Petrovská, B., Bergougnoux, V., Vrána, J., Pecinka, A., Doležel, J., and Šebela, M.

Frontiers in Plant Science

DOI: <https://doi.org/10.3389/fpls.2021.723674>

IF (2021): 6.63

Abstract:

Proteins play a major role in the three-dimensional organization of nuclear genome and its function. While histones arrange DNA into a nucleosome fiber, other proteins contribute to higher-order chromatin structures in interphase nuclei, and mitotic/meiotic chromosomes. Despite the key role of proteins in maintaining genome integrity and transferring hereditary information to daughter cells and progenies, the knowledge about their function remains fragmentary. This is particularly true for the proteins of condensed chromosomes and, in particular, chromosomes of plants. Here, we purified barley mitotic metaphase chromosomes by a flow cytometric sorting and characterized their proteins. Peptides from tryptic protein digests were fractionated either on a cation exchanger or reversed-phase microgradient system before liquid chromatography coupled to tandem mass spectrometry. Chromosomal proteins comprising almost 900 identifications were classified based on a combination of software prediction, available database localization information, sequence homology, and domain representation. A biological context evaluation indicated the presence of several groups of abundant proteins including histones, topoisomerase 2, POLYMERASE 2, CONDENSIN subunits, and many proteins with chromatin-related functions. Proteins involved in processes related to DNA replication, transcription, and repair as well as nucleolar proteins were found. We have experimentally validated the presence of FIBRILLARIN 1, one of the nucleolar proteins, on metaphase chromosomes, suggesting that plant chromosomes are coated with proteins during mitosis, similar to those of human and animals. These results improve significantly the knowledge of plant chromosomal proteins and provide a basis for their functional characterization and comparative phylogenetic analyses.

5 CONTRIBUTION TO THE PUBLICATIONS

5.1 Image analysis workflows to reveal the spatial organization of cell nuclei and chromosomes

Randall, R.S.[†], Jourdain, C.[†], Nowicka, A.[†], **Kaduchová, K.**[†], Kubová, M.[†], Ayoub, M.A.[†], Schubert, V.[†], Tatout, Ch.[†], Colas, I.[†], Kalyanikrishna, Desset, S., Mermet, S., Stevens, A., Kubalova, I., Mandáková, T., Heckmann, S., Lysak, M.A., Panatta, M., Santoro, R., Schubert, D., Pecinka, A., Routh, D., and Baroux, C., (2022). Image analysis workflows to reveal the spatial organization of cell nuclei and chromosomes. *Nucleus*, 13, 277-299. doi: 10.1080/19491034.2022.2144013.

[†]Authors contributed equally

My contribution:

- Performed microscopy scanning of my barley fluorescent marker lines CFP-H2B and RFP-CENH3.
- Wrote the Workflow text (Workflow 7) of the image post-processing procedure.
- Prepared an Excel table for Workflow (Workflow 7) of the image post-processing procedure containing detailed information on rendering.
- Prepared Figure 7, capturing individual steps of image post-processing.
- Wrote part of the Abstract and Introduction corresponding to Workflow 7 and was involved in preparing the manuscript.

5.2 Spatial organization and dynamics of chromosomes during barley mitosis

Kaduchová, K., Marchetti, C., Ovečka, M., Galuszka, M., Bergougnoux, V., Šamaj, J., and Pecinka, A. (2023). Spatial organization and dynamics of chromosomes during barley mitosis. *The Plant Journal*, 115, 602-613. doi: 10.1111/tpj.16355.

My contribution:

- Designed a cloning strategy for constructing EYFP-FIB1, CFP-H2B, and EYFP-H2B.
- Performed cloning of EYFP-FIB1, CFP-H2B, and EYFP-H2B constructs.
- Transformed the EYFP-H2B construct into the immature barley embryos and did subsequent selection and regeneration of transgenic calli.
- Performed genotyping and microscopy verification of EYFP-FIB1, CFP-H2B, and EYFP-H2B transgenic plants based on the presence of a specific fluorescence signal.
- Performed crossing between single and multi-fluorescent marker lines (FMLs) (including mCHERRY-TUA3 line) and microscopy selection of intended marker combinations.
- Performed confocal *in vivo* microscopy analysis of all single and multi-FMLs, including time-lapse scanning for mitosis length measurement.
- Did all measurements present in the manuscript and made quantifications and statistical analyses.
- Did surface rendering in Imaris Bitplane software.
- Prepared all Figures and Tables present in the manuscript and wrote the manuscript text.

This research article was highly appreciated by the research community and selected as the “Research Highlight” article and used for the corresponding issue’s cover page.

5.3 EasyClick: An improved system for confocal microscopy of live roots with a user-optimized sample holder

Kaduchová, K., Čmiel, V., Koláčková, V., and Pecinka, A. (2023). 3D print user-optimized sample holder for confocal microscopy of plant roots. *Planta*, *in press*

My contribution:

- Participated in the design of the sample holder.
- Performed optimization and testing of individual holder prototypes.
- Did time-lapse scanning of roots growing without and in the microscopy holder.
- Measured and quantified the growth speed of roots grown without and in microscopy holders.
- Prepared all Figures present in the manuscript and wrote the manuscript text.

5.4 Proteome analysis of condensed barley mitotic chromosomes

Perutka, Z., **Kaduchová, K.**, Chamrád, I., Beinhauer, J., Lenobel, R., Petrovská, B., Bergougnoux, V., Vrána, J., Pecinka, A., Doležel, J., and Šebela, M. (2021). Proteome analysis of condensed barley mitotic chromosomes. *Frontiers in Plant Science*, 12, 723674. doi: 10.3389/fpls.2021.723674.

My contribution:

- Designed a cloning strategy for creating EYFP-FIB1 construct and did the cloning.
- Performed microscopy verification of EYFP-FIB1 transgenic line based on the presence of a specific fluorescence signal.
- Did immunolocalization staining of sorted metaphase chromosomes and RNase A treatment of sorted chromosomes.
- Did confocal microscopy of both treated and untreated sorted metaphase chromosomes.
- Prepared Figures 5 and 6 and was involved in preparing the manuscript.

6 PUBLISHED CONFERENCE ABSTRACTS

6.1 Towards *in vivo* analysis of chromatin dynamics in barley

(Appendix V)

poster presentation

6.2 *In planta* microscopy of barley fluorescent marker lines

(Appendix VI)

oral presentation

6.3 Developing system for tracking *in planta* chromatin dynamics in barley (*Hordeum vulgare*)

(Appendix VI)

poster presentation

“Best poster prize”

6.4 Developing system for *in planta* tracking of chromatin dynamics in barley (*Hordeum vulgare*)

(Appendix VIII)

poster presentation

6.5 Analysis of *in vivo* chromatin dynamics during mitotic division in barley (*Hordeum vulgare*)

(Appendix IX)

oral presentation

“Best flash-talk prize”

6.6 Live analysis of barley nuclei and chromosomes using fluorescent marker lines

(Appendix X)

oral presentation

6.7 Towards understanding of spatial *in vivo* dynamics of mitotic division in barley (*Hordeum vulgare*)

(Appendix X)

oral presentation

6.8 Towards understanding of spatial *in vivo* dynamics of mitotic division in barley (*Hordeum vulgare*)

(Appendix XI)

oral presentation

“Best conference talk prize”

6.1. Towards *in vivo* analysis of chromatin dynamics in barley

Lahnerová, K., Stromšíková, H., Střelcová, K., Doležel, J., Bergougnoux-Fojtík, V, and Pecinka, A.

In: Abstract book of the 4th INDEPTH meeting ,“Impact of chromatin domains on plant phenotypes“

Madrid, Spain, 2019

Abstract:

The organization of chromatin in cell nuclei is dynamic and undergoes changes during cell cycle and cell tissue differentiation. This is necessary for correct segregation of genetic information, regulation of gene expression, DNA replication etc. While there is growing information about *in vivo* dynamics of nuclear domains in plant species with small genomes represented mainly by *Arabidopsis thaliana*, such data are practically missing in plants with large and complex genomes. We will present our efforts in developing a series of *Hordeum vulgare* ($2n = 2x = 14$; 5 Gbp/1C) marker lines carrying fluorescently labelled fusion proteins indicative of specific chromosome and nuclear domains such as centromere, telomere and nucleolus. Production of multi-marker lines will enable comprehensive analysis of chromatin dynamics in both wild type and mutant plants under ambient and stress conditions.

6.2. *In planta* microscopy of barley fluorescent marker lines

Lahnerová, K., Stromšíková, H., Střelcová, K., Mičúchová, A., Bergougnoux-Fojtík, V, Šamaj, J., and Pecinka, A.

In: „INDEPTH Imaris Training School 2020“

Zürich, Switzerland, 2020

Abstract:

The organization of chromatin in cell nuclei is dynamic and undergoes changes during cell cycle and cell tissue differentiation. In course of my Ph.D. project, I am developing series of barley (*Hordeum vulgare*, $2n = 2x = 14$; 5 Gbp/1C) marker lines carrying fluorescently labelled fusion proteins indicative of specific chromosome and nuclear domains such as the centromere (CENH3-RFP), telomere (TRB1-GFP), nucleolus (YFP-FIB1), chromatin (H2B-CFP) etc. After crossing of individual marker lines, I will apply confocal microscopy to study 3D *in vivo* dynamics of nuclear compartments in barley. To get the best possible images and information using my reporter lines, I would like to improve my image analysis skills using Imaris. Therefore, I am very much interested to join the INDEPTH-organized training school on image analysis.

6.3. Developing system for tracking *in planta* chromatin dynamics in barley (*Hordeum vulgare*)

Lahnerová, K., Stromšíková, H., Střelcová, K., Mičúchová, A., Bergougnoux-Fojtík, V, Šamaj, J., and Pecinka, A.

In: Abstract book of the „1st Czech Plant Nucleus Workshop 2021 (CPNW2021)“

Olomouc, Czech Republic, 2021

Abstract:

The structure and the dynamics of chromosome and chromatin organization in cell nuclei may change rapidly during cell cycle, in different cell tissues or in response to environmental stimuli. Owing to the limited experimental resources, little is known about chromosome and chromatin dynamics in plants with large genomes. During my Ph.D. project, I am developing a series of stable barley (*Hordeum vulgare*, $2n = 2x = 14$; 5 Gbp/1C) transgenic lines carrying translational fusions of nuclear and fluorescent proteins. These reporter lines will be indicative of specific chromosome and nuclear domains such as the centromere (RFP-CENH3), nucleolus (YFP-FIB1), chromatin (CFP/GFP/YFP-H2B), nuclear membrane (SUN1B-CFP). In addition, the lines will be combined with the existing markers for specific cellular proteins e.g. microtubules (mCherry-TUB) etc. Single as well as multi-marker lines are subject of confocal microscopy to study 3D *in vivo* dynamics of nuclear domains. This set of fluorescent marker lines will help in better understanding of chromatin organization in cereals with large and complex genomes and in the detailed investigating of various cell types focusing on their exact position in the plant tissue.

This poster won “The best poster prize of the 1st Czech Plant Nucleus Workshop 2021”.

6.4. Developing system for *in planta* tracking of chromatin dynamics in barley (*Hordeum vulgare*)

Kaduchová, K., Stromšíková, H., Střelcová, K., Mičúchová, A., Křižňanská, H. Bergougnoux-Fojtík, V, Galuszka, P., Šamaj, J., and Pecinka, A.

In: Abstract book of the „Cytogenetics meeting 2021“

Görlitz, Germany, 2021

Abstract:

The structure and the dynamics of chromosome and chromatin organization in cell nuclei may change rapidly during cell cycle, in different cell tissues or in response to environmental stimuli. Owing to the limited experimental resources, little is known about chromosome and chromatin dynamics in plants with large genomes. During my Ph.D. project, I am developing a series of stable barley (*Hordeum vulgare*, $2n = 2x = 14$; 5,1 Gbp/1C) transgenic lines carrying translational fusions of nuclear and fluorescent proteins. These reporter lines will be indicative of specific chromosome and nuclear domains such as the centromere (RFP-CENH3), nucleolus (YFP-FIB1), chromatin (CFP/GFP/YFP-H2B), nuclear membrane (SUN1B-CFP). In addition, the lines will be combined with the existing markers for specific cellular proteins e.g. microtubules (mCherry-TUB) etc. Single as well as multi-marker lines are subject of confocal microscopy to study 3D *in vivo* dynamics of nuclear domains. This set of fluorescent marker lines will help in better understanding of chromatin organization in cereals with large and complex genomes and in the detailed investigating of various cell types focusing on their exact position in the plant tissue

6.5. Analysis of *in vivo* chromatin dynamics during mitotic division in barley (*Hordeum vulgare*)

Kaduchová, K., Střelcová, K., Mičúchová, A., Galuszka, P., Bergougnoux-Fojtík, V, Šamaj, J., and Pecinka, A.

In: Abstract book of the „7th European Workshop on Plant Chromatin 2022 (EWPC2022)”

Průhonice, Praha, 2022

Abstract:

The structure and the dynamics of chromatin organization in cell nuclei is not strict and may change rapidly during cell cycle, in different cell tissues and in response to environmental stimuli. The most rapid changes of cell architecture occur during the cell divisions such as mitosis and meiosis, where chromatin arrangement is changed due to its condensation into compact chromosomes and their even distribution into the newly emerging daughter cells. To study the dynamics of mitosis in plants, it is necessary to use appropriate system enabling *in vivo* and *in planta* investigation of the key processes. To this end, we developed a series of barley (*Hordeum vulgare*, $2n = 2x = 14$; 5 Gbp/1C) marker lines carrying fluorescently labelled fusion proteins that are indicative of specific chromosome and nuclear domains such as the chromatin (GFP/YFP/CFP-H2B), microtubules (mCHERRY-TUA3), centromere (RFP-CENH3) and nucleolus (YFP-FIB1). The combinations of different markers provide a universal and unique system for analysis of 3D *in vivo* dynamics of nuclear compartments in barley cells suitable for diverse microscopy applications.

This oral presentation won “The best flash-talk of the 7th European Workshop on Plant Chromatin 2022 prize”.

6.6. Live analysis of barley nuclei and chromosomes using fluorescent marker lines

Kaduchová, K., Galuszka, P., Bergougnoux-Fojtík, V, Šamaj, J., and Pecinka, A.

In: Abstract book of the „2nd EPI-CATCH Conference“

Crete, Greece, 2022

Abstract:

The structure and the dynamics of chromatin organization in cell nuclei is not strict and may change rapidly during cell cycle, in different cell tissues and in response to environmental stimuli. The most rapid changes of cell architecture occur during the cell divisions such as mitosis and meiosis, where chromatin arrangement is changed due to its condensation into compact chromosomes and their even distribution into the newly emerging daughter cells. To study the dynamics of mitosis in plants, it is necessary to use appropriate system enabling *in vivo* and *in planta* investigation of the key processes. To this end, we developed a series of barley (*Hordeum vulgare*, $2n = 2x = 14$; 5 Gbp/1C) marker lines carrying fluorescently labelled fusion proteins that are indicative of specific chromosome and nuclear domains such as the chromatin (GFP/YFP/CFP-H2B), microtubules (mCHERRY-TUA3), centromere (RFP-CENH3) and nucleolus (YFP-FIB1). The combinations of different markers provide a universal and unique system for analysis of 3D *in vivo* dynamics of nuclear compartments in barley cells suitable for diverse microscopy applications.

6.7. Towards understanding of spatial *in vivo* dynamics of mitotic division in barley (*Hordeum vulgare*)

Kaduchová, K., Marchetti, C., Ovečka, M., Galuszka, P., Bergougnoux, V, Šamaj, J., and Pecinka, A.

In: Abstract book of the „3rd EPI-CATCH Conference“

Sofia, Bulgaria, 2023

Abstract:

The structure and the dynamics of chromatin organization in cell nuclei are not strict and may change rapidly during the cell cycle, in different tissues, and in response to abiotic and biotic stimuli. The most rapid changes in the cell architecture occur during the cell divisions. In mitosis the chromatin arrangement is changed due to its condensation into compact chromosomes which are subsequently distributed into the newly emerging daughter cells. To study the dynamics of mitosis in plants with large genomes, we developed a series of unique barley marker lines carrying fluorescently labeled fusion proteins that are indicative of specific chromosomal/nuclear domains such as the chromatin (GFP/YFP/CFP-H2B), microtubules (mCHERRY-TUA3) and nucleolus (YFP-FIB1). With these lines, we were able to measure the length of mitotic division in barley root cells and reveal the dynamics of tagged cellular structures. Moreover, we found that the condensation of mitotic chromosomes does not reach its maximum in metaphase but proceeds until telophase where the newly formed daughter cells emerge.

6.8. Towards understanding of spatial in vivo dynamics of mitotic division in barley (*Hordeum vulgare*)

Kaduchová, K., Marchetti, C., Ovečka, M., Galuszka, P., Bergougnoux, V, Šamaj, J., and Pecinka, A.

In: Abstract book of the „2nd Czech Plant Nucleus Workshop” (CPNW2023)

Brno, Czech Republic, 2023

Abstract:

The structure and the dynamics of chromatin organization in cell nuclei are not strict and may change rapidly during the cell cycle, in different tissues, and response to abiotic and biotic stimuli. The most rapid changes in cell architecture occur during cell divisions. In mitosis, the chromatin arrangement is changed due to its condensation into compact chromosomes, which are subsequently distributed into the newly emerging daughter cells. To study the dynamics of mitosis in plants with large genomes, we developed a series of unique barley marker lines carrying fluorescently labelled fusion proteins that are indicative of specific chromosomal/nuclear domains such as the chromatin (GFP/YFP/CFP-H2B), microtubules (mCHERRY-TUA3) and nucleolus (YFP-FIB1). With these lines, we were able to measure the length of mitotic division in barley root cells and reveal the dynamics of tagged cellular structures. Moreover, we found that the condensation of mitotic chromosomes does not reach its maximum in metaphase but proceeds until telophase where the newly formed daughter cells emerge.

This oral presentation won “The best talk of the 2nd Czech Plant Nucleus Workshop 2023 prize”.

7 DISCUSSION

7.1 Development of the fluorescent marker lines for *in vivo* nuclear and cellular organization and dynamics studies in barley

The ability to observe cell behavior in living plants in real time opened up new possibilities for studying comprehensive biological processes. Live cell imaging has allowed us to investigate tissue and organ development, as well as the regulation of metabolic pathways and the mobility of proteins both within and between cells.

The progress in live microscopy has been fueled by the development of various fluorescent proteins, differing in terms of stability, conformation, and excitation/emission spectra (Lambert, 2019, Valuchova *et al.*, 2020, Prusicki *et al.*, 2021, Silveira *et al.*, 2022). This diversity has enabled labelling of a wide range of proteins with different fluorescent tags and their simultaneous visualization in living cells using fluorescent marker (reporter) lines. Until now, an extensive platform of diverse lines has been developed and applied for dynamic and localization studies in the model plant *Arabidopsis thaliana*, such as fluorescent lines for diverse cellular and nuclear compartments, tracking of the cell cycle, mitosis, and meiosis progression (Boisnard-Lorig *et al.*, 2001, Ubeda-Tomas *et al.*, 2009, Yin *et al.*, 2014). These lines become even more valuable when combined with different mutants as change in marker protein localization is visible in a mutant background.

Compared to *Arabidopsis*, the development of mutants and fluorescent marker lines for *in vivo* studies in cereal crop plants is a more challenging process. Cereal crops have a longer life cycle which extends the required time, are more difficult to transform, and the regeneration and selection of transgenic plants is time- and space-demanding. Moreover, already optimized construct designs for marker proteins tested in *Arabidopsis* are frequently not applicable for crops due to species-specific protein structures and the potential influence of the N' or C'-terminal positioning of fluorescent tags (Chenal *et al.*, 2002). This was confirmed also in this study.

Initially, we tested the localization of created fusion proteins in the barley leaf protoplast system (Shan *et al.*, 2014). We observed specific localization of both N' and C' tagged variants of H2B (nucleus), N' tagged FIB1 (nucleolus) and C' tagged CENH3 (centromeres). Nevertheless, we noticed differences in the localization of distinct fusion protein variants (e.g., H2B-CFP and CENH3-RFP, C'-terminal fusions) between

protoplasts and plants regenerated after transformation. In regenerated plants, we could not detect any fluorescent signal for both of these fusion proteins. Leaf protoplasts do not divide and have changed transcription and translation regulation (Bai *et al.*, 2014). We speculate that the lack of active cell division restricts the CENH3-RFP ability to load to DNA, which normally happens during the G2 phase (Lermontova *et al.*, 2006). In the case of H2B-CFP and also TRB1-GFP, we were not able to detect any fluorescent signal in plants nuclei or cells, however we did not further test the specific cause.

Despite these features, in total 12 different FLMs and also their variously crossed combinations were developed during my Ph.D. project. Several of these lines are still unpublished and will be used for future research. However, it has to be emphasized that although these lines show fluorescence at expected cellular domains, we cannot make firm conclusions concerning the functionality of the tagged proteins because all these lines carry also fully functional endogenous copies.

Despite the challenges of marker line development, sets of marker lines for various proteins or their native promoters have been successfully established until now for some crop species with the lead of maize. As for example fluorescent fusions of FLOWERING LOCUS T-LIKE for tracking a flowering induction, DECREASE IN DNA METHYLATION 1 facilitating DNA methylation, HISTONE H1 for chromatin structure, RAN-GAP for nuclear envelope, TANGLED 1 for preprophase band formation and many others (Wu *et al.*, 2013). These lines have significantly helped with uncovering the regulation of plant developmental processes. However, only a few marker lines have been developed for other crop species such as rice, wheat, or barley (Furtado and Henry, 2005, Wu *et al.*, 2016, Xue *et al.*, 2016, Kirschner *et al.*, 2018, Luginbuehl *et al.*, 2020). Besides, none of these marker lines are as versatile for complex cellular and nuclear *in vivo* microscopy as those available for maize.

The substantial advantage of the FML system for *in vivo* studies in barley lies in the larger dimensions of barley cells, nuclei, and their compartments. Compared to *Arabidopsis* and even maize, the process of chromosome condensation and decondensation can be easily tracked *in vivo*, same as the progression of mitosis, meiosis, and cytokinesis. Moreover, the Rabl chromosome arrangement is a valuable marker for nuclear orientation in a cellular space. These features could together help to uncover new and unique aspects of cell nuclear dynamics.

7.2 Live imaging uncovers unique features of barley genome dynamics

Live imaging puts new insights into the dynamical cell processes. Using a double CFP-H2B RFP-CENH3 line, we observed that the mitotic spindle was often deflected from the expected orientation parallel to the root division axis in most anaphase cells. Typically, tilting of the mitotic spindle and emerging phragmoplast is associated with changes in cell shape and cell division plane morphology caused by local or tissue-level stress (Rasmussen and Bellinger, 2018). It can also occur in mutants with defective PPB establishments, such as *Arabidopsis* TONNEAU1 RECRUITMENT MOTIF_{6,7,8} (TRM_{6,7,8}), or maize TANGLED1 (TAN1) (Smith *et al.*, 2001) and MAIZE LINC KASH SINE-LIKE2 (MLKS2) (Gumber *et al.*, 2019, Allsman *et al.*, 2023). Interestingly, this deflection of the mitotic spindle appears to be natural in barley. Newly formed cell walls do not show any deviations, and the root architecture remains unchanged.

It was proposed that the size of the chromosomes or limited cell space could influence the mechanism of mitotic spindle dynamics and chromosome condensation. Generally, it is assumed that intense mitotic chromatin condensation proceeds during prophase (Feitoza *et al.*, 2017). Based on our observations in barley and in other studies, it is likely that chromatin condensation starts earlier, as also supported by the presence of mitosis-specific histone H3 modifications H3T3p, H3T11p, and H3S10p (Houben *et al.*, 1999, Wilkins *et al.*, 2014). It is possible that in the fast-cycling barley root cells, chromatin condensation and early-mitotic microtubule assembly are not completely synchronized, as chromosome-like structures are visible before the PPB emergence. We speculate that CONDENSIN II, which is localized in the nucleus during the interphase, might play a key role in early chromatin condensation, binding to the chromatin before the nuclear envelope breakdown (Ono *et al.*, 2004). Alternatively, some fast-cycling cell populations might be able to undergo interphase with semi-condensed chromosomes. Nevertheless, additional FMLs and experiments would be needed for testing these hypotheses.

Moreover, our data showed that chromosome condensation does not reach the maximum in mitotic metaphase but proceeds until telophase. This trend has been described in mammalian cells but not in plants (Mora-Bermudez *et al.*, 2007). Functionally, it is suggested to prevent the cleavage of long chromosome arm ends or the elimination of lagging chromosomes, ensuring the proper assembly of a balanced mitotic spindle (Schubert and Oud, 1997, Hudakova *et al.*, 2002, Neurohr *et al.*, 2011).

Additionally, we observed the association of EYFP-tagged FIB1 RNA methyltransferase within the surface of condensing chromosomes, persisting from prometaphase until telophase, which was lost after RNase A treatment. It suggests that plant mitotic chromosomes are coated with a plant alternative of the perichromosomal layer observed in Animalia cells. The components of this layer, including proteins and RNA molecules, are mostly involved in chromosome compaction, cell cycle regulation, protein synthesis, and cell formation in Animalia (Gautier *et al.*, 1992, Takagi *et al.*, 1999). However, complete composition and cellular functions specific for the plant perichromosomal layer have not yet been characterized.

The main advantage and importance of *in vivo* microscopy using marker lines lies in their ability to monitor the progress of favorable traits in live during distinct time periods. This significantly aids in filling gaps in knowledge obtained from fixed-state *in vitro* approaches, as observed using multi-FMLs for a more accurate definition of the mitosis in barley root cells by simultaneous detection of independent protein markers.

When comparing the length of the cell cycle and mitosis of barley root cells obtained by immunolabelling of tagged base analogs incorporated into the genomic DNA, we observed differences between resulting times compared to our *in vivo* measurements (Benneth and Finch, 1972, Schwammenhoferova and Ondrej, 1978, Kwasniewska *et al.*, 2018). There was a decrease in the duration of both mitosis and its individual phases. The overall length of mitosis was reduced by more than 38 % (Benneth and Finch, 1972). We also noticed similar shortening for individual mitotic phases, especially for anaphase and telophase, where the reduction was over 51 %. However, we suspect that these changes in the expected durations of phases are likely due to technical factors, such as variations in growth conditions (temperature difference), light intensities, the supply of growth media, or differences among barley cultivars.

7.3 *In planta* microscopy brings challenges in mounting of living samples

Despite the pronounced advantages of *in vivo* microscopy techniques, there are challenges arising from the requirements of the microscopy setup. Plant *in vivo* microscopy faces unique challenges compared to animal models, including strong autofluorescence of chlorophyll and secondary metabolites, interference of cell walls, and

plant growth affected by gravitropism (reviewed in Chen *et al.*, 1999). To overcome these limitations and obtain high-quality live cell microscopy data, approaches have been developed and optimized for plant *in vivo* time-lapse microscopy. For instance, advanced sample tracking softwares, setups guiding sample growth, or chambers simulating natural growth conditions (Grossmann *et al.*, 2011, Ovecka *et al.*, 2015, Vyplelova *et al.*, 2018, Rahni and Birnbaum, 2019).

During the time-lapse microscopy on a confocal microscope (horizontal sample positioning), we observed prominent root rotations, side movements and root natural circumnutation (reviewed in Chen *et al.*, 1999, Migliaccio *et al.*, 2013). Moreover, roots often grew from the vision field during the time-lapse due to the unpredictable root growth direction. These issues made the time-lapse analysis challenging. However, none of the previously developed horizontal living sample mounting setups which we tested improved the scanning efficiency due to the barley roots larger diameter (Grossmann *et al.*, 2011, Rahni and Birnbaum, 2019). There have been developed systems enabling a transformation of the classical confocal microscopes (horizontal sample positioning) into a mode where samples are placed vertically during the scanning (von Wangenheim *et al.*, 2017, Feldhaus *et al.*, 2021). However, these systems require specialized assembling adds-on components on the microscope body or specific software. They are also difficult to implement in our conditions where most users apply microscopy on fixed, horizontally mounted, samples.

The EasyClick microscopy sample holder is a valuable tool for live cell imaging of cereal crop plant roots with larger diameters, where plantlets are placed horizontally during the scanning. Compared to other alternative sample horizontal mounting methods (Rahni and Birnbaum, 2019), it is easy to assemble and handle. Besides, it can be used for microscopy of different cereal crops roots thanks to the exchangeable ‘metal plate with growth channels’ component optimized for different root diameters. Currently, it is optimized for inverted confocal microscopes but can be easily adapted for upright microscope variants.

In conclusion, the valuable insights obtained through the development and *in vivo* analysis of FMLs underscore the importance of live microscopy done on non-model plant species. They strongly expand the complexity of knowledge about plant genome organization and dynamics and are essential for understanding the regulation of growth

and development of plant species with unsubstantial agronomic importance. With *in planta* time-lapse microscopy, it is possible to observe immediate plant reactions and track them in time. In the future, developed fluorescent marker lines could be used for complex analysis of how barley responds to drought, heat, or salinity stress.

8 CONCLUSIONS

Understanding the organization and dynamics of the nuclear genome plays an irreplaceable role in uncovering the regulation of biological processes controlling organism development. To investigate these processes in living plants with large genomes, we developed translational fusion fluorescent marker lines (FMLs) of barley marking chromatin, nucleolus, microtubules, and centromeres. These lines should serve as a platform for understanding the nuclear dynamics of other agriculturally essential crop species comparable with barley.

Using the developed multi-marker FMLs, we performed a time-lapse *in vivo* analysis of mitotic division in barley root cells. This allowed us to distinguish and describe individual mitotic phases and uncover specific features of mitosis in barley root cells. For instance, we observed early preprophase chromosome condensation in almost half of the dividing cells, which progressed until the telophase. We also discovered specific localization of FIBRILLARIN1 protein onto the surface of condensed chromosomes, where it interacts with RNA molecules. Additionally, we found that during barley anaphase chromosome division, the chromosomes tend to tilt more towards the cell wall corners rather than into the cell wall centers, which we quantified by establishing our protocol for measuring anaphase division angles using Imaris bitplane software.

Moreover, we designed and developed a user-optimized EasyClick microscopy sample holder. This holder allows precise cell-level time-lapse *in vivo* microscopy of fast-growing roots of greater thickness and is dedicated specifically for cereal crop roots microscopy analysis.

9 REFERENCES

- Afonso, C.L., Harkins, K.R., Thomascompton, M.A., Krejci, A.E. and Galbraith, D.W. (1985) Selection of somatic hybrid plants in *Nicotiana* through fluorescence-activated sorting of protoplasts. *Bio-Technology*, **3**, 811-816.
- AGI (2000) The Arabidopsis Genome Initiative. Analysis of the genome sequence of the flowering plant *Arabidopsis thaliana*. *Nature*, **408**, 796-815.
- Alipour, E. and Marko, J.F. (2012) Self-organization of domain structures by DNA-loop-extruding enzymes. *Nucleic Acids Research*, **40**, 11202-11212.
- Allsman, L.A., Bellinger, M.A., Huang, V., Duong, M., Contreras, A., Romero, A.N., Verboonen, B., Sidhu, S., Zhang, X., Steinkraus, H., Uyehara, A.N., Martinez, S.E., Sinclair, R.M., Soriano, G.S., Diep, B., Dawson Byrd, V., Noriega, A., Drakakaki, G., Sylvester, A.W. and Rasmussen, C.G. (2023) Subcellular positioning during cell division and cell plate formation in maize. **14**.
- Ambrose, J.C. and Cyr, R. (2008) Mitotic spindle organization by the preprophase band. *Molecular Plant*, **1**, 950-960.
- Anderson, D.E., Losada, A., Erickson, H.P. and Hirano, T. (2002) Condensin and cohesin display different arm conformations with characteristic hinge angles. *Journal of Cell Biology*, **156**, 419-424.
- Anton, T., Leonhardt, H. and Markaki, Y. (2016) Visualization of genomic loci in living cells with a fluorescent CRISPR/Cas9 system. *Nuclear Envelope: Methods and Protocols*, **1411**, 407-417.
- Ashley, T. (1979) Specific end-to-end attachment of chromosomes in *Ornithogalum virens*. *Journal of Cell Science*, **38**, 357-367.
- Badr, A., Muller, K., Schafer-Pregl, R., El Rabey, H., Effgen, S., Ibrahim, H.H., Pozzi, C., Rohde, W. and Salamini, F. (2000) On the origin and domestication history of barley (*Hordeum vulgare*). *Molecular Biology and Evolution*, **17**, 499-510.
- Bai, Y., Han, N., Wu, J.X., Yang, Y.N., Wang, J.H., Zhu, M.Y. and Bian, H.W. (2014) A transient gene expression system using barley protoplasts to evaluate microRNAs for post-transcriptional regulation of their target genes. *Plant Cell Tissue and Organ Culture*, **119**, 211-219.
- Bajer, A. (1959) Change of length and volume of mitotic chromosomes in living cells. *Hereditas*, **45**, 579-596.
- Baurle, I. and Trindade, I. (2020) Chromatin regulation of somatic abiotic stress memory. *Journal of Experimental Botany*, **71**, 5269-5279.
- Beliveau, B.J., Boettiger, A.N., Avendano, M.S., Jungmann, R., McCole, R.B., Joyce, E.F., Kim-Kiselak, C., Bantignies, F., Fonseka, C.Y., Erceg, J., Hannan, M.A., Hoang, H.G., Colognori, D., Lee, J.T., Shih, W.M., Yin, P., Zhuang, X.W. and Wu, C.T. (2015) Single-molecule super-resolution imaging of chromosomes and in situ haplotype visualization using Oligopaint FISH probes. *Nature Communications*, **6**.
- Benneth, M. and Finch, R. (1972) The mitotic cycle time of root meristem cells of *Hordeum vulgare*. **25**, 399-444.
- Berckmans, B. and De Veylder, L. (2009) Transcriptional control of the cell cycle. *Current Opinion in Plant Biology*, **12**, 599-605.
- Bevan, M.W., Flavell, R.B. and Chilton, M.D. (1983) A chimaeric antibiotic-resistance gene as a selectable marker for plant-cell transformation. *Nature*, **304**, 184-187.
- Binarova, P., Cenklova, V., Prochazkova, J., Doskocilova, A., Volc, J., Vrlik, M. and Bogre, L. (2006) gamma-Tubulin is essential for acentrosomal microtubule

- nucleation and coordination of late mitotic events in Arabidopsis. *Plant Cell*, **18**, 1199-1212.
- Bishop, J., Swan, H., Valente, F. and Nutzmann, H.W.** (2021) The plant nuclear envelope and its role in gene transcription. *Frontiers in Plant Science*, **12**.
- Boisnard-Lorig, C., Colon-Carmona, A., Bauch, W., Hodge, S., Doerner, P., Bancharel, E., Dumas, C., Haseloff, J. and Berger, F.** (2001) Dynamic analyses of the expression of the HISTONE :: YFP fusion protein in arabidopsis show that syncytial endosperm is divided in mitotic domains. *Plant Cell*, **13**, 495-509.
- Boruc, J., Van den Daele, H., Hollunder, J., Rombauts, S., Mylle, E., Hilson, P., Inze, D., De Veylder, L. and Russinova, E.** (2010) Functional modules in the Arabidopsis core cell cycle binary protein-protein interaction network. *Plant Cell*, **22**, 1264-1280.
- Boudaoud, A., Burian, A., Borowska-Wykret, D., Uyttewaal, M., Wrzalik, R., Kwiatkowska, D. and Hamant, O.** (2014) FibrilTool, an ImageJ plug-in to quantify fibrillar structures in raw microscopy images. *Nature Protocols*, **9**, 457-463.
- Boudolf, V., Lammens, T., Boruc, J., Van Leene, J., Van Den Daele, H., Maes, S., Van Isterdael, G., Russinova, E., Kondorosi, E., Witters, E., De Jaeger, G., Inze, D. and De Veylder, L.** (2009) CDKB1;1 forms a functional complex with CYCA2;3 to suppress endocycle onset. *Plant Physiology*, **150**, 1482-1493.
- Brassac, J. and Blattner, F.R.** (2015) Species-level phylogeny and polyploid relationships in *Hordeum* (Poaceae) inferred by Next-Generation Sequencing and in silico cloning of multiple nuclear loci. *Systematic Biology*, **64**, 792-808.
- Brenchley, R., Spannagl, M., Pfeifer, M., Barker, G.L.A., D'Amore, R., Allen, A.M., McKenzie, N., Kramer, M., Kerhornou, A., Bolser, D., Kay, S., Waite, D., Trick, M., Bancroft, I., Gu, Y., Huo, N., Luo, M.C., Sehgal, S., Gill, B., Kianian, S., Anderson, O., Kersey, P., Dvorak, J., McCombie, W.R., Hall, A., Mayer, K.F.X., Edwards, K.J., Bevan, M.W. and Hall, N.** (2012) Analysis of the breadwheat genome using whole-genome shotgun sequencing. *Nature*, **491**, 705-710.
- Bücherl, C., Aker, J., de Vries, S. and Borst, J.W.** (2010) Probing protein-protein interactions with FRET-FLIM. In: Hennig, L., Köhler, C. (eds.) *Plant Developmental Biology*. **655**, 389-399.
- Callamaras, N. and Parker, I.** (1999) Construction of a confocal microscope for real-time x-y and x-z imaging. *Cell Calcium*, **26**, 271-279.
- Cardullo, R.A. and Hinchcliffe, E.H.** (2013) Post-processing for statistical image analysis in light microscopy. *Digital Microscopy, 4th Edition*, **114**, 285-315.
- Carninci, P., Kvam, C., Kitamura, A., Ohsumi, T., Okazaki, Y., Itoh, M., Kamiya, M., Shibata, K., Sasaki, N., Izawa, M., Muramatsu, M., Hayashizaki, Y. and Schneider, C.** (1996) High-efficiency full-length cDNA cloning by biotinylated CAP trapper. *Genomics*, **37**, 327-336.
- Casale, F., Van Inghelandt, D., Weisweiler, M., Li, J.Q. and Stich, B.** (2022) Genomic prediction of the recombination rate variation in barley: A route to highly recombinogenic genotypes. *Plant Biotechnology Journal*, **20**, 676-690.
- Caudron, M., Bunt, G., Bastiaens, P. and Karsenti, E.** (2005) Spatial coordination of spindle assembly by chromosome-mediated signaling gradients. *Science*, **309**, 1373-1376.
- CGIAR** (2023) <https://cropgenebank.sgrp.cgiar.org/index.php/barley-mainmenu-250>. Vized on 2023/08/22.

- Chabaud, M., de Carvalho-Niebel, F. and Barker, D.G.** (2003) Efficient transformation of *Medicago truncatula* cv. Jemalong using the hypervirulent *Agrobacterium tumefaciens* strain AGL1. *Plant Cell Reports*, **22**, 46-51.
- Chen, R.J., Rosen, E. and Masson, P.H.** (1999) Gravitropism in higher plants. *Plant Physiology*, **120**, 343-350.
- Chenal, A., Nizard, P., Forge, V., Pugniere, M., Roy, M.O., Mani, J.C., Guillain, F. and Gillet, D.** (2002) Does fusion of domains from unrelated proteins affect their folding pathways and the structural changes involved in their function? A case study with the diphtheria toxin T domain. *Protein Engineering*, **15**, 383-391.
- Chilton, M.D., Drummond, M.H., Merlo, D.J., Sciaky, D., Montoya, A.L., Gordon, M.P. and Nester, E.W.** (1977) Stable incorporation of plasmid DNA into higher plant cells: molecular basis of crown gall tumorigenesis. *Cell*, **11**, 263-271.
- Ciska, M. and de la Espina, S.M.D.** (2014) The intriguing plant nuclear lamina. *Frontiers in Plant Science*, **5**.
- Close, T.J., Bhat, P.R., Lonardi, S., Wu, Y.H., Rostoks, N., Ramsay, L., Druka, A., Stein, N., Svensson, J.T., Wanamaker, S., Bozdag, S., Roose, M.L., Moscou, M.J., Chao, S.A.M., Varshney, R.K., Szucs, P., Sato, K., Hayes, P.M., Matthews, D.E., Kleinhofs, A., Muehlbauer, G.J., DeYoung, J., Marshall, D.F., Madishetty, K., Fenton, R.D., Condamine, P., Graner, A. and Waugh, R.** (2009) Development and implementation of high-throughput SNP genotyping in barley. *Bmc Genomics*, **10**.
- Concia, L., Veluchamy, A., Ramirez-Prado, J.S., Martin-Ramirez, A., Huang, Y., Perez, M., Domenichini, S., Granados, N.R.Y., Kim, S., Blein, T., Duncan, S., Pichot, C., Manza-Mianza, D., Juery, C., Paux, E., Moore, G., Hirt, H., Bergounioux, C., Crespi, M., Mahfouz, M.M., Bendahmane, A., Liu, C., Hall, A., Raynaud, C., Latrasse, D. and Benhamed, M.** (2020) Wheat chromatin architecture is organized in genome territories and transcription factories. *Genome Biology*, **21**.
- Cowan, C.R., Carlton, P.M. and Cande, W.Z.** (2001) The polar arrangement of telomeres in interphase and meiosis. Rab1 organization and the bouquet. *Plant Physiology*, **125**, 532-538.
- Cowley, D.O., Rivera-Perez, J.A., Schliekelman, M., He, Y.J., Oliver, T.G., Lu, L., O'Quinn, R., Salmon, E.D., Magnuson, T. and Van Dyke, T.** (2009) Aurora-A kinase is essential for bipolar spindle formation and early development. *Molecular and Cellular Biology*, **29**, 1059-1071.
- DaSilva, L.L.P., Snapp, E.L., Denecke, J., Lippincott-Schwartz, J., Hawes, C. and Brandizzi, F.** (2004) Endoplasmic reticulum export sites and golgi bodies behave as single mobile secretory units in plant cells. *Plant Cell*, **16**, 1753-1771.
- De Luca, G.M.R., Breedijk, R.M.P., Brandt, R.A.J., Zeelenberg, C.H.C., de Jong, B.E., Timmermans, W., Azar, L.N., Hoebe, R.A., Stallinga, S. and Manders, E.M.M.** (2013) Re-scan confocal microscopy: scanning twice for better resolution. *Biomedical Optics Express*, **4**, 2644-2656.
- de Reuille, P.B., Routier-Kierzkowska, A.L., Kierzkowski, D., Bassel, G.W., Schupbach, T., Tauriello, G., Bajpai, N., Strauss, S., Weber, A., Kiss, A., Burian, A., Hofhuis, H., Sapala, A., Lipowczan, M., Heimlicher, M.B., Robinson, S., Bayer, E.M., Basler, K., Koumoutsakos, P., Roeder, A.H.K., Aegerter-Wilmsen, T., Nakayama, N., Tsiantis, M., Hay, A., Kwiatkowska, D., Xenarios, I., Kuhlemeier, C. and Smith, R.S.** (2015) MorphoGraphX: A platform for quantifying morphogenesis in 4D. *Elife*, **4**.

- De Saeger, J., Park, J., Chung, H.S., Hernalsteens, J.P., Van Lijsebettens, M., Inze, D., Van Montagu, M. and Depuydt, S.** (2021) Agrobacterium strains and strain improvement: Present and outlook. *Biotechnology Advances*, **53**.
- Debernardi, J.M., Tricoli, D.M., Ercoli, M.F., Hayta, S., Ronald, P., Palatnik, J.F. and Dubcovsky, J.** (2020) A GRF-GIF chimeric protein improves the regeneration efficiency of transgenic plants. *Nature Biotechnology*, **38**, 1274-+.
- Dekker, J., Rippe, K., Dekker, M. and Kleckner, N.** (2002) Capturing chromosome conformation. *Science*, **295**, 1306-1311.
- Demidov, D., Van Damme, D., Geelen, D., Blattner, F.R. and Houben, A.** (2005) Identification and dynamics of two classes of Aurora-like kinases in arabidopsis and other plants. *Plant Cell*, **17**, 836-848.
- Dogan, E.S. and Liu, C.** (2018) Three-dimensional chromatin packing and positioning of plant genomes. *Nature Plants*, **4**, 521-529.
- Dong, P.F., Tu, X.Y., Chu, P.Y., Lu, P.T., Zhu, N., Grierson, D., Du, B.J., Li, P.H. and Zhong, S.L.** (2017) 3D chromatin architecture of large plant genomes determined by local A/B compartments. *Molecular Plant*, **10**, 1497-1509.
- Dostie, J., Richmond, T.A., Arnaout, R.A., Selzer, R.R., Lee, W.L., Honan, T.A., Rubio, E.D., Krumm, A., Lamb, J., Nusbaum, C., Green, R.D. and Dekker, J.** (2006) Chromosome Conformation Capture Carbon Copy (5C): A massively parallel solution for mapping interactions between genomic elements. *Genome Research*, **16**, 1299-1309.
- Dreissig, S., Mascher, M. and Heckmann, S.** (2019) Variation in recombination rate is shaped by domestication and environmental conditions in barley. *Molecular Biology and Evolution*, **36**, 2029-2039.
- Dreissig, S., Schiml, S., Schindele, P., Weiss, O., Rutten, T., Schubert, V., Gladilin, E., Mette, M.F., Puchta, H. and Houben, A.** (2017) Live-cell CRISPR imaging in plants reveals dynamic telomere movements. *Plant Journal*, **91**, 565-573.
- Dumur, T., Duncan, S., Graumann, K., Desset, S., Randall, R.S., Scheid, O.M., Prodanov, D., Tatout, C. and Baroux, C.** (2019) Probing the 3D architecture of the plant nucleus with microscopy approaches: challenges and solutions. *Nucleus*, **10**, 181-212.
- Egecioglu, D. and Brickner, J.H.** (2011) Gene positioning and expression. *Current Opinion in Cell Biology*, **23**, 338-345.
- Elliott, A.D.** (2020) Confocal microscopy: Principles and modern practices: Curr Protoc Cytom, pp. 1-18.
- Erguvan, O., Louveaux, M., Hamant, O. and Verger, S.** (2019) ImageJ SurfCut: a user-friendly pipeline for high-throughput extraction of cell contours from 3D image stacks. *Bmc Biology*, **17**.
- Evans, D.E., Irons, S.L. and Graumann, K.e.a.** (2009) The plant nuclear envelope. In: Meier, I, editor. Functional organisation of the plant nucleus. 9-28.
- FAO** (2022 - October) FAO publications catalogue 2022. Rome.
- Feitoza, L., Costa, L. and Guerra, M.** (2017) Condensation patterns of prophase/prometaphase chromosome are correlated with H4K5 histone acetylation and genomic DNA contents in plants. *Plos One*, **12**.
- Feldhaus, C., Kolb, M., Küppers, M., Hardy, S. and Palmisano, R.** (2021) GraviKit: an easy-to-implement microscope add-on for observation of gravitation dependent processes. (preprint): bioRxiv.
- Fernandez, R., Das, P., Mirabet, V., Moscardi, E., Traas, J., Verdeil, J.L., Malandain, G. and Godin, C.** (2010) Imaging plant growth in 4D: robust tissue reconstruction and lineaging at cell resolution. *Nature Methods*, **7**, 547-U594.

- Fouquet, C., Gilles, J.F., Heck, N., Dos Santos, M., Schwartzmann, R., Cannaya, V., Morel, M.P., Davidson, R.S., Trembleau, A. and Bolte, S.** (2015) Improving axial resolution in confocal microscopy with new high refractive index mounting media. *Plos One*, **10**.
- Fraley, R.T., Rogers, S.G., Horsch, R.B., Sanders, P.R., Flick, J.S., Adams, S.P., Bittner, M.L., Brand, L.A., Fink, C.L., Fry, J.S., Galluppi, G.R., Goldberg, S.B., Hoffmann, N.L. and Woo, S.C.** (1983) Expression of bacterial genes in plant cells. *Proceedings of the National Academy of Sciences of the United States of America-Biological Sciences*, **80**, 4803-4807.
- Fransz, P., de Jong, J.H., Lysak, M., Castiglione, M.R. and Schubert, I.** (2002) Interphase chromosomes in Arabidopsis are organized as well defined chromocenters from which euchromatin loops emanate. *Proceedings of the National Academy of Sciences of the United States of America*, **99**, 14584-14589.
- Fricker, M., Runions, J. and Moore, I.** (2006) Quantitative fluorescence microscopy: From art to science. *Annual Review of Plant Biology*, **57**, 79-107.
- Fromont-Racine, M., Senger, B., Saveanu, C. and Fasiolo, F.** (2003) Ribosome assembly in eukaryotes. *Gene*, **313**, 17-42.
- Fudenberg, G. and Imakaev, M.** (2017) FISHing for captured contacts: towards reconciling FISH and 3C. *Nature Methods*, **14**, 673-678.
- Fujimoto, S., Yonemura, M., Matsunaga, S., Nakagawa, T., Uchiyama, S. and Fukui, K.** (2005) Characterization and dynamic analysis of Arabidopsis condensin subunits, AtCAP-H and AtCAP-H2. *Planta*, **222**, 293-300.
- Furtado, A. and Henry, R.J.** (2005) The wheat Em promoter drives reporter gene expression in embryo and aleurone tissue of transgenic barley and rice. *Plant Biotechnology Journal*, **3**, 421-434.
- Gautier, T., Dauphinvillemant, C., Andre, C., Masson, C., Arnoult, J. and Hernandezverdun, D.** (1992) Identification and characterization of a new set of nucleolar ribonucleoproteins which line the chromosomes during mitosis. *Experimental Cell Research*, **200**, 5-15.
- Gautier, T., Fomproix, N., Masson, C., Azumgelade, M.C., Gas, N. and Hernandezverdun, D.** (1994) Fate of specific nucleolar perichromosomal proteins during mitosis: cellular distribution and association with U3 snoRNA. *Biology of the Cell*, **82**, 81-93.
- Gerlach, W.L. and Bedbrook, J.R.** (1979) Cloning and characterization of ribosomal-RNA genes from wheat and barley. *Nucleic Acids Research*, **7**, 1869-1885.
- Gibcus, J.H., Samejima, K., Goloborodko, A., Samejima, I., Naumova, N., Nuebler, J., Kanemaki, M.T., Xie, L.F., Paulson, J.R., Earnshaw, W.C., Mirny, L.A. and Dekker, J.** (2018) A pathway for mitotic chromosome formation. *Science*, **359**, eaa06135.
- Goto, C., Tamura, K., Fukao, Y., Shimada, T. and Hara-Nishimura, I.** (2014) The novel nuclear envelope protein KAKU4 modulates nuclear morphology in Arabidopsis. *Plant Cell*, **26**, 2143-2155.
- Goto, T. and Wang, J.C.** (1982) Yeast DNA topoisomerase II and ATP-dependent type II topoisomerase that catalyzes the catenation, decatenation, unknotting, and relaxation of double-stranded DNA rings. *Journal of Biological Chemistry*, **257**, 5866-5872.
- GrainGenes** (2023) https://wheat.pw.usda.gov/GG3/barley_bldv. Visited on 2023/08/22.

- Grandjean, O., Vernoux, T., Laufs, P., Belcram, K., Mizukami, Y. and Traas, J.** (2004) In vivo analysis of cell division, cell growth, and differentiation at the shoot apical meristem in arabidopsis. *Plant Cell*, **16**, 74-87.
- Graumann, K. and Evans, D.E.** (2011) Nuclear envelope dynamics during plant cell division suggest common mechanisms between kingdoms. *Biochemical Journal*, **435**, 661-667.
- Green, L.C., Kalitsis, P., Chang, T.M., Cipetic, M., Kim, J.H., Marshall, O., Turnbull, L., Whitchurch, C.B., Vagnarelli, P., Samejima, K., Earnshaw, W.C., Choo, K.H.A. and Hudson, D.F.** (2012) Contrasting roles of condensin I and condensin II in mitotic chromosome formation. *Journal of Cell Science*, **125**, 1591-1604.
- Grossmann, G., Guo, W.J., Ehrhardt, D.W., Frommer, W.B., Sit, R.V., Quake, S.R. and Meier, M.** (2011) The RootChip: An integrated microfluidic chip for plant science. *Plant Cell*, **23**, 4234-4240.
- Gumber, H.K., McKenna, J.F., Tolmie, A.F., Jalovec, A.M., Kartick, A.C., Graumann, K. and Bass, H.W.** (2019) MLKS2 is an ARM domain and F-actin-associated KASH protein that functions in stomatal complex development and meiotic chromosome segregation. *Nucleus*, **10**, 144-166.
- Guo, A.Y., Zhang, Y.M., Wang, L., Bai, D., Xu, Y.P. and Wu, W.Q.** (2021) Single-molecule imaging in living plant cells: A methodological review. *International Journal of Molecular Sciences*, **22**.
- Gutierrez, C.** (2009) The Arabidopsis cell cycle division: The Arabidopsis Book, pp. 1-19.
- Guttinger, S., Laurell, E. and Kutay, U.** (2009) Orchestrating nuclear envelope disassembly and reassembly during mitosis. *Nature Reviews Molecular Cell Biology*, **10**, 178-191.
- Haizel, T., Merkle, T., Pay, A., Fejes, E. and Nagy, F.** (1997) Characterization of proteins that interact with the GTP-bound form of the regulatory GTPase ran in Arabidopsis. *Plant Journal*, **11**, 93-103.
- Hamano, T., Dwiranti, A., Kaneyoshi, K., Fukuda, S., Kometani, R., Nakao, M., Takata, H., Uchiyama, S., Ohmido, N. and Fukui, K.** (2014) Chromosome interior observation by focused Ion Beam/Scanning Electron Microscopy (FIB/SEM) using ionic liquid technique. *Microscopy and Microanalysis*, **20**, 1340-1347.
- Harper, L., Golubovskaya, I. and Cande, W.Z.** (2004) A bouquet of chromosomes. *Journal of Cell Science*, **117**, 4025-4032.
- HarvEST:Barley** (2015) HarvEST:Barley. Version 2.26.
- Harwood, W.A., Bartlett, J.G., Alves, S.C., Perry, M., Smedley, M.A., Leyland, N., Snape, J.W.** (2009) Barley transformation using Agrobacterium-mediated techniques. **478**, 137-147.
- Hashimoto, T.** (2015) Microtubules in plants: The Arabidopsis Book.
- Hayashi, K. and Matsunaga, S.** (2019) Heat and chilling stress induce nucleolus morphological changes. *Journal of Plant Research*, **132**, 395-403.
- Hernandez, M.R., Davis, M.B., Jiang, J.H., Brouhard, E.A., Severson, A.F. and Csankovszki, G.** (2018) Condensin I protects meiotic cohesin from WAPL-1 mediated removal. *Plos Genetics*, **14**.
- Hernandez-Verdun, D.** (2011) Assembly and disassembly of the nucleolus during the cell cycle. *Nucleus*, **2**, 189-194.
- Hernandez-Verdun, D. and Gautier, T.** (1994) The chromosome periphery during mitosis. *Bioessays*, **16**, 179-185.

- Herreraestrella, L., Depicker, A., Vanmontagu, M. and Schell, J.** (1983) Expression of chimaeric genes transferred into plant cells using a Ti-plasmid delivered vector. *Nature*, **303**, 209-213.
- Higuchi, K., Ono, K., Araki, S., Nakamura, S., Uesugi, T., Makishima, T., Ikari, A., Hanaoka, T. and Sue, M.** (2017) Elongation of barley roots in high-pH nutrient solution is supported by both cell proliferation and differentiation in the root apex. *Plant Cell and Environment*, **40**, 1609-1617.
- Higuchi, R., Dollinger, G., Walsh, P.S. and Griffith, R.** (1992) Simultaneous amplification of specific DNA sequences. *Bio-Technology*, **10**, 413-417.
- Hinchliffe, A. and Harwood, W.A.** (2019) Agrobacterium-mediated transformation of barley immature embryos. *BARLEY: Methods and Protocols*, **1900**, 115-126.
- Hindson, B.J., Ness, K.D., Masquelier, D.A., Belgrader, P., Heredia, N.J., Makarewicz, A.J., Bright, I.J., Lucero, M.Y., Hiddessen, A.L., Legler, T.C., Kitano, T.K., Hodel, M.R., Petersen, J.F., Wyatt, P.W., Steenblock, E.R., Shah, P.H., Bousse, L.J., Troup, C.B., Mellen, J.C., Wittmann, D.K., Erndt, N.G., Cauley, T.H., Koehler, R.T., So, A.P., Dube, S., Rose, K.A., Montesclaros, L., Wang, S.L., Stumbo, D.P., Hodges, S.P., Romine, S., Milanovich, F.P., White, H.E., Regan, J.F., Karlin-Neumann, G.A., Hindson, C.M., Saxonov, S. and Colston, B.W.** (2011) High-throughput droplet digital PCR system for absolute quantitation of DNA copy number. *Analytical Chemistry*, **83**, 8604-8610.
- Hink, M.A., Bisseling, T. and Visser, A.** (2002) Imaging protein-protein interactions in living cells. *Plant Molecular Biology*, **50**, 871-883.
- Hisano, H., Tsujimura, M., Yoshida, H., Terachi, T. and Sato, K.** (2016) Mitochondrial genome sequences from wild and cultivated barley (*Hordeum vulgare*). *Bmc Genomics*, **17**.
- Hoencamp, C., Dudchenko, O., Elbatsh, A.M.O., Brahmachari, S., Raaijmakers, J.A., van Schaik, T., Cacciato, A.S., Contessoto, V.G., van Heesbeen, R., van den Broek, B., Mhaskar, A.N., Teunissen, H., St Hilaire, B.G., Weisz, D., Omer, A.D., Pham, M., Colaric, Z., Yang, Z.Z., Rao, S.S.P., Mitra, N., Lui, C., Yao, W.J., Khan, R., Moroz, L.L., Kohn, A., St Leger, J., Mena, A., Holcroft, K., Gambetta, M.C., Lim, F.B.A., Farley, E., Stein, N., Haddad, A., Chauss, D., Mutlu, A.S., Wang, M.C., Young, N.D., Hildebrandt, E., Cheng, H.H., Knight, C.J., Burnham, T.L.U., Hovel, K.A., Beel, A.J., Mattei, P.J., Kornberg, R.D., Warren, W.C., Cary, G., Gomez-Skarmeta, J.L., Hinman, V., Lindblad-Toh, K., Di Palma, F., Maeshima, K., Multani, A.S., Sen, P., Nel-Themaat, L., Behringer, R.R., Kaur, P., Medema, R.H., van Steensel, B., de Wit, E., Onuchic, J.N., Di Pierro, M., Aiden, E.L. and Rowland, B.D.** (2021) 3D genomics across the tree of life reveals condensin II as a determinant of architecture type. *Science*, **372**, 984-+.
- Hotta, T., Fujita, S., Uchimura, S., Noguchi, M., Demura, T., Muto, E. and Hashimoto, T.** (2016) Affinity purification and characterization of functional tubulin from cell suspension cultures of *Arabidopsis* and tobacco. *Plant Physiology*, **170**, 1189-1205.
- Houben, A., Wako, T., Furushima-Shimogawara, R., Presting, G., Kunzel, G., Schubert, I. and Fukui, K.** (1999) The cell cycle dependent phosphorylation of histone H3 is correlated with the condensation of plant mitotic chromosomes. *Plant Journal*, **18**, 675-679.

- Hua, W., Zhu, J.H., Shang, Y., Wang, J.M., Jia, Q.J., Lin, F. and Yang, J.M.** (2013) Establishment of a highly efficient regeneration method from the scraped broken embryo of mature barley seed. *Canadian Journal of Plant Science*, **93**, 1029-1035.
- Huang, Y., Rodriguez-Granados, N.Y., Latrasse, D., Raynaud, C., Benhamed, M. and Ramirez-Prado, J.S.** (2020) The matrix revolutions: towards the decoding of the plant chromatin three-dimensional reality. *Journal of Experimental Botany*, **71**, 5129-5147.
- Hudakova, S., Kunzel, G., Endo, T.R. and Schubert, I.** (2002) Barley chromosome arms longer than half of the spindle axis interfere with nuclear divisions. *Cytogenetic and Genome Research*, **98**, 101-107.
- Huff, J.** (2015) The Airyscan detector from ZEISS: confocal imaging with improved signal-to-noise ratio and super-resolution. *Nature Methods*, **12**.
- Ibidi** (2023) Confocal microscopy. <https://ibidi.com/content/216-confocal-microscopy>. Visited on 2023/08/25.
- IBSC, I.B.S.C.** (2012) A physical, genetic and functional sequence assembly of the barley genome. **491**, 711-716.
- Imaris Imaris** (RRID:SCR_007370).
- Inze, D. and De Veylder, L.** (2006) Cell cycle regulation in plant development. *Annual Review of Genetics*, **40**, 77-105.
- IPK_Genbank** (2023) <https://www.ipk-gatersleben.de/en/research/genebank>. Visited on 23/08/22.
- Ishii, T., Schubert, V., Khosravi, S., Dreissig, S., Metje-Sprink, J., Sprink, T., Fuchs, J., Meister, A. and Houben, A.** (2019) RNA-guided endonuclease - in situ labelling (RGEN-ISL): a fast CRISPR/Cas9-based method to label genomic sequences in various species. *New Phytologist*, **222**, 1652-1661.
- Jacobs, B., Schneider, R., Molenaar, J., Filion, L. and Deinum, E.E.** (2022) Microtubule nucleation complex behavior is critical for cortical array homogeneity and xylem wall patterning. *Proceedings of the National Academy of Sciences of the United States of America*, **119**.
- Jia, J.Z., Xie, Y.L., Cheng, J.F., Kong, C.Z., Wang, M.Y., Gao, L.F., Zhao, F., Guo, J.Y., Wang, K., Li, G.W., Cui, D.Q., Hu, T.Z., Zhao, G.Y., Wang, D.W., Ru, Z.G. and Zhang, Y.J.** (2021) Homology-mediated inter-chromosomal interactions in hexaploid wheat lead to specific subgenome territories following polyploidization and introgression. *Genome Biology*, **22**.
- Jiao, Y.N., Li, J.P., Tang, H.B. and Paterson, A.H.** (2014) Integrated syntenic and phylogenomic analyses reveal an ancient genome duplication in Monocots. *Plant Cell*, **26**, 2792-2802.
- Jones, T., Lowe, K., Hoerster, G., Anand, A., Wu, E., Wang, N., Arling, M., Lenderts, B. and Gordon-Kamm, W.** (2019) Maize Transformation Using the Morphogenic Genes Baby Boom and Wuschel2. *TRANSGENIC PLANTS: Methods and Protocols*, **1864**, 81-93.
- Jonkman, J. and Brown, C.M.** (2015) Any way you slice it - A comparison of confocal microscopy techniques. *Journal of Biomolecular Techniques*, **25**, 54-65.
- Kaduchová, K., Marchetti, C., Ovečka, M., Galuszka, P., Bergognoux, V., Šamaj, J. and Pecinka, A.** (2023) Spatial organization and dynamics of chromosomes and microtubules during barley mitosis. **115**, 602-613.
- Kalinina, N.O., Makarova, S., Makhotenko, A., Love, A.J. and Taliansky, M.** (2018) The multiple functions of the nucleolus in plant development, disease and stress responses. *Frontiers in Plant Science*, **9**.

- Kato, N. and Lam, E.** (2003) Chromatin of endoreduplicated pavement cells has greater range of movement than that of diploid guard cells in *Arabidopsis thaliana*. *Journal of Cell Science*, **116**, 2195-2201.
- Khosravi, S., Schindele, P., Gladilin, E., Dunemann, F., Rutten, T., Puchta, H. and Houben, A.** (2020) Application of aptamers improves CRISPR-based live imaging of plant telomeres. *Frontiers in Plant Science*, **11**.
- Kierzkowski, D., Runions, A., Vuolo, F., Strauss, S., Lymbouridou, R., Routier-Kierzkowska, A.L., Wilson-Sanchez, D., Jenke, H., Galinha, C., Mosca, G., Zhang, Z.J., Canales, C., Dello Ioio, R., Huijser, P., Smith, R.S. and Tsiantis, M.** (2019) A growth-based framework for leaf shape development and diversity. *Cell*, **177**, 1405-1418.
- Kim, E., Gonzalez, A.M., Pradhan, B., van der Torre, J. and Dekker, C.** (2022) Condensin-driven loop extrusion on supercoiled DNA. *Nature Structural & Molecular Biology*, **29**, 719-727.
- Kimura, Y., Kuroda, C. and Masuda, K.** (2010) Differential nuclear envelope assembly at the end of mitosis in suspension-cultured *Apium graveolens* cells. *Chromosoma*, **119**, 195-204.
- Kireeva, N., Lakonishok, M., Kireev, I., Hirano, T. and Belmont, A.S.** (2004) Visualization of early chromosome condensation: a hierarchical folding, axial glue model of chromosome structure. *Journal of Cell Biology*, **166**, 775-785.
- Kirienko, D.R., Luo, A.D. and Sylvester, A.W.** (2012) Reliable transient transformation of intact maize leaf cells for functional genomics and experimental study. *Plant Physiology*, **159**, 1309-1318.
- Kirik, A., Ehrhardt, D.W. and Kirik, V.** (2012) TONNEAU2/FASS regulates the geometry of microtubule nucleation and cortical array organization in interphase *Arabidopsis* cells. *Plant Cell*, **24**, 1158-1170.
- Kirschner, G.K., Stahl, Y., Imani, J., von Korff, M. and Simon, R.** (2018) Fluorescent reporter lines for auxin and cytokinin signalling in barley (*Hordeum vulgare*). *Plos One*, **13**.
- Kiss, A., Moreau, T., Mirabet, V., Calugaru, C.I., Boudaoud, A. and Das, P.** (2017) Segmentation of 3D images of plant tissues at multiple scales using the level set method. *Plant Methods*, **13**.
- Komaki, S. and Sugimoto, K.** (2012) Control of the Plant Cell Cycle by Developmental and Environmental Cues. *Plant and Cell Physiology*, **53**, 953-964.
- Komis, G., Samajova, O., Ovecka, M. and Samaj, J.** (2015) Super-resolution microscopy in plant cell imaging. *Trends in Plant Science*, **20**, 834-843.
- Křižňanská, H.** (2022) Selection and analysis of fluorescent marker lines of barley (*Hordeum vulgare*). Diploma Thesis: Palacký University, Olomouc, Czech Republic.
- Kubalova, I., Camara, A.S., Capal, P., Beseda, T., Rouillard, J.M., Krause, G.M., Holusova, K., Toegelova, H., Himmelbach, A., Stein, N., Houben, A., Dolezel, J., Mascher, M., Simkova, H. and Schubert, V.** (2023) Helical coiling of metaphase chromatids. *Nucleic Acids Research*.
- Kubalova, I., Nemeckova, A., Weisshart, K., Hribova, E. and Schubert, V.** (2021) Comparing super-resolution microscopy techniques to analyze chromosomes. *International Journal of Molecular Sciences*, **22**.
- Kumar, S., Patial, M. and Sharma, R.** (2020) Efficient barley breeding. In: Gosal, S., Wani, S. (eds) Accelerated plant breeding, volume 1: Springer, Cham.
- Kuznetsova, M.A., Chaban, I.A. and Sheval, E.V.** (2017) Visualization of chromosome condensation in plants with large chromosomes. *Bmc Plant Biology*, **17**.

- Kwasniewska, J., Zubrzycka, K. and Kus, A.** (2018) Impact of mutagens on DNA replication in barley chromosomes. *International Journal of Molecular Sciences*, **19**.
- Lafontaine, D.L.J.** (2019) Birth of nucleolar compartments: Phase separation-driven ribosomal RNA sorting and processing. *Molecular Cell*, **76**, 694-696.
- Lambert, T.J.** (2019) FPbase: a community-editable fluorescent protein database. *Nature Methods*, **16**, 277-278.
- Leland, B.A. and King, M.C.** (2014) Using LacO arrays to monitor DNA double-strand break dynamics in live *Schizosaccharomyces pombe* cells. *Cancer Genomics and Proteomics: Methods and Protocols, 2nd Edition*, **1176**, 127-141.
- Lermontova, I., Schubert, V., Fuchs, J., Klatte, S., Macas, J. and Schubert, I.** (2006) Loading of Arabidopsis centromeric histone CENH3 occurs mainly during G2 and requires the presence of the histone fold domain. *Plant Cell*, **18**, 2443-2451.
- Li, G., Fullwood, M.J., Xu, H., Mulawadi, F.H., Velkov, S., Vega, V., Ariyaratne, P.N., Bin Mohamed, Y., Ooi, H.S., Tennakoon, C., Wei, C.L., Ruan, Y.J. and Sung, W.K.** (2010) ChIA-PET tool for comprehensive chromatin interaction analysis with paired-end tag sequencing. *Genome Biology*, **11**.
- Li, J., Wang, Y.T., Zou, W.X., Jian, L.F., Fu, Y. and Zhao, J.** (2021) AtNUF2 modulates spindle microtubule organization and chromosome segregation during mitosis. *Plant Journal*, **107**, 801-816.
- Li, J., Xu, Y.Y. and Chong, K.** (2012) The novel functions of kinesin motor proteins in plants. *Protoplasma*, **249**, 95-100.
- Lieberman-Aiden, E., van Berkum, N.L., Williams, L., Imakaev, M., Ragoczy, T., Telling, A., Amit, I., Lajoie, B.R., Sabo, P.J., Dorschner, M.O., Sandstrom, R., Bernstein, B., Bender, M.A., Groudine, M., Gnirke, A., Stamatoyannopoulos, J., Mirny, L.A., Lander, E.S. and Dekker, J.** (2009) Comprehensive mapping of long-range interactions reveals folding principles of the human genome. *Science*, **326**, 289-293.
- Liew, L.C., Narsai, R., Wang, Y., Berkowitz, O., Whelan, J. and Lewsey, M.G.** (2020) Temporal tissue-specific regulation of transcriptomes during barley (*Hordeum vulgare*) seed germination. *Plant Journal*, **101**, 700-715.
- Liu, Y.G., Mitsukawa, N., Oosumi, T. and Whittier, R.F.** (1995) Efficient isolation and mapping of Arabidopsis thaliana T-DNA insert junctions by thermal asymmetric interlaced PCR. *Plant Journal*, **8**, 457-463.
- Lockhead, S., Moskaleva, A., Kamenz, J., Chen, Y.X., Kang, M.J., Reddy, A.R., Santos, S.D.M. and Ferrell, J.E.** (2020) The apparent requirement for protein synthesis during G2 phase is due to checkpoint activation. *Cell Reports*, **32**.
- Long, Y., Tahl, Y.S., Weidtkamp-Peters, S., Postma, M., Zhou, W., Oedhart, J.G., Sanchez-Perez, M.I., Adella, T., Simon, R., Scheres, B. and Blilou, I.** (2017) In vivo FRET-FLIM reveals cell-type-specific protein interactions in Arabidopsis roots. *Nature*, **548**, 97-102.
- Luginbuehl, L.H., El-Sharnouby, S., Wang, N. and Hibberd, J.M.** (2020) Fluorescent reporters for functional analysis in rice leaves. *Plant Direct*, **4**.
- Lysak, M.A.** (2022) Celebrating Mendel, McClintock, and Darlington: On end-to-end chromosome fusions and nested chromosome fusions. *Plant Cell*, **34**, 2475-2491.
- Maeshima, K. and Laemmli, U.K.** (2003) A two-step scaffolding model for mitotic chromosome assembly. *Developmental Cell*, **4**, 467-480.
- Manuelidis, L. and Chen, T.L.** (1990) A unified model of eukaryotic chromosomes. *Cytometry*, **11**, 8-25.

- Margolin, G., Gregoret, I.V., Cickovski, T.M., Li, C.L., Shi, W., Alber, M.S. and Goodson, H.V.** (2012) The mechanisms of microtubule catastrophe and rescue: implications from analysis of a dimer-scale computational model. *Molecular Biology of the Cell*, **23**, 642-656.
- Marthe, C., Kumlehn, J. and Hensel, G.** (2015) Barley (*Hordeum vulgare* L.) transformation using immature embryos. *Agrobacterium Protocols, Vol 1, 3rd Edition*, **1223**, 71-83.
- Mascher, M.** (2021) Pseudomolecules and annotation of the third version of the reference genome sequence assembly of barley cv. Morex [Morex V3]: e!DAL - Plant Genomics and Phenomics Research Data Repository (PGP), IPK Gatersleben, Seeland OT Gatersleben, Corrensstraße 3, 06466, Germany.
- Mascher, M., Gundlach, H., Himmelbach, A., Beier, S., Twardziok, S.O., Wicker, T., Radchuk, V., Dockter, C., Hedley, P.E., Russell, J., Bayer, M., Ramsay, L., Liu, H., Haberer, G., Zhang, X.Q., Zhang, Q.S., Barrero, R.A., Li, L., Taudien, S., Groth, M., Felder, M., Hastie, A., Simkova, H., Stankova, H., Vrana, J., Chan, S., Munoz-Amatrian, M., Ounit, R., Wanamaker, S., Bolser, D., Colmsee, C., Schmutz, T., Aliyeva-Schnorr, L., Grasso, S., Tanskanen, J., Chailyan, A., Sampath, D., Heavens, D., Clissold, L., Cao, S.J., Chapman, B., Dai, F., Han, Y., Li, H., Li, X., Lin, C.Y., McCooke, J.K., Tan, C., Wang, P.H., Wang, S.B., Yin, S.Y., Zhou, G.F., Poland, J.A., Bellgard, M.I., Borisjuk, L., Houben, A., Dolezel, J., Ayling, S., Lonardi, S., Kersey, P., Lagridge, P., Muehlbauer, G.J., Clark, M.D., Caccamo, M., Schulman, A.H., Mayer, K.F.X., Platzer, M., Close, T.J., Scholz, U., Hansson, M., Zhang, G.P., Braumann, I., Spannagl, M., Li, C.D., Waugh, R. and Stein, N.** (2017) A chromosome conformation capture ordered sequence of the barley genome. *Nature*, **544**, 426-433.
- Mascher, M., Muehlbauer, G.J., Rokhsar, D.S., Chapman, J., Schmutz, J., Barry, K., Munoz-Amatrian, M., Close, T.J., Wise, R.P., Schulman, A.H., Himmelbach, A., Mayer, K.F.X., Scholz, U., Poland, J.A., Stein, N. and Waugh, R.** (2013) Anchoring and ordering NGS contig assemblies by population sequencing (POPSEQ). *Plant Journal*, **76**, 718-727.
- Mascher, M., Wicker, T., Jenkins, J., Plott, C., Lux, T., Koh, C.S., Ens, J., Gundlach, H., Boston, L.B., Tulpova, Z., Holden, S., Hernandez-Pinzon, I., Scholz, U., Mayer, K.F.X., Spannagl, M., Pozniak, C.J., Sharpe, A.G., Simkova, H., Moscou, M.J., Grimwood, J., Schmutz, J. and Stein, N.** (2021) Long-read sequence assembly: a technical evaluation in barley. *Plant Cell*, **33**, 1888-1906.
- Masuda, K., Haruyama, S. and Fujino, K.** (1999) Assembly and disassembly of the peripheral architecture of the plant cell nucleus during mitosis. *Planta*, **210**, 165-167.
- Matsumoto, T., Tanaka, T., Sakai, H., Amano, N., Kanamori, H., Kurita, K., Kikuta, A., Kamiya, K., Yamamoto, M., Ikawa, H., Fujii, N., Hori, K., Itoh, T. and Sato, K.** (2011) Comprehensive sequence analysis of 24,783 barley full-length cDNAs derived from 12 clone libraries. *Plant Physiology*, **156**, 20-28.
- Matzke, A.J.M., Huettel, B., van der Winden, J. and Matzke, M.** (2005) Use of two-color fluorescence-tagged transgenes to study interphase chromosomes in living plants. *Plant Physiology*, **139**, 1586-1596.
- Mayer, K.F.X., Waugh, R., Langridge, P., Close, T.J., Wise, R.P., Graner, A., Matsumoto, T., Sato, K., Schulman, A., Muehlbauer, G.J., Stein, N., Ariyadasa, R., Schulte, D., Poursarebani, N., Zhou, R.N., Steuernagel, B., Mascher, M., Scholz, U., Shi, B.J., Madishetty, K., Svensson, J.T., Bhat, P.,**

- Moscou, M., Resnik, J., Hedley, P., Liu, H., Morris, J., Frenkel, Z., Korol, A., Berges, H., Taudien, S., Groth, M., Felder, M., Lonardi, S., Duma, D., Alpert, M., Cordero, F., Beccuti, M., Ciardo, G., Ma, Y., Wanamaker, S., Platzer, M., Brown, J.W.S., Fincher, G.B., Sampath, D., Swarbreck, D., Scalabrin, S., Zuccolo, A., Vendramin, V., Morgante, M. and Int Barley Genome Sequencing, C. (2012) A physical, genetic and functional sequence assembly of the barley genome. *Nature*, **491**, 711-+.
- McFarlane, H.E., Doring, A. and Persson, S. (2014) The cell biology of cellulose synthesis. *Annual Review of Plant Biology*, Vol 65, **65**, 69-94.
- Menges, M., de Jager, S.M., Gruissem, W. and Murray, J.A.H. (2005) Global analysis of the core cell cycle regulators of Arabidopsis identifies novel genes, reveals multiple and highly specific profiles of expression and provides a coherent model for plant cell cycle control. *Plant Journal*, **41**, 546-566.
- Meschichi, A., Ingouff, M., Picart, C., Mirouze, M., Desset, S., Gallardo, F., Bystricky, K., Picault, N., Rosa, S. and Pontvianne, F. (2021) ANCHOR: A technical approach to monitor single-copy locus localization in planta. *Frontiers in Plant Science*, **12**, :677849.
- Middleton, C.P., Senerchia, N., Stein, N., Akhunov, E.D., Keller, B., Wicker, T. and Kilian, B. (2014) Sequencing of chloroplast genomes from wheat, barley, rye and their relatives provides a detailed insight into the evolution of the Triticeae tribe. *Plos One*, **9**.
- Migliaccio, F., Tassone, P. and Fortunati, A. (2013) Circumnutation as an autonomous root movement in plants. *American Journal of Botany*, **100**, 4-13.
- Miyawaki, A. (2011) Development of probes for cellular functions using fluorescent proteins and fluorescence resonance energy transfer. *Annual Review of Biochemistry*, **80**, 357-373.
- Mora-Bermudez, F., Gerlich, D. and Ellenberg, J. (2007) Maximal chromosome compaction occurs by axial shortening in anaphase and depends on Aurora kinase. *Nature Cell Biology*, **9**, 822-831.
- Mrizova, K., Holaskova, E., Oz, M.T., Jiskrova, E., Frebort, I. and Galuszka, P. (2014) Transgenic barley: A prospective tool for biotechnology and agriculture. *Biotechnology Advances*, **32**, 137-157.
- Mumbach, M.R., Rubin, A.J., Flynn, R.A., Dai, C., Khavari, P.A., Greenleaf, W.J. and Chang, H.Y. (2016) HiChIP: efficient and sensitive analysis of protein-directed genome architecture. *Nature Methods*, **13**, 919-922.
- Munoz-Amatriain, M., Moscou, M.J., Bhat, P.R., Svensson, J.T., Bartos, J., Suchankova, P., Simkova, H., Endo, T.R., Fenton, R.D., Lonardi, S., Castillo, A.M., Chao, S.M., Cistue, L., Cuesta-Marcos, A., Forrest, K.L., Hayden, M.J., Hayes, P.M., Horsley, R.D., Makoto, K., Moody, D., Sato, K., Valles, M.P., Wulff, B.B.H., Muehlbauer, G.J., Dolezel, J. and Close, T.J. (2011) An improved consensus linkage map of barley based on flow-sorted chromosomes and single nucleotide polymorphism markers. *Plant Genome*, **4**, 238-249.
- Nagaki, K., Furuta, T., Yamaji, N., Kuniyoshi, D., Ishihara, M., Kishima, Y., Murata, M., Hoshino, A. and Takatsuka, H. (2021) Effectiveness of Create ML in microscopy image classifications: a simple and inexpensive deep learning pipeline for non-data scientists. *Chromosome Research*, **29**, 361-371.
- Nagano, T., Lubling, Y., Stevens, T.J., Schoenfelder, S., Yaffe, E., Dean, W., Laue, E.D., Tanay, A. and Fraser, P. (2013) Single-cell Hi-C reveals cell-to-cell variability in chromosome structure. *Nature*, **502**, 59-644.

- Nasmyth, K. and Haering, C.H.** (2005) The structure and function of SMC and Kleisin complexes. *Annual Review of Biochemistry*, **74**, 595-648.
- Naumova, N., Imakaev, M., Fudenberg, G., Zhan, Y., Lajoie, B.R., Mirny, L.A. and Dekker, J.** (2013) Organization of the mitotic chromosome. *Science*, **342**, 948-953.
- Navratilova, P., Toegelova, H., Tulpova, Z., Kuo, Y.T., Stein, N., Dolezel, J., Houben, A., Simkova, H. and Mascher, M.** (2022) Prospects of telomere-to-telomere assembly in barley: Analysis of sequence gaps in the MorexV3 reference genome. *Plant Biotechnology Journal*, **20**, 1373-1386.
- Neurohr, E., Naegeli, A., Titos, I., Theler, D., Greber, B., Barral, Y. and Mendoza, M.** (2011) A midzone-based ruler adjusts chromosome compaction to anaphase spindle length. *Molecular Biology of the Cell*, **22**.
- NordGen** (2023) <https://bgs.nordgen.org>. Visited on 2023/08/22.
- Nowicka, A., Ferkova, L., Said, M., Kovacik, M., Zwyrtkova, J., Baroux, C. and Pecinka, A.** (2023) Non-Rabl chromosome organization in endoreduplicated nuclei of barley embryo and endosperm tissues. *Journal of Experimental Botany*.
- Ohnuki, Y.** (1965) Demonstration of the spiral structure of human chromosomes: Nature, pp. 916-917.
- Oko, Y., Ito, N. and Sakamoto, T.** (2020) The mechanisms and significance of the positional control of centromeres and telomeres in plants. *Journal of Plant Research*, **133**, 471-478.
- Ono, T., Fang, Y., Spector, D.L. and Hirano, T.** (2004) Spatial and temporal regulation of condensins I and II in mitotic chromosome assembly in human cells. *Molecular Biology of the Cell*, **15**, 3296-3308.
- Ovecka, M., Vaskebova, L., Komis, G., Luptovciak, I., Smertenko, A. and Samaj, J.** (2015) Preparation of plants for developmental and cellular imaging by light-sheet microscopy. *Nature Protocols*, **10**, 1234-1247.
- Paddock, S.W.** (1999) Confocal laser scanning microscopy. *Biotechniques*, **27**, 992-+.
- Palozola, K.C., Liu, H., Nicetto, D. and Zaret, K.S.** (2017) Low-level, global transcription during mitosis and dynamic gene reactivation during mitotic exit. *Chromosome Segregation and Structure, Vol 82, 2017*, **82**, 197-205.
- Parry, G.** (2014) Components of the Arabidopsis nuclear pore complex play multiple diverse roles in control of plant growth. *Journal of Experimental Botany*, **65**, 6057-6067.
- Pecinka, A., Kato, N., Meister, A., Probst, A.V., Schubert, I. and Lam, E.** (2005) Tandem repetitive transgenes and fluorescent chromatin tags alter local interphase chromosome arrangement in Arabidopsis thaliana. *Journal of Cell Science*, **118**, 3751-3758.
- Pecinka, A. and Mittelsten Scheid, O.** (2012) Stress-induced chromatin changes: a critical view on their heritability. *Plant and Cell Physiology*, **53**, 801-808.
- Pecinka, A., Schubert, V., Meister, A., Kreth, G., Klatter, M., Lysak, M.A., Fuchs, J. and Schubert, I.** (2004) Chromosome territory arrangement and homologous pairing in nuclei of Arabidopsis thaliana are predominantly random except for NOR-bearing chromosomes. *Chromosoma*, **113**, 258-269.
- Peirats-Llobet, M., Yi, C., Liew, L.C., Berkowitz, O., Narsai, R., Lewsey, M.G. and Whelan, J.** (2023) Spatially resolved transcriptomic analysis of the germinating barley grain: Nucleic Acid Research.
- Pontvianne, F., Blevins, T., Chandrasekhara, C., Mozgova, I., Hassel, C., Pontes, O.M.F., Tucker, S., Mokros, P., Muchova, V., Fajkus, J. and Pikaard, C.S.** (2013) Subnuclear partitioning of rRNA genes between the nucleolus and

- nucleoplasm reflects alternative epiallelic states. *Genes & Development*, **27**, 1545-1550.
- Pradillo, M., Knoll, A., Oliver, C., Varas, J., Corredor, E., Puchta, H. and Santos, J.L.** (2015) Involvement of the cohesin cofactor PDS5 (SP076) during meiosis and DNA repair in *Arabidopsis thaliana*. *Frontiers in Plant Science*, **6**.
- Prieto, P., Santos, A.P., Moore, G. and Shaw, P.** (2004) Chromosomes associate premeiotically and in xylem vessel cells via their telomeres and centromeres in diploid rice (*Oryza sativa*). *Chromosoma*, **112**, 300-307.
- Probst, A.V. and Mittelsten Scheid, O.** (2015) Stress-induced structural changes in plant chromatin. *Current Opinion in Plant Biology*, **27**, 8-16.
- Prusicki, M.A., Balboni, M., Sofroni, K., Hamamura, Y. and Schnittger, A.** (2021) Caught in the act: Live-cell imaging of plant meiosis. *Frontiers in Plant Science*, **12**.
- Rabl, C.** (1885) Über Zelltheilung: Morphologisches Jahrbuch, pp. 214-330.
- Rahni, R. and Birnbaum, K.D.** (2019) Week-long imaging of cell divisions in the *Arabidopsis* root meristem. *Plant Methods*, **15**.
- Rasmussen, C.G. and Bellinger, M.** (2018) An overview of plant division-plane orientation. *New Phytologist*, **219**, 505-512.
- Rasmussen, C.G., Humphries, J.A. and Smith, L.G.** (2011) Determination of symmetric and asymmetric division planes in plant cells. *Annual Review of Plant Biology*, Vol 62, **62**, 387-409.
- Reddy, G.V., Gordon, S.P. and Meyerowitz, E.M.** (2007) Unravelling developmental dynamics: transient intervention and live imaging in plants. *Nature Reviews Molecular Cell Biology*, **8**, 491-501.
- Risueno, M.C., Medina, F.J. and Moreno Diaz de la Espina, S.** (1982) Nucleolar fibrillar centres in plant meristematic cells: ultrastructure, cytochemistry and autoradiography: *Journal of Cell Science*, pp. 313-329.
- Rodley, G.A., Scobie, R.S., Bates, R.H.T. and Lewitt, R.M.** (1976) Possible conformation for double-stranded polynucleotides. *Proceedings of the National Academy of Sciences of the United States of America*, **73**, 2959-2963.
- Rosa, S., De Lucia, F., Mylne, J.S., Zhu, D., Ohmido, N., Pendle, A., Kato, N., Shaw, P. and Dean, C.** (2013) Physical clustering of FLC alleles during Polycomb-mediated epigenetic silencing in vernalization. *Genes & Development*, **27**, 1845-1850.
- Saad, H., Gallardo, F., Dalvai, M., Tanguy-le-Gac, N., Lane, D. and Bystricky, K.** (2014) DNA dynamics during early double-strand break processing revealed by non-intrusive imaging of living cells. *Plos Genetics*, **10**.
- Saez-Vasquez, J. and Medina, F.J.** (2008) The plant nucleolus. *Botanical Research: Incorporating Advances in Plant Pathology*, Vol. 47, **47**, 1-46.
- Sakamoto, T., Sakamoto, Y., Grob, S., Slane, D., Yamashita, T., Ito, N., Oko, Y., Sugiyama, T., Higaki, T., Hasezawa, S., Tanaka, M., Matsui, A., Seki, M., Suzuki, T., Grossniklaus, U. and Matsunaga, S.** (2022) Two-step regulation of centromere distribution by condensin II and the nuclear envelope proteins. *Nature Plants*, **8**, 940-953.
- Sakamoto, T., Sugiyama, T., Yamashita, T. and Matsunaga, S.** (2019) Plant condensin II is required for the correct spatial relationship between centromeres and rDNA arrays. *Nucleus*, **10**, 116-125.
- Sakamoto, Y.** (2020) Nuclear lamina CRWN proteins regulate chromatin organization, gene expression, and nuclear body formation in plants. *Journal of Plant Research*, **133**, 457-462.

- Sakamoto, Y. and Takagi, S.** (2013) LITTLE NUCLEI 1 and 4 regulate nuclear morphology in *Arabidopsis thaliana*. *Plant and Cell Physiology*, **54**, 622-633.
- Santos, A.P., Ferreira, L., Maroco, J. and Oliveira, M.M.** (2011) Abiotic stress and induced DNA hypomethylation cause interphase chromatin structural changes in rice rDNA loci. *Cytogenetic and Genome Research*, **132**, 297-303.
- Santos, A.P. and Shaw, P.** (2004) Interphase chromosomes and the Rab1 configuration: does genome size matter? *Journal of Microscopy*, **214**, 201-206.
- Sato, K.** (2020) History and future perspectives of barley genomics. *DNA Research*, **27**.
- Sato, K., Shin-I, T., Seki, M., Shinozaki, K., Yoshida, H., Takeda, K., Yamazaki, Y., Conte, M. and Kohara, Y.** (2009) Development of 5006 full-length cDNAs in barley: A tool for accessing cereal genomics resources. *DNA Research*, **16**, 81-89.
- Sato, K., Tanaka, T., Shigenobu, S., Motoi, Y., Wu, J.Z. and Itoh, T.** (2016) Improvement of barley genome annotations by deciphering the Haruna Nijo genome. *DNA Research*, **23**, 21-28.
- Savino, T.M., Gebrane-Younes, J., De Mey, J., Sibarita, J.B. and Hernandez-Verdun, D.** (2001) Nucleolar assembly of the rRNA processing machinery in living cells. *Journal of Cell Biology*, **153**, 1097-1110.
- Schaper, A., Rossle, M., Formanek, H., Jovin, T.M. and Wanner, G.** (2000) Complementary visualization of mitotic barley chromatin by field-emission scanning electron microscopy and scanning force microscopy. *Journal of Structural Biology*, **129**, 17-29.
- Schindelin, J., Arganda-Carreras, I., Frise, E., Kaynig, V., Longair, M., Pietzsch, T., Preibisch, S., Rueden, C., Saalfeld, S., Schmid, B., Tinevez, J.Y., White, D.J., Hartenstein, V., Eliceiri, K., Tomancak, P. and Cardona, A.** (2012) Fiji: an open-source platform for biological-image analysis. *Nature Methods*, **9**, 676-682.
- Schloissnig, S., Kawaguchi, A., Nowoshilow, S., Falcon, F., Otsuki, L., Tardivo, P., Timoshevskaya, N., Keinath, M.C., Smith, J.J., Voss, S.R. and Tanaka, E.M.** (2021) The giant axolotl genome uncovers the evolution scaling, and transcriptional control of complex gene loci. *Proceedings of the National Academy of Sciences of the United States of America*, **118**.
- Schubert, I. and Oud, J.L.** (1997) There is an upper limit of chromosome size for normal development of an organism. *Cell*, **88**, 515-520.
- Schubert, V.** (2017) Super-resolution microscopy: Applications in plant cell research. *Frontiers in Plant Science*, **8**.
- Schwammenhoferova, K. and Ondrej, M.** (1978) Mitotic-cycle kinetics of root-meristems of isolated barley embryos and intact seedlings - labeling of nuclei by tetraploidy. *Biologia Plantarum*, **20**, 409-417.
- Schwille, P., MeyerAlmes, F.J. and Rigler, R.** (1997) Dual-color fluorescence cross-correlation spectroscopy for multicomponent diffusional analysis in solution. *Biophysical Journal*, **72**, 1878-1886.
- Shan, Q.W., Wang, Y.P., Li, J. and Gao, C.X.** (2014) Genome editing in rice and wheat using the CRISPR/Cas system. *Nature Protocols*, **9**, 2395-2410.
- Shan, W., Kubova, M., Mandakova, T. and Lysak, M.A.** (2021) Nuclear organization in crucifer genomes: nucleolus-associated telomere clustering is not a universal interphase configuration in Brassicaceae. *Plant Journal*, **108**, 528-540.
- Sharma, V.K., Hansch, R., Mendel, R.R. and Schulze, J.** (2004) A highly efficient plant regeneration system through multiple shoot differentiation from commercial cultivars of barley (*Hordeum vulgare* L.) using meristematic shoot segments excised from germinated mature embryos. *Plant Cell Reports*, **23**, 9-16.

- Shaw, P. and Brown, J.** (2012) Nucleoli: composition, function, and dynamics. *Plant Physiology*, **158**, 44-51.
- Shaw, S.L., Kamyar, R. and Ehrhardt, D.W.** (2003) Sustained microtubule treadmilling in Arabidopsis cortical arrays. *Science*, **300**, 1715-1718.
- Shintomi, K. and Hirano, T.** (2010) Sister chromatid resolution: a cohesin releasing network and beyond. *Chromosoma*, **119**, 459-467.
- Silveira, S.R., Le Gloanec, C., Gomez-Felipe, A., Routier-Kierzkowska, A.L. and Kierzkowski, D.** (2022) Live-imaging provides an atlas of cellular growth dynamics in the stamen. *Plant Physiology*, **188**, 769-781.
- Simonis, M., Kooren, J. and de Laat, W.** (2007) An evaluation of 3C-based methods to capture DNA interactions. *Nature Methods*, **4**, 895-901.
- Singh, S., Nandha, P.S. and Singh, J.** (2017) Transposon-based genetic diversity assessment in wild and cultivated barley. *Crop Journal*, **5**, 296-304.
- Sirri, V., Hernandez-Verdun, D. and Roussel, P.** (2002) Cyclin-dependent kinases govern formation and maintenance of the nucleolus. *Journal of Cell Biology*, **156**, 969-981.
- Smertenko, A., Assaad, F., Baluska, F., Bezanilla, M., Buschmann, H., Drakakaki, G., Hauser, M.T., Janson, M., Mineyuki, Y., Moore, I., Muller, S., Murata, T., Otegui, M.S., Panteris, E., Rasmussen, C., Schmit, A.C., Samaj, J., Samuels, L., Staehelin, L.A., Van Damme, D., Wasteneys, G. and Zarsky, V.** (2017) Plant cytokinesis: Terminology for structures and processes. *Trends in Cell Biology*, **27**, 885-894.
- Smith, L.G., Gerttula, S.M., Han, S.C. and Levy, J.** (2001) TANGLED1: A microtubule binding protein required for the spatial control of cytokinesis in maize. *Journal of Cell Biology*, **152**, 231-236.
- Solovei, I., Cavallo, A., Schermelleh, L., Jaunin, F., Scasselati, C., Cmarko, D., Cremer, C., Fakan, S. and Cremer, T.** (2002) Spatial preservation of nuclear chromatin architecture during three-dimensional fluorescence in situ hybridization (3D-FISH). *Experimental Cell Research*, **276**, 10-23.
- Soppe, W.J.J., Jasencakova, Z., Houben, A., Kakutani, T., Meister, A., Huang, M.S., Jacobsen, S.E., Schubert, I. and Fransz, P.F.** (2002) DNA methylation controls histone H3 lysine 9 methylation and heterochromatin assembly in Arabidopsis. *Embo Journal*, **21**, 6549-6559.
- Southern, E.M.** (1975) Detection of specific sequences among DNA fragments separated by gel electrophoresis. *Journal of Molecular Biology*, **98**, 503-517.
- Stein, N., Prasad, M., Scholz, U., Thiel, T., Zhang, H., Wolf, M., Kota, R., Varshney, R.K., Perovic, G., Grosse, I. and Graner, A.** (2007) A 1000-loci transcript map of the barley genome: new anchoring points for integrative grass genomics: Theoretical and applied genetics, pp. 823-839.
- Stepinski, D.** (2014) Functional ultrastructure of the plant nucleolus. *Protoplasma*, **251**, 1285-1306.
- Stoppin, V., Vantard, M., Schmit, A.C. and Lambert, A.M.** (1994) Isolated plant nuclei microtubule assembly: The nuclear surface in higher plants has centrosome-like activity. *Plant Cell*, **6**, 1099-1106.
- Sun, M.X., Biggs, R., Hornick, J. and Marko, J.F.** (2018) Condensin controls mitotic chromosome stiffness and stability without forming a structurally contiguous scaffold. *Chromosome Research*, **26**, 277-295.
- Swanston, J.S., Wilhelmson, A., Ritala, A. and Gibson, B.R.** (2014) Malting, Brewing, and Distilling. *Barley: Chemistry and Technology, 2nd Edition*, 193-222.

- Takagi, M., Matsuoka, Y., Kurihara, T. and Yoneda, Y.** (1999) Chmadrin: a novel Ki-67 antigen-related perichromosomal protein possibly implicated in higher order chromatin structure. *Journal of Cell Science*, **112**, 2463-2472.
- Tamura, K., Fukao, Y., Iwamoto, M., Haraguchi, T. and Hara-Nishimura, I.** (2010) Identification and characterization of nuclear pore complex components in *Arabidopsis thaliana*. *Plant Cell*, **22**, 4084-4097.
- Tanaka, T., Ishikawa, G., Ogiso-Tanaka, E., Yanagisawa, T. and Sato, K.** (2019) Development of genome-wide SNP markers for barley via reference-based RNA-seq analysis. *Frontiers in Plant Science*, **10**.
- Tang, Y., Dong, Q.L., Wang, T.Y., Gong, L. and Gu, Y.N.** (2022) PNET2 is a component of the plant nuclear lamina and is required for proper genome organization and activity. *Developmental Cell*, **57**, 19-31.
- Tang, Y., Huang, A.B. and Gu, Y.N.** (2020) Global profiling of plant nuclear membrane proteome in *Arabidopsis*. *Nature Plants*, **6**, 838-847.
- Tatout, C., Evans, D.E., Vanrobays, E., Probst, A.V. and Graumann, K.** (2014) The plant LINC complex at the nuclear envelope. *Chromosome Research*, **22**, 241-252.
- Thomas, J.B. and Kaltsikes, P.J.** (1976) Bouquet-like attachment plate for telomeres in leptotene of rye revealed by heterochromatin staining. *Heredity*, **36**, 155-162.
- Thomas, W.T.B., Hayes, P.M. and Dahleen, L.S.** (2011) Application of molecular genetics and transformation to barley improvement. In: Steven E. Ullrich (ed.): *Barley: production, improvement, and uses*: Wiley-Blackwell, New Jersey, pp. 122-143.
- Tiang, C.L., He, Y. and Pawlowski, W.P.** (2012) Chromosome Organization and Dynamics during Interphase, Mitosis, and Meiosis in Plants. *Plant Physiology*, **158**, 26-34.
- Tomastikova, E., Demidov, D., Jerabkova, H., Binarova, P., Houben, A., Dolezel, J. and Petrovska, B.** (2015) TPX2 protein of *Arabidopsis* activates Aurora kinase 1, but not Aurora kinase 3 in vitro. *Plant Molecular Biology Reporter*, **33**, 1988-1995.
- Ubeda-Tomas, S., Federici, F., Casimiro, I., Beemster, G.T.S., Bhalerao, R., Swarup, R., Doerner, P., Haseloff, J. and Bennett, M.J.** (2009) Gibberellin signaling in the endodermis controls *Arabidopsis* root meristem size. *Current Biology*, **19**, 1194-1199.
- Ullrich, S.E.** (2014) The Barley Crop: Origin and Taxonomy, Production, and End Uses. *Barley: Chemistry and Technology, 2nd Edition*, 1-9.
- USDA** (2023) <https://www.ars.usda.gov>. Vided on 2023/08/22.
- Valuchova, S., Mikulkova, P., Pecinkova, J., Klimova, J., Krumnikl, M., Binar, P., Heckmann, S., Tomancak, P. and Riha, K.** (2020) Imaging plant germline differentiation within *Arabidopsis* flowers by light sheet microscopy. *Elife*, **9**.
- van Damme, D., Bouget, F.Y., van Poucke, K., Inze, D. and Geelen, D.** (2004) Molecular dissection of plant cytokinesis and phragmoplast structure: a survey of GFP-tagged proteins. *Plant Journal*, **40**, 386-398.
- Van Leene, J., Boruc, J., De Jaeger, G., Russinova, E. and De Veylder, L.** (2011) A kaleidoscopic view of the *Arabidopsis* core cell cycle interactome. *Trends in Plant Science*, **16**, 141-150.
- van Steensel, B. and Belmont, A.S.** (2017) Lamina-associated domains: Links with chromosome architecture, heterochromatin, and gene repression. *Cell*, **169**, 780-791.

- Vinje, M.A., Henson, C.A., Duke, S.H., Simmons, C.H., Le, K., Hall, E. and Hirsch, C.D.** (2021) Description and functional analysis of the transcriptome from malting barley. *Genomics*, **113**, 3310-3324.
- Vodermaier, H.C.** (2004) APC/C and SCF: Controlling each other and the cell cycle. *Current Biology*, **14**, R787-R796.
- von Bothmer, R., Jacobsen, N., Baden, C., Jorgensen, R.B. and Linde-Laursen, I.** (1995) An ecogeographical study of the genus *Hordeum* (2nd edition), pp. 195.
- von Bothmer, R., Sato, K., Komatsuda, T., Yasuda, S. and Fischbeck, G.** (2003) The domestication of cultivated barley. In *Diversity in Barley (Hordeum vulgare)* (In: R. von Bothmer, T.v.H., H. Knüpffer and K. Sato (eds) ed. Amsterdam, The Netherlands: Elsevier Sciences B.V, pp. 9-27.
- von Chamier, L., Laine, R.F. and Henriques, R.** (2019) Artificial intelligence for microscopy: what you should know. *Biochemical Society Transactions*, **47**, 1029-1040.
- von Wangenheim, D., Hauschild, R., Fendrych, M., Barone, V., Benkova, E. and Friml, J.** (2017) Live tracking of moving samples in confocal microscopy for vertically grown roots. *Elife*, **6**.
- Vos, J.W., Pieuchot, L., Evrard, J.L., Janski, N., Bergdoll, M., de Ronde, D., Perez, L.H., Sardon, T., Vernos, I. and Schmit, A.C.** (2008) The plant TPX2 protein regulates prospindle assembly before nuclear envelope breakdown. *Plant Cell*, **20**, 2783-2797.
- Vyplelova, P., Ovecka, M., Komis, G. and Samaj, J.** (2018) Advanced microscopy methods for bioimaging of mitotic microtubules in plants. *Mitosis and Meiosis, Pt B*, **145**, 129-158.
- Wang, C.M., Liu, C., Roqueiro, D., Grimm, D., Schwab, R., Becker, C., Lanz, C. and Weigel, D.** (2015) Genome-wide analysis of local chromatin packing in *Arabidopsis thaliana*. *Genome Research*, **25**, 246-256.
- Wang, H.Y., Dittmer, T.A. and Richards, E.J.** (2013) *Arabidopsis* CROWDED NUCLEI (CRWN) proteins are required for nuclear size control and heterochromatin organization. *Bmc Plant Biology*, **13**.
- Wanner, G., Formanek, H., Martin, R. and Herrmann, R.G.** (1991) High-resolution scanning electron microscopy of plant chromosomes. *Chromosoma*, **100**, 103-109.
- Watanabe, K., Pecinka, A., Meister, A., Schubert, I. and Lam, E.** (2005) DNA hypomethylation reduces homologous pairing of inserted tandem repeat arrays in somatic nuclei of *Arabidopsis thaliana*. *Plant Journal*, **44**, 531-540.
- Weimer, A.K., Demidov, D., Lermontova, I., Beeckman, T. and Van Damme, D.** (2016) Aurora kinases throughout plant development. *Trends in Plant Science*, **21**, 69-79.
- Wicker, T., Schulman, A.H., Tanskanen, J., Spannagl, M., Twardziok, S., Mascher, M., Springer, N.M., Li, Q., Waugh, R., Li, C.D., Zhang, G.P., Stein, N., Mayer, K.F.X. and Gundlach, H.** (2017) The repetitive landscape of the 5100 Mbp barley genome. *Mobile DNA*, **8**.
- Wilkins, B.J., Rall, N.A., Ostwal, Y., Kruitwagen, T., Hiragami-Hamada, K., Winkler, M., Barral, Y., Fischle, W. and Neumann, H.** (2014) A cascade of histone modifications induces chromatin condensation in mitosis. *Science*, **343**, 77-80.
- Wolffe, A.P. and Hayes, J.J.** (1999) Chromatin disruption and modification. *Nucleic Acids Research*, **27**, 711-720.

- Wolny, A., Cerrone, L., Vijayan, A., Tofanelli, R., Barro, A.V., Louveaux, M., Wenzl, C., Strauss, S., Wilson-Sanchez, D., Lymbouridou, R., Steigleder, S.S., Pape, C., Bailoni, A., Duran-Nebreda, S., Bassel, G.W., Lohmann, J.U., Tsiantis, M., Hamprecht, F.A., Schneitz, K., Maizel, A. and Kreshuk, A.** (2020) Accurate and versatile 3D segmentation of plant tissues at cellular resolution. *Elife*, **9**.
- Wu, Q.Y., Luo, A.D., Zadrozny, T., Sylvester, A. and Jackson, D.** (2013) Fluorescent protein marker lines in maize: generation and applications. *International Journal of Developmental Biology*, **57**, 535-543.
- Wu, T.M., Lin, K.C., Liao, W.S., Chao, Y.Y., Yang, L.H., Chen, S.Y., Lu, C.A. and Hong, C.Y.** (2016) A set of GFP-based organelle marker lines combined with DsRed-based gateway vectors for subcellular localization study in rice (*Oryza sativa* L.). *Plant Molecular Biology*, **90**, 107-115.
- Wu, Y., Wu, X.D., Lu, R., Zhang, J., Toro, L. and Stefani, E.** (2015) Resonant scanning with large field of view reduces photobleaching and enhances fluorescence yield in STED microscopy. *Scientific Reports*, **5**.
- Xu, X.F.M., Zhao, Q., Rodrigo-Peiris, T., Brkljacic, J., He, C.S., Muller, S. and Meier, I.** (2008) RanGAP1 is a continuous marker of the Arabidopsis cell division plane. *Proceedings of the National Academy of Sciences of the United States of America*, **105**, 18637-18642.
- Xu, X.M., Meulia, T. and Meier, I.** (2007) Anchorage of plant RanGAP to the nuclear envelope nuclear-pore-associated involves novel proteins. *Current Biology*, **17**, 1157-1163.
- Xue, G.P., Rae, A.L., White, R.G., Drenth, J., Richardson, T. and McIntyre, C.L.** (2016) A strong root-specific expression system for stable transgene expression in bread wheat. *Plant Cell Reports*, **35**, 469-481.
- Ye, X., Shrawat, A., Moeller, L., Rode, R., Rivlin, A., Kelm, D., Martinell, B.J., Williams, E.J., Paisley, A., Duncan, D.R. and Armstrong, C.L.** (2023) Agrobacterium-mediated direct transformation of wheat maize embryos through organogenesis. **14**.
- Yin, K., Ueda, M., Takagi, H., Kajihara, T., Aki, S.S., Nobusawa, T., Umeda-Hara, C. and Umeda, M.** (2014) A dual-color marker system for in vivo visualization of cell cycle progression in Arabidopsis. *Plant Journal*, **80**, 541-552.
- Yiu, S.H.** (1993) Food microscopy and the nutritional quality of cereal foods. *Food Structure*, **12**, 123-133.
- Yu, Y., Tomkins, J.P., Waugh, R., Frisch, D.A., Kudrna, D., Kleinhofs, A., Brueggeman, R.S., Muehlbauer, G.J., Wise, R.P. and Wing, R.A.** (2000) A bacterial artificial chromosome library for barley (*Hordeum vulgare* L.) and the identification of clones containing putative resistance genes. *Theoretical and Applied Genetics*, **101**, 1093-1099.
- Zeder, M.A.** (2008) Domestication and early agriculture in the Mediterranean basin: origins, diffusion, and impact. *Proceedings of the National Academy of Sciences of the United States of America*, **105**, 11597-11604.
- Zelazny, E., Borst, J.W., Muylaert, M., Batoko, H., Hemminga, M.A. and Chaumont, F.** (2007) FRET imaging in living maize cells reveals that plasma membrane aquaporins interact to regulate their subcellular localization. *Proceedings of the National Academy of Sciences of the United States of America*, **104**, 12359-12364.
- Zhao, L., Wang, S.Q., Cao, Z.L., Ouyang, W.Z., Zhang, Q., Xie, L., Zheng, R.Q., Guo, M.R., Ma, M., Hu, Z., Sung, W.K., Zhang, Q.F., Li, G.L. and Li, X.W.**

- (2019) Chromatin loops associated with active genes and heterochromatin shape rice genome architecture for transcriptional regulation. *Nature Communications*, **10**.
- Zhao, Z., Tavoosidana, G., Sjolinder, M., Gondor, A., Mariano, P., Wang, S., Kanduri, C., Lezcano, M., Sandhu, K.S., Singh, U., Pant, V., Tiwari, V., Kurukuti, S. and Ohlsson, R.** (2006) Circular chromosome conformation capture (4C) uncovers extensive networks of epigenetically regulated intra- and interchromosomal interactions. *Nature Genetics*, **38**, 1341-1347.
- Zheng, B.L., Chen, X.M. and McCormick, S.** (2011) The anaphase-promoting complex is a dual integrator that regulates both microRNA-mediated transcriptional regulation of Cyclin B1 and degradation of Cyclin B1 during Arabidopsis male gametophyte development. *Plant Cell*, **23**, 1033-1046.
- Zheng, Y.X., Wong, M.L., Alberts, B. and Mitchison, T.** (1995) Nucleation of microtubule assembly by gamma-tubulin-containing ring complex. *Nature*, **378**, 578-583.
- Zhou, S.L., Jiang, W., Zhao, Y. and Zhou, D.X.** (2019) Single-cell three-dimensional genome structures of rice gametes and unicellular zygotes. *Nature Plants*, **5**, 795-800.

10 LIST OF ABBREVIATIONS

3C	chromosome conformation capture
3D	three dimensional
4C	circular chromosome conformation capture
5C	3C-carbon copy
AFLP	amplified fragment length polymorphism
AGL1	<i>Agrobacterium tumefaciens</i> strain AGL1
ANCHOR	approach to monitor single-copy locus localization <i>in planta</i>
APC/C	ANAPHASE-PROMOTING COMPLEX/CYCLOSOME
BAC	bacterial artificial chromosome
BBM	BABY BOOM
bp	base pair
CAP-H	CONDENSIN-1 COMPLEX SUBUNIT H
CAP-H2	CONDENSIN-2 COMPLEX SUBUNIT H2
Cas9	CRISPR-associated protein 9
CCD	charge-coupled device
CDK	CYCLIN-DEPENDENT KINASES
cDNA	copy DNA
CDS	coding sequence
CENH3	CENTROMERIC HISTONE 3
CESA	CELLULOSE SYNTHASE
CFP	CYAN FLUORESCENT PROTEIN
ChIA-PET	chromatin interaction analysis with paired-end tag
ChIP	chromatin immunoprecipitation
ChIP-seq	chromatin immunoprecipitation with sequencing
CKI	CYCLIN-DEPENDENT KINASE INHIBITOR
COST	European cooperation in science and technology
CPNW	Czech plant nucleus workshop
CRWN	CROWDED NUCLEI
CSC	CELLULOSE SYNTHASE COMPLEX

CTCF	CCCTC-BINDING FACTOR
CYC	CYCLIN
dCas9	dead CRISPR associated protein 9
<i>ddm1</i>	<i>decrease in DNA methylation1</i>
ddPCR	digital droplet polymerase chain reaction
DNA	deoxyribonucleic acid
EHA105	<i>Agrobacterium tumefaciens</i> strain EHA105
EPI-CATCH	Epigenetic mechanisms of crop adaptation to climate change
EST	expressed sequence tags
EWPC	European workshop on plant chromatin
EYFP	ENHANCED YELLOW FLUORESCENT PROTEIN
FACS	fluorescence activated cell sorting
FCCS	fluorescence cross-correlation spectroscopy
FCS	fluorescence correlation spectroscopy
FIB1	FIBRILLARIN1
FISH	fluorescence in situ hybridization
FLIM	fluorescence-lifetime imaging microscopy
FLIP	fluorescence loss in photobleaching
FML	fluorescent marker line
FRAP	fluorescence recovery after photobleaching
FRET	Förster resonance energy transfer
G1	cell cycle phase G1
G2	cell cycle phase G2
Gbp	giga base pair
GFP	GREEN FLUORESCENT PROTEIN
GFR4	GROWTH-REGULATING FACTOR4
GIF1	GRF-INTERACTING FACTOR1
GTP	guanosine 5'-triphosphate
GW3101	<i>Agrobacterium tumefaciens</i> strain GW3101
H2B	HISTONE 2B

H3	histone 3
H3S10p	histone 3 serine 10 phosphorylation
H3T11p	histone 3 threonine 11 phosphorylation
H3T3p	histone 3 threonine 3 phosphorylation
Hi-C	high-throughput chromosome conformation capture
HiChIP	high-throughput chromatin immunoprecipitation
INDEPTH	Impact of Nuclear Domains On Gene Expression and Plant Traits
INM	inner nuclear membrane
ITS	internal transcribed spacer
KAKU4	JAPANESE FOR NUCLEUS 4
KASH	KLARSICHT ANC-1 SYNE HOMOLOGY
kbp	kilo base pair
LacI	lactose inhibitor
<i>lacO</i>	lactose operone
LBA4404	<i>Agrobacterium tumefaciens</i> strain LBA4404
LINC	LINKER OF NUCLEOSKELETON
LSCM	laser scanning confocal microscope
MAP	MITOGEN-ACTIVATED PROTEIN
Mbp	mega base pair
<i>met1</i>	<i>methyltransferase1</i>
mCHERRY	MONOMERIC CHERRY RED FLUORESCENT PROTEIN
MLKS2	MAIZE LINC KASH SINE-LIKE2
MTOC	microtubule-organizing center
NA	numerical aperture
NDC80	FOUR-PROTEIN NUCLEAR DIVISION CYCLE80
NE	nuclear envelope
NEAP	NUCLEAR ENVELOPE ASSOCIATED PROTEIN
NL	nuclear lamina
NOP52	NUCLEOLAR PROTEIN52
NOR	nucleolus organizing region

NPC	nuclear pore complex
NUF2	NUCLEAR FILAMENT-CONTAINING2 PROTEIN
NuMA	NUCLEAR MITOTIC APPARATHUS PROTEIN
NUP	NUCLEOPORIN
ONM	outer nuclear membrane
PALM	photo-activated localization microscopy
ParB	bacterial centromere-binding protein
<i>parS</i>	bacterial centromere or partition site
PCR	polymerase chain reaction
PDS5	PRECOCIOUS DISSOCIATION OF SISTERS 5
PNB	prenucleolar bodies
PNET1,2	PLANT NUCLEAR ENVELOPE TRANSMEMBRANE1,2
POL I	POLYMERASE I
PPB	preprophase band
pre-rRNA	pre-ribosomal ribonucleic acid
qPCR	quantitative polymerase chain reaction
RAE1	RIBONUCLEIC ACID EXPORT1
RanGAP	GTPase ACTIVATING PROTEIN
RanGDP	Ras-related nuclear protein guanosine 5'-diphosphate
RanGTP	Ras-related nuclear protein guanosine 5'-triphosphate
RFP	RED FLUORESCENT PROTEIN
RNA	ribonucleic acid
rRNA	ribosomal ribonucleic acid
S	synthesis cell cycle phase
SCC1	SISTER CHROMATID COHESION1
SCF	SKP-CULLIN1-F-BOX E3 LIGASE
sgRNA	single guide ribonucleic acid
SIM	structured illumination microscopy
siRNA	small interfering RNA
SMC	structural maintenance of chromosomes

snoRNA	small nucleolar ribonucleic acid
snoRNP	small nucleolar ribonucleoprotein
SNP	single nucleotide polymorphism
snRNA	spliceosomal small nucleolar ribonucleic acid
snRNP	spliceosomal small nucleolar ribonucleoprotein
STED	stimulated emission depletion
SUN	SAD1/UNC84 DOMAIN-CONTAINING PROTEIN
TADs	topologically associated domains
TAIL-PCR	thermal asymmetric interlaced polymerase chain reaction
TALEN	transcription activator-like effector nucleases
TAN1	TANGLED1
T-DNA	transferred DNA
TPX2	TARGETING PROTEIN FOR XKLP2
TRM6,7,8	TONNEAU1 RECRUITMENT MOTIF6,7,8
TUA3	TUBULIN ALPHA CHAIN 3
WAPL	WINGS APART-LIKE
WUS2	WUSCHEL 2
ZF	zinc finger
γ -TuRC	γ -TUBULIN RING COMPLEXES

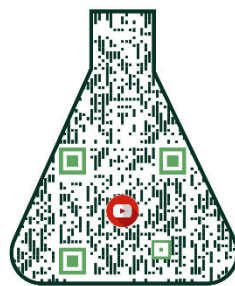
11 SUPPLEMENTARY MATERIAL

11.1 Supplementary video 1.



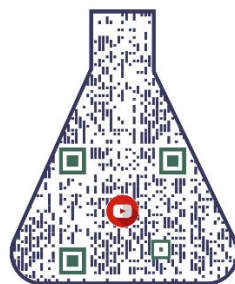
Time-lapse microscopy of nucleoli (EYFP-FIB1) and microtubules (mCHERRY-TUA3) in barley roots. The root was photographed for 22 min and 45 sec in 30-sec intervals.

11.2 Supplementary video 2.



Time-lapse microscopy of chromatin (EYFP-H2B) and microtubules (mCherry-TUA3) in barley roots. The root was photographed for 36 min and 45 sec in 30-sec intervals.

11.3 Supplementary video 3.



Time-lapse microscopy of chromatin (CFP-H2B) and nucleoli (EYFP-FIB1) in barley roots. The root was photographed for 23 min and 30 sec in 15-sec intervals.

12 LIST OF APPENDICES

First author publications

- Appendix I Image analysis workflows to reveal the spatial organization of cell nuclei and chromosomes
- Appendix II Spatial organization and dynamics of chromosomes during barley mitosis
- Appendix III 3D print user-optimized sample holder for confocal microscopy of plant roots

Co-authorship publications

- Appendix IV Proteome analysis of condensed barley mitotic chromosomes

Published abstracts – poster presentation

- Appendix V Towards in vivo analysis of chromatin dynamics in barley
- Appendix VI Developing system for tracking in planta chromatin dynamics in barley (*Hordeum vulgare*)

Appendix I

Image analysis workflows to reveal the spatial organization of cell nuclei and chromosomes

Randall, R.S.[†], Jourdain, C.[†], Nowicka, A.[†], **Kaduchová, K.**[†], Kubová, M.[†], Ayoub, M.A.[†], Schubert, V.[†], Tatout, Ch.[†], Colas, I.[†], Kalyanikrishna, Desset, S., Mermet, S., Stevens, A., Kubalova, I., Mandáková, T., Heckmann, S., Lysak, M.A., Panatta, M., Santoro, R., Schubert, D., Pecinka, A., Routh, D., and Baroux, C.

[†]Authors contributed equally

Nucleus

DOI: <https://doi.org/10.1080/19491034.2022.2144013>

IF (2022): 3.45



Image analysis workflows to reveal the spatial organization of cell nuclei and chromosomes

Ricardo S Randall, Claire Jourdain, Anna Nowicka, Kateřina Kaduchová, Michaela Kubová, Mohammad A. Ayoub, Veit Schubert, Christophe Tatout, Isabelle Colas, Kalyanikrishna, Sophie Desset, Sarah Mermet, Aurélia Boulaflous-Stevens, Ivona Kubalová, Terezie Mandáková, Stefan Heckmann, Martin A. Lysak, Martina Panatta, Raffaella Santoro, Daniel Schubert, Ales Pecinka, Devin Routh & Célia Baroux

To cite this article: Ricardo S Randall, Claire Jourdain, Anna Nowicka, Kateřina Kaduchová, Michaela Kubová, Mohammad A. Ayoub, Veit Schubert, Christophe Tatout, Isabelle Colas, Kalyanikrishna, Sophie Desset, Sarah Mermet, Aurélia Boulaflous-Stevens, Ivona Kubalová, Terezie Mandáková, Stefan Heckmann, Martin A. Lysak, Martina Panatta, Raffaella Santoro, Daniel Schubert, Ales Pecinka, Devin Routh & Célia Baroux (2022) Image analysis workflows to reveal the spatial organization of cell nuclei and chromosomes, *Nucleus*, 13:1, 277-299, DOI: [10.1080/19491034.2022.2144013](https://doi.org/10.1080/19491034.2022.2144013)

To link to this article: <https://doi.org/10.1080/19491034.2022.2144013>



© 2022 The Author(s). Published by Informa UK Limited, trading as Taylor & Francis Group.



[View supplementary material](#)



Published online: 29 Nov 2022.



[Submit your article to this journal](#)



[View related articles](#)



[View Crossmark data](#)

RESEARCH PAPER

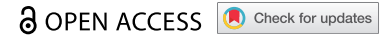










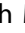













Image analysis workflows to reveal the spatial organization of cell nuclei and chromosomes

Ricardo S Randall ^{ar*}, Claire Jourdain ^{br*}, Anna Nowicka ^{cr*}, Kateřina Kaduchová ^{cr*}, Michaela Kubová ^{dr*}, Mohammad A. Ayoub ^{er*}, Veit Schubert ^{er*}, Christophe Tatout ^{fr*}, Isabelle Colas ^{gr*}, Kalyanikrishna ^b, Sophie Desset ^f, Sarah Mermet ^f, Aurélia Boulaflous-Stevens ^f, Ivona Kubalová ^e, Terezie Mandáková ^d, Stefan Heckmann ^e, Martin A. Lysak ^h, Martina Panatta ⁱ, Raffaella Santoro ⁱ, Daniel Schubert ^b, Ales Pecinka ^c, Devin Routh^j, and Célia Baroux ^a

^aDepartment of Plant and Microbial Biology, Zürich-Basel Plant Science Center, University of Zürich, Zürich, Switzerland; ^bInstitute of Biology, Freie Universität Berlin, Germany; ^cCentre of the Region Haná for Biotechnological and Agricultural Research (CRH), Institute of Experimental Botany, v. v. i. (IEB), Olomouc, Czech Republic; ^dCentral European Institute of Technology (CEITEC) and Department of Experimental Biology, Masaryk University, Brno, Czech Republic; ^eLeibniz Institute of Plant Genetics and Crop Plant Research (IPK) Gatersleben, D-06466 Seeland, Germany; ^fInstitut Génétique, Reproduction et Développement (GrED), Université Clermont Auvergne, CNRS, INSERM, 63001 Clermont-Ferrand, France; ^gThe James Hutton Institute, Errol Road, Invergowrie, DD2 5DA, Scotland UK; ^hCentral European Institute of Technology (CEITEC) and National Centre for Biomolecular Research, Masaryk University, Brno, Czech Republic; ⁱDepartment of Molecular Mechanisms of Disease, DMMD, University of Zürich, Zürich, Switzerland; ^jService and Support for Science IT (S3IT), Universität Zürich, Zürich, Switzerland

ABSTRACT

Nucleus, chromatin, and chromosome organization studies heavily rely on fluorescence microscopy imaging to elucidate the distribution and abundance of structural and regulatory components. Three-dimensional (3D) image stacks are a source of quantitative data on signal intensity level and distribution and on the type and shape of distribution patterns in space. Their analysis can lead to novel insights that are otherwise missed in qualitative-only analyses. Quantitative image analysis requires specific software and workflows for image rendering, processing, segmentation, setting measurement points and reference frames and exporting target data before further numerical processing and plotting. These tasks often call for the development of customized computational scripts and require an expertise that is not broadly available to the community of experimental biologists. Yet, the increasing accessibility of high- and super-resolution imaging methods fuels the demand for user-friendly image analysis workflows. Here, we provide a compendium of strategies developed by participants of a training school from the COST action INDEPTH to analyze the spatial distribution of nuclear and chromosomal signals from 3D image stacks, acquired by diffraction-limited confocal microscopy and super-resolution microscopy methods (SIM and STED). While the examples make use of one specific commercial software package, the workflows can easily be adapted to concurrent commercial and open-source software. The aim is to encourage biologists lacking custom-script-based expertise to venture into quantitative image analysis and to better exploit the discovery potential of their images.

Abbreviations: 3D FISH: three-dimensional fluorescence in situ hybridization; 3D: three-dimensional; ASY1: ASYNAPTIC 1; CC: chromocenters; CO: Crossover; DAPI: 4',6-diamidino-2-phenylindole; DMC1: DNA MEIOTIC RECOMBINASE 1; DSB: Double-Strand Break; FISH: fluorescence in situ hybridization; GFP: GREEN FLUORESCENT PROTEIN; HEI10: HUMAN ENHANCER OF INVASION 10; NCO: Non-Crossover; NE: Nuclear Envelope; Oligo-FISH: oligonucleotide fluorescence in situ hybridization; RNPII: RNA Polymerase II; SC: Synaptonemal Complex; SIM: structured illumination microscopy; ZMM (ZIP: MSH4: MSH5 and MER3 proteins); ZYP1: ZIPPER-LIKE PROTEIN 1.

ARTICLE HISTORY

Received 28 June 2022
Revised 27 October 2022
Accepted 31 October 2022



KEYWORDS


Nucleus; chromatin; 3D organization; spatial distribution; image analysis; segmentation; quantification; mitosis; meiosis; chromosome; metaphase; pachytene; crossovers; nuclear speckles; nuclear bodies; RNA Pol II; transcription factories; oligo FISH; STED imaging; SIM

Introduction

Elucidating the spatial organization of eukaryotic genomes, their structural and compositional

dynamics during cellular processes and functional relationship with the nucleus, is a keystone of three-dimensional (3D) genomics. 3D genomics

CONTACT Célia Baroux  cbaroux@botinst.uzh.ch  Department of Plant and Microbial Biology, Zürich-Basel Plant Science Center, University of Zürich, Zürich, Switzerland
*equal contribution

 Supplemental data for this article can be accessed online at <https://doi.org/10.1080/19491034.2022.2144013>

© 2022 The Author(s). Published by Informa UK Limited, trading as Taylor & Francis Group.
This is an Open Access article distributed under the terms of the Creative Commons Attribution License (<http://creativecommons.org/licenses/by/4.0/>), which permits unrestricted use, distribution, and reproduction in any medium, provided the original work is properly cited.

aims to decipher the functional, 3D organizing principles of the chromosomes, chromatin domains and nucleus that contribute to transcription, replication, repair, and recombination. Understanding the 3D genome requires multidisciplinary methods including high-throughput, sequencing-based, molecular profiling techniques, computational simulation-based biophysical and mathematical modeling, and microscopy imaging at high-to-super resolution and in three-dimensions [1,2]. Microscopy followed by image analysis provides the opportunity to measure chromosome and chromatin structures down to the nanoscale, with a few kilobase resolution. This can inform on the genomic interactions *in situ* and the spatial organization of genomic domains in relation to the 3D nuclear space and its functional compartments [3,4].

Venturing into these opportunities to probe for the spatial organization of the genome *in situ* requires dedicated imaging and image analysis procedures, recently captured by the concept of quantitative, data-driven microscopy [1]. Quantitative image analysis for nuclear and chromosomal studies can be implemented at different levels of complexity, depending on the research question and, often, the expertise available. For instance, a simple level consists of scoring structures or patterns on the image based on user-defined classification. This can be applied when the immunolabelled chromatin protein, or FISH-labeled genomic domain, shows a very distinct distribution pattern (e.g. punctuate vs diffuse), varying between treatments or genotypes. In this case, quantifying the relative occurrence of pattern categories by scoring may be sufficient to address the original question. Manual scoring can also be used to quantify a moderate number of labeled regions (e.g., number of FISH signals or nuclear bodies). These categorical, quantitative approaches have the virtue to be accessible to all experimentalists, without sophisticated software. They allow to characterize relatively simple signal distribution patterns, providing, however, a limited number of samples, and double-blind scoring to avoid cognitive biases. Yet, for many images (e.g., from high-throughput imaging), images with multiple

labels, showing complex spatial patterns of signal distribution, with continuous (rather than discrete) variation in signal abundance, or a combination of all, require computationally driven processing approaches for quantitative analyses. A core step required is image segmentation. This process partitions the image based on the signal distribution into digital objects identifying biologically relevant structures. Various image segmentation methods and algorithms exist. These perform differently depending on the signal distribution [5], with deep-learning approaches for automated segmentation tasks at a large scale being continuously developed [6]. Once the image is segmented, multiple features can be extracted from the 3D digital objects, for instance, object number, size and shape; signal intensity and variance per object type, texture of the signal, channel and position in the image; distance relationships, and spatial distribution. Practically, these features are highly relevant to analyze the spatial organization of chromatin, chromosome and nuclear components *in situ*.

The field of chromatin, chromosome and nuclear organization studies would greatly benefit from the broader deployment of image processing-based quantitative analyses [2,3]. Several tools and packages have been developed in the past years based on open-source software, including for the 3D spatial analysis of nuclear organization [7–11]. Yet, a major hurdle for most ‘biology-only’ oriented labs is the lack of computational expertise for customizing the image processing scripts, for large data handling, the lack of template workflows, or a combination thereof. Key concepts, from image acquisition to quantitative data, have been framed in recent years, for applications in cell biology, but also to set good practice and standards in the field [1,12]. Efforts are undertaken to promote education and support in image analysis for scientists dealing with biological images [13]. This resource paper contributes to these efforts by providing a compendium of image analysis workflows for nucleus, chromatin and chromosome studies, taking seven case-studies as examples developed by participants of the training school of the INDEPTH COST action [14].

The workflows are based on a user-friendly, commercial image processing software (Imaris, Bitplane, Switzerland) but are conceptually applicable to concurrent (commercial or open source) software as discussed in this paper. In addition, although they largely borrow examples from plant nuclei and chromosomes, they remain transferable to the study of animal nuclei. Indeed, the organization of the nucleus, including the nuclear envelope, chromatin domains and chromosomes, share common organizing principles in plants and animals [15–18]

The workflows associated with each case study are briefly described below and are illustrated in the related figures. Each workflow is associated with a Supplemental File folder that includes a step-by-step guideline (text); a table summarizing the main step functions and parameters used on the training image; one or two training images per workflow; and, for workflow 1, a video tutorial. Training image datasets are available on the INDEPTH-OMERO repository [13,14].¹

Analyzing the spatial distribution of transcription clusters

In mammals, a radial gradient model of transcription in the nucleus has been proposed [19,20]. In plants, including the *Arabidopsis thaliana* (*Arabidopsis*) plant model, little is known about the spatial, 3D distribution of transcription. Transcriptional activity in the nucleus can be visualized *in situ* by immunolabeling the active isoform of RNA Polymerase II (RNPII). In *Arabidopsis*, super-resolution imaging of RNPII has shown a reticulate pattern throughout the nucleoplasm along which distributed clusters of variable size and intensity exist [21,22].

To resolve the spatial distribution of RNPII signals in *Arabidopsis* nuclei in 3D, we imaged RNPII and DNA using 3D-STED microscopy. To quantify RNPII foci distribution, we designed an image analysis workflow (Figure 1a and Supplemental File 1). Sample preparation and imaging are described elsewhere [23]. Deconvolved STED images are segmented using the Imapris software (Bitplane, Switzerland) to create digital objects corresponding to the nucleus, the nucleolus, the chromocenters and

the RNPII signals (Figure 1b-d, Supplemental File 1 – Video 1). The surface object corresponding to the nucleus is also used to apply a 3D mask to separate the true image from the background signal (compare the framed regions in Figure 1b-c). While the nucleus and nucleolus are segmented based on smoothed, manual contours, heterochromatin is segmented using the supervised automated tool. Chromocenters (CCs) are typically large, brightly stained regions. In *Arabidopsis* nuclei, these are discrete and relatively easy to segment (Figure 1d, inset d1). Super-resolution imaging revealed that additional heterochromatin regions, which we termed nanochromocenters (nanoCC), can also be segmented (Figure 1d, inset d2). RNPII signal shows a complex nuclear distribution in *Arabidopsis* nuclei: rather than being discrete, it spreads unevenly in a reticulated manner with, however, clearly identifiable local clusters [22]. Our aim was to segment the image to discretize RNPII signal and focus on the clusters, considering their variable size, to further analyze their variability in intensity, size and spatial distribution. We applied the growing spot function in an iterative manner and could capture 70–80% of the RNPII signal in spots of variable size (Figure 1e, inset e2). This stepwise segmentation resulted in a digital image composed of objects capturing the nucleus, the nucleolus, the chromocenters and RNPII clusters (Figure 1f). Variables of interest, such as signal intensity per channel, object size and shape and distance between objects (spot-to-spot, spot-to-surface) were exported for each object type and channel.

The high number of variables, object type, channels, image replicates and levels of comparison (such as genotypes and treatment) dramatically increases data complexity. To facilitate data exploration, we built a stand-alone data visualization interface named *DataViz* (<https://github.com/barouxlab/DataViz>) which allows one to interactively plot all, or a subset of, data. This also enables custom variable creation for the normalization of distances and intensity per image (Figure 1g-i, Supplemental File 1 – *Dataviz_guidelines*). Here, we provide a few examples of violin plots (Figure 1g), density distributions (Figure 1h) and scatter plots with

a Workflow 1 (overview)

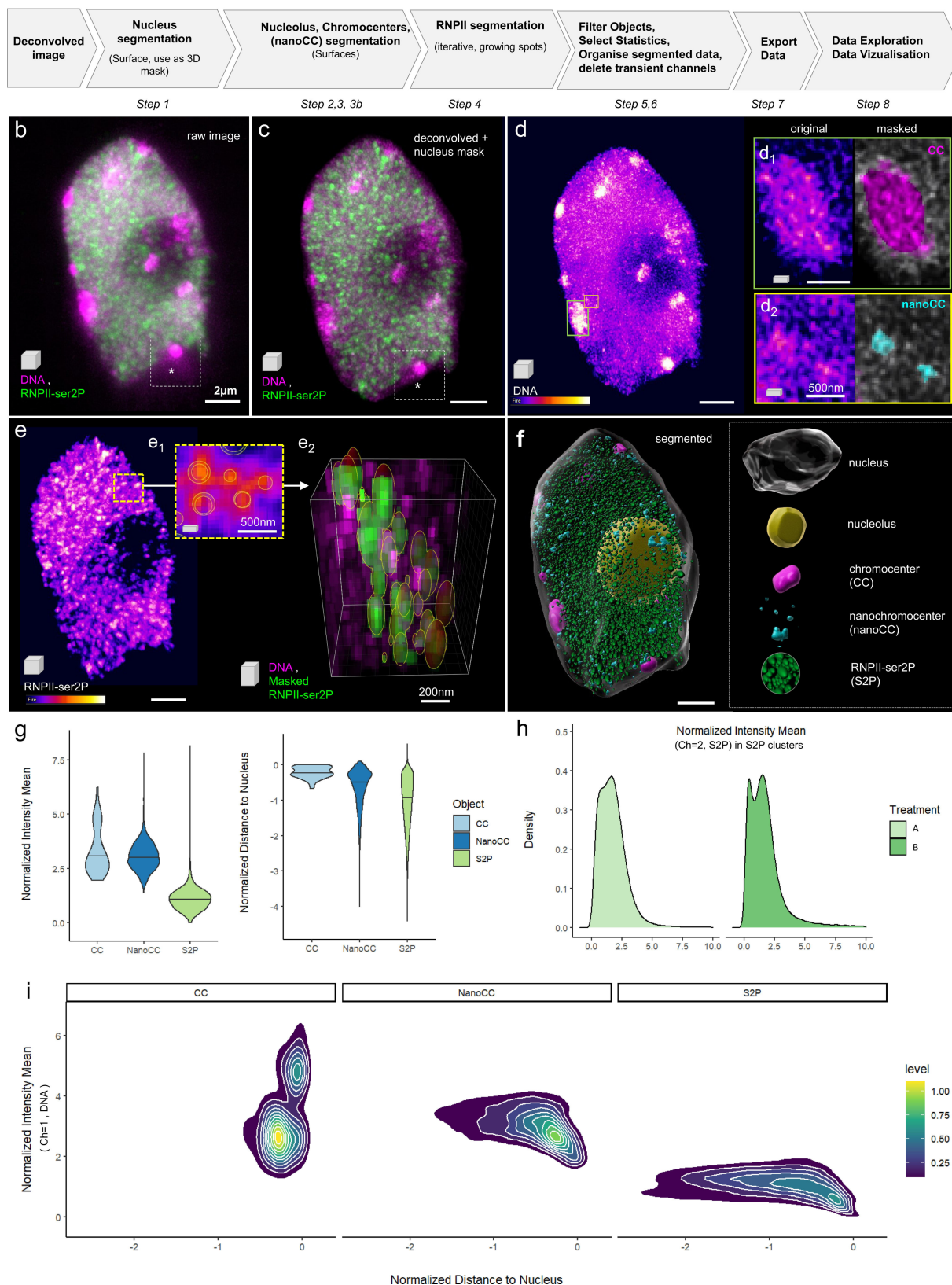


Figure 1. Analysis of the spatial distribution of RNA Pol II clusters in intact nuclei. (a) Overview of the workflow illustrated in b-i; (b) 3D projection of a 3D-STED image reporting on immunolabelled RNA Pol II (isoform phosphorylated on SerP, green, RNPII-ser2P) and DNA (magenta, Hoechst 580CP [26]), raw image; (c) Same image following deconvolution, nucleus contour segmentation and masking; (d) Intensity-coded coloring mode (Fire) of the DNA channel and frames magnified in the insets showing examples of

density contours (Figure 1i). The mean intensity, normalized per nucleus, of the DNA signal shows that the average and range of chromatin compaction in CC and nanoCC is largely similar, while nanoCC occasionally shows a higher compaction (upper tail of the violin plot, Figure 1g). By contrast, and as expected for transcriptionally active regions, chromatin is, on average, 2–3x less condensed in the RNPII-S2P clusters (Figure 1g). Also, plotting the shortest distance of each object to the nucleus surface (Figure 1g, right plot: the negative values indicate distance toward the nucleus interior), confirms the peripheral localization of CC as already described [24,25], an apparent enrichment of the nanoCC toward the periphery (although less pronounced than CC), and spreading of the RNPII-S2P clusters from the periphery toward the nuclear interior (with an apparent decreasing occurrence linked to the presence of the nucleolus). Further, plotting the density distribution of RNPII-S2P signals in the clusters (normalized mean intensity) allows detecting different structures of the RNPII landscape between different treatments (A and B in the example provided Figure 1h). Finally, DataViz enables exploring the relationship between two continuous variables using scatter plots, with or without density contours. In the example provided Figure 1i, we interrogated the relationship between the distance to the nucleus boundary and the mean DNA intensity for each of the nuclear domains segmented as CC, nanoCC and S2P clusters. The plots suggested (i) two categories of CC distinctive mostly by their intensity but slightly different with regard to their peripheral position and

that (ii) nanoCC and transcription clusters closer to the periphery are on average less compact than their counterparts located more toward the nuclear interior. These are only a few examples of the numerous possible plots that collectively contribute to data mining and discovery.

The segmentation process described in detail in the supplemental material corresponds to a user-supervised workflow. The input values (threshold, smoothing factor, or filtering values) are either software-defined values (and depend on image attributes) or customized by the user to best capture the biological objects. The parameters are then saved and re-applied for subsequent image replicate analyses. If the image quality is highly reproducible, it is further possible to apply automated batch-segmentation (following the software provider's instructions). For a trained user, the workflow takes *ca.* 45 min per image or less. Finally, this workflow can be further applied for the analysis of other types of nuclear signals showing punctate distribution similar to that in our example.

Analysis of the spatial distribution of proteins located at the nuclear periphery

To date, the distribution of nuclear envelope (NE)-associated proteins is poorly documented in plants. 3D microscopy-based observations may provide new insights into the organization of chromatin domains at the nuclear periphery at the single-cell level.

In this example, we developed a workflow to quantify the spatial pattern of a protein heterogeneously distributed within the NE (Figure 2a).

chromocenters (CC, d1) and nanochromocenters (nanoCC, d2) in the original channel (left) and after segmentation and pseudo-coloring (right); **(e)** Intensity-coded coloring mode (Fire) of the RNPII-ser2P channel showing a dense distribution of clusters with identifiable intensity peaks, enabling segmentation as adaptive spots (e1, e2), e1: single plane showing the spot contours; e2, 3D segment of the image after segmentation, clusters pseudo-colored in green, DNA in magenta. **(f)** Fully segmented image containing surface (nucleus, nucleolus, CC and nanoCC) and spot objects (RNPII-ser2P, abbreviated S2P). **(g-i)** Data exploration using *DataViz* (github.com/barouxlabs/DataViz, Supplemental File 1- *Dataviz_guidelines*). **(g)**, Violin plots showing a similar DNA density distribution in CC and nanoCC but much lower density in S2P clusters (intensity mean, DNA channel, normalized per image) and a sharp peripheral location of CC as formerly described (Andrey et al., 2010; Fransz et al., 2002), contrasting with the more dispersed distribution of nanoCC and S2P clusters (distance to nucleus surface (0) normalized using the nucleus center of mass as reference); **(h)** Example showing an application of the workflow, to compare the distribution of RNPII cluster intensities between two treatments: A and B. **(i)** Another example illustrating one of the many analyses enabled by the workflow and *DataViz*, with density scatter plots of DNA intensity means in RNPII clusters as a function of their distance to the nucleus surface. Scale bars: b-f, 2 μ m; insets, as indicated.

a Workflow 2 (overview)

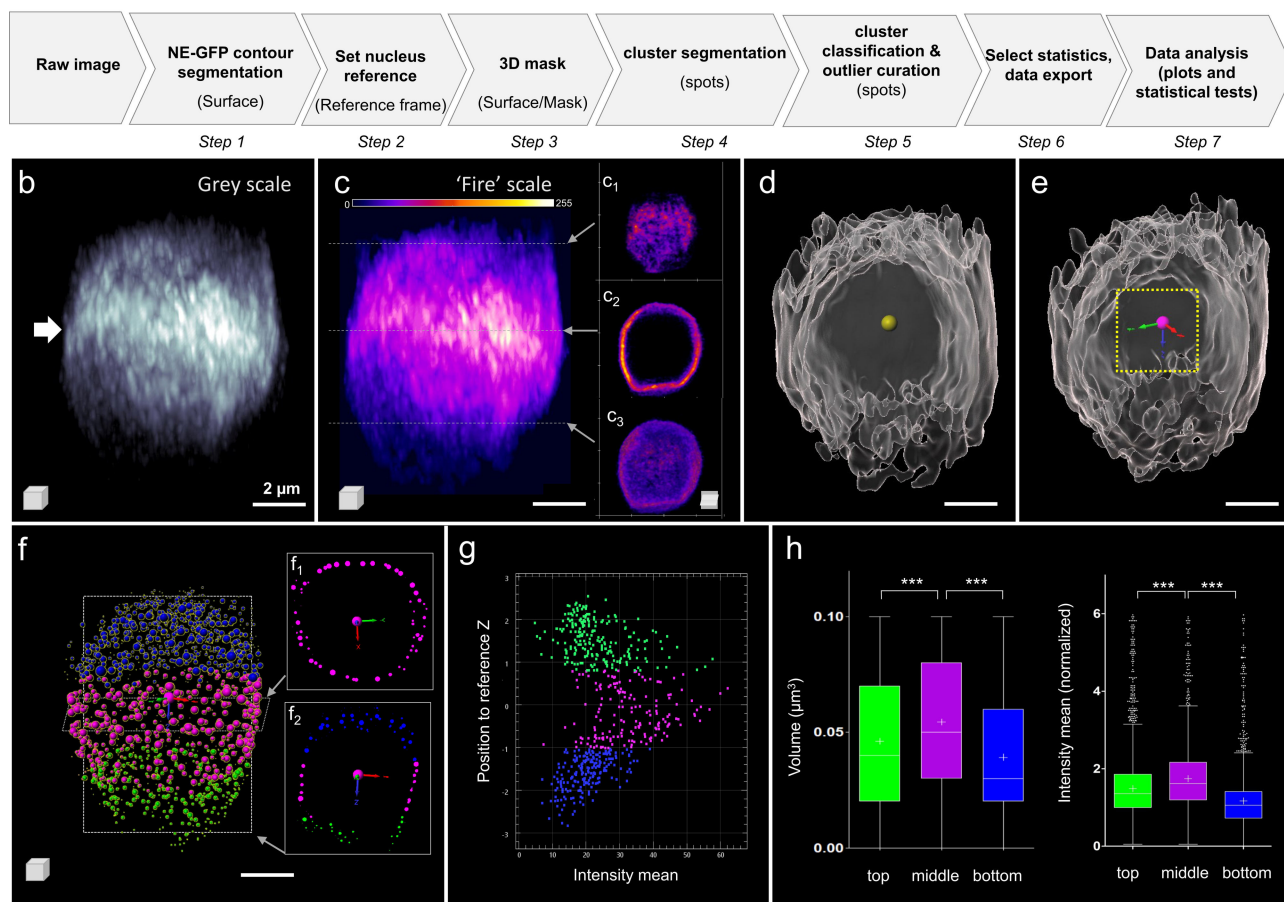


Figure 2. Analysis of the spatial distribution of a fluorescently tagged protein associated with the nuclear envelope. (a) Overview of the Image analysis workflow. Details of the parameters are in supplements. (b) Raw image of NE-GFP (Nuclear Envelope – associated protein fused to GFP) signal in a root nucleus; 3D rendering in gray levels suggests an enrichment of the protein at the equatorial region of the nucleus (white arrow). (c) Same image (3D) as in (b) using a fire color scale for NE-GFP signal intensities display (0–255); c1-c3 insets: cross sections at selected top, middle and bottom planes, respectively. (d) Result of the segmentation of the NE-GFP signal domain as a surface (gray); a spot (yellow) is created at the surface' center-of-mass. (e) A new XYZ coordinate system (reference frame) is docked at the center-of-mass. (f) The NE-GFP signal is segmented as spots of adaptive size ('growing spots') using the channel masked by the surface; spots are classified according to their axial (z) position, the equatorial region is defined $\pm 2 \mu\text{m}$ around the origin. Three spot classes are created located at the top, middle and bottom of the nucleus (blue, magenta, green, respectively). f1, f2 insets: XY and XZ sections. (g) The intensity mean of the spots is plotted as a function of their axial position (z) relative to the new reference frame for the image shown in (b-f). The colors indicate the 'top', 'middle' and 'bottom' classes, respectively. (h) The volume and normalized intensity mean of NE-GFP spots are plotted for each class, for $n = 8$ nuclei images segmented following this workflow. Kruskal-Wallis and Dunn's multiple comparison tests with bottom vs middle and top vs middle indicate statistically significant differences with $P < 0.001$ (***) for both variables. Scale bars: $2 \mu\text{m}$.

We imaged *Arabidopsis* root nuclei expressing a GFP-tagged protein associated with the NE (NE-GFP, *Tatout*, *Mermet*, *Boulaflous-Stevens*, unpublished) from 1 week old seedlings using a confocal microscope equipped with an Airyscan module [27] (Supplemental File 2-Figure 2). The NE-GFP protein is located at the NE and forms clusters of variable size; these clusters appear to be asymmetrically distributed (arrow, Figure 2b). Intensity-based

coloring of the signal confirmed the enrichment of NE-GFP at the equatorial plane of the nucleus, in contrast to that at the top and bottom poles (Figure 2c and insets). The first step in our procedure was to segment the global domain of NE-GFP signal using the 'Surface' function of Imaris (Figure 2d). Subsequently, we created a spot at the center of mass of the segmented NE-GFP surface (yellow spot, Figure 2d) and used it to create a 'Reference

frame' object (Figure 2e). This new XYZ coordinate system at the nucleus' center allows to classify the NE-GFP clusters at a later stage. The NE-GFP clusters are segmented as spots of adaptive size on the NE-GFP domain masked on the surface created at step 1 (Step 3–4, Supplemental File 2). Spots were classified into three categories (top:blue, middle:magenta, bottom:green) according to their axial position in the coordinate system defined at step 2 (Step 5, Figure 2f). The 'middle' class is defined by a region encompassing the origin of this coordinate system from -2 to $+2$ μm along the z-axis. The 'top' and 'bottom' classes capture the spots above and below this equatorial region, respectively. In addition, this step included curation of the segmentation results to (i) keep spots strictly located at the periphery (removing outliers located internally due to surface invaginations) and (ii) to select spots of biologically relevant size (up to 600 nm diameter, ~ 1.1 μm^3 ; detailed procedure in Supplemental File 2). A 2D-plot of the mean intensity of segmented NE-GFP spots according to their axial (x) position in this coordinated system revealed higher signal intensity among spots located at the equatorial plane ('middle' class, Figure 2g). The segmentation of multiple images supported this finding (Figure 2h). Importantly, as fluorescence intensities varied between images, the mean intensity of each spot was normalized, following export, using the mean intensity within the NE-GFP surface for each image (Figure 2h). This analysis revealed that both the volume and mean intensity of NE-GFP clusters in the equatorial plane ('middle' class) are significantly different from that of the clusters located at the polar regions ('top' and 'bottom' classes; Figure 2h, Kruskal-Wallis and Dunn's multiple comparison test with $P < 0.0001$ for all pairs).

In conclusion, this image analysis workflow enables quantification of the spatial heterogeneity of proteins associated with the nuclear envelope. In combination with mutant genetics, this approach enables one to assess the quantitative influence of candidate regulators and that of intrinsic (protein) domains on spatial protein localization.

Analysis of protein distribution on meiotic chromosomes

Meiosis is a special type of cell division occurring during sexual reproduction and enabling genetic recombination. During the first stage of meiosis, prophase I, homologous chromosomes align along their entire length by a protein structure called the synaptonemal complex (SC). This process is essential for crossover (CO) formation in many eukaryotes. Prophase I is itself divided into five substages – leptotene, zygotene, pachytene, diplotene and diakinesis. Each stage can be monitored by immunostaining specific proteins involved in SC formation. The most common targets are ASY1 (ASYNAPTIC 1) and ZYP1 (ZIPPER-LIKE 1) [28]. During prophase I, homologous recombination starts with the formation of SPO11-programmed DNA double-strand breaks (DSB) [29]. These DSBs are subsequently processed and recombinases such as DMC1 (DNA MEIOTIC RECOMBINASE 1) mediate strand invasion, essential for CO formation [30]. In barley, a large number of DSBs are formed [31], but only 13–22 (depending on the cultivar and scoring method) are repaired to crossover (CO), while the rest are repaired as non-crossovers (NCO) [32,33]. What controls the fate of DSB (CO vs NCO) is poorly understood. A current hypothesis involves HEI10 (HUMAN ENHANCER OF INVASION 10), a ZMM class-of-protein in the CO repair pathway, as an early indicator [34].

To elucidate whether HEI10 also contributes to DSB fate designation in barley, one approach is to elucidate the dynamics of HEI10 foci along prophase chromosomes at early, mid, and late stages, and in relation to DMC1 at early prophase. This approach requires 3D imaging of (immunostained) meiotic proteins on prophase chromosomes and the scoring of HEI10 vs DMC1 foci in relation to the prophase stage. We describe here a workflow to process 3D-SIM images to enable the scoring and classification of DMC1 and HEI10 foci depending on their size and intensity.

The workflow (Figure 3a) is illustrated with two images of barley male meiocytes labeled for components of the SC (ASY1, ZYP1), processed DSBs

a Workflow 3 (overview)

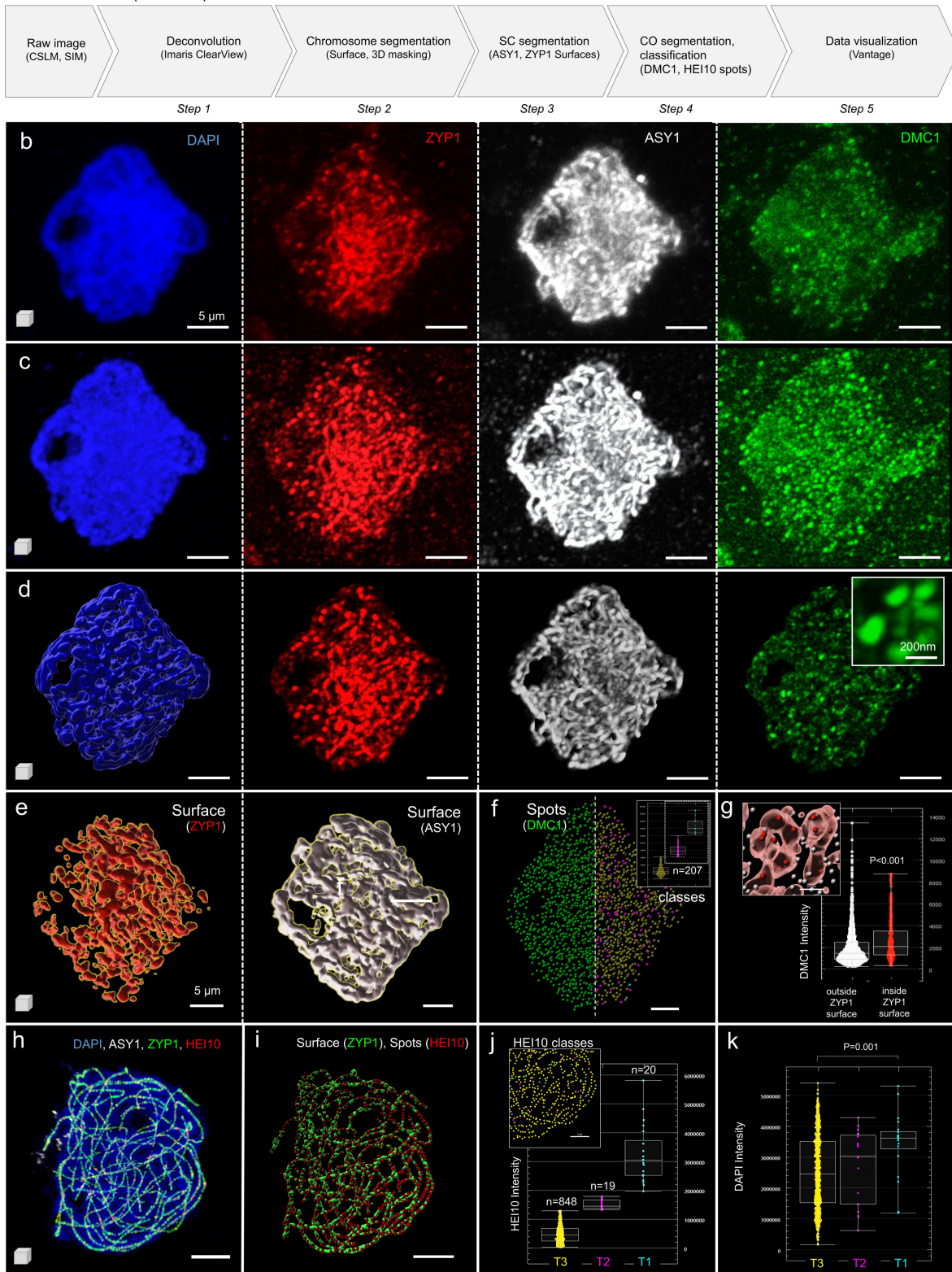


Figure 3. Analysis of crossover distribution in meiocytes. (a) Overview of the image analysis workflow in 5 steps illustrated on two images marking the synaptonemal complex (SC) and crossovers (CO) with different components (provided in Supplemental File 3): image 3a (b-g) represents a barley meiocyte at zygotene stage immunostained for DMC1, ZYP1 and ASY1 and counterstained for DNA using DAPI. The image was acquired by confocal microscopy (ZEISS LSM 710) as described (Colas et al., 2019). Image 3b (h-k) represents a barley meiocyte at the late pachytene stage immunostained for ASY1 (Ch = 2), ZYP1 (Ch = 3) and HEI10 (Ch = 4) and counterstained for DNA using DAPI (Ch = 1). The image was acquired by 3D-SIM as described previously (Hesse et al., 2019). (b) Original image acquired by confocal imaging, the different labeling are indicated.

(DMC1) and recombination intermediates (HEI10). The first image, shown in [Figure 3b-g](#) and provided in Supplemental File 3 – [Image 3a](#), shows a zygotene stage nucleus labeled with ASY1 (white), ZYP1 (red), DMC1 (green) and counterstained with DAPI (blue), was acquired on a confocal microscope (Zeiss LSM 710) as per Colas *et al.* [33]. The second image, shown in [Figure 3h-k](#) and provided in Supplemental File 3 – [Image 3b](#), shows a pachytene stage nucleus labeled with ASY1 (white), ZYP1 (green), HEI10 (red) and counterstained with DAPI (blue), was acquired using 3D-SIM similar as for rye [35]. The aim of both images was to segment HEI10 or DMC1 foci and to analyze their distribution relative to the SC, their size and their intensity. For this, the chromosomes, SC complex and HEI10 or DMC1 foci are segmented separately. The detailed strategies used for filtering and classifying the HEI10 or DMC1 foci are explained in the detailed workflow descriptions (Supplemental Files 3). In brief, the image analysis followed the steps of deconvolution (optional depending on the imaging method), chromosome segmentation, SC segmentation, CO foci segmentation and classification before data export ([Figure 3a](#)).

The effect of deconvolution is shown for the first image acquired by confocal microscopy to reconstruct the image at optical resolution (compare the panels [Figure 3b](#) and [3c](#)). This step is essential for properly estimating the CO diameter later ([Figure 3d](#), DMC1 channel inset). Next, the DNA (DAPI) staining was used to generate a 3D surface of the chromosomes serving as a mask to remove signal noise in the image (compare the panels [Figure 3c](#) and [3d](#)). Note that here, the aim was not to segment the chromosomes very precisely, as the masking

would result in the exclusion of ASY1, ZYP1 and DMC1 foci that do not entirely colocalize with DNA at that meiotic stage. Hence, permissive criteria were preferred in this case. Next, the SC complex was segmented on both the ASY1 and ZYP1 channels, creating two distinct surfaces ([Figure 3e](#), red: surface ZYP1, white: surface ASY1). Finally, DMC1 foci were segmented as spot objects using an estimated seed size of 200 nm ([Figure 3f](#)). The algorithm detects all possible foci with both low and high intensities. Classical studies have so far focused on high-intensity foci, whose abundance falls within a few hundred [31,33]. By contrast, the workflow described here enables one to capture all foci, first, irrespective of their intensity, and to classify them according to intensity, during the creation process ([Figure 3f](#), right panel). In this example, three classes were created ([Figure 3f](#) plot, yellow, magenta and cyan classes). Alternatively, spots can be classified after data export based on normalized signal intensity in a third-party software application (for instance, using DataViz, see Workflow1). In an intensity sum-based classification, we scored 217 DMC1 spots with medium-to-high intensity ([Figure 3f](#) plot, magenta and cyan classes) as previously reported for a similar stage of meiosis [31,33]. The remaining low-intensity spots ([Figure 3f](#) plot, yellow class) may correspond to either immunolabeling noise or unbound proteins. Next, we asked whether DMC1 localization was correlated with the SC. Indeed, following the classification of DMC1 spots in two groups, inside or outside the ZYP1 surface, we found a significant enrichment of DMC1 signal (based on intensity mean) when foci colocalize with ZYP1 ([Figure 3g](#)). This is one of the many

(c) image following deconvolution to resolve the SC and immunostained CO. (d) segmentation of the chromosomes as surface and masking of the ZYP1, ASY1 and DMC1 channels to remove background signal. It allows resolving DMC1 foci at high resolution (inset). (e) SC segmentation using the ZYP1 and ASY1 masked channels (f) DMC1 foci segmentation (left) and classification according to their intensity (right and inset = intensity plot per category), (g) classification of DMC1 foci according to their distance relative to the ZYP1 surface. (h) Original 3d SIM image (image 3b), (i) same image following ZYP1 and HEI10 segmentation, (j) HEI10 spots were classified according to their intensity (T1, T2, T3 on graph and inset); 20 foci were scored (automatic) for the T1 class as described in earlier studies, (k) HEI10 classes differ by the DNA density. Scale bars: 5 μ m except for the inset d, DMC1 channel (200 nm), Plots (f, g, j, k): Imaris Vantage.

examples of correlative analyses that can be carried-out in such segmented images.

The second image (Figure 3h) was analyzed similarly, but deconvolution, chromosome segmentation and masking were omitted in this case. The ZYP1 surface (Figure 3i, green) was used to mask the HEI10 channel to specifically focus on HEI10 foci (Figure 3i, red) colocalizing with ZYP1. HEI10 spots objects were then classified according to their intensity, considering notably the first and next 2% quantile versus the rest to create three classes, T1, T2 and T3, respectively (Figure 3j). This approach was formerly described to analyze CO distribution during meiosis in a fungal species [36]. The surprisingly high number of low-intensity HEI10 foci (T3 class) detected by the segmentation in this late pachytene-stage nucleus suggests the need for further investigation to understand their nature and possible function. To further describe the properties of HEI10 classes, we investigated different relationships and found that in most cells, typically high-intensity HEI10 foci (T1) localize, on average, on chromosome regions with higher DNA compaction (DAPI mean intensity) compared to low-intensity HEI10 foci (T3) (Figure 3k).

This image processing workflow facilitates the scoring of class I CO and NCO foci across multiple images, stages and genotypes, a task largely done manually until now. In addition, segmentation is near-exhaustive and includes low-intensity foci that were discarded from manual scoring in former studies. This raises the question of the dynamics of HEI10 and DMC1 foci formation, with possible intermediate stages represented by low-intensity foci. In addition, it opens the possibility to refine the analysis of CO/NCO spatial organization and their fine-scale structure. For instance, the localization of CO/NCO foci can be measured relatively to the SC components as a function of their intensity, and as a function of local chromatin compaction.

Analysis of nuclear speckle distribution

A distinguishing feature of nuclear topography is the ability to accommodate a variety of subnuclear compartments including nuclear bodies. Nuclear bodies are membraneless compartments

that spatially partition the nuclear environment and are thought to facilitate enzymatic reactions [37,38]. Similar to membrane-bound organelles, they maintain an effective steady-state structure, but likely by different mechanisms [39]. The first-identified and best-characterized plant nuclear bodies are the nucleolus and Cajal bodies. Several other smaller structures have, however, also been identified, including speckles, paraspeckles, coiled bodies and photobodies [40–42]. Unmasking the mechanisms by which cells assemble, maintain and regulate nuclear bodies and speckles, and the environmental and developmental factors contributing to the process, will shed light on their biological functions. For instance, splicing regulator (SR) proteins in plants localize as speckles, the size and shape of which are dependent on cell type, metabolic state and transcriptional activity [41–43].

One way to elucidate the speckle dynamics of nuclear bodies, which are not membrane-bound, is through microscopy imaging and image analysis. This approach enables the analysis of their spatial distribution and their composition relative to other nuclear components and DNA (chromatin) density. In this example, we showcase a simple image analysis workflow for analyzing the distribution of nuclear speckles and bodies. We used two images: Supplemental File 4 – image 4a reports on the nuclear localization of a plant chromatin remodeler: a SWI/SNF subunit (called SSSU here) forming nuclear speckles in leaf nuclei. Supplemental File 4 – image 4b reports on the nuclear localization of a mammalian chromatin protein (here called CP) and of H3K27me3 forming large nuclear bodies in nuclei of mouse naive pluripotent embryonic stem cells [44]. CP is a Baz-related subunit of the ISWI (Imitation SWItch) family remodeling complex factor, interacting with SNF2H, a SWI/SNF related remodeler [45] (Santoro, Panatta, unpublished).

SSSU was found to interact with PWO1 and CRWN1 (Kalyanikrishna, Jourdain, Schubert, unpublished), a set of proteins involved in epigenetic gene regulation and chromatin organization at the nuclear periphery [46]. CRWN1 (CROWDED NUCLEI 1), a nuclear lamina candidate in Arabidopsis, interacts with PWO1 (PROLINE-TRYPTOPHANE-TRYPTOPHANE-PROLINE

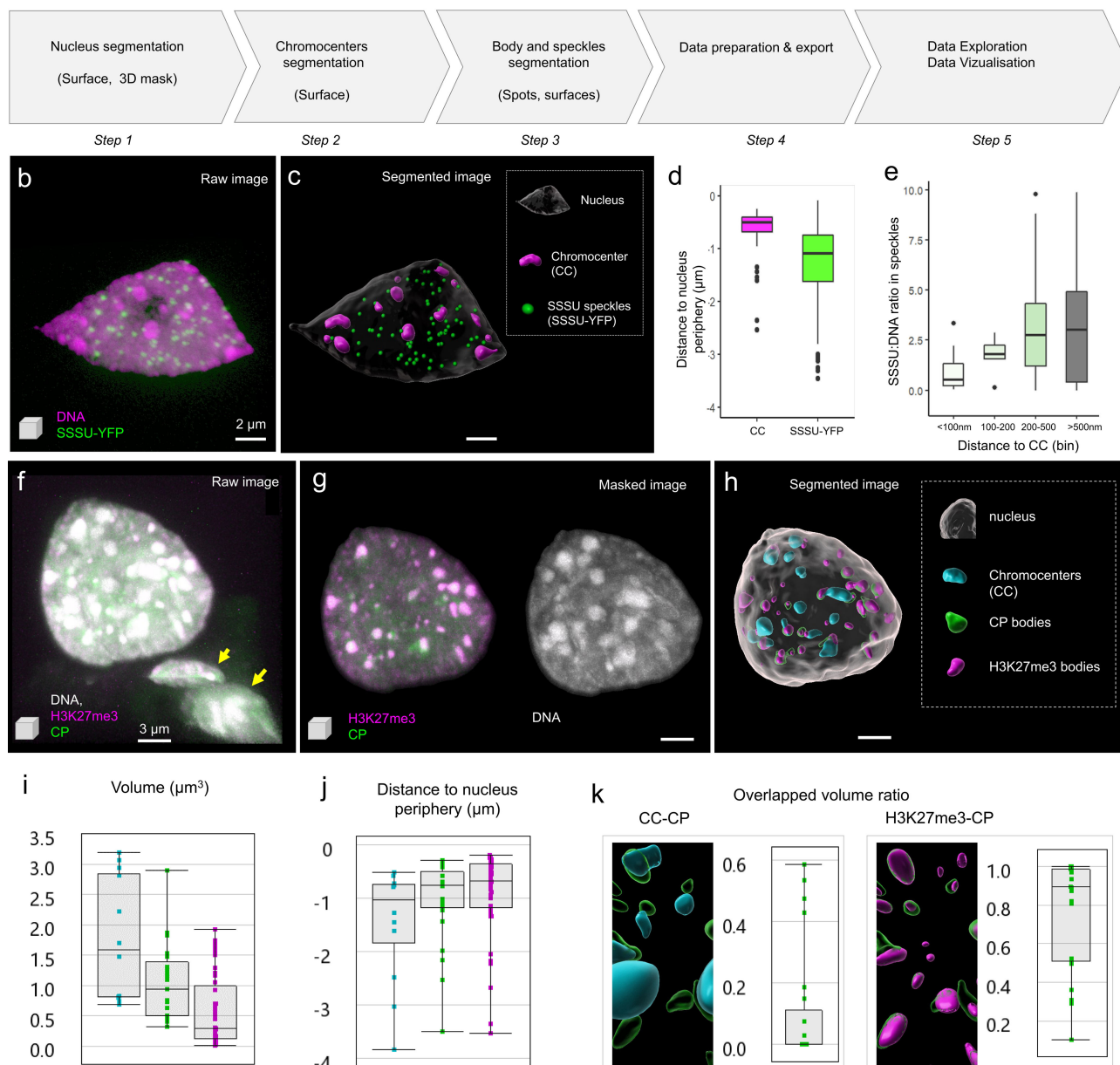
a Workflow 4 (overview)


Figure 4. Analysis of the spatial distribution of nuclear speckles and bodies. (a) Overview of the image analysis workflow, details and training images are provided in Supplemental Files 4. The analysis of two images (Supplemental File 4 – image 4a and 4b) representing plant and animal nuclei are shown in (b-e) and (f-k), respectively. (b) Raw, STED image (3D projection) showing an isolated leaf nucleus stained for DNA (magenta, Hoechst 580CP [26]), and immunostained for SSSU (green). (c) Segmentation result: the nucleus, chromocenters (CC) and the nuclear speckles (SSSU) were segmented as surface objects (legend, right panel). (d) The position of CC and SSSU speckles was plotted relative to the nucleus' periphery defined by the surface's boundary (0 = at the boundary; negative values = toward the interior), $n = 9$ nuclei analyzed. (e) The relative enrichment of SSSU on chromatin was plotted as the SSSU:DNA mean signal intensity ratio for different classes of speckles defined by their distance to CC (in μm). Plots were generated using Dataviz (see Workflow 1) using data from $n = 10$ segmented nuclei. (f) Confocal image (3D projection) of a nucleus from a mouse naïve pluripotent embryonic stem cell stained for DNA (gray, DAPI), immunostained for the chromatin protein under study (CP, green) and H3K27me3 (magenta) forming large nuclear bodies; the arrows show truncated nuclei in the field of view undesirable for downstream analyses and eliminated upon masking at the next step. (g) Same image after 3D masking using the nucleus surface created at step 1. (h) Results of image segmentation: the nucleus, chromocenters (CC) and the nuclear bodies (CP and H3K27me3) were segmented as surface objects (legend, right panel). (i-k) Quantitative analysis of CC and nuclear bodies: volume: (i) distance to the nucleus periphery (j) and overlapping volume ratios (k, left: CC and CP overlap, right: CP and H3K27me3 overlap). Plots were generated using Imaris Vantage. Scale bar: (a-b), 2 μm ; (f-h), 3 μm .

INTERACTOR OF POLYCOMBS1), a plant-specific protein associated with histones and PRC2 (POLYCOMBREPRESSIVE COMPLEX 2) [46]. Due to its possible interaction with CRWN1, we asked whether SSSU is also located preferentially at the nuclear periphery. To answer this question, we tagged SSSU with YFP (YELLOW FLUORESCENT PROTEIN) and imaged nuclei expressing SSSU-YFP using STED microscopy. The image analysis workflow consists of only a few steps (Figure 4a): STED images reporting on the immunolabeled SSSU-YFP and DNA counterstaining (Figure 4b) were segmented for the nucleus, chromocenters (CC) and SSSU-speckles, using the surface tool. For segmentation of the nucleus, smooth, manual contours were used, while for segmenting CCs, automated, parameter-controlled settings were applied. SSSU speckles were segmented as spot objects of ca. 200 nm diameter. Segmentation data of several images were exported and plotted using DataViz (see workflow 1, Supplemental File 1 – [Dataviz_guidelines](#)). SSSU-YFP speckles showed a broad spatial distribution, with no clear preferential enrichment toward the periphery (Figure 4d), in contrast to chromocenters as previously shown [24,25]. We found, however, that SSSU speckles are not uniform: they differ in their relative enrichment (SSSU:DNA ratio), which correlates with the proximity to CC (Figure 4e). Our analysis demonstrates that the nuclear speckles formed by SSSU are not preferentially enriched at the nuclear periphery as would have been expected from their biochemical interaction with CRWN1. The analysis suggests a differential enrichment depending on the proximity to other nuclear bodies, the CC, a relationship whose functional relevance remains to be investigated. This preliminary finding was unexpected and was revealed thanks to the possibility to explore multiple relationships between distance and intensity measurements in DataViz using segmentation data generated using this workflow.

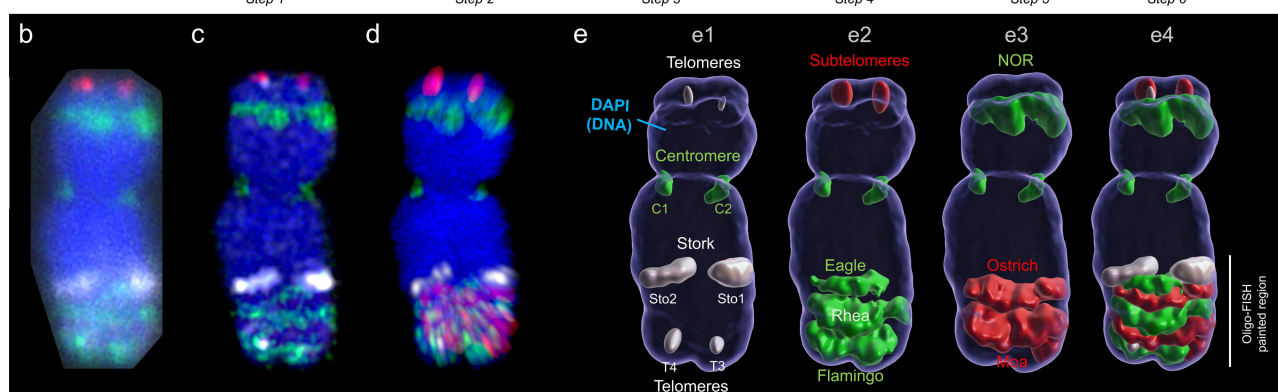
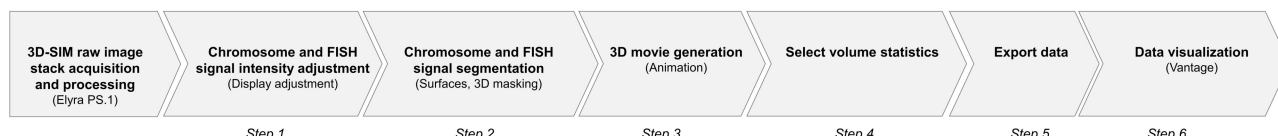
In the second example, we were interested in the CP protein localization relative to the repressive nuclear compartments formed by heterochromatin (chromocenters) and H3K27me3 in nuclei of mouse naive pluripotent embryonic stem cells. Nuclei stained for DNA and immunostained for CP and

H3K27me3 were imaged at high resolution by confocal microscopy (Figure 4f). To analyze the distribution of CP bodies, we segmented the nucleus, the chromocenters (CC), CP and H3K27me3 nuclear bodies, as surfaces of adaptive size (Figure 4g-h). Volume measurements show that CP bodies are smaller than CC but larger than H3K27me3 bodies (Figure 4i, $p < 0.001$, Wilcoxon test) and are similarly distributed toward the periphery compared to CC and H3K27me3 bodies (Figure 4j). The image shows an intricate relationship between CP bodies, CC and H3K27me3 bodies. Measuring the overlapped volume ratio is a useful approach to quantify the fraction of spatially colocalizing bodies (Figure 4k), revealing in our case a frequent overlap of 50% or more of CP bodies with H3K27me3 bodies. Conversely, the overlap with CCs is less frequent and occurs to a lower extent (<20%). This image analysis workflow thus allows one to quantify features of the nuclear body distribution that are otherwise underappreciated with qualitative data alone. Based on this simple workflow, further processing steps can be implemented that would contribute to a refined analysis of the spatial pattern of CP proteins relative to chromatin density and H3K27me3 levels. This can include, for instance, the creation of intensity-based colocalization or ratio channels (not shown).

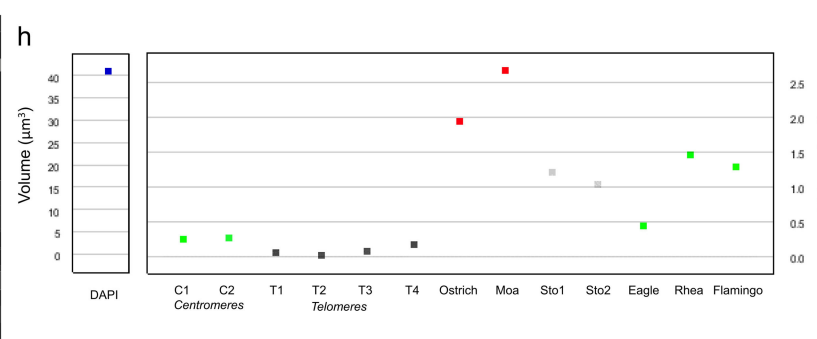
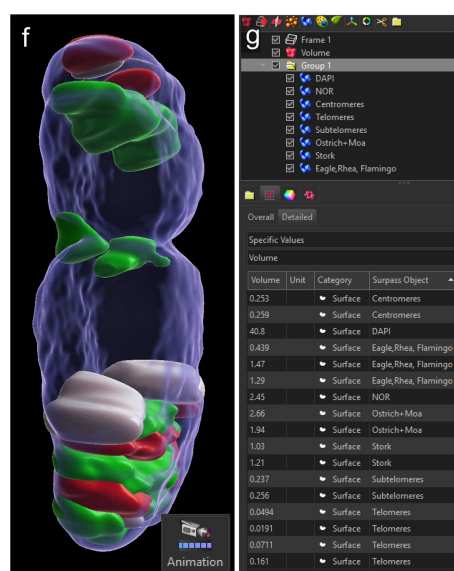
Analysis of the higher-order chromatin organization in mitotic chromosomes

During mitosis, chromosomes reassemble into compact bodies resulting from increased chromatin fiber looping within the chromatids [47]. How sister chromatids resolve into distinct structures and which topological rearrangement contributes to the final organization start being understood. Yet, questions remain concerning the molecular mechanisms and the regulation of this dynamic process [47]. Also, whether the topological arrangement in mitotic chromosomes is conserved during evolution is not well known and is motivating for comparative investigations in less-well-studied models [48].

a Workflow 5 (overview)



b 3D-SIM raw data (Single slice) **c** 3D-SIM processed (Single slice) **d** Signal intensity adjusted (3D rendering) **e** Chromosome and FISH signals segmented



h Data visualization (Vantage)

Figure 5. Analysis of the metaphase chromosome ultrastructure using volume measurement of oligo-FISH labeled regions.

(a) Overview of the image analysis workflow. (b) 3D-SIM raw image slice from a stack containing 30 slices at widefield resolution. (c) 3D-SIM processed image slice showing increased super-resolution. (d) Display adjustment to optimize the visualization of signals with varying intensities. (e) Segmentation results: the chromosome is segmented using the DAPI channel and the generated 3D surface is used as a mask to specifically retain chromosomal FISH signals and exclude the background. The segmentation is presented sequentially for different FISH probe groups (e1-e3), and the result is shown in the merge (e4). e1, telomere, centromere, and Stork probes; e2, Subtelomeres, Eagle, Rhea and Flamingo probes; e3, 45SrDNA (Nucleolus Organizing Region, NOR), Ostrich and Moa probes. The Oligo-FISH probes label the bottom part of chromosome 5HL. (f) Side view of a 3D movie generated via the 'Animation' tool (Supplemental File 5 – video 1). (g) Volume data are read in the 'Statistics' Tab for selected surfaces. (h) Data visualization using the 'Vantage' tool for individual objects (top).

Oligo-FISH combined with spatial super-resolution structured illumination microscopy (3D-SIM) is a useful approach for resolving helical versus non-helical arrangement of chromatin fibers in

chromatids. For instance, this method allowed us to confirm that the chromatids of barley metaphase chromosomes are formed by a helically wound ~400 nm chromatin fiber, the so-called

chromonema [49]. Additionally, by measuring the volume of oligo-FISH painted regions and based on the DNA quantity used for the probes, it was possible to calculate the chromatin compaction. With this approach, different chromatin densities were found along the barley chromosome arm 5 HL. Interstitial arm regions were ~ 1.7 times more compact than regions adjacent to the subtelomeres (34.1 vs. 19.5 Mb/ μm^3 , respectively) [49].

Workflow 5 describes the processing procedure to segment an individual 5 H chromosome and the different FISH signals to obtain quantitative measurements on the degree of chromatin compaction (Figure 5a; Supplemental File 5). In this example, centromeres, 45SrDNA (NOR, nucleolus organizing regions) telomeres, and subtelomeres of somatic metaphase chromosomes were labeled with specific FISH probes as described [49]. In addition, half- and full helical turns of the chromonema were painted by oligo-FISH at the long arm of chromosome 5H (Figure 5, probes were named according to birds: Stork, Eagle, Ostrich, Rhea, Moa, Flamingo) [49]. 3D-SIM raw data image stacks (Figure 5b) were acquired using an Elyra PS.1 microscope system equipped with a 63 \times /1.4 Oil Plan-Apochromat objective, processed with the software ZENBlack (Carl Zeiss GmbH) (Figure 5c) [50] and converted into an Imaris file. DAPI and FISH signal intensities were adjusted for improving the visualization using the 'Display Adjustment' tool (Figure 5d). The DAPI-labeled chromosome was segmented using the surface tool, and the surface was used to mask the image to remove the background signal outside this region of interest. Additional surfaces of the other, differently colored FISH signals were generated (Figure 5e-f, Supplemental File 5 – Video 1). The surface volume data were established (Figure 5g), exported for further analysis by compiling several images, and used to calculate the volumetric density of the different FISH-labeled regions along the chromosome [49]. An example plot for one chromosome is shown in Figure 5h using Vantage.

Analysis of centromere and telomere positioning

Arabidopsis and barley are eukaryotic models contrasting in their 3D interphase chromosome

organization. Arabidopsis has a small genome of about 157 Mbp per haploid DNA content (1C) packed into 5 chromosomes ($2n = 10$), whereas the barley genome is large, with around 5.1 Gbp/1C divided into 7 chromosomes ($2n = 14$) [51,52]. In Arabidopsis, centromeres are distributed relatively equally around the nuclear periphery to which they are attached, while telomeres are associated with nucleoli and each chromosome occupies a discrete territory within the nuclear space [53]. In barley, interphase chromosomes are organized in the so-called Rabl configuration with the centromeres and telomeres clustered at opposite nuclear poles [52]. While the Rabl configuration has long been thought to be prevalent among monocot species, recent studies show that it also occurs in dicot species and that variations exist within the same phylogenetic group [54]. In addition, this peculiar organization can occur in a tissue-specific manner, as in rice [55]. To better characterize the occurrence of Rabl vs. non-Rabl configurations and their possible intermediates, in different species and tissue types, there is a need to define an image analysis workflow quantifying telomere and centromere distribution in the nuclear space. We present such a workflow (overview Figure 6a) illustrated with two examples, corresponding to studies of chromosome organization in a monocot species (barley, Figure 6b-f) and in a dicot species (*Limnanthes floccosa* subsp. *bellingermaniana*, Figure 6g-j). Details, parameters, and demo images are available in Supplemental Files 6.

A first example is given for barley nuclei (Figure 6b-f). Nuclei extracted from seeds (Figure 6b) were flow-sorted as described [56] and labeled by FISH using fluorescently labeled oligoprobes (Cy3-labeled *CEREBA*-centromeric repeat; [57] and Cy5-labeled Arabidopsis-type telomeric repeats [58]). Z-stack images were acquired with an epifluorescence microscope connected with a spinning disk (Andor, Oxford Instruments, UK). Centromeric and telomeric FISH signals and the DNA counterstain (DAPI) were pseudo-colored in magenta, yellow, and gray, respectively. Two types of seed nuclei are shown (Type I, Type II, Figure 6c). Images are first

a Workflow 6 (overview)

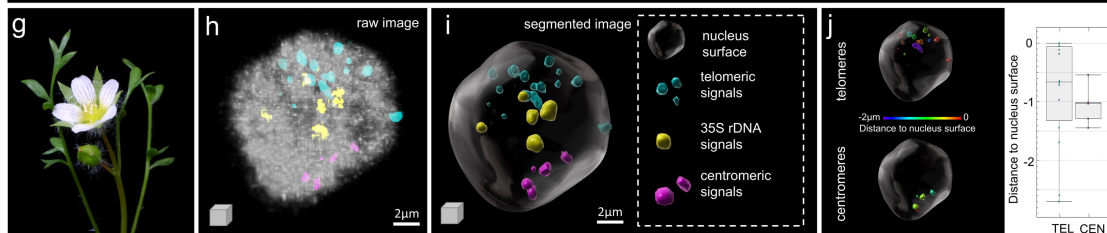
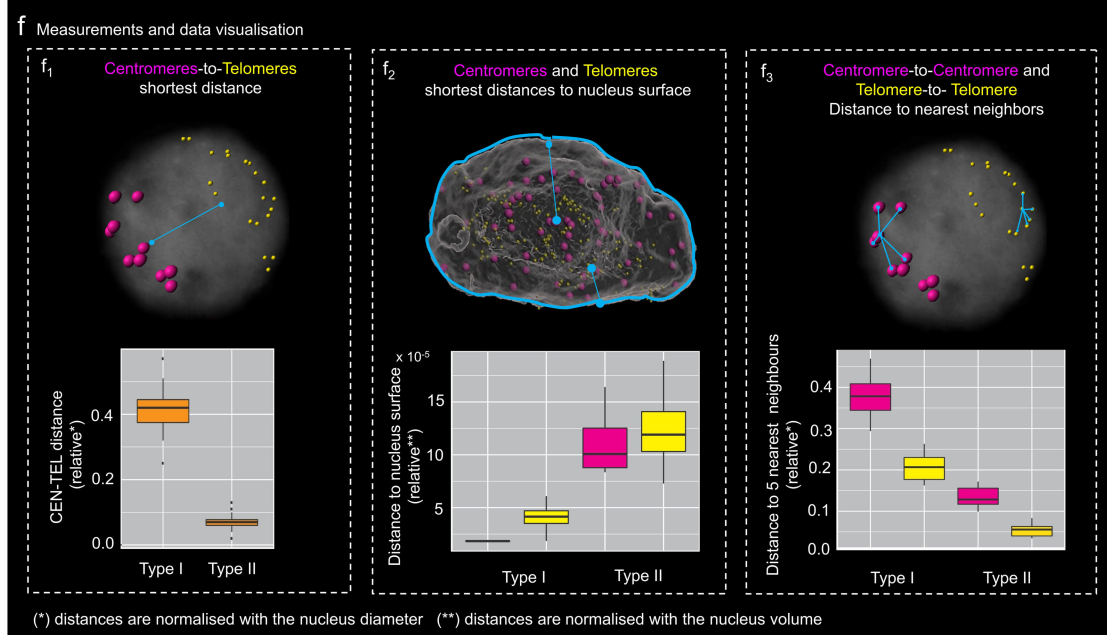
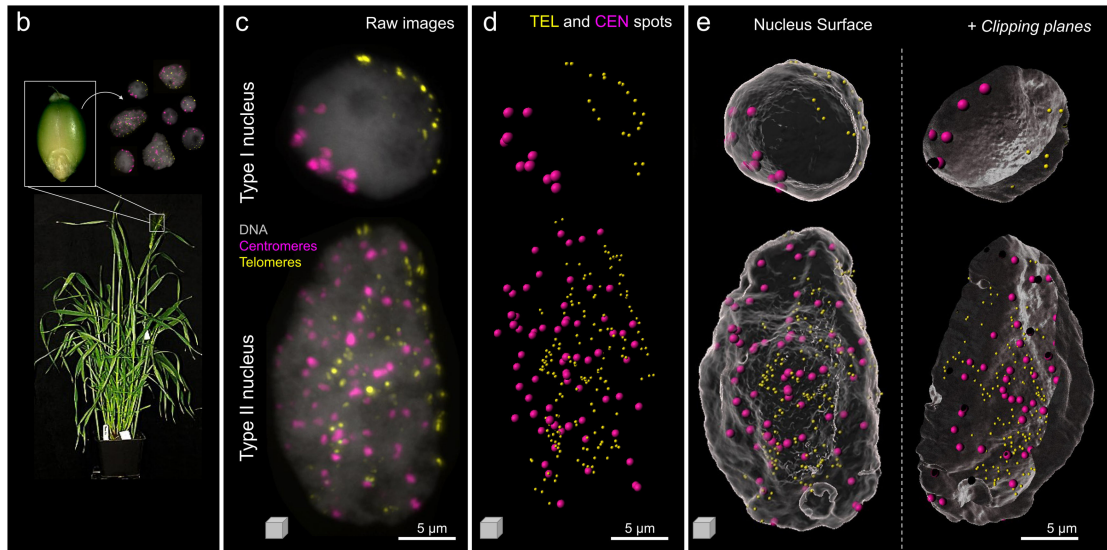
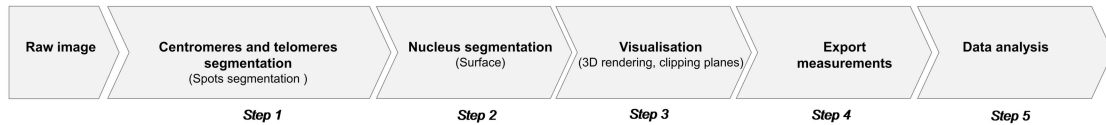


Figure 6. Analysis of centromere and telomere positioning in the interphase nucleus (continued). (a) Workflow overview showing the main steps to process the 3D image and identify centromeres and telomeres and their position in an interphase nucleus. The workflow is illustrated with seed nuclei from barley (a-f) and leaf nuclei from *Limnanthes* (g-i). (b) Barley plant, seeds and isolated nuclei stained by FISH for centromere and telomeric repeats (see main text for details). (c) Raw images (3D projections) of type I and type II nuclei showing centromeric (magenta) and telomeric (yellow) FISH probes signals, counterstained for DNA (DAPI, gray). (d) Telomeric (TEL) and centromeric (CEN) signals were segmented as spots. (e) 3D rendering together with nucleus surfaces (gray)

segmented on the channels reporting on FISH signals to create spot objects corresponding to centromeres (CEN) and telomeres (TEL), (Figure 6d) using the automated tool. The spot diameter is adjusted to the average size of FISH foci (ca 300 nm). The nuclear surface is rendered using a low smoothing factor (Figure 6e). For a better visualization of the spot distribution inside the nucleus, the surface is set to transparent or can be digitally sectioned using a clipping plane (Figure 6e). This segmentation and 3D visualization approach allowed us to realize that the seed nuclei population was composed of two categories of nuclei. In type I nuclei, centromeric and telomeric spots are grouped to opposite sides of the nucleus, reflecting Rab1-like features. In type II nuclei, they distribute in the whole 3D nuclear space, which corresponds to a non-Rab1 configuration. To support this observation by quantitative measurements, we exported three types of distance measurements (Figure 6f): (i) shortest distance between centromeric and telomeric spots (Figure 6f₁), (ii) shortest distance of centromeres and telomeres to the surface, corresponding to the nucleus border (Figure 6f₂), and (iii) average distance to top five neighboring spots for each group (centromeres, telomeres, Figure 6f₃). Because distances depend on the nucleus size, we normalized them using the nucleus diameter (graphs shown in Figure 6f express relative distances). The quantitative analysis shown in Figure 6f based on ca. 20 nuclei supported a contrasted spatial distribution of telomeres and centromeres in the two categories, with notably clear segregation of telomere and centromere groups in Type I nuclei (f1), located closely to the nuclear surface (f2). We

also noticed a shorter distance between telomeres and centromeres in Type II nuclei, which was unexpected. Because this type of nuclei is frequently highly endoreduplicated, this led us to investigate further the relationship between ploidy and chromosomal organization (Nowicka, Pecinka et al., submitted).

A second example is shown using nuclei from *L. floccosa* subsp. *bellingermana* (Figure 6g-j). Nuclei extraction from different types of tissue, FISH protocol and imaging were previously described by [54,59–61]. A similar procedure was applied to segment the nucleus based on DAPI staining (gray) and FISH signal reporting on the telomeres (cyan), centromeres (magenta) and 35S rDNA loci (yellow) (Figure 6h-i). In this example, centromeres and telomeres clearly showed clustering toward the nuclear periphery as shown with a median distance of spots around 0.6 μm (TEL) to 1 μm (CEN) in a nucleus of ca. 12 μm diameter (Figure 6j). We used this workflow for the analysis of nuclear organization in *Crucifera* genomes [54], in seven diploid species with up to 26-fold variation in genome size. This allowed to unveil species-specific patterns in nuclear organization [54].

For a trained user, the workflow takes approximately 20 minutes or less per image. This workflow can be used to compare the spatial distribution of chromosomes at interphase using centromeres and telomeres as references. Distance measurements across image replicates offer the possibility to detect quantitative differences invisible to the eye, between tissue types and cell types and to characterize potential mutant phenotypes in genetic analyses.

following segmentation, whole nuclei (left) or clipped (right), exposing the CEN and TEL signals in the interior of the nucleus. (f) The distribution of telomeres and centromeres is described according to three measurements derived from spot-to-spot or spot-to-surface statistics: shortest distance between centromeres and telomeres (f1), shortest distance of centromeres to the nucleus surface and shortest distance of telomeres to the nucleus surface (f2), inter-centromere and inter-telomere distances computed as the average distance to the nearest 5 neighbor spots of the same category (f3). In blue, schematic representation of the measured distance. Distances were exported and normalized to the nucleus diameter (f1, f3) or nucleus volume (f2) and plotted using the ggplot GUI online tool (<https://shiny.gmw.rug.nl/ggplotgui/>). The lower and upper hinges of the boxplots correspond to the first and third quartiles of the data, respectively, the black lines within the boxes mark the median. Five to ten nuclei were used for each measurement. Black spots beyond the whiskers represent outliers. (g-j) Illustration of the workflow on a *Limnanthes* leaf nucleus, (g) *Limnanthes floccosa* subsp. *bellingermana*, (h) Raw image (3D projection) of a nucleus stained for centromeric repeats (magenta), telomeric repeats (cyan) and rDNA repeats (yellow) by FISH, counterstained for DNA (DAPI, gray), imaged by confocal laser scanning microscopy, (i) 3D nucleus following segmentation of FISH signals and DNA as surfaces. (j) Distance of the different segmented groups relative to the nucleus surface were plotted in Imaris Vantage; images showing a distance-coded coloring are shown for centromeres (CEN) and telomeres (TEL).

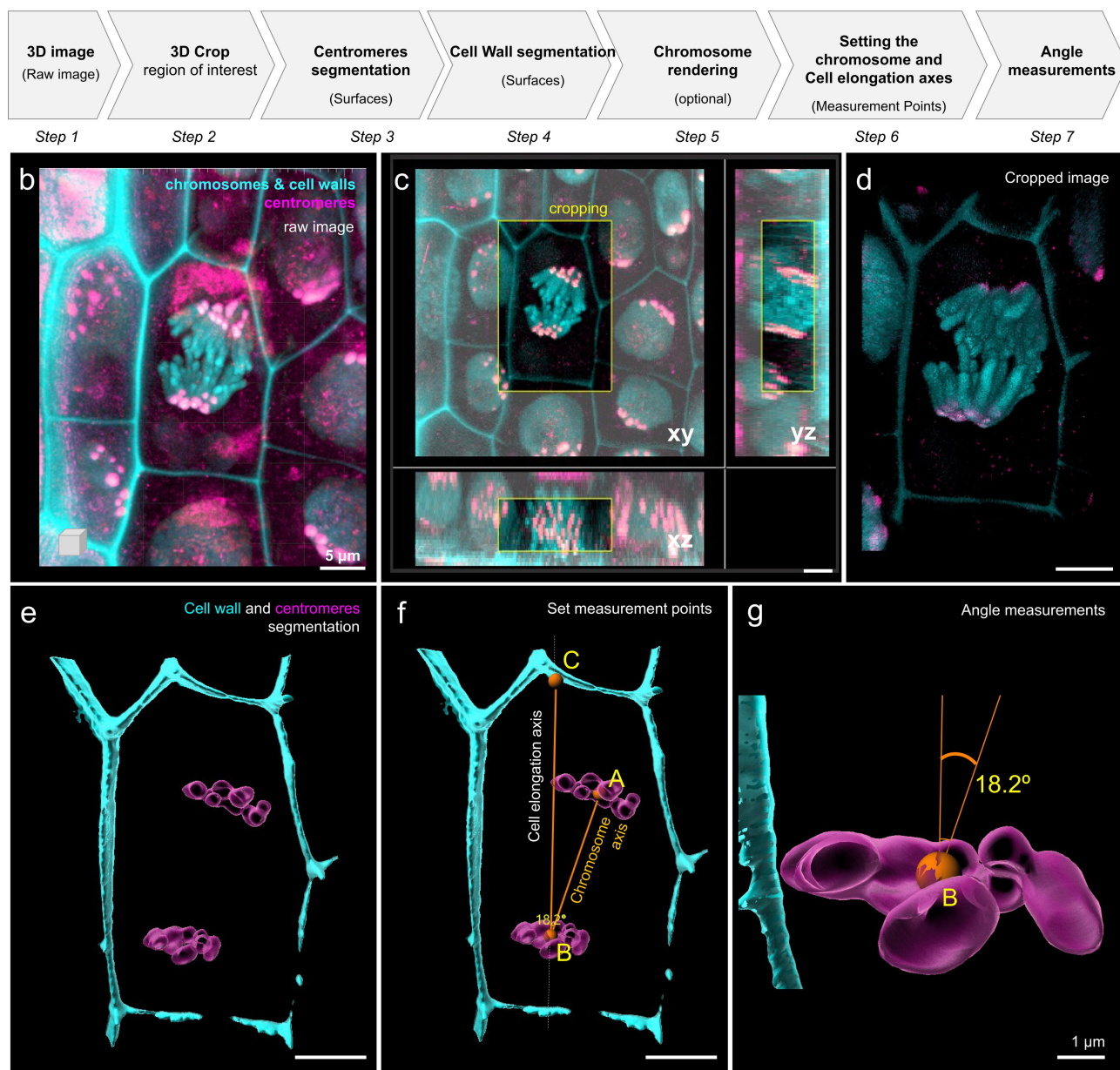
a Workflow 7 (overview)

Figure 7. Division angle measurement using surface-rendered cellular structures in living barley root cells. (next page).

(a) Workflow overview showing the sequence of tasks to process a raw picture up to the setting of measurement lines within the 3D cell space. (b) Confocal imaging of barley root tissue from a young seedling expressing CFP-H2B marking the chromosomes (cyan) and RFP-CenH3 marking the centromeres (magenta). In addition, cell wall autofluorescence upon UV excitation was used to mark the cell's boundaries (cyan). The image is a partial projection from a z-stack. (c) 3D cropping of the image to select a region of interest containing a dividing cell in mitotic anaphase (yellow frame). Orthogonal projections are shown in xy, yz and xz. (d) The cropped image is rendered in 3D using the 'blend' mode. (e) 'Surface' rendering of segmented centromeres (magenta) and the cell wall (cyan). (f) Setting of 'Measurement points' and their connective lines. AB defines the axis along which chromosomes are pulled (orthogonal to the chromosome plates), BC defines the cell's elongation axis. (g) Detailed visualization of the lower metaphase plate and angle formed between both axes defined by AB and BC measurement lines. The angle is measured in 3D by Imaris. Scale bars: b-f, 5 μm ; g, 1 μm .

Analysis of mitotic chromosome orientation during division

Mitosis is the process by which organisms increase the number of cells. In plants, the highest number of mitotically active cells can be found in the root and shoot apical meristems (RAM and SAM, respectively) [62]. We focused the analysis on chromosome organization and orientation in living barley roots. Both cell division orientation and cell elongation contribute to the oriented growth of the root. Changes in the mitotic division orientation affect root shape and anatomy [63]. In *Vicia faba*, chromosome positioning correlates with the cell division plane and ultimately cell shape [64]. Notably, it was speculated that cell size could be a limiting factor forcing the spindle axis to be tilted, deviating slightly from the main axis of cell and organ elongation. Analyzing the orientation of mitotic chromosomes during cell division is thus relevant to understand this intricate relationship.

We designed a 3D microscopic image analysis workflow described in Figure 7a and detailed in Supplemental Files 7 containing a protocol and troubleshooting tips. We used barley chromatin and centromere fluorescent marker lines (FMLs) expressing translational fusions of histone H2B with CYAN FLUORESCENT PROTEIN (CFP-H2B) and -CENTROMERIC HISTONE H3 with RED FLUORESCENT PROTEIN (RFP-CENH3), respectively (Kaduchová, Pecinka et al., in preparation). Z-stack images were acquired using a Leica TCS SP8 STED3X confocal microscope equipped with a Leica Application Suite X (LAS-X) software version 3.5.5 with a Leica Lightning module (Leica, Buffalo Grove, IL, USA) (Leica Microsystems, Wetzlar, Germany). In addition, we took advantage of the fact that barley cell walls have an autofluorescence detectable in CFP emission spectra [65], allowing simultaneous visualization of chromosomes, centromeres, and cell walls. Centromere signals were pseudo-colored in magenta, chromatin with cell walls in cyan. The raw image (Figure 7b) presenting several cells in the root was cropped around one cell showing chromosomes at anaphase (Figure 7c). Centromeres were segmented with the ‘spots’ tool

(Figure 7d). Chromosomes and cell walls were segmented using the ‘surface’ tool (Figure 7e). Using the tool ‘Measurement point’, we created spots (connected by a measurement line) at key positions, providing information on the cell elongation axis (A-B), on the pulling axis of the chromosomes (A'-B) and a reference axis (B-C) (Figure 7f, see Supplemental File 7 for detailed explanation), which allowed for angle measurements (Figure 7g).

For a trained user, the workflow takes approximately 30 min per image. This workflow will allow one to measure the relationship between the orientation of the spindle axis during division and cell shape (elongation) and its variation between tissue and cell types. In addition, the possibility to measure this relationship opens the possibility to quantify the effect of genetic or environmental factors with large or subtle effects on the cell division axis.

Conclusive remarks

We present here a set of seven image analysis workflows enabling the quantitative study of the spatial organization of chromosomes and chromatin components. The workflows cover applications for studies at interphase (workflows 1, 2, 4, 6), mitosis (workflow 5, 7) or meiosis (workflow 3). Workflows 1, 2 and 4 demonstrated the possibility to discover spatial distribution patterns, taking as examples transcription clusters, nuclear bodies and speckles and nuclear envelope-associated proteins. Such patterns were revealed thanks to the exploration of possible relationships between distance and intensity measurements among the different objects of the segmented images. Workflow 6, exploring genome organization at interphase, illustrates the quantitative power of image segmentation to precisely measure the spatial positioning in the nuclear space and the clustering of telomeres and centromeres. These features describe different types of 3D genome organization depending on cell type and species. The interest in performing image analysis for chromosome studies was further illustrated with workflows 3 and 5 focusing on condensed

chromosomes at meiosis or mitosis, respectively. Workflow 1 demonstrates the usefulness of image segmentation for quantifying the number and distribution of crossover components on meiotic chromosomes and revealing the possible enrichment in relation to the synaptonemal complex and that of chromosomal regions. Workflow 5 shows that volumetric measurements of FISH signals enable determining chromatin density (compaction) in different genomic regions. Finally, workflow 7 proposes an approach to measure the angles between chromosome and cell elongation axes and to investigate the relationship between cell division orientation and chromosomal positioning.

Image segmentation delivers a wealth of information related to signal intensity, distribution pattern (texture), shape, size and distance relationships between segmented objects [1]. Thus, images become associated with many variables and entry types, generating big data. Those can either be explored in a non-hypothesis-driven way using multidimensional data analysis (Bagheri et al., 2022) or in a hypothesis-driven manner following a careful choice of data for export. Even when exporting a selective number of image descriptors, the analysis of replicate image datasets, in different conditions (treatments or genotypes), labeled for multiple components, quickly generates a large numerical dataset. Versatile data visualization interfaces become handy at this stage. Here, we provided some examples among the numerous available solutions. We developed a customized Shiny-based (shiny.rstudio.com/) data visualization interface, DataViz, for processing (normalizing, filtering), exploring and plotting intensity, morphology and distance measurement data exported from segmented images. Normalization of intensity or distance measurements per image is important for considering variations that may arise between images during sample preparation, imaging or image acquisition [1,12]. The examples provided here propose different strategies depending on the image analysis question. Versatile data visualization greatly facilitates the explorative work, which in turn has the potential to seed discoveries, revealing

unexpected patterns or relationships and driving further analyses or experiments.

Although these workflows were developed to analyze nuclei and chromosome organization mostly in plant cells, these are conceptually applicable to nuclei of other species. An example is shown in workflow 4 with the analysis of nuclear bodies in mouse embryonic stem cells. In addition, these image analysis workflows are expected to inspire cell biologists beyond the study of the nucleus and its constituents. For instance, transposed at the cellular scale, workflow 1 or 4 could be applied to analyze the spatial distribution of vesicles or cytoplasmic bodies within a cell, using cell segmentation modules to create the initial surface object (see, for instance, but not exhaustive, references [66–68]).

Finally, while based on a particular (commercial) software piece, the concept of these workflows is expected to be transferable to other concurrent software offering similar image analysis tools (Supplementary File 8 – Table 1). One example is the 3D ImageJ Suite [8,10] popularized by the NEUBIAS COST action [8] which also offers a set of Fiji-based plugins for analyzing the spatial distribution of nuclear signals.

The increasing number of user-friendly platforms and the growing performance of segmentation algorithms greatly facilitate image analysis. Yet, this progress should not elude the need to reflect on the pertinence of the segmentation applied relative to the image features extracted by the process – and that will ultimately be interpreted in a biological context. Segmentation is influenced by the image quality, and specific metrics have been proposed to control for it [69]. In addition, when establishing a segmentation pipeline for the first time, several thresholds relative, for instance, to signal intensity, contrast and seed size must be adjusted that influence object detection. These thresholds influence the results in terms of the number, size, shape and texture of objects (discussed in [1,3]). In a semi-automated, user-guided segmentation such as proposed here, how to decide on a specific threshold or cutoff values can be difficult (of note, this type of decision is similar to those met in

bioinformatics analyses to select sequencing reads based on their quality, replication and cutoff levels). Threshold values must be justified with sufficient criteria to be reproduced and understood by peer users. Alternatively, and when image quality is relatively homogeneous in a dataset, it is possible to use values automatically proposed by the algorithm as those are usually derived from image-based statistical parameters. We address this issue and propose solutions for each workflow in their detailed description (supplemental files 1–7). Yet, the rapid emergence of machine-learning (ML) based segmentation algorithms is expected to ease the application of optimal segmentation parameters, although an initial investment is required to train the algorithm with ground-truth images (discussed in [1,12]). Eventually, and perhaps most importantly, the image analysis becomes only relevant when two or more biological conditions are compared. Sample preparation and image analysis done in the same conditions and by the same user, ideally in a blind analysis design, will average possible technical and cognitive biases throughout the datasets. This will, in turn, allow us to draw relevant conclusions relative to the type and the order of magnitude of changes correlated with a treatment, a genotype or cell type, for a given spatial pattern describing nuclear, chromatin or chromosome organization.

The compendium of workflows presented here, with its illustrations, training images and detailed guidelines, aims at inspiring experimentalists in the field of chromatin, chromosome and nucleus organization studies, with no or little expertise in image processing. This effort responds to the rapid development of microscopy imaging techniques and the needs of a wider community to have well documented and conceptually accessible image analysis tools [13]. Ultimately, this allows to exploit image data to an unprecedented level of analysis.

Note

1. <https://omero.bio.fsu.edu/webclient/userdata/?experimenter=-1> folder IDP 3008_Randall-Baroux2022

Acknowledgments

We acknowledge the microscopy imaging facilities of the University of Zürich (Jana Doehner, Urs Ziegler; ZMB), of the CEITEC at the Masaryk University (CELLIM, supported by the MEYS CR project no. LM2018129), and of the Auvergne Bioimaging platform (CLIC microscopy facility). The authors acknowledge the ‘INDEPTH’ COST Action CA16212 for funding of the Training School during which the workflows were developed, Peter Majer and Michael Mahler (Bitplane AG) for suggestions during the training school.

Disclosure statement

No potential conflict of interest was reported by the author(s).

Author contribution

The work was conceived by CB; carried out and conceptually refined by CB, RSR, DR, CJ, AN, KK, MK, MAA, VS, CT, IC, K, MP, IK, AS, SM, and SD; supervised by CB, CT, VS, ML, SH, RS, DS, and AP; and written by CB, RSR, CJ, AN, KK, MK, MAA, VS, CT, and IC. All authors read and revised the manuscript.

Funding

This work was funded by grants from the Swiss National Science Foundation [310030_185186 and IZCOZ0_198171 to CB, 310030_201268 to RS]; the Velux Stiftung (project 1107 to CB); the Ricola foundation (to CB); the ERC Grant Shuffle (Project ID: 669182) and Biotechnology and Biological Sciences Research Council (BB/T008636/1) to IC; the Deutsche Forschungsgemeinschaft to VS (Schu 762/11-1); the UZH-FUB Global Strategy and Partnerships Funding Scheme (grant to K); the Deutsche Akademische Austauschdienst Dienst (grant to K); the International Max Planck Research School for Biology and Computation (project IMPRS-BAC to CJ); the Czech Science Foundation (project 18-20134Sto MAL, 21-02929S to AP); the Operational Programme Research, Development and Education – “Project Internal Grant Agency of Masaryk University” (No. CZ.02.2.69/0.0/0.0/19_073/0016943 to MAL and MK) and ‘Plants as a tool for sustainable global development’ (No. CZ.02.1.01/0.0/0.0/16_019/0000827 to KK and AP); the German Federal Ministry of Education and Research (BMBF) in frame of the grant HERBY (FKZ-031B0188 to SH); the Purkyně fellowship to AP; the European Research Council (H2020 European Research Council ERC-AdG -787074-NucleolusChromatin to R.S.); CT, AS, SM and SD are supported by CNRS, INSERM, Université Clermont Auvergne (UCA), Agence Nationale de la Recherche (project grants 16-IDEX-0001 CAP 20-25 CIR1 and CIR3).

ORCID

Ricardo S Randall  <http://orcid.org/0000-0002-2778-519X>
 Claire Jourdain  <http://orcid.org/0000-0002-3568-580X>
 Anna Nowicka  <http://orcid.org/0000-0002-5762-3482>
 Kateřina Kaduchová  <http://orcid.org/0000-0001-9259-5942>
 Michaela Kubová  <http://orcid.org/0000-0003-3474-7324>
 Mohammad A. Ayoub  <http://orcid.org/0000-0001-9371-3277>
 Veit Schubert  <http://orcid.org/0000-0002-3072-0485>
 Christophe Tatout  <http://orcid.org/0000-0001-5215-2338>
 Isabelle Colas  <http://orcid.org/0000-0001-6980-9906>
 Kalyanikrishna  <http://orcid.org/0000-0002-8026-246X>
 Sophie Desset  <http://orcid.org/0000-0002-4897-4977>
 Sarah Mermet  <http://orcid.org/0000-0001-6839-3224>
 Aurélia Boulafloous-Stevens  <http://orcid.org/0000-0003-1378-2569>
 Ivona Kubalová  <http://orcid.org/0000-0002-5673-9715>
 Terezie Mandáková  <http://orcid.org/0000-0001-6485-0563>
 Stefan Heckmann  <http://orcid.org/0000-0002-0189-8428>
 Martin A. Lysak  <http://orcid.org/0000-0003-0318-4194>
 Martina Panatta  <http://orcid.org/0000-0002-8180-8380>
 Raffaella Santoro  <http://orcid.org/0000-0001-9894-2896>
 Daniel Schubert  <http://orcid.org/0000-0003-2390-0733>
 Ales Pecinka  <http://orcid.org/0000-0001-9277-1766>
 Célia Baroux  <http://orcid.org/0000-0001-6307-2229>

References

- [1] Bagheri N, Carpenter AE, Lundberg E, et al. The new era of quantitative cell imaging-challenges and opportunities. *Mol Cell*. 2022;82:241–247.
- [2] Jerkovic I, Cavalli G. Understanding 3D genome organization by multidisciplinary methods. *Nat Rev Mol Cell Biol*. 2021;22:511–528.
- [3] Dumur T, Duncan S, Graumann K, et al. Probing the 3D architecture of the plant nucleus with microscopy approaches: challenges and solutions. *Nucleus*. 2019;10(1):181–212.
- [4] Boettiger A, Murphy S. Advances in chromatin imaging at kilobase-scale resolution. *Trends Genet*. 2020;36:273–287.
- [5] Dar AS, Padha D. Medical image segmentation: a review of recent techniques, advancements and a comprehensive comparison. *Int J Comput Sci Eng*. 2019;7:114–124.
- [6] Lucas AM, Ryder PV, Li B, et al. Open-source deep-learning software for bioimage segmentation. *Mol Biol Cell*. 2021;32:823–829.
- [7] Shivanandan A, Radenovic A, Sbalzarini IF. MosaicIA: an ImageJ/Fiji plugin for spatial pattern and interaction analysis. *BMC Bioinformatics*. 2013;14:349.
- [8] Boudier T. Fiji 3D image suite. 2020. <https://imagej.net/media/plugins/3d-imagej-suite/neubias-3dsuite.pdf>
- [9] Boudier T, Andrey P. Spatial statistics 2D/3D. 2012. https://imagejdocu.list.lu/plugin/analysis/spatial_statistics_2d_3d/start
- [10] Ollion J, Cochenne J, Loll F, et al. TANGO: a generic tool for high-throughput 3D image analysis for studying nuclear organization. *Bioinformatics*. 2013;29:1840–1841.
- [11] Arpon J, Gaudin V, Andrey P. A method for testing random spatial models on nuclear object distributions. *Methods Mol Biol*. 2018;1675:493–507.
- [12] Caicedo JC, Cooper S, Heigwer F, et al. Data-analysis strategies for image-based cell profiling. *Nat Methods*. 2017;14:849–863.
- [13] Jamali N, Dobson ETA, Eliceiri KW, et al. BioImage Analysis Survey: community experiences and needs for the future. *Biological Imaging*. 2020;1:e4.
- [14] Tatout C, Mougeot G, Parry G, et al. The INDEPTH (Impact of nuclear domains on gene expression and plant traits) academy – a community resource for plant science. *J Exp Bot*. 2022;73:1926–1933.
- [15] van Driel R, Franz P. Nuclear architecture and genome functioning in plants and animals: what can we learn from both? *Exp Cell Res*. 2004;296:86–90.
- [16] Dong P, Tu X, Liang Z, et al. Plant and animal chromatin three-dimensional organization: similar structures but different functions. *J Exp Bot*. 2020;71:5119–5128.
- [17] Andrey P, Kiêu K, Kress C, et al. Statistical analysis of 3D images detects regular spatial distributions of centromeres and chromocenters in animal and plant nuclei. *PLoS Comput Biol*. 2010;6:e1000853.
- [18] Bishop J, Swan H, Valente F, et al. The plant nuclear envelope and its role in gene transcription. *Front Plant Sci*. 2021;12:674209.
- [19] Cremer M, Schmid VJ, Kraus F, et al. Initial high-resolution microscopic mapping of active and inactive regulatory sequences proves non-random 3D arrangements in chromatin domain clusters. *Epigenetics Chromatin*. 2017;10:39.
- [20] Girelli G, Custodio J, Kallas T, et al. GPSeq reveals the radial organization of chromatin in the cell nucleus. *Nat Biotechnol*. 2020;38:1184–1193.
- [21] Schubert V. RNA polymerase II forms transcription networks in rye and Arabidopsis nuclei and its amount increases with endopolyploidy. *Cytogenet Genome Res*. 2014;143:69–77.
- [22] Schubert V, Weissbart K. Abundance and distribution of RNA polymerase II in Arabidopsis interphase nuclei. *J Exp Bot*. 2015;66:1687–1698.
- [23] Ashenafi MS, Baroux C. Automated 3D gene position analysis using a customized imaris plugin: xTFISHInsideNucleus. *Methods Mol Biol*. 2018;1675:591–613.
- [24] Andrey P, Kieu K, Kress C, et al. Statistical analysis of 3D images detects regular spatial distributions of

- centromeres and chromocenters in animal and plant nuclei. *PLoS Comput Biol.* **2010**;6:e1000853.
- [25] Fransz P, De Jong JH, Lysak M, et al. Interphase chromosomes in *Arabidopsis* are organized as well defined chromocenters from which euchromatin loops emanate. *Proc Natl Acad Sci U S A.* **2002**;99:14584–14589.
- [26] Bucevicius J, Keller-Findeisen J, Gilat T, et al. Rhodamine-Hoechst positional isomers for highly efficient staining of heterochromatin. *Chem Sci.* **2019**;10:1962–1970.
- [27] Huff J. The Airyscan detector from ZEISS: confocal imaging with improved signal-to-noise ratio and super-resolution. *Nat Methods.* **2015**;12:i–ii.
- [28] Orr JN, Lewandowska D, Waugh R, et al. Chromosome synapsis and recombination in cereals. *Annu Plant Rev Online.* 1–26. doi:10.1002/9781119312994.apr0710.
- [29] Keeney S. Spo11 and the formation of DNA double-strand breaks in meiosis. *Genome Dyn Stab.* **2008**;2:81–123.
- [30] Bishop DK. RecA homologs Dmc1 and Rad51 interact to form multiple nuclear complexes prior to meiotic chromosome synapsis. *Cell.* **1994**;79:1081–1092.
- [31] Higgins JD, Perry RM, Barakate A, et al. Spatiotemporal asymmetry of the meiotic program underlies the predominantly distal distribution of meiotic crossovers in barley. *Plant Cell.* **2012**;24:4096–4109.
- [32] Barakate A, Higgins JD, Vivera S, et al. The synaptonemal complex protein ZYP1 is required for imposition of meiotic crossovers in barley. *Plant Cell.* **2014**;26:729–740.
- [33] Colas I, Barakate A, Macaulay M, et al. desynaptic5 carries a spontaneous semi-dominant mutation affecting Disrupted Meiotic cDNA 1 in barley. *J Exp Bot.* **2019**;70:2683–2698.
- [34] Serra H, Lambing C, Griffin CH, et al. Massive crossover elevation via combination of HEI10 and recq4a recq4b during *Arabidopsis* meiosis. *Proc Natl Acad Sci U S A.* **2018**;115:2437–2442.
- [35] Hesse S, Zelkowski M, Mikhailova EI, et al. Ultrastructure and dynamics of synaptonemal complex components during meiotic pairing and synapsis of standard (A) and Accessory (B) rye chromosomes. *Front Plant Sci.* **2019**;10:773.
- [36] De Muyt A, Zhang L, Piolot T, et al. E3 ligase Hei10: a multifaceted structure-based signaling molecule with roles within and beyond meiosis. *Genes Dev.* **2014**;28:1111–1123.
- [37] Matera AG, Izaguire-Sierra M, Praveen K, et al. Nuclear bodies: random aggregates of sticky proteins or crucibles of macromolecular assembly? *Dev Cell.* **2009**;17:639–647.
- [38] Stanek D, Fox AH. Nuclear bodies: news insights into structure and function. *Curr Opin Cell Biol.* **2017**;46:94–101.
- [39] Mao YS, Zhang B, Spector DL. Biogenesis and function of nuclear bodies. *Trends Genet.* **2011**;27:295–306.
- [40] Ali GS, Golovkin M, Reddy AS. Nuclear localization and in vivo dynamics of a plant-specific serine/arginine-rich protein. *Plant J.* **2003**;36:883–893.
- [41] Docquier S, Tillemans V, Deltour R, et al. Nuclear bodies and compartmentalization of pre-mRNA splicing factors in higher plants. *Chromosoma.* **2004**;112:255–266.
- [42] Reddy AS, Day IS, Gohring J, et al. Localization and dynamics of nuclear speckles in plants. *Plant Physiol.* **2012**;158:67–77.
- [43] Lorkovic ZJ, Hilscher J, Barta A. Use of fluorescent protein tags to study nuclear organization of the spliceosomal machinery in transiently transformed living plant cells. *Mol Biol Cell.* **2004**;15:3233–3243.
- [44] Tosolini M, Brochard V, Adenot P, et al. Contrasting epigenetic states of heterochromatin in the different types of mouse pluripotent stem cells. *Sci Rep.* **2018**;8:5776.
- [45] Gioacchini N, Peterson CL. Chromatin remodeling: a complex affair. *EMBO Rep.* **2017**;18:1673–1674.
- [46] Mikulski P, Hohenstatt ML, Farrona S, et al. The chromatin-associated protein PWO1 interacts with plant nuclear lamin-like components to regulate nuclear size. *Plant Cell.* **2019**;31:1141–1154.
- [47] Batty P, Gerlich DW. Mitotic chromosome mechanics: how cells segregate their genome. *Trends Cell Biol.* **2019**;29:717–726.
- [48] Beseda T, Capal P, Kubalova I, et al. Mitotic chromosome organization: general rules meet species-specific variability. *Comput Struct Biotechnol J.* **2020**;18:1311–1319.
- [49] Kubalová I, Câmara AS, Cápál P, et al. Helical metaphase chromatid coiling is conserved. *bioRxiv.* **2021**;2021:460607.
- [50] Weisshart K, Fuchs J, Schubert V. Structured illumination microscopy (SIM) and photoactivated localization microscopy (PALM) to analyze the abundance and distribution of RNA Polymerase II molecules on flow-sorted *Arabidopsis* nuclei. *Bio-protocol.* **2016**;6:e1725.
- [51] Bennett MD, Leitch IJ, Price HJ, et al. Comparisons with *Caenorhabditis* (approximately 100 Mb) and *Drosophila* (approximately 175 Mb) using flow cytometry show genome size in *Arabidopsis* to be approximately 157 Mb and thus approximately 25% larger than the *Arabidopsis* genome initiative estimate of approximately 125 Mb. *Ann Bot.* **2003**;91:547–557.
- [52] Mascher M, Gundlach H, Himmelbach A, et al. A chromosome conformation capture ordered sequence of the barley genome. *Nature.* **2017**;544:427–433.
- [53] Pecinka A, Schubert V, Meister A, et al. Chromosome territory arrangement and homologous pairing in nuclei of *Arabidopsis thaliana* are predominantly random except for NOR-bearing chromosomes. *Chromosoma.* **2004**;113:258–269.
- [54] Shan W, Kubova M, Mandakova T, et al. Nuclear organization in crucifer genomes: nucleolus-associated

- telomere clustering is not a universal interphase configuration in Brassicaceae. *Plant J.* **2021**;108:528–540.
- [55] Santos AP, Shaw P. Interphase chromosomes and the Rab1 configuration: does genome size matter? *J Microsc.* **2004**;214:201–206.
- [56] Nowicka A, Kovacik M, Tokarz B, et al. Dynamics of endoreduplication in developing barley seeds. *J Exp Bot.* **2021**;72:268–282.
- [57] Hudakova S, Michalek W, Presting GG, et al. Sequence organization of barley centromeres. *Nucleic Acids Res.* **2001**;29:5029–5035.
- [58] Richards EJ, Ausubel FM. Isolation of a higher eukaryotic telomere from *Arabidopsis thaliana*. *Cell.* **1988**;53:127–136.
- [59] Hurel A, Phillips D, Vrielynck N, et al. A cytological approach to studying meiotic recombination and chromosome dynamics in *Arabidopsis thaliana* male meiocytes in three dimensions. *Plant J.* **2018**;95:385–396.
- [60] Mandakova T, Lysak MA. Chromosome preparation for cytogenetic analyses in *Arabidopsis*. *Curr Protoc Plant Biol.* **2016**;1:43–51.
- [61] Mandakova T, Lysak MA. Painting of *Arabidopsis* chromosomes with chromosome-specific BAC clones. *Curr Protoc Plant Biol.* **2016**;1:359–371.
- [62] Kirschner GK, Stahl Y, Von Korff M, et al. Unique and conserved features of the barley root meristem. *Front Plant Sci.* **2017**;8:1240.
- [63] Van Norman JM. Asymmetry and cell polarity in root development. *Dev Biol.* **2016**;419:165–174.
- [64] Oud JL, Nanninga N. Cell shape, chromosome orientation and the position of the plane of division in *Vicia faba* root cortex cells. *J Cell Sci.* **1992**;103:847–855.
- [65] Donaldson L. Autofluorescence in plants. *Molecules.* **2020**;25:2393.
- [66] Mendocilla Sato E, Baroux C. Analysis of 3D cellular organization of fixed plant tissues using a user-guided platform for image segmentation. *Bio-protocol.* **2017**;7:e2355.
- [67] Ota R, Ide T, Michiue T. A rapid segmentation method of cell boundary for developing embryos using machine learning with a personal computer. *Dev Growth Differ.* **2021**;63(8):406–416.
- [68] Kesler B, Li G, Thiemicke A, et al. Automated cell boundary and 3D nuclear segmentation of cells in suspension. *Sci Rep.* **2019**;9:10237.
- [69] Bray MA, Fraser AN, Hasaka TP, et al. Workflow and metrics for image quality control in large-scale high-content screens. *J Biomol Screen.* **2012**;17:266–274.

Appendix II

Spatial organization and dynamics of chromosomes during barley mitosis

Kaduchová, K., Marchetti, C., Ovečka, M., Galuszka, M., Bergougnoux, V., Šamaj, J.,
and Pecinka, A.

The Plant Journal

DOI: <https://doi.org/10.1111/tpj.16355>

IF (2022): 7.2

Spatial organization and dynamics of chromosomes and microtubules during barley mitosis

Kateřina Kaduchová^{1,2}, Cintia Marchetti³, Miroslav Ovečka⁴, Petr Galuszka^{5,†}, Véronique Bergougnoux³, Jozef Šamaj⁴ and Ales Pecinka^{1,*} 

¹Institute of Experimental Botany (IEB), Czech Academy of Sciences, Centre of the Region Haná for Biotechnological and Agricultural Research, Šlechtitelů 31, Olomouc 77900, Czech Republic,

²Department of Cell Biology and Genetics, Faculty of Science, Palacký University, Šlechtitelů 27, 78371 Olomouc, Czech Republic,

³Centre of the Region Haná for Biotechnological and Agricultural Research, Czech Advanced Technology and Research Institute (CATRIN), Palacký University, Šlechtitelů 27, 77900 Olomouc, Czech Republic,

⁴Department of Biotechnology, Faculty of Science, Palacký University Olomouc, Šlechtitelů 27, 77900 Olomouc, Czech Republic, and

⁵Department of Molecular Biology, Centre of the Region Haná for Biotechnological and Agricultural Research, Faculty of Science, Palacký University, Šlechtitelů 27, 77900 Olomouc, Czech Republic

Received 26 January 2023; revised 28 May 2023; accepted 7 June 2023; published online 16 June 2023.

*For correspondence (e-mail pecinka@ueb.cas.cz)

†Deceased

SUMMARY

Mitosis and cytokinesis are fundamental processes through which somatic cells increase their numbers and allow plant growth and development. Here, we analyzed the organization and dynamics of mitotic chromosomes, nucleoli, and microtubules in living cells of barley root primary meristems using a series of newly developed stable fluorescent protein translational fusion lines and time-lapse confocal microscopy. The median duration of mitosis from prophase until the end of telophase was 65.2 and 78.2 min until the end of cytokinesis. We showed that barley chromosomes frequently start condensation before mitotic pre-prophase as defined by the organization of microtubules and maintain it even after entering into the new interphase. Furthermore, we found that the process of chromosome condensation does not finish at metaphase, but gradually continues until the end of mitosis. In summary, our study features resources for *in vivo* analysis of barley nuclei and chromosomes and their dynamics during mitotic cell cycle.

Keywords: *Hordeum vulgare*, barley, mitosis, 3D nuclear organization, chromosomes, chromatin, microtubules, live imaging, confocal microscopy, crops.

Linked article: This paper is the subject of a Research Highlight article. To view this Research Highlight article visit <https://doi.org/10.1111/tpj.16392>.

INTRODUCTION

Mitosis is the main process of cell division by which organisms increase the number of cells and regulate their growth and development. During the cell cycle, the cells duplicate the majority of cellular components, genetic material, organelles, and other macromolecules, which are equally distributed into the newly emerging daughter cells (Gutierrez, 2009). The mitotic cell division and its regulation are studied in great detail in several fungal and metazoan models, including humans (Kimata et al., 2020; Kraikivski et al., 2015; Levine & Holland, 2018; Pintard & Bowerman, 2019). However, the amount of information about the kinetics and molecular control of mitotic division

in plants is still limited. Mitosis in plants differs from that in metazoa by some unique features due to the absence of a centrosomes (Ambrose & Cyr, 2008), the formation of phragmoplast, and the centrifugal emergence of new cell wall between daughter cells (Gutierrez, 2009; Smertenko et al., 2017). During the late G2 phase, cortical microtubules reorganize to create a structure characteristic of mitotic pre-prophase called pre-prophase band (PPB), indicating the position and orientation of the future division plane in plant cells (Ambrose & Cyr, 2008; Rasmussen & Bellinger, 2018). Microtubular PPB remains through prophase until it rearranges in prometaphase to give rise to the bipolar mitotic spindle composed mainly of

microtubules, microtubule-associated proteins, and kinases (Ambrose & Cyr, 2008; Liu & Lee, 2022; Smertenko et al., 2017; Zhang & Dawe, 2011). Mitotic spindle kinetochore microtubules attach chromosomes by interaction with their kinetochore structures and migrate them to form the metaphase band which helps to separate chromatids of individual chromosomes equally into the daughter cells by pulling them to the opposite cell poles in anaphase. Daughter cells are then separated by another plant-specific structure, phragmoplast (Smertenko et al., 2017). Phragmoplast is formed by a bipolar array of microtubules and actin filaments together with cytokinetic vesicles creating a cell plate that will separate sister cells during cytokinesis (Donaldson, 2020; Smertenko et al., 2017). In parallel to microtubule dynamics, specific changes occur in the cell nucleus. The chromosome organization and dynamics are controlled by the activity of structural maintenance of chromosomes (SMC) complexes. The chromosomes condense by the activity of Condensin I and II complexes into the rodlike structures with sister chromatids being held together along the arms and particularly in centromeric regions by the Cohesin complex (Fomproix et al., 1998; Gibcus et al., 2018; Hernandez-Verdun, 2011). Nucleoli disperse at the beginning of mitosis and reemerge in course of telophase around 45S rDNA loci (Hernandez-Verdun, 2011; Perutka et al., 2021).

Knowledge of the molecular mechanisms governing plant mitosis is based mostly on model species *Arabidopsis thaliana* where a broad range of genetic and molecular tools is available (Echevarria et al., 2021; Gutierrez, 2009; Liu & Qu, 2008; Noir et al., 2015). Despite many advantages of *Arabidopsis*, the small size of its chromosomes may hinder the resolution of specific chromosomal structures during mitosis. Moreover, *Arabidopsis* chromosomes enter mitosis from a rather unique rosette-like interphase organization. Most importantly, whether the observations made in *Arabidopsis* mitosis are representative also for phylogenetically distant plant species with a different genome structure and 3D organization remains unclear, for instance in important crops from the *Triticeae* tribe such as *Hordeum vulgare* (barley) or *Triticum aestivum* (bread wheat). In these species, interphase chromosomes occupy the Rab1 configuration (Rab1, 1885) with centromeres and telomeres grouping at opposite nuclear poles. Chromosomes in Rab1 configuration can possibly be condensed in early mitosis and can interact with kinetochores directly after the nuclear envelope breakdown in early prometaphase (Rosa & Shaw, 2013; Zhang & Dawe, 2011). This may simplify the formation of the mitotic spindle and speed up cell division. Until now, the knowledge about mitotic dynamics and the proportion of cells in different cell cycle stages in *Triticeae* is based on the combination of replication-coupled chromosome labeling with modified nucleotides and flow sorting which enabled to set length of the different cell cycle

stages (Baiza et al., 1989; Demchenko & Demchenko, 2001; Mickelson-Young et al., 2016). The flow sorting technique of interphase nuclei or metaphase chromosomes in combination with fluorescence *in situ* hybridization (FISH) and immunostaining extended knowledge about their structure and organization (Fuchs et al., 2006; Jasencakova et al., 2001). Nuclei, chromosomes, and microtubules were also studied using microtubular drugs such as taxol, oryzalin, and colchicine combined with cytochemical staining of nuclei and chromosomes or with tubulin immunolocalization (Baluska et al., 1997). However, these techniques based on fixed samples cannot provide information about the kinetics of chromatin, nucleoli, and microtubules and the duration of mitotic stages.

In this study, we present a unique analysis of the nuclear organization and dynamics of mitosis in root meristematic cells of living barley plants. We provide a comprehensive overview of the organization of several nuclear domains and microtubules and show that chromosome condensation precedes and outlasts mitosis in some cells and that multiple factors need to be considered for the correct estimation of each cell cycle stage. In addition, we estimated the duration of individual mitotic phases and show that chromosome condensation gradually continues throughout the entire mitosis in barley.

RESULTS

Development of fluorescent marker lines (FMLs) for *in vivo* analysis of mitosis, nuclear, and microtubule organization in barley

We selected the barley homologs of HISTONE H2B (H2B), TUBULIN ALPHA 3 (TUA3), and FIBRILLARIN 1 (FIB1) as candidates for the development of barley fluorescent marker lines (FMLs) (Boisnard-Lorig et al., 2001; Ludwig et al., 1987; Reichow et al., 2007). These proteins were N-terminally and translationally fused with different variants of fluorescent proteins resulting in CYAN FLUORESCENT PROTEIN-H2B (CFP-H2B), ENHANCED YELLOW FLUORESCENT PROTEIN-H2B (EYFP-H2B), mCHERRY-TUA3, and EYFP-FIB1 under the control of maize *UBIQUITIN 1* (*ZmUBI1*) promoter. The signals of fluorescent proteins and their subcellular localization were monitored using confocal microscopy in barley root apical meristems (Figure 1). To minimize tissue damage by the excitation laser, we focused primarily on the epidermal and outer cortex cell layers and kept the laser intensity at moderately low level ($\leq 46\%$ of the possible maximum intensity). Only diploid plants with fluorescent signals in chromatin (CFP-H2B and EYFP-H2B), microtubules (mCHERRY-TUA3), and nucleolus (EYFP-FIB1) were used for the experiments. Furthermore, the single FMLs were crossed to obtain combined FMLs with two or three fluorescently labeled compartments (Figure 1). The list of all FMLs used in this

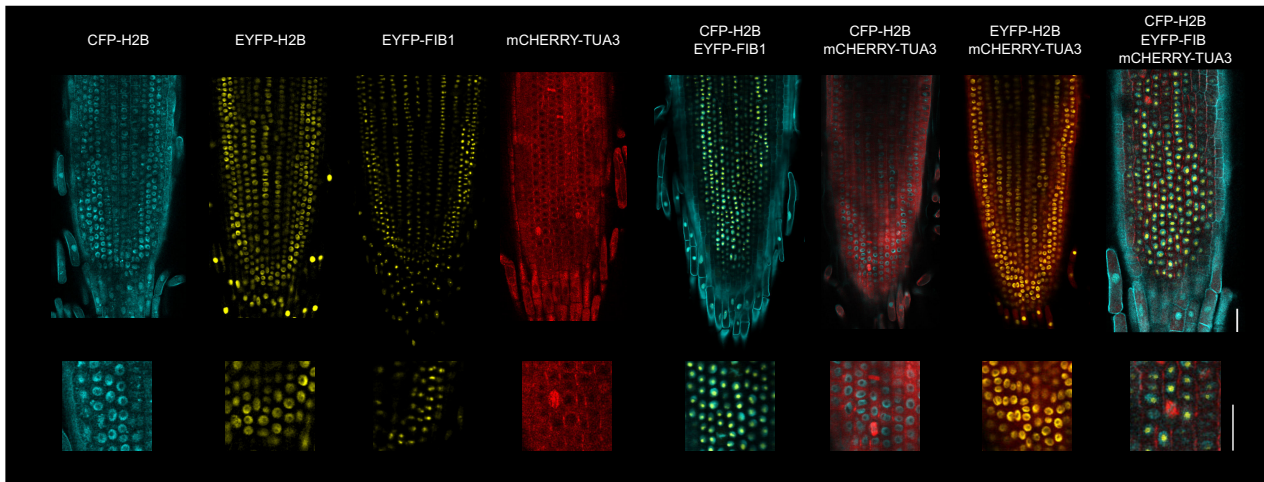


Figure 1. Overview of barley fluorescent marker lines developed and used in this study. Representative confocal microscopy optical longitudinal sections of roots from single, double, and triple fluorescent marker lines. Multimarker lines were generated by crossing single lines. The squares indicate selected magnified regions that are shown below each root. Scale bars = 20 μm .

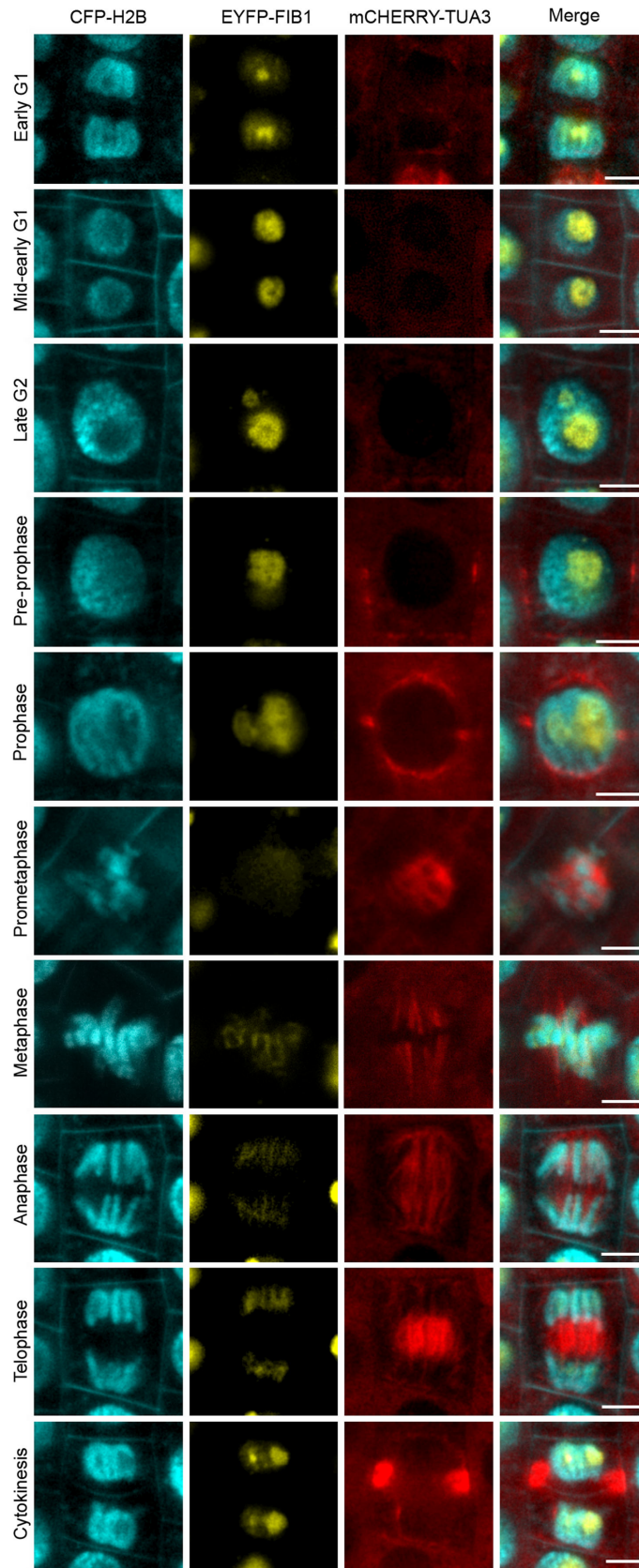
study is provided in Table S1. The constitutive overexpression of the translational fusion proteins might negatively affect various cellular processes and cause reduced plant fitness. To exclude such effects, we monitored single and combined FMLs at approximately Z70–Z90 Zadoks scale stages corresponding to maturing plants (Zadoks, 1985) and also looked at their dry grains (Figure S1). The only line that showed a phenotypic difference relative to the non-transgenic plants was CFP-H2B mCHERRY-TUA3 double FML with slightly shorter stems and fewer tillers (Figure S1). However, the localization of the fluorescent fusion proteins was the same as in the single FMLs. Hence, we successfully established a series of barley single and multiple FMLs for *in planta* detection of chromatin, microtubules, and nucleoli.

Analysis of nuclear and mitotic chromosome organization using FMLs

At first, we determined individual stages of the cell cycle using parameters such as the nucleus size, condensation and compaction of chromatin, morphology of nucleoli, arrangement of microtubules, and cell shapes (Figure 2). The cells in early G1 were observed typically shortly after the cytokinesis and were prominent by their still partially condensed chromosomes, resembling a relaxed telophase figure. The mitotic microtubule network persisted around newly reconstructed nuclei but dispersed homogenously

through the cytoplasm from mid-G1 to late G2. Afterward, the microtubules became prominently visible in the cytoplasm, later arranged themselves around the nucleus periphery, and finally formed a pre-prophase band (PPB). Another typical sign of G1 cells was a prominent shape visualized using autofluorescence in the CFP emission spectrum (Donaldson, 2020). The cell walls of G1 cells parallel with the main root axis (x white lines; Figure 3a) were distinctly shorter compared with those perpendicular to the main root axis (y red lines; Figure 3a), reaching significantly differentiated mean x/y ratios of 0.62 (G1 cells) and 1.3 (G2 cells) (one-way ANOVA and Tukey HSD significance test, $P \leq 0.01$; Figure 3b). The number and structure of nucleoli were other dynamic parameters (Figure 3c–e). A typical early G1 nucleus contained three to four small and dense nucleoli, the latter indicated by the intense and uniform EYFP-FIB1 signals that progressively fused into one or two nucleoli in late G2 (Figure 3d). We also noted a significant increase (one-way ANOVA and Tukey HSD significance test, $P \leq 0.05$) in nucleoli total volume from 102.93 μm^3 in early G1 to 188.56 μm^3 (+83.2%) in late G2 nuclei (Figure 3d). This might reflect an increased ribosome synthesis initiated during the S phase and continuing in the G2 phase (Hernandez-Verdun, 2011; Lockhead et al., 2020). After the S phase, G2 cell nuclei increased significantly (one-way ANOVA and Tukey HSD significance test, $P \leq 0.05$) their volume from 286.74 μm^3 (early G1) to

Figure 2. Localization of fluorescent marker proteins in different cell cycle phases. The rows represent images of typical barley epidermal cells corresponding to individual cell cycle phases. The columns show signals of individual marker proteins: CFP-H2B for chromosomes (cyan), mCHERRY-TUA3 for microtubules (red), EYFP-FIB1 for nucleolus (yellow), and their combination (merge). Non-nuclear/chromosomal signals in the first column correspond to cell walls that are visible due to cell wall autofluorescence in the CFP emission spectrum. Scale bars = 5 μm .



493.08 μm^3 (late G2; +71.9%) and/or area from 49.19 μm^2 (early G1) to 71.29 μm^2 (late G2; +44.9%) (Figure 3F,G). The phases from mid-G1 to mid-G2 could not be unambiguously distinguished with our FMLs due to the absence of stage-specific structures formed by the selected marker proteins.

Next, we focused on mitotically dividing root cells (Figure 2). A typical mitotic pre-prophase was hallmarked by the presence of PPB surrounding the nucleus. The band appeared on single confocal optical sections as two bright spots of mCHERRY-TUA3 at the opposite sides of the nucleus. The pre-prophase nuclei were characterized by the presence of one or two large nucleoli undergoing relaxation as the cell progressed through mitosis. To our surprise, the chromatin structure of pre-prophase cells (as defined by the PPB) was not uniform. Around 40% of the pre-prophase cells contained at least partially condensed chromosomes with visible chromatin folds and loops, especially when examined using the EYFP-H2B line with a strong signal (Figure 4A,B). This suggests that the chromatin condensation is initiated already during mitotic pre-prophase and/or that the chromosome condensation is maintained during the interphase in some barley cells. During prophase, the microtubules formed a prominent spherical structure around the whole nucleus on single confocal optical sections, which was persistent until the nuclear envelope breakdown (inferred indirectly based on the relocalization of microtubules) at the start of prometaphase. Chromatin condensation progressed in prophase cells and the sister chromatids became even more prominent. At this stage, the nucleolus rapidly changed its structure from a weakly relaxed sphere in pre-prophase and relaxed conformation in prophase to a diffuse EYFP-FIB1 signal in prometaphase. At the end of prometaphase, a weak EYFP-FIB1 signal was distributed equally throughout the whole cell. After the nuclear envelope breakdown, mCHERRY-TUA3-tagged microtubules formed a mitotic spindle in the central part of the cell and connected with the chromosomes at the region of centromeric constrictions (Video S1, 4 min; left mitotic cell). Subsequently, the chromosomes moved into the central part of the cell to form a typical metaphase band, and even the sister chromatids of individual chromosomes were distinguishable (Figure 2). The sister chromatids were aligned alongside each other, suggesting their persisting cohesion. Besides the random EYFP-FIB1 localization in the cytoplasm, the protein was enriched on the surface of the condensed chromosomes from metaphase until the telophase. In anaphase, the chromosomes were pulled to the opposite poles of the mitotic spindle. Interestingly, we found that the chromosome condensation did not stop at metaphase but gradually continued until the end of mitosis (Figure 2). The approximate average chromosome arm length significantly shortened from 8.05 μm in prophase to 5.76 μm in

metaphase, 4.71 μm in anaphase, and reached a minimal length of 4.25 μm in telophase, corresponding to a 47% reduction from the beginning till the end of karyokinesis ($P \leq 0.05$, one-way ANOVA; Figure 4c). During the transition from anaphase to telophase (Figure 2), the mitotic spindle was assembled by a set of polar microtubules. In addition, the microtubules assembled in the central part of cell division plane, where the early phragmoplast was initiated. The phragmoplast was visible by using molecular marker mCHERRY-TUA3, and forming cell plate was detectable in the CFP emission spectrum owing to the autofluorescence of cell wall components. From mid-telophase, the chromosome structure became gradually relaxed and the nuclear envelope was formed, thus reconstituting the daughter cell nuclei. However, the individual chromosome arms were distinguishable and maintained the same orientation as in the anaphase stage. In parallel, microtubules reorganized to support an extension and formation of late phragmoplast visible during the telophase as a double-layered disk along a cell division plane visualized by the mCHERRY-TUA3 marker. At the cytokinesis, the phragmoplast gradually decomposed from the centre to the periphery during progressive extension. In parallel, the EYFP-FIB1 signals disappeared from the chromosomes and nucleoli started to form (Figure 2). Each of the daughter cells contained typically three to four nucleoli (Figure 3b). Two nucleoli signals were larger and persisted in the nuclei almost through the whole interphase until the late G2 where they eventually fused into a single large one.

Determining the duration of barley mitotic stages

The time of mitosis defines the speed of cell division. Therefore, we analyzed the time of individual mitotic stages based on live imaging of 131 dividing cells (Figure 4d). Time-lapse recordings of cells undergoing mitotic division are captured in supplementary video files (EYFP-H2B mCHERRY-TUA3; Video S1; EYFP-FIB1 mCHERRY-TUA3, Video S2; CFP-H2B EYFP-FIB1, Video S3). We defined the start and the end of individual stages based on the configuration of marker proteins (Figure 2). We started the measurements at the beginning of prophase when microtubules formed bright PPB surrounding the nucleus. The prophase had a median duration of 32.6 min and was relatively variable in length as the shortest one took 19.5 min while the longest was 41.6 min. Prometaphase started with the breakdown of the nuclear envelope, which was visible as a loss of perinuclear spherical microtubule signal and spreading of the FIB1 signal through the cellular space and ended with microtubules forming a mitotic spindle with individually distinguishable chromosomes located in the central part of the cell. This stage had a median length of 7.2 min, and it varied from 3.4 min to 15.9 min (with some outliers up to 17 min). The median metaphase length was 9 min, and the shortest

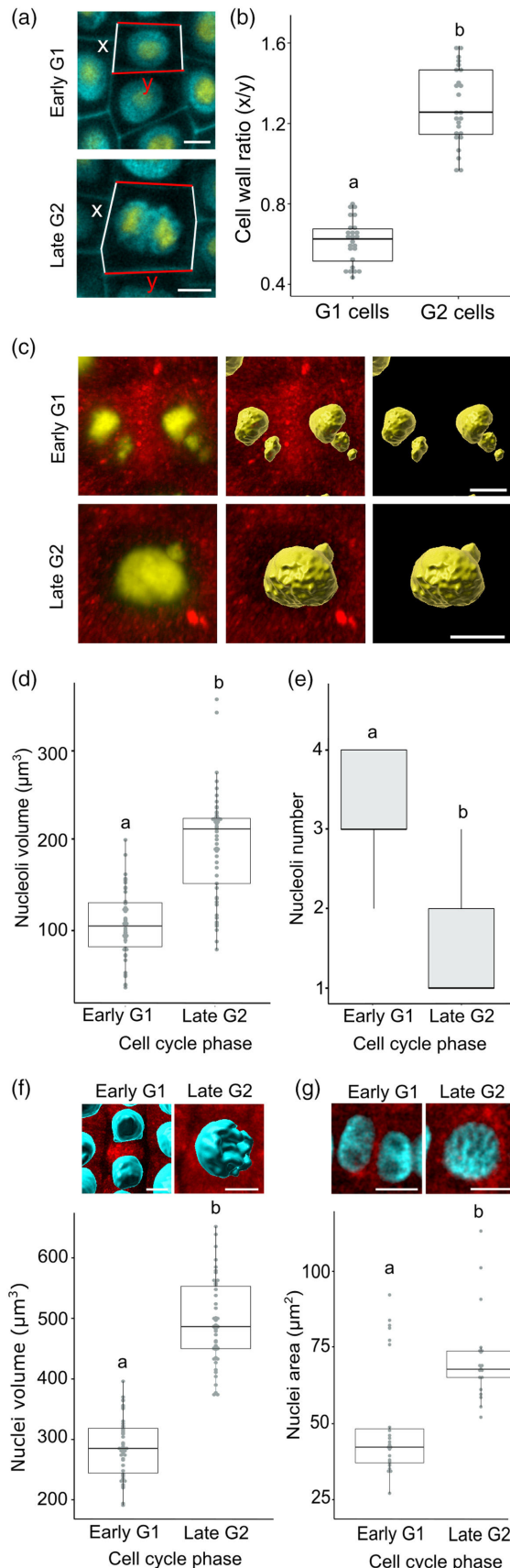


Figure 3. Nuclear and nucleolar parameters of barley G1 and G2 cells. (a) Representative images of early G1 and late G2 cells expressing nucleolar (EYFP-FIB1; yellow) and nuclear (CFP-H2B; cyan) fluorescent markers; auto-fluorescent cell walls are visible in cyan channel. The white lines (x) show cell walls linear, and red lines (y) show cell walls perpendicular with the main root growth axis. (b) The box plots show the cumulative cell wall ratio of x/y . The black lines within the boxes mark the median, whiskers mark 10 and 90 percent intervals. The lower and upper hinges of the boxplots correspond to the first and third quartiles of the data. A total of 50 nuclei were measured for G1 ($n = 25$) and G2 cells ($n = 25$). Different letters indicate significant differences ($P \leq 0.01$, one-way ANOVA, factor 1 = cell walls ratio), and grouping was done using the Tukey and Fisher methods. Scale bars = 5 μm . (c) 3D projection of cells in early G1 and late G2 expressing nucleolar (EYFP-FIB1; yellow) and microtubular (mCHERRY-TUA3; red) fluorescent markers before and after 3D surface rendering made in IMARIS bitplane software (rendering parameters: surface detail 0.149 μm ; absolute intensity thresholding; 89% voxels above 10). Scale bars = 5 μm . (d) Number of nucleoli per cell in early G1 and late G2 phases. A total of 100 nucleoli were measured for G1 ($n = 50$) and G2 nuclei ($n = 50$). The boxplot design and statistics are the same as in (b). (e) Nucleoli total volume per cell in early G1 and late G2 phases. A total of 90 nucleoli were measured for G1 ($n = 45$) and G2 nuclei ($n = 45$). The boxplot design and statistics is the same as in (b). (f) Nuclei volume per cell in early G1 and late G2 phases. A total of 100 nuclei were measured for G1 ($n = 50$) and G2 ($n = 50$) nuclei. The boxplot design and statistics is the same as in (b). (g) Nuclei area per cell in early G1 and late G2 phases. A total of 48 nuclei were measured for G1 ($n = 27$) and G2 ($n = 21$). The boxplot design and statistics are the same as in (b).

observed metaphase lasted only 4.1 min, while the longest was 18.8 min (outliers from 20.9 min to 47.3 min). Rarely, we observed entire chromosomes or chromatin fragments lagging behind and not being aligned at the metaphase band. These defects occasionally transformed into prolonged cohesion of sister chromatids. Such cells had slower progress into the anaphase but mostly were able to finish the whole mitotic division (Figure 4e). The onset of telophase was marked by a termination of chromosome movement to the opposite cell poles and by a translocation of the mCHERRY-TUA3 signals from the spindle and cell poles to the cell central plane. The end of telophase was defined by the establishment of compact nucleoli as indicated by the EYFP-FIB1 signals. The median duration of telophase was 10.3 min and varied from 6.6 min to 17.6 min (outliers from 19.5 min to 29.3 min). The cytokinesis started by the mCHERRY-TUA3 signals forming two parallel lines, each on one side of the emerging early phragmoplast, at the cell central plane (phragmoplast microtubules were oriented perpendicularly to the cell division plane), and ended when late phragmoplast connected to the mother cell walls and mCHERRY-TUA3 signals disappeared from the cell central plane. The typical cytokinesis lasted 13 min, but its time was relatively variable (4.5 to 27 min).

All measurements were used to calculate the total length of mitosis in barley root meristematic cells (Figure 4d). It has to be emphasized that only three mitoses

could be monitored from the beginning of prophase until the end of cytokinesis. In most cases ($n = 128$), the live imaging started during or terminated before the end of the given mitotic division. Therefore, we performed the calculations based on the median length of each mitotic phase, and a typical mitosis of barley root apical meristem cell takes 65.2 min from prophase to the end of telophase or 78.2 min until the end of cytokinesis under our experimental conditions.

DISCUSSION

Mitosis represents the most common way how plants increase their cell number and biomass. Here, we analyzed the organization of chromosomes, microtubules, and nucleoli and measured the duration of mitotic division stages in barley root apical meristem cells.

The large size of chromosomes makes barley a favorite model for analyzing chromosome organization, dynamics, and epigenetic regulation during mitosis (Rotasperti et al., 2020). Barley chromosomes show (i) Rab1 organization during interphase; (ii) replication initiated on rDNA genes, followed by euchromatin, centromeres, and pericentromeres; (iii) unique and conserved features compared with other plants (Jasencakova et al., 2001; Kuznetsova et al., 2017; Wako et al., 2005). However, the published data are based on fixed roots or isolated nuclei/chromosomes. Therefore, our aim was to explore *in vivo* dynamics of cell division in living barley roots. To this end, we developed a series of FMLs designed to visualize chromatin, nucleolus, and microtubules (Table S1). The presence of single recombinant proteins did not affect plant growth and development, but ThemCherry-TUA3 CFP-H2B double reporter line showed a weakly reduced growth. Nevertheless, marker protein localization was not affected in this line. Hence, the series of our marker lines represents a unique robust tool for *in vivo* analysis of specific cellular components in barley.

With the set of barley FMLs, we defined the organization of chromatin, nucleolus, and microtubules at

individual cell cycle and mitotic stages (Figure 5). The most dynamic structure were the microtubules whose organization and dynamics was generally described earlier in plants (Bajer & Allen, 1966; Hamada, 2014; Marc, 1997; Mirabet et al., 2018; Rasmussen, 2016). Long-term live cell imaging using light-sheet fluorescence microscopy confirmed dynamic properties of mitotic microtubules in dividing root meristematic cells of crop, *Medicago sativa* (Vyplelova et al., 2017), and leaf meristems of maize (*Zea mays*) (Rasmussen, 2016). We observed unexpected dynamics for the nucleolar marker FIB1. Early G1 nuclei showed mostly four nucleoli that fused into one-to-two large nucleoli in late G2 cells, and the volume of nucleoli increased from the early G1 to the late G2 phase, which might reflect an increased ribosome activity initiated during the S phase and partly continuing until the end of the G2 phase (Hernandez-Verdun, 2011; Lockhead et al., 2020). Alternatively, the larger volume of nucleoli could represent their relaxation in preparation for mitotic pre-prophase (Kalinina et al., 2018). From prometaphase on, nucleoli were no longer visible as shape-defined structures, but the EYFP-FIB1 signal was detected weakly in the cytoplasm and enriched on the surface of chromosomes from anaphase until cytokinesis as we demonstrated recently (Perutka et al., 2021). This is consistent with the observations of the perichromosomal layer in human and animal cells where some proteins involved in nucleolus-associated processes (e.g., rRNA biogenesis) localize on the surface of mitotic chromosomes and are equally distributed into newly formed daughter cells (Gautier et al., 1992; Perutka et al., 2021; Van Hooser et al., 2005).

Almost 40% of pre-prophase nuclei (defined by microtubule organization) contained condensed chromosomes contradicting the general assumption that intense condensation starts during the mitotic prophase (Feitoza et al., 2017). Nevertheless, our observation is supported by an earlier study where signals for mitosis-specific histone H3 modifications H3T3p, H3T11p, and H3S10p were found in pre-mitotic nuclei of barley (Houben et al., 1999; Wilkins

Figure 4. Chromosomes condensation and duration of mitosis in barley root cells.

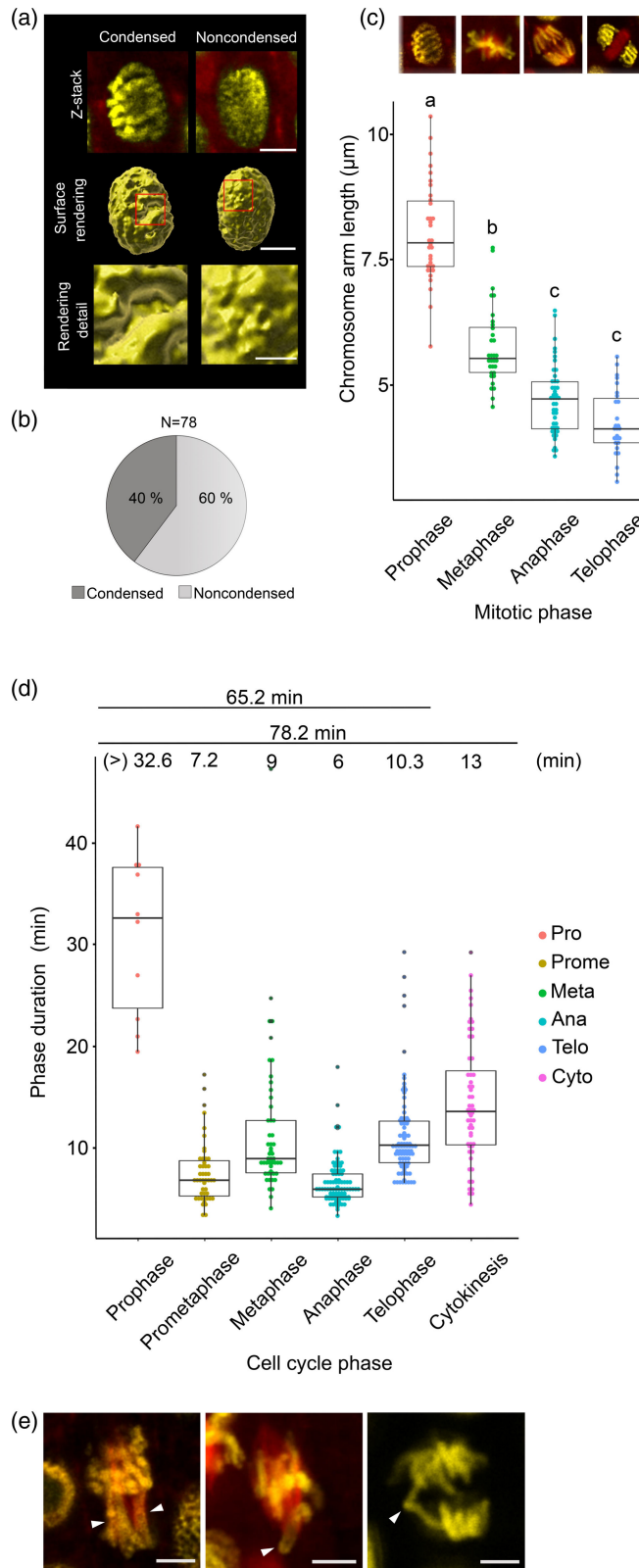
(a) Confocal microscopy-based 3D projection of pre-prophase nuclei (Z-stack) with condensed (left) and non-condensed (right) chromatin visualized by EYFP-H2B (yellow) and microtubules with mCHERRY-TUA3 (red). The next rows show surface rendering of whole nuclei and detail of a region indicated by red square, in Imaris bitplane (rendering parameters: surface detail 0.4 μm ; absolute intensity thresholding; 90% voxels above 10). Scale bars of whole nuclei = 5 μm and insets = 2 μm .

(b) Percentage of pre-prophase cells ($n = 78$) with condensed and non-condensed chromosomes.

(c) Average chromosome arm length in different mitotic phases. The lower and upper hinges of the boxplots correspond to the first and third quartiles of the data, respectively, and the thick black line within the boxes marks the median. The lower and the upper whiskers mark 10 and 90 percent intervals, respectively. A total of $n = 138$ chromosomes were measured: prophase $n = 34$, metaphase $n = 32$, anaphase $n = 45$, and telophase $n = 27$. Different letters indicate significant differences ($P \leq 0.05$, one-way ANOVA, factor 1 = nucleoli number), and grouping was done using Tukey's and Fisher's exact methods. Scale bars = 5 μm .

(d) Duration of individual mitotic stages. A total of $n = 337$ phase lengths were measured: prophase $n = 10$, prometaphase = 47, metaphase $n = 50$, anaphase $n = 88$, telophase $n = 86$, cytokinesis $n = 56$. The boxplot design and statistics are the same as in (c).

(e) Examples of defective mitosis using EYFP-H2B (yellow) and mCHERRY-TUA3 (red) fluorescent marker lines. The defects are marked by white arrowheads. From left: abnormal chromosome condensation and prometaphase–metaphase alignment, lagging chromosome, prolonged cohesion between sister chromatids. Scale bars = 5 μm .



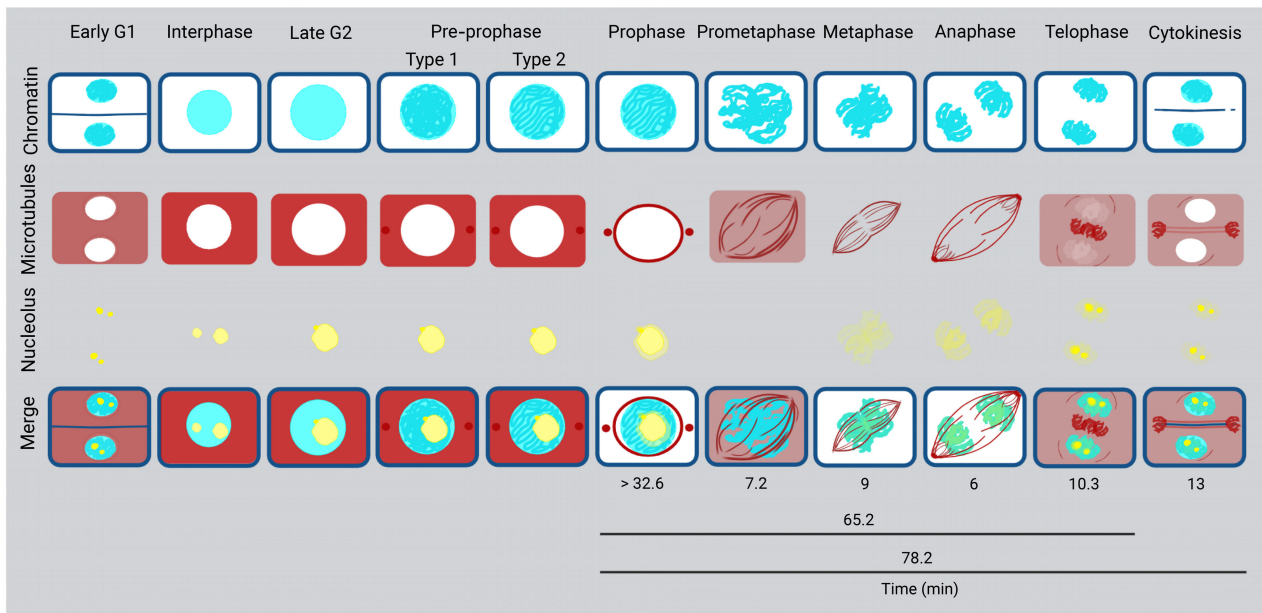


Figure 5. An atlas of barley cell cycle as visualized using fluorescent marker lines described in this study. Chromatin and cell walls = light blue, microtubules = red, and nucleolus = yellow. The time indicates median duration of individual mitotic stages and whole mitosis, > symbol indicates non-defined start of prophase.

et al., 2014). This suggests that chromosomes are spiraled before the dissolution of the nuclear envelope in many barley nuclei, likely by the activity of nuclear Condensin II (Hirota et al., 2004). Importantly, this indicates that chromosome condensation and microtubule organization are at least partially asynchronous and chromosome condensation starts well ahead of nuclear envelope dissolution in barley. We found condensed chromosomes also in nuclei of G0/G1 cells suggesting delayed decondensation. Speculatively, some fast-cycling barley nuclei might even undergo interphase with semi-condensed chromosomes. However, testing this possibility will require developing new interphase-specific FLMs.

The dissolution of the nuclear envelope allows the translocation of Condensin I from the cytoplasm to chromosomes and the establishment of compact metaphase chromosome structure (Ono et al., 2004). Measurements of chromosome arm length over different mitotic stages revealed that their condensation did not stop at metaphase but continued in other stages, and the chromosomes were shortest at telophase. This extends the findings in mammalian cells, where chromosomes reached maximum compaction at anaphase (Mora-Bermudez et al., 2007). The post-metaphase chromosome compaction is controlled by the Aurora kinase in a Condensin-independent manner (Neurohr et al., 2011; Wilkins et al., 2014). The progressive chromosome compaction might help establishing a balanced mitotic spindle (Neurohr et al., 2011, Wilkins et al., 2014) and/or to prevent a cleavage of the long chromosome arms and/or lagging chromosomes by newly

emerging furrow in animals or phragmoplast in plants (Hudakova et al., 2002; Mora-Bermudez et al., 2007; Schubert & Oud, 1997).

Previous studies estimated the duration of the whole barley cell cycle, by immunolabeling of tagged base analogs incorporated into the genomic DNA, to be 8.5 to 15 h (Kwasniewska & Jaskowiak, 2016; Schwammenhoferova & Ondrej, 1978). The G1 took from 1.3 to 4.5 h, S phase from 3.5 to 6.5 h, G2 from 3 to 5 h, and mitosis 1 to 2 h. Individual mitotic phases were estimated as follows: prophase 48 min, metaphase 23.4 min, anaphase 12.6 min, and telophase 21 min, corresponding to a total of 105 min (= 1.75 h). We measured average mitosis from prophase to telophase to be 65.2 min, making it 39.8 min (38%) shorter compared with previous data (Benneth & Finch, 1972). The differences included all stages, but were greater for the last ones (reduction relative to Benneth & Finch, 1972 in parentheses): prophase 32.6 min (32%), prometaphase + metaphase 16.2 min (31%), anaphase 6 min (52%), and telophase 10.3 min (51%). Except for technology advancements, this may arise from the use of various methodologies with different sensitivities toward determining the start and end of mitosis, growth conditions (mainly temperature differences), and genotypes (Brown, 1951; Kwasniewska & Jaskowiak, 2016; Schwammenhoferova & Ondrej, 1978).

In conclusion, we developed a unique set of barley reporter lines that allowed generating the most detailed atlas of barley mitosis and cytokinesis up to date by live cell imaging and estimating the duration of individual mitotic stages. Altogether, our results set up a solid

platform for future studies of chromosome and microtubule dynamics in the context of barley development and stress responses.

EXPERIMENTAL PROCEDURES

Plant growth and embryo dissection

Two-row spring-type *H. vulgare* L. cv. Golden Promise (GP) was used in this study. For germination, seeds were soaked in tap water on wet filter paper, stratified in the dark at 4°C for 48 h, and then transferred to 24°C for 48 h. The germinating plantlets were put into coconut fiber pots (Rosteto) filled with a mixture of substrate (Klasmann) and sand (3:1 v/v) and were grown in a phyto-chamber with 12-h day (200 $\mu\text{mol}^{-1}\text{m}^2\text{sec}^{-1}$, 15°C)/12-h night (0 $\mu\text{mol}^{-1}\text{m}^2\text{sec}^{-1}$, 13°C) and 70% relative humidity regime. Two weeks later, the plants were replanted into 3-liter pots. After the emergence of the fourth leaf, plants were fertilized with 12 g of grass fertilizer (Compo), grown for another 6 weeks, and then fertilized with 100 mL 2% (w/v) Hakaphos ROT fertilizer (Compo) once per week until seed maturation. Crosses between the FMLs were done according to Thomas et al. (2019). The mature F1 hybrid seeds were surface sterilized as described (Marthe et al., 2015) and soaked in sterile water at 4°C overnight, and the embryos were manually extracted under a binocular microscope using tweezers in sterile conditions. Dissected embryos were placed on sterile plates with Murashige–Skoog (½ MS) medium with 0.6% agar (w/v). The plates were sealed and cultivated under 16-h light (30 $\mu\text{mol}^{-1}\text{m}^2\text{sec}^{-1}$)/8-h dark cycles at 21°C in the Percival chamber for 7 days.

Nucleic acids isolation and cDNA synthesis

The plant tissues were flash-frozen in liquid nitrogen and kept at –80°C until use. Genomic DNA was isolated with a NucleoSpin® Plant II isolation kit (Macherey-Nagel) according to the manufacturer's instructions or via the protocol of Edwards (Edwards et al., 1991). Total RNA from roots and immature flowers was isolated using the RNeasy isolation kit (Qiagen) with additional on-column DNase I digestion. Isolated RNA was stored at –80°C until cDNA synthesis. The cDNA was obtained by reverse transcription (Transcriptor High Fidelity cDNA Synthesis Kit; Roche) using anchored-oligo(dT)₁₈ primers and standard reaction conditions.

Cloning reporter constructs and barley transformation

Primers used in this study are listed in Table S2. The development of the *ZmProUBI1:YFP-HvFIBRILLARIN1:T35S* (EYFP-FIB1) reporter line was described earlier (Perutka et al., 2021). The fusion construct *ZmUBI1:CFP-HvH2B:T35S* (CFP-H2B) was generated in a procedure analogous to *EYFP-FIB1*. CDS sequence of GP *HISTONE 2B* (*HvH2B*; HORVU.MOREX.r3.3HG0252240) was amplified from cDNA with the primers H2B_fwd and H2B_rev including stop codon, reamplified with specific primers containing *attB* sites and cloned into the *pDONR2r-P3* by BP reaction. The final *CFP-H2B* expression cassette was created by LR multisite reaction subcloning three entry vectors *pEN-L4-UBIL-R1* (*ZmUBI1*), *pEN-L1-C-L2* with *CFP* sequence, and *pDONR-P2r-P3* containing *HvH2B* CDS into the *pH7m34GW* destination vector. The cloning of the *ZmUBI1:EYFP-HvH2B:T35S* fusion construct (EYFP-H2B) followed the strategy for *CFP-H2B*, using *pEN-L1-Y-L2* coding EYFP instead of *pEN-L1-C-L2*.

The *mCHERRY TUBULIN ALPHA CHAIN 3* (*HvTUA3*; HORVU.MOREX.r3.4HG0338800) fragment was synthesized by the GeneArt® Gene Synthesis (Thermo Fisher Scientific) and cloned into

the vector *pMK-RQ* (AmpR) (GeneArt, Thermo Fischer Scientific, Waltham, USA) and subcloned into the Gateway™ Entry Vector *pENTR1A*, through specific restriction sites presented in the synthesized fragment. The resulting entry clone was subcloned into the *pBRACT 214* vector (provided by John Innes Centre, Norwich, UK), downstream of the *ZmUBI1* promoter via Gateway LR recombination reaction. The final cassette contains *ZmUBI1:mCHERRY-TUA3:Tnos* (*mCherry-TUA3*) and the *hpt* gene driven by the *CaMV35Spro*.

All final constructs were verified by Sanger sequencing using a commercial service (SeqMe, Czech Republic) and transformed into *Agrobacterium tumefaciens* strain AGL1 (together with the helper vector *pSoup* for the construct *mCHERRY-TUA3*). After transformation, the plasmids were isolated from AGL1, their integrity was verified by enzymatic restriction, and the AGL1 cultures were mixed 1:1 v/v with 100% glycerol and stored at –80°C until use.

Immature embryos were dissected approximately 14 days after pollination and transformed according to the previously described protocols (Harwood et al., 2009; Marthe et al., 2015). After the transformation, 25 embryos were placed on a 10-cm-diameter Petri dish with selection media containing 1 mL/L hygromycin (50 mg/mL; Roche) and 0.6% (w/v) Phytoagar (Duchefa Biochemie) for 2 weeks, then young embryonic calli were transferred onto the fresh Petri dishes containing the same media (16 calli per dish) and then after 2 weeks, the calli were transferred onto Petri dishes with regeneration media containing 500 $\mu\text{L/L}$ hygromycin (50 mg/mL) and 0.6% (w/v) Phytoagar (10 calli per dish). After another 2 weeks, calli with emerging shoots were transferred onto fresh regeneration media until roots were visible. Young plantlets with roots were transferred into the sterile PTC containers (Duchefa Biochemie) containing regeneration media without hygromycin or directly into the coconut fiber pots (Rosteto). All regenerated plants were genotyped for the presence of the *hpt* resistance gene, and the negative plants were excluded.

Genotyping of transgenic plants

Regenerated plants were genotyped for the presence of *Hyg* selection marker by PCR with primer pairs *Hyg_fwd/Hyg_rev* (EYFP-FIB1, CFP-H2B, and EYFP-H2B lines) or *Hyg2_fwd/Hyg2_rev* (*mCHERRY-TUA3* line). Plants of individual FMLs were additionally PCR genotyped for the presence of the respective fluorescent protein gene using primer pairs *YFP_fwd/YFP_rev*, *CFP_fwd/CFP_rev*, and *mCHERRY_fwd/mCHERRY_rev* for detection of *YFP*, *CFP*, and *mCHERRY*, respectively. PCR amplification was done using DreamTaq Polymerase (Thermo Fisher Scientific, Waltham, USA) and standard reaction conditions. The amplification products were monitored on 1% agarose gels stained with ethidium bromide 0.5 $\mu\text{g ml}^{-1}$. The primers used in this study are provided in Table S2.

Ploidy measurements

Around 2-cm-long leaf samples were cut off each of the selected FMLs and used for the nuclei isolation as described in Dolezel et al. (1994) with modifications. The ploidy was analyzed on Partec PAS I flow cytometer with the use of cv. Golden Promise as a diploid standard. DNA was stained with the 4',6'-diamidino-2-phenylindole (DAPI).

Microscopy

For the time-lapse analysis, seeds of FMLs were surface sterilized as described (Marthe et al., 2015), soaked in sterile water at 4°C

for 48 h, and placed on the wet filter paper at 24°C for 48 h to germinate. To increase the seed germination of F1 crosses, embryos of sterilized and cold-stratified seeds were dissected under a binocular microscope with pinnets and put on the plates with ½ MS medium in sterile conditions. Plates were placed into the Percival chamber (16 h light 30 μmol⁻¹ m² sec⁻¹) at 21°C for 48 h. Small plantlets were put on a slide with a chamber made by both-sided tape into a water drop and covered with a cover slip.

Microscopic images were acquired using a Leica TCS SP8 STED3X confocal microscope (Leica Microsystems, Wetzlar, Germany), equipped with an HC PL APO CS2 20x/0.75 DRY objective, HC PL APO CS2 63x/1.40 Oil objective, hybrid detectors (HyD), and the Leica Application Suite X (LAS-X) software version 3.5.5 with the Leica Lightning module (Leica, Buffalo Grove, IL, USA). Time-lapse confocal Z-stack images of approximately 20–30 μm width were captured in line (EYFP-FIB1 mCherry-TUA3 and EYFP-H2B mCherry-TUA3 double lines) or sequential (CFP-H2B mCherry-TUA3, CFP-H2B EYFP-FIB1 double lines, and EYFP-FIB1 CFP-H2B mCherry-TUA3 triple line) scanning modes depending on the specific combination of detected fluorophores. We used 508 nm (EYFP), 405 nm (CFP), and 514 nm (mCherry or EYFP-FIB1) laser lines for excitation and appropriate emission spectrum. Individual Z-stack scans were done every 30-sec or 45-sec intervals. Images were processed in Adobe pre-hybridize shop version 12.0 (Adobe Systems), Imaris version 9.7.2 (Oxford Instruments), ImageJ Fiji version 1.53c (Schindelin et al., 2012), and Inkscape (Inkscape project).

The average chromosome arm length was estimated by measuring individually distinguishable arms from end to the primary constriction (Ramesh & Singh, 1996).

ACKNOWLEDGMENTS

We thank E. Jahnová for the help with genotyping and media preparation; P. Čápal and J. Weiserová for the assistance with nuclei sorting; and K. Strelcová, V. Svobodová, A. Mičuchová, and I. Hradilová for the help with barley transformation and plant regeneration.

AUTHOR CONTRIBUTIONS

KK designed and cloned CFP-H2B, EYFP-H2B, and YFP-FIB1 FLM constructs and performed a selection of the transgenic lines and confocal microscopy under the supervision of AP. The transformation of *CFP-H2B* and *YFP-FIB1* constructs was performed under the supervision of VB; PG and JŠ designed *mCherry-TUA3* construct; CM and MO performed transformation, selection, and basic characterization of mCherry-TUA3 reporter barley line; AP and KK designed and supervised the project.

CONFLICT OF INTEREST STATEMENT

The authors declare that the research was conducted in the absence of any commercial or financial relationships that could be construed as a potential conflict of interest.

FUNDING INFORMATION

Multiple authors were supported by the ERDF project 'Plants as a tool for sustainable global development' (No. CZ.02.1.01/0.0/0.0/16_019/0000827). The work was further supported by the MEYS INTER-COST grant LTC18026,

GAČR grant 21-02929S and Purkyně fellowship from the Czech Acad Sci to A.P.

SUPPORTING INFORMATION

Additional Supporting Information may be found in the online version of this article.

Figure S1. Phenotypes of transgenic FML plants and seeds.

File S1. Amino acid sequences of proteins used for the creation of fluorescent marker lines.

Table S1. Fluorescent marker lines (FMLs) of barley used in this study.

Table S2. Primers used in this study.

Video S1. Time-lapse microscopy of nucleoli (EYFP-FIB1) and microtubules (mCherry-TUA3) in barley roots. The root was photographed for 22 min and 45 sec in 30-sec intervals.

Video S2. Time-lapse microscopy of chromatin (EYFP-H2B) and microtubules (mCherry-TUA3) in barley roots. The root was photographed for 36 min and 45 sec in 30-sec intervals.

Video S3. Time-lapse microscopy of chromatin (CFP-H2B) and nucleoli (EYFP-FIB1) in barley roots. The root was photographed for 23 min and 30 sec in 15-sec intervals.

OPEN RESEARCH BADGES



This article has earned an Open Data badge for making publicly available the digitally-shareable data necessary to reproduce the reported results. The data is available at [[insert provided URL from Open Research Disclosure Form]].

REFERENCES

- Ambrose, J.C. & Cyr, R. (2008) Mitotic spindle organization by the preprophase band. *Molecular Plant*, **1**, 950–960.
- Baiza, A.M., Vazquezramos, J.M. & Dejimenez, E.S. (1989) DNA-synthesis and cell-division in embryonic maize tissues during germination. *Journal of Plant Physiology*, **135**, 416–421.
- Bajer, A. & Allen, R.D. (1966) Structure and organization of the living mitotic spindle of *Haemanthus endosperm*. *Science*, **151**, 572–574.
- Baluska, F., Samaj, J., Volkmann, D. & Barlow, P.W. (1997) Impact of taxol-mediated stabilization of microtubules on nuclear morphology, ploidy levels and cell growth in maize roots. *Biology of the Cell*, **89**, 221–231.
- Benneth, M. & Finch, R. (1972) The mitotic cycle time of root meristem cells of *Hordeum vulgare*. *Caryologia*, **25**, 399–444.
- Boisnard-Lorig, C., Colon-Carmona, A., Bauch, W., Hodge, S., Doerner, P., Bancharrel, E. et al. (2001) Dynamic analyses of the expression of the HIS-TONE::YFP fusion protein in arabidopsis show that syncytial endosperm is divided in mitotic domains. *Plant Cell*, **13**, 495–509.
- Brown, R. (1951) The effects of temperature on the durations of the different stages of cell division in the root-tip. *Journal of Experimental Botany*, **2**, 96–110.
- Demchenko, N.P. & Demchenko, K.N. (2001) Resumption of DNA synthesis and cell division in wheat roots as related to lateral root initiation. *Russian Journal of Plant Physiology*, **48**, 755–763.
- Dolezel, J., Lucretti, S. & Schubert, I. (1994) Plant chromosome analysis and sorting by flow cytometry. *Critical Reviews in Plant Sciences*, **13**, 275–309.
- Donaldson, L. (2020) Autofluorescence in plants. *Molecules*, **25**, 2393.
- Echevarria, C., Gutierrez, C. & Desvoyes, B. (2021) Tools for assessing cell-cycle progression in plants. *Plant and Cell Physiology*, **62**, 1231–1238.
- Edwards, K., Johnstone, C. & Thompson, C. (1991) A simple and rapid method for the preparation of plant genomic DNA for PCR analysis. *Nucleic Acids Research*, **19**, 1349.

- Feitoza, L., Costa, L. & Guerra, M. (2017) Condensation patterns of prophase/prometaphase chromosome are correlated with H4K5 histone acetylation and genomic DNA contents in plants. *PLoS One*, **12**, e0183341.
- Fomproix, N., Gebrane-Younes, J. & Hernandez-Verdun, D. (1998) Effects of anti-fibrillar antibodies on building of functional nucleoli at the end of mitosis. *Journal of Cell Science*, **111**, 359–372.
- Fuchs, J., Demidov, D., Houben, A. & Schubert, I. (2006) Chromosomal histone modification patterns - from conservation to diversity. *Trends in Plant Science*, **11**, 199–208.
- Gautier, T., Dauphinvillermant, C., Andre, C., Masson, C., Arnoult, J. & Hernandezverdun, D. (1992) Identification and characterization of a new set of nucleolar ribonucleoproteins which line the chromosomes during mitosis. *Experimental Cell Research*, **200**, 5–15.
- Gibcus, J.H., Samejima, K., Goloborodko, A., Samejima, I., Naumova, N., Nuebler, J. *et al.* (2018) A pathway for mitotic chromosome formation. *Science*, **359**, 652.
- Gutierrez, C. (2009) The *Arabidopsis* cell cycle division. *Arabidopsis Book*, **7**, e0120.
- Hamada, T. (2014) Microtubule organization and microtubule-associated proteins in plant cells. *International Review of Cell and Molecular Biology*, **312**(312), 1–52.
- Harwood, W.A., Bartlett, J.G., Alves, S.C., Perry, M., Smedley, M.A., Leyland, N. *et al.* (2009) Barley transformation using agrobacterium-mediated techniques. *Methods in Molecular Biology*, **478**, 137–147.
- Hernandez-Verdun, D. (2011) Assembly and disassembly of the nucleolus during the cell cycle. *Nucleus*, **2**, 189–194.
- Hirota, T., Gerlich, D., Koch, B., Ellenberg, J. & Peters, J.M. (2004) Distinct functions of condensin I and II in mitotic chromosome assembly. *Journal of Cell Science*, **117**, 6435–6445.
- Houben, A., Wako, T., Furushima-Shimogawara, R., Presting, G., Kunzel, G., Schubert, I. *et al.* (1999) The cell cycle dependent phosphorylation of histone H3 is correlated with the condensation of plant mitotic chromosomes. *Plant Journal*, **18**, 675–679.
- Hudakova, S., Kunzel, G., Endo, T.R. & Schubert, I. (2002) Barley chromosome arms longer than half of the spindle axis interfere with nuclear divisions. *Cytogenetic and Genome Research*, **98**, 101–107.
- Jasencakova, Z., Meister, A. & Schubert, I. (2001) Chromatin organization and its relation to replication and histone acetylation during the cell cycle in barley. *Chromosoma*, **110**, 83–92.
- Kalinina, N.O., Makarova, S., Makhontenko, A., Love, A.J. & Taliensky, M. (2018) The multiple functions of the nucleolus in plant development, disease and stress responses. *Frontiers in Plant Science*, **9**, 132.
- Kimata, Y., Leturcq, M. & Aradhya, R. (2020) Emerging roles of metazoan cell cycle regulators as coordinators of the cell cycle and differentiation. *FEBS Letters*, **594**, 2061–2083.
- Kraikivski, P., Chen, K.C., Laomettacht, T., Murali, T.M. & Tyson, J.J. (2015) From START to FINISH: computational analysis of cell cycle control in budding yeast. *NPJ Systems Biology and Applications*, **1**, 15016.
- Kuznetsova, M.A., Chaban, I.A. & Sheval, E.V. (2017) Visualization of chromosome condensation in plants with large chromosomes. *BMC Plant Biology*, **17**, 153.
- Kwasniewska, J. & Jaskowiak, J. (2016) Transcriptional activity of rRNA genes in barley cells after mutagenic treatment. *PLoS One*, **11**, e0156865.
- Levine, M.S. & Holland, A.J. (2018) The impact of mitotic errors on cell proliferation and tumorigenesis. *Genes & Development*, **32**, 620–638.
- Liu, B. & Lee, Y.R.J. (2022) Spindle assembly and mitosis in plants. *Annual Review of Plant Biology*, **73**, 227–254.
- Liu, J.J. & Qu, L.J. (2008) Meiotic and mitotic cell cycle mutants involved in gametophyte development in *Arabidopsis*. *Molecular Plant*, **1**, 564–574.
- Lockhead, S., Moskaleva, A., Kamenz, J., Chen, Y.X., Kang, M.J., Reddy, A.R. *et al.* (2020) The apparent requirement for protein synthesis during G2 phase is due to checkpoint activation. *Cell Reports*, **32**, 107901.
- Ludwig, S.R., Oppenheimer, D.G., Silflow, C.D. & Snustad, D.P. (1987) Characterization of the *alpha*-tubulin gene family of *Arabidopsis thaliana*. *Proceedings of the National Academy of Sciences of the United States of America*, **84**, 5833–5837.
- Marc, J. (1997) Microtubule-organizing centres in plants. *Trends in Plant Science*, **2**, 223–230.
- Marthe, C., Kumlehn, J. & Hensel, G. (2015) Barley (*Hordeum vulgare* L.) transformation using immature embryos. *Methods in Molecular Biology*, **1223**, 71–83.
- Mickelson-Young, L., Wear, E., Mulvaney, P., Lee, T.J., Szymanski, E.S., Allen, G. *et al.* (2016) A flow cytometric method for estimating S-phase duration in plants. *Journal of Experimental Botany*, **67**, 6077–6087.
- Mirabet, V., Krupinski, P., Hamant, O., Meyerowitz, E.M., Jonsson, H. & Boudaoud, A. (2018) The self-organization of plant microtubules inside the cell volume yields their cortical localization, stable alignment, and sensitivity to external cues. *PLoS Computational Biology*, **14**, e1006011.
- Mora-Bermudez, F., Gerlich, D. & Ellenberg, J. (2007) Maximal chromosome compaction occurs by axial shortening in anaphase and depends on Aurora kinase. *Nature Cell Biology*, **9**, 822–U170.
- Neurohr, E., Naegeli, A., Titos, I., Theler, D., Greber, B., Barral, Y. *et al.* (2011) A midzone-based ruler adjusts chromosome compaction to anaphase spindle length. *Science*, **332**, 465–468.
- Noir, S., Marrocco, K., Masoud, K., Thomann, A., Gusti, A., Bitrian, M. *et al.* (2015) The control of *Arabidopsis thaliana* growth by cell proliferation and endoreplication requires the F-box protein FBL17. *Plant Cell*, **27**, 1461–1476.
- Ono, T., Fang, Y., Spector, D.L. & Hirano, T. (2004) Spatial and temporal regulation of condensins I and II in mitotic chromosome assembly in human cells. *Molecular Biology of the Cell*, **15**, 3296–3308.
- Perutka, Z., Kaduchova, K., Chamrad, I., Beinhauer, J., Lenobel, R., Petrovska, B. *et al.* (2021) Proteome analysis of condensed barley mitotic chromosomes. *Frontiers in Plant Science*, **12**, e723674.
- Pintard, L. & Bowerman, B. (2019) Mitotic cell division in *Caenorhabditis elegans*. *Genetics*, **211**, 35–73.
- Rabl, C. (1885) *Über Zelltheilung: Morphologisches Jahrbuch*, Leipzig: W. Engelmann; **10**, pp. 214–330.
- Ramesh, B. & Singh, V.P. (1996) Somatic karyotype analysis in barley (*Hordeum vulgare*). *Indian Journal of Genetics and Plant Breeding*, **56**, 248–255.
- Rasmussen, C.G. (2016) Using live-cell markers in maize to analyze cell division orientation and timing. *Plant Cell Division: Methods and Protocols*, **1370**, 209–225.
- Rasmussen, C.G. & Bellinger, M. (2018) An overview of plant division-plane orientation. *New Phytologist*, **219**, 505–512.
- Reichow, S.L., Hamma, T., Ferre-D'Amare, A.R. & Varani, G. (2007) The structure and function of small nucleolar ribonucleoproteins. *Nucleic Acids Research*, **35**, 1452–1464.
- Rosa, S. & Shaw, P. (2013) Insights into chromatin structure and dynamics in plants. *Biology*, **2**, 1378–1410.
- Rotaspart, L., Sansoni, F., Mizzotti, C., Tadini, L. & Pesaresi, P. (2020) Barley's second spring as a model organism for chloroplast research. *Plants*, **9**, 803.
- Schindelin, J., Arganda-Carreras, I., Frise, E., Kaynig, V., Longair, M., Pietzsch, T. *et al.* (2012) Fiji: an open-source platform for biological-image analysis. *Nature Methods*, **9**, 676–682.
- Schubert, I. & Oud, J.L. (1997) There is an upper limit of chromosome size for normal development of an organism. *Cell*, **88**, 515–520.
- Schwammenhoferova, K. & Ondrej, M. (1978) Mitotic-cycle kinetics of root-meristems of isolated barley embryos and intact seedlings - labeling of nuclei by tetraploidy. *Biologia Plantarum*, **20**, 409–417.
- Smertenko, A., Assaad, F., Baluska, F., Bezanilla, M., Buschmann, H., Drakaki, G. *et al.* (2017) Plant cytokinesis: terminology for structures and processes. *Trends in Cell Biology*, **27**, 885–894.
- Thomas, W.T.B., Bull, H., Booth, A., Hamilton, R., Forster, B.P. & Franckowiak, J.D. (2019) A practical guide to barley crossing. *Methods in Molecular Biology*, **1900**, 21–36.
- Van Hooser, A.A., Yuh, P. & Heald, R. (2005) The perichromosomal layer. *Chromosoma*, **114**, 377–388.
- Vyplelová, P., Ovečka, M. & Šamaj, J. (2017) Alfalfa root growth rate correlates with progression of microtubules during mitosis and cytokinesis as revealed by environmental light-sheet microscopy. *Frontiers in Plant Science*, **8**, 1870.
- Wako, T., Murakami, Y. & Fukui, K. (2005) Comprehensive analysis of dynamics of histone H4 acetylation in mitotic barley cells. *Genes & Genetic Systems*, **80**, 269–276.
- Wilkins, B.J., Rall, N.A., Ostwal, Y., Kruitwagen, T., Hiragami-Hamada, K., Winkler, M. *et al.* (2014) A cascade of histone modifications induces chromatin condensation in mitosis. *Science*, **343**, 77–80.
- Zadoks, J.C. (1985) A decimal code for the growth-stages of cereals. *Current Contents/Agriculture Biology & Environmental Sciences*, **14**, 415–421.
- Zhang, H. & Dawe, R.K. (2011) Mechanisms of plant spindle formation. *Chromosome Research*, **19**, 335–344.

Appendix III

EasyClick: An improved system for confocal microscopy of live roots with a user-optimized sample holder

Kaduchová, K., Čmiel, V., Koláčková, V., and Pecinka, A.

Planta

in press

IF (2021): 4.45

1 **EasyClick: An improved system for confocal microscopy of live roots**
2 **with a user-optimized sample holder**

3

4 **Kateřina Kaduchov^{1,2}, Vratislav miel ³, Veronika Kolckov ¹, Ales Pecinka ¹**

5

6 ¹Institute of Experimental Botany of the Czech Academy of Sciences, Centre of Plant Structural
7 and Functional Genomics, Šlechtitel 31, 779 00 Olomouc, Czech Republic.

8 ²Department of Cell Biology and Genetics, Faculty of Science, Palacky University, 779 00
9 Olomouc, Czech Republic.

10 ³Department of Biomedical Engineering, Faculty of Electrical Engineering and Communication,
11 Brno University of Technology, Technick 3082/12, 61600 Brno, Czech Republic.

12

13 ORCID:

14 Kateřina Kaduchov: 0000-0001-9259-5942

15 Vratislav miel: 0000-0002-0441-9840

16 Veronika Kolckov: 0000-0002-5416-8947

17 Ales Pecinka: 0000-0001-9277-1766

18

19 ***Correspondence:**

20 Aleř Peinka, pecinka@ueb.cas.cz

21 Vratislav miel, cmiel@vut.cz

22

23

24 **Keywords:** Barley, Confocal microscopy, EasyClick, Growth, *Hordeum vulgare*, Live cell
25 imaging, Plant, Root, .

26

27 **Main Conclusions**

28 We describe a user-optimized sample holder EasyClick for medium-sized plants that reduces
29 root side movements and thus greatly extends the duration of live cell confocal microscopy.

30

31 **Abbreviations**

32 3D Three Dimensional

33 EYFP Enhanced Yellow Fluorescent Protein

2

3 **Abstract**

4 Preparation and mounting of the samples are key factors for successful live cell microscopy.
5 To acquire biologically relevant data, it is necessary to minimize stress and avoid physical
6 damage to plant tissues during the installation of the sample into the microscope. This is
7 challenging, particularly when the whole plant is mounted as the living sample needs to be
8 properly anchored in the microscopic system to obtain high-quality and high-resolution data.
9 Here, we present a user-optimized sample holder EasyClick for live cell inverted confocal
10 microscopic analysis of plant roots with diameters from 0.3 to 0.7 mm. The EasyClick holder
11 was tested on an inverted confocal microscope using germinating plants of several cereals.
12 Nevertheless, it can be directly used on other types of inverted microscopes from various
13 producers and on different plant species. The EasyClick holder effectively restricts root lateral
14 and vertical movements. This greatly improves the conditions for time-lapse microscopy of the
15 samples of interest.

16

17 **Introduction**

18 High-quality live cell microscopy is essential for understanding the principles of plant cell
19 biology (Nagy et al. 2012; Hamant et al. 2019). At the confocal (180 nm lateral and 500 nm
20 axial) resolution, mutual cell-cell, cell-molecule and/or molecule-molecule interactions can be
21 explored (Fouquet et al. 2015; Elliott 2020). Compared to confocal *in vivo* analysis of animal
22 cell cultures or early developmental stages of small-to-middle sized animal models (e.g.
23 *Drosophila melanogaster*, *Danio rerio*), plant researchers are facing a variety of difficulties
24 when setting experiments, including strong autofluorescence of chlorophyll and secondary
25 metabolites, interference of the cell walls and plant growth affected by gravitropism. The
26 gravity-directed growth controls both the upward growth of the shoot and leaves and the
27 downward growth of roots, enabling the proper uptake of water and ions required for plant
28 development (Chen et al. 1999). Due to gravitropism, plants placed in a non-vertical direction
29 can quickly react and point their growth in the vertical direction again. As amyloplasts are not
30 fixed in the root cap cells, they sprinkle frequently during growth which makes the root rotate
31 and twist along the elongation axis (Rahni and Birnbaum 2019). In standard confocal
32 microscopes, the sample is placed horizontally during the scanning. When the living plant is
33 set between glass slides, the root immediately reacts to rotate. These moves regularly reach
34 a growth rate 120 - 800 $\mu\text{m}\cdot\text{h}^{-1}$ in various model plants, e.g. 120 - 150 $\mu\text{m}\cdot\text{h}^{-1}$ in *Arabidopsis*
35 *thaliana*, $\sim 700 \mu\text{m}\cdot\text{h}^{-1}$ in barley (*Hordeum vulgare*) or $\sim 800 \mu\text{m}\cdot\text{h}^{-1}$ in rice (*Oryza sativa*)

1 (Yazdanbakhsh and Fisahn 2010; Higuchi et al. 2017). Taken together, the stochastic root
2 movements make live cell microscopy of the root apical meristems challenging.

3 There are several approaches how to prevent or restrict excessive root movements on a
4 microscopic slide. Root movements in the x-y axis leading to root twisting were previously
5 decreased by placing the plant between two nylon strings fixed on a slide or into the
6 microscopic slide chambers used for cell culture chemical treatments (Grossmann et al. 2011;
7 Rahni and Birnbaum 2019). The movement in the z-axis is normally restricted by covering the
8 sample with a coverslip but sometimes this limitation is not enough, especially when the roots
9 with a wider diameter are analyzed. In some setups, the coverslip can be replaced by the
10 agarose block placed on the top of the lying root which pushes it equally down onto a slide
11 surface (Rahni and Birnbaum 2019).

12 Even though all these approaches improved plant root microscopy quality, the preparation of
13 the plant sample itself is time-consuming and not user-friendly in these systems. To increase
14 sample preparation effectiveness and enable long-term microscopy scanning, we co-
15 developed a custom-optimized microscopy holder EasyClick facilitating plant root analysis.
16 The tested version of the holder is primarily designed for the microscopy of plants with a root
17 diameter from 0.3 to 0.7 mm, which includes e.g. several cereal crops such as barley, wheat,
18 or rye.

19

20 **Materials and methods**

21 **Rapid movements of barley roots in a standard microscopy setup**

22 Recently, we established a series of barley fluorescent marker lines for monitoring nuclear
23 compartments and microtubules (Kaduchová et al. 2023). During this analysis, we noted rapid
24 movements of barley root apices in the frontal, lateral, and vertical directions. This had a major
25 negative impact on the duration of individual scanning windows and the identification of the
26 cells (Fig. 1A). Due to these movements, a cell or mitotic division of interest frequently
27 appeared out of the focus or even the scanned area. To mitigate this issue, we tested a
28 prototype of a microscopy holder named EasyClick (Pragolab s.r.o., Praha, Czech Republic;
29 catalog numbers of individual parts: VIV0004, VIV0013, T220007, T220008, T220009) that
30 was designed to reduce root movements by defining the growth direction and decreasing the
31 probability of root damage during the mounting.

32

33 **Preparation of the plant sample**

1 The initial optimization was done using the wild-type two-row spring barley (*Hordeum vulgare*
2 L.) cultivar Golden Promise (PI 343079; from the National small grains collection of the national
3 plant germplasm system of the United States Department of Agriculture-Agricultural Research
4 Service) and fluorescent marker line ENHANCED YELLOW FLUORESCENT PROTEIN -
5 HISTONE 2B (EYFP-H2B) in Golden Promise background (Kaduchová et al. 2023). Dry barley
6 seeds were stratified on the wet filter paper soaked in tap water at 4°C for 48 h in the dark and
7 then transferred to 24 °C for 48 h to germinate in the dark.

8

9 **Mounting of the sample into the EasyClick microscopy holder**

10 The principle of the EasyClick microscopy holder components and their assembly are shown
11 in Figs. 1B-D. The EasyClick consists of a three dimensional (3D)-printed plastic holder matrix
12 (PA11 material, powder laser sintering SLS) with embedded magnets on both sides, a stainless
13 steel metal plate (food and gastronomy industry use, 0.5 mm thickness) with 37 mm long
14 growth channels of different widths, a 0.5 mm thick polymethyl methacrylate plastic seal, and
15 a large coverslip (60 x 45 mm; Karl Hecht, Sondheim vor der Rhön, Německo) (Figs. 1B-D).
16 3D printed holder matrix was permanently fixed with the plastic seal (quick drying glue; Kavan,
17 Pardubice, Czech Republic). The remaining parts (metal plate, coverslip) are removable and
18 fixed via magnets (Fig. 1D).

19 During the fixation of the sample, the metal plate was put on the back side of the 3D-printed
20 matrix on the plastic seal where it was held with magnets. In the second step, a few drops of
21 liquid growth media were dripped on the metal surface. After covering the metal plate with a
22 large coverslip, the liquid media filled the metal plate channels. The large cover slip was
23 afterwards fixed on the metal plate with magnets. Subsequently, the plant sample was placed
24 into one of two positions bordered by raised holder edges making small 18 × 41 × 6 mm plant
25 containers (Fig. 1D). The construction of the EasyClick metal plate with ground edges allowed
26 for easy penetration of the root into the selected channel. After setting plants in proper
27 positions, the containers were filled with liquid growth media, alternatively, containers can be
28 covered with a wet tissue to reduce transpiration. A liquid was refilled with a Pasteur pipette
29 during the time-lapse experiments without any plant growth disruption and microscopy stage
30 movements. The EasyClick holder is easily fitted into the universal microscope stage mounting
31 system (Fig. 1E). Microscopic images were acquired using a Leica TCS SP8 STED3X confocal
32 microscope (Leica Microsystems, Wetzlar, Germany), equipped with an HC PL APO CS2
33 20x/0.75 DRY and HC PL APO CS2 639/1.40 Oil objective, hybrid detectors (HyD), and the
34 Leica Application Suite X (LAS-X) software version 3.5.5 with the Leica Lightning module
35 (Leica, Buffalo Grove, IL, USA). Time-lapse confocal Z-stack images of EYFP-H2B of

1 approximately 20–30 μm width were captured using 508 nm laser excitation line and
2 appropriate emission spectrum in 4-min intervals. Single time-lapse scans of roots in
3 transmission light were captured in 1-min intervals. Images were processed in Adobe pre-
4 hybridize shop version 12.0 (Adobe Systems), Imaris version 9.7.2 (Oxford Instruments), and
5 Inkscape (Inkscape project).

6 Three different custom-optimized variants of the metal plates (Type 1-3), differing in the growth
7 channel widths (0.4 mm; 0.5 mm, and 0.7 mm), were used depending on the size of the roots
8 of the analyzed plant (Fig. 1D). For each metal plate, up to two roots of two different plant
9 samples were installed and analyzed in short time intervals (four roots per metal plate in total).
10 More than 4 cm length of the channels enables the time-lapse scanning theoretically of more
11 than 48 h (counted for root growth rate of $600 \mu\text{m}\cdot\text{h}^{-1}$ when 1 cm long root is placed into 4 cm
12 channel). However, we recommend to use young (one or two days old) seedlings with roots
13 approximately 1-2 cm long for the microscopy analysis. Such roots can be easily placed into
14 the holder channel without a risk of damage caused by their length and can use the whole
15 channel length for growth. Due to the non-transparent material of the metal plate, we
16 recommend first navigating the root tip in the channel directly to the light path of the objective
17 and only then focusing at the Z-axis.

18

19 **Results**

20 During the microscopy analysis, the root movements in the y-axis (axis perpendicular to the
21 root growth axis) are limited by channel walls. Channel width should be selected so that it leads
22 the root straight while providing enough space for its growth (Figs. 1B-D). A test 28 min
23 scanning revealed that the root grew out of the analysis field under standard settings
24 (microscopy slide without any root restrictions) nevertheless the root placed in the EasyClick
25 microscopy holder remained in the scanning field and could still be analysed even after this
26 scanning time (Fig. 2, red arrowheads).

27 Similarly, the EasyClick channels reduce root twisting in the z-axis due to the thickness of the
28 metal plate ($500 \mu\text{m}$), roughly corresponds to the diameter of wider barley roots. This enables
29 root growth in the proximity of the coverslip in a limited space. Despite the optimized channel
30 z-axis height, it is still challenging to precisely set a root cell layer for detailed microscopy
31 analysis where the focal plane and vertical position of the object of interest will not change in
32 time. Furthermore, the conically shaped meristematic zone represents the most problematic
33 part of the root in our microscopy analysis. As the root grows, the cells in this region are pushed
34 into the higher scanning layers due to the production of new cells via mitotic divisions (Figs.
35 2C,D; cyan arrowheads). This may even lead to a change of the focus plane from epidermal

1 cell layer (Fig. 2D, 0 - 12 min) to the first cortex cell layer (Fig. 2D, 16 - 28 min). The holder
2 cannot solve completely this problem but reduces it by stabilizing the samples in several
3 directions.

4 Finally, we assessed whether the EasyClick holder affects barley root growth along its main
5 growth axis (Fig. 3A). We compared the root growth rate of unrestricted roots placed on a
6 microscopy slide (without holder) and roots placed in a microscopy holder during the 32-minute
7 time-lapse scanning. For better clarity, we calculated the root growth rate for a reference time
8 of 1 h. There was a greater variability as to the root growth rate in unrestricted conditions on
9 the microscopy slide, but the median growth rate was almost the same ($P = 0.801$) for both
10 conditions (in holder $604.1 \mu\text{m}\cdot\text{h}^{-1}$; without holder on slide $573.7 \mu\text{m}\cdot\text{h}^{-1}$). Afterward, we
11 measured the growth rate of roots after 24 h in the holder and on a microscopy slide. Although
12 the median root growth rate of samples from the holder ($167.3 \mu\text{m}\cdot\text{h}^{-1}$) and on a microscopy
13 slide ($302.8 \mu\text{m}\cdot\text{h}^{-1}$) differed by 1.8-fold, it was not significant ($P = 0.187$), possibly due to a
14 relatively large variation between individual roots (Fig. 3A). When comparing the growth rate
15 between 1 h and 24 h setups, the reduction was not significant for the free growing roots ($P =$
16 0.077), but opposite was true for the roots in holder ($P = 0.001$; Fig. 3A).

17 Finally, we tested the versatility of the EasyClick holder for root microscopy of different
18 crops (Fig. 3B). The Type 1 metal plate (0.4 mm channel width) fitted for the rye (*Secale*
19 *cereale*), and Type 2 metal plate (0.5 mm channel width) for the barley, wheat (*Triticum*
20 *aestivum*), and oat (*Avena sativa*). The Type 3 metal plate (0.7 mm channel width) was ideal
21 for some of the oat and wheat roots with a wider diameter. We also attempted to test the
22 germinating roots of several other crops such as faba bean (*Vicia faba*), garden pea (*Pisum*
23 *sativum*) and maize (*Zea mays*), but their roots were too thick even for the Type 3 plate (not
24 shown).

25

26 **Discussion**

27 Several systems for monitoring the growth of living plant roots in microscopes were already
28 described and can improve imaging of various plants as demonstrated for e.g. *Arabidopsis*
29 *thaliana* and *Medicago truncatula* (Grossmann et al. 2011; Ovecka et al. 2015; Berthet and
30 Maizel 2016; von Wangenheim et al. 2017). Specialized systems have been engineered to
31 explore interactions between plant roots and microbes or worms (Parashar and Pandey 2011;
32 Vernet et al. 2022).

33 The systems can be divided into two main groups based on the direction of plant root
34 cultivation: (i) vertical and (ii) horizontal. The vertical systems frequently utilize either light sheet

1 microscopy technology and the samples are mounted in different types of capillaries (Ovecka
2 et al. 2015; Vernet et al. 2022) or less often also confocal microscopy (von Wangenheim et al.
3 2017). The vertical confocal systems are typically based on microscopes that are turned 90°
4 to bring the slides with samples in a vertical position (von Wangenheim et al. 2017). The
5 advantage of these systems is that the roots can growth more-or-less straight towards the
6 center of gravity as typical for many plants (Chen et al. 1999; Migliaccio et al. 2013). The other
7 main direction of systems forces plants to grow in a horizontal position. These systems are
8 explored for various complex setups combining microscopy with microfluidic systems
9 (Grossmann et al. 2011; Parashar and Pandey 2011) or simply when the access to vertical
10 systems is not available (Rahni and Birnbaum 2019). The EasyClick system represents the
11 latter setup and is so far the only system that was tested and successfully used to on temperate
12 cereals (Kaduchová et al. 2023).

13 The horizontal growth of the plants is an obvious limitation for studies where root
14 gravitropism is essential for understanding given processes. It also has to be noted that not all
15 roots under natural conditions grow straight down and that soil contains various objects (e.g.
16 stones) that can cause roots to grow horizontally for some time until the object can be
17 bypassed. Therefore, the tendency of the root to bend towards the center of gravity might
18 represent a rather technical than biological problem. For applications where vertical growth is
19 needed, the EasyClick system could possibly be adapted for mounting into a 90° turned
20 confocal microscope (von Wangenheim et al. 2017). Alternatively, an add-on on horizontal
21 microscopes allowing observations in a vertical manner such as GraviKit could be applied
22 (Feldhaus et al. 2021).

23 The forward and to some extent also side movements of the conically shaped root tips
24 represents a major challenge for live cell microscopy analysis because the cells of interest
25 dynamically change their position in all directions. Therefore, it is essential to precisely fix the
26 living sample in space for a certain time while simulating more-or-less natural conditions for its
27 growth. Our initial trials to lead barley roots between two stretched fishing strings fixed on a
28 microscopy glass as described (Rahni and Birnbaum 2019), or covering the root with a block
29 of agar did not work well due to its thickness. Therefore, we tested the EasyClick microscopy
30 holder, which guides roots through narrow channels without disturbing their growth. There
31 were no significant differences in the rate of root growth freely on the microscopic slide versus
32 EasyClick at 1 h and then after 24 h. However, this parameter is relatively highly variable
33 between individual roots which could mask some subtle trends. While there were no significant
34 differences between mounting methods, there was a clear reduction in the root growth rate
35 after 24 h for both approaches and the difference was even statistically significant for the
36 holder. The cause of this is unknown and we could not find data for barley root growth rate in

1 specific types of soil. We hypothesize that barley roots might grow slower in soil than in free
2 space on microscopic slides and that they also naturally reduce their growth rate over time.

3 The great advantage of this system is a quick and easy assembly minimizing plant
4 damage and reducing stress. As the EasyClick holder permits plants to be grown for several
5 hours or even days, it is possible to firstly set two plants into the holder, let them grow for a
6 distinct time to overcome potential manipulation stress, and then apply some highly-sensitive
7 analyses like microtubule or chromosome dynamics (Kaduchová et al. 2023). Using of different
8 growth media will also allow for assessing mid- and long-term effects of specific nutrients,
9 treatments, or stresses. However, the growth compartments on the tested EasyClick model
10 were not separated by a watertight wall which means that only one type of growth media can
11 be applied at the time. The system can be used practically for germinating plants of a wide
12 range of species with root diameters below 0.7 mm. We demonstrated it by using EasyClick in
13 combination with different cereal species. However, the current set of metal plates might be
14 exclusive for species with larger roots such as e.g. garden pea, faba bean or maize. Their roots
15 were too thick even for the Type 3 metal plate.

16 One limitation noted in our analyses was the conical shape of the root tip. When
17 focused on a rhizodermal layer close to the tip, the frontal proliferation of the root and its
18 thickening caused a switch of the focus to cortex cell layer(s) and the disappearance of the
19 initially monitored cells. There are several possible solutions. First, using a lower magnification
20 with a greater focal depth. Second, extending the size of the z-stack. However, this might lead
21 to longer scanning times and exposure of plant cells to the laser. Finally, the microscopy could
22 focus on a position more distal from the root tip that already underwent the expansion and will
23 not change much anymore.

24 In conclusion, the tested 3D-printed EasyClick microscopy holder is a useful addition
25 to the microscopy toolbox for live cell confocal imaging within the roots of plants with root
26 diameter from 0.3 to 0.7 mm. The holder can help plant researchers perform precise confocal
27 microscopy analysis in a user-friendly manner. Moreover, this microscopy holder enables a
28 high-quality analysis on a wide range of confocal microscopes, where the sample is placed
29 horizontally during the scanning in the majority of cases. We envision future development of
30 the upright version of the EasyClick holder that will extend its use also to non-inverted confocal
31 microscopes.

32

33 **Acknowledgements**

1 We thank Dr. Martin Kopecký from Pragolab s.r.o. for providing early access to the EasyClick
2 microscopy sample holder and connecting researchers working on this project, we
3 acknowledge H. Tvardíková and E. Jahnová for help with harvesting and cleaning the barley
4 seeds.

5

6 **Author contribution**

7 K.K. managed the experimental design and tested EasyClick for various conditions, K.K. and
8 V.Č. optimized the design of the EasyClick microscopy holder; V.Č. performed the 3D models,
9 the printing of the holder matrix and produced the metal plates; K.K., and V.K. optimized the
10 confocal microscopy settings for live microscopy; K.K. performed microscopy; A.P. and K.K.
11 designed and supervised the project.

12

13 **Funding**

14 The work was further supported by the GAČR grant 21-02929S to A.P.

15

16 **Declarations**

17

18 **Competing interests**

19 The authors declare no personal or financial conflict of interest.

20

21 **Availability of data and materials**

22 Data are available within the article.

23

24 **References**

- 25 Berthet B, Maizel A (2016) Light sheet microscopy and live imaging of plants. *J Microsc* 263 (2):158-
26 164. doi:10.1111/jmi.12393
- 27 Chen RJ, Rosen E, Masson PH (1999) Gravitropism in higher plants. *Plant Physiol* 120 (2):343-350.
28 doi:10.1104/pp.120.2.343
- 29 Elliott AD (2020) Confocal microscopy: Principles and modern practices. *Curr Protoc Cytom* 92: e68.
30 doi:10.1002/cpcy.68.
- 31 Feldhaus C, Kolb M, Küppers M, Hardy S, Palmisano R (2021) GraviKit: An easy-to-implement
32 microscope add-on for observation of gravitation dependent processes. (preprint). *bioRxiv*.
33 doi:10.1101/2021.08.30.458259
- 34 Fouquet C, Gilles JF, Heck N, Dos Santos M, Schwartzmann R, Cannaya V, Morel MP, Davidson RS,
35 Trembleau A, Bolte S (2015) Improving axial resolution in confocal microscopy with new high

1 refractive index mounting media. Plos One 10 (3):e0121096.
2 doi:10.1371/journal.pone.0121096
3 Grossmann G, Guo WJ, Ehrhardt DW, Frommer WB, Sit RV, Quake SR, Meier M (2011) The RootChip:
4 An integrated microfluidic chip for plant science. Plant Cell 23 (12):4234-4240.
5 doi:10.1105/tpc.111.092577
6 Hamant O, Das P, Burian A (2019) Time-lapse imaging of developing shoot meristems using a confocal
7 laser scanning microscope. Plant cell morphogenesis: Methods and protocols, 2nd Edition
8 1992:257-268. doi:10.1007/978-1-4939-9469-4_17
9 Higuchi K, Ono K, Araki S, Nakamura S, Uesugi T, Makishima T, Ikari A, Hanaoka T, Sue M (2017)
10 Elongation of barley roots in high-pH nutrient solution is supported by both cell proliferation
11 and differentiation in the root apex. Plant Cell Environ 40 (8):1609-1617.
12 doi:10.1111/pce.12969
13 Kaduchová K, Marchetti C, Ovečka M, Galuszka P, Bergougnoux V, Šamaj J, Pecinka A (2023) Spatial
14 organization and dynamics of chromosomes and microtubules during barley mitosis. Plant J
15 115:602-613. doi:10.1111/tpj.16392
16 Migliaccio F, Tassone P, Fortunati A (2013) Circumnutation as an autonomous root movement in plants.
17 Am J Bot 100 (1):4-13. doi:10.3732/ajb.1200314
18 Nagy G, Kiraly G, Banfalvi G (2012) Optimization of cell cycle measurement by time-lapse microscopy.
19 Laboratory methods in cell biology: Biochemistry and cell culture 112:143-161.
20 doi:10.1016/b978-0-12-405914-6.00007-x
21 Ovečka M, Vaskebova L, Komis G, Luptovciak I, Smertenko A, Samaj J (2015) Preparation of plants for
22 developmental and cellular imaging by light-sheet microscopy. Nat Protoc 10 (8):1234-1247.
23 doi:10.1038/nprot.2015.081
24 Parashar A, Pandey S (2011) Plant-in-chip: Microfluidic system for studying root growth and pathogenic
25 interactions in Arabidopsis. Appl Phys Lett 98 (26). doi:10.1063/1.3604788
26 Rahni R, Birnbaum KD (2019) Week-long imaging of cell divisions in the Arabidopsis root meristem.
27 Plant Methods 15. doi:10.1186/s13007-019-0417-9
28 Vernet H, Fullana AM, Sorribas FJ, Gualda EJ (2022) Development of microscopic techniques for the
29 visualization of plant-root-knot nematode interaction. Plants-Basel 11 (9).
30 doi:10.3390/plants11091165
31 von Wangenheim D, Hauschild R, Fendrych M, Barone V, Benkova E, Friml J (2017) Live tracking of
32 moving samples in confocal microscopy for vertically grown roots. Elife 6.
33 doi:10.7554/eLife.26792
34 Yazdanbakhsh N, Fisahn J (2010) Analysis of Arabidopsis thaliana root growth kinetics with high
35 temporal and spatial resolution. Annals of Botany 105 (5):783-791. doi:10.1093/aob/mcq048

36

37 Fig. legends

38 **Fig. 1.** Barley root movements during time-lapse scanning and description of the microscopy
39 EasyClick holder. **A** Time-lapse of barley free root growth on a microscopy slide using
40 transmission light microscopy. Total scanning time 29 min. Scale bar = 200 µm. **B** 3D model
41 of individual EasyClick parts. **C** Three types of the metal plate differing in the growth channel
42 widths (0.4, 0.5 and 0.7 mm). **D** Detailed view of germinating barley plants in the holder. Scale
43 bars = 1 cm. **E** Installation of the EasyClick holder in the inverted microscope.

44

45 **Fig. 2.** Live cell confocal microscopy (CLSM) imaging of root apical meristems without and
46 with EasyClick holder. **A** Representative free growth of a root from two days old barley plant

1 without holder. Nuclei and chromosomes were visualized with the chromatin marker eYFP-
2 H2B. Scanning time = 28 min. Scale bar = 100 μm . **B** Channel-directed root movement with
3 EasyClick holder using the same fluorescent marker line as in (B). Scale bar = 100 μm . **C**
4 Detailed time-lapse single-cell layer scanning of root growing on a microscopy slide without
5 the holder. Note the shifts in both the horizontal (red arrowhead) and vertical (cyan arrowhead)
6 directions. Arrowheads of the same colour mark particular cell tracked in time. Scale bar = 10
7 μm . **D** Situation as in **C** with improved parameters due to EasyClick holder use. Arrowheads
8 of the same colour mark particular cell tracked in time. Scale bar = 10 μm .

9
10 **Fig. 3.** Root growth rate and mounting of roots from various cereals. **A** Roots growth rate from
11 two days old barley plants grown freely on a microscopic slide (Without holder 1 h; $n = 9$ roots),
12 shortly after introduction into the EasyClick (Holder 1 h; $n = 9$ roots), after 24 h of freely growing
13 on a microscopy slide (Without holder 24h; $n = 9$), and after 24 h in the EasyClick (Holder 24
14 h; $n = 9$). The total recording time of 32 min and the values were transformed to 1 h of total
15 growth time. The horizontal black lines within the boxes mark the median, the lower and upper
16 hinges of the boxplots correspond to the first and third quartiles of the data, and the whiskers
17 mark 10 and 90 % intervals. Asterisks above the boxes indicate statistically significant
18 differences. The significance level = 0.05, Kruskal-Wallis test with post-hoc Dunn's test, $P =$
19 0.002. Scale bar = 0.2 mm. **B** Examples of roots of other cereals introduced into the EasyClick
20 system. For the roots of wheat and oat plants we used Type 2 metal plate (0.5 mm channels)
21 and for the roots of rye we used Type 1 plate (0.4 mm channels).

22

Appendix IV

Proteome analysis of condensed barley mitotic chromosomes

Perutka, Z., **Kaduchová, K.**, Chamrád, I., Beinhauer, J., Lenobel, R., Petrovská, B.,
Bergougnoux, V., Vrána, J., Pecinka, A., Doležel, J., and Šebela, M.

Frontiers in Plant Science

DOI: <https://doi.org/10.3389/fpls.2021.723674>

IF (2021): 6.63



Proteome Analysis of Condensed Barley Mitotic Chromosomes

Zdeněk Perutka¹, Kateřina Kaduchová², Ivo Chamrád¹, Jana Beinhauer¹, René Lenobel¹, Beáta Petrovská², Véronique Bergougnoux^{3†}, Jan Vrána², Ales Pecinka², Jaroslav Doležel^{2*} and Marek Šebela^{1*}

¹Department of Protein Biochemistry and Proteomics, Faculty of Science, Centre of the Region Haná for Biotechnological and Agricultural Research, Palacký University Olomouc, Olomouc, Czechia, ²Institute of Experimental Botany of the Czech Academy of Sciences, Centre of the Region Haná for Biotechnological and Agricultural Research, Olomouc, Czechia, ³Department of Molecular Biology, Faculty of Science, Centre of the Region Haná for Biotechnological and Agricultural Research, Palacký University Olomouc, Olomouc, Czechia

OPEN ACCESS

Edited by:

Hans-Peter Mock,
Leibniz Institute of Plant Genetics
and Crop Plant Research (IPK),
Germany

Reviewed by:

Tiago Santana Balbuena,
São Paulo State University, Brazil
Xiaojian Yin,
China Pharmaceutical University,
China

*Correspondence:

Marek Šebela
marek.sebela@upol.cz
Jaroslav Doležel
dolezel@ueb.cas.cz

†Present address:

Véronique Bergougnoux,
Centre of the Region Haná for
Biotechnological and Agricultural
Research, Czech Advanced
Technology and Research Institute
(CATRIN), Palacký University
Olomouc, Olomouc, Czechia

Specialty section:

This article was submitted to
Plant Proteomics and Protein
Structural Biology,
a section of the journal
Frontiers in Plant Science

Received: 11 June 2021

Accepted: 21 July 2021

Published: 23 August 2021

Citation:

Perutka Z, Kaduchová K, Chamrád I,
Beinhauer J, Lenobel R, Petrovská B,
Bergougnoux V, Vrána J, Pecinka A,
Doležel J and Šebela M (2021)
Proteome Analysis of Condensed
Barley Mitotic Chromosomes.
Front. Plant Sci. 12:723674.
doi: 10.3389/fpls.2021.723674

Proteins play a major role in the three-dimensional organization of nuclear genome and its function. While histones arrange DNA into a nucleosome fiber, other proteins contribute to higher-order chromatin structures in interphase nuclei, and mitotic/meiotic chromosomes. Despite the key role of proteins in maintaining genome integrity and transferring hereditary information to daughter cells and progenies, the knowledge about their function remains fragmentary. This is particularly true for the proteins of condensed chromosomes and, in particular, chromosomes of plants. Here, we purified barley mitotic metaphase chromosomes by a flow cytometric sorting and characterized their proteins. Peptides from tryptic protein digests were fractionated either on a cation exchanger or reversed-phase microgradient system before liquid chromatography coupled to tandem mass spectrometry. Chromosomal proteins comprising almost 900 identifications were classified based on a combination of software prediction, available database localization information, sequence homology, and domain representation. A biological context evaluation indicated the presence of several groups of abundant proteins including histones, topoisomerase 2, POLYMERASE 2, condensin subunits, and many proteins with chromatin-related functions. Proteins involved in processes related to DNA replication, transcription, and repair as well as nucleolar proteins were found. We have experimentally validated the presence of FIBRILLARIN 1, one of the nucleolar proteins, on metaphase chromosomes, suggesting that plant chromosomes are coated with proteins during mitosis, similar to those of human and animals. These results improve significantly the knowledge of plant chromosomal proteins and provide a basis for their functional characterization and comparative phylogenetic analyses.

Keywords: barley, chromatin, FIBRILLARIN 1, flow cytometric sorting, mass spectrometry, mitotic chromosome, perichromosomal layer, protein prediction

INTRODUCTION

Nuclear DNA in eukaryotes is tightly associated with various proteins to form chromatin (Fierz and Poirer, 2019). The nucleoprotein complex not only participates in DNA packaging so that it fits the small nuclear volume, but also plays an important role in functional organization of DNA in the three-dimensional nuclear space, DNA damage repair, and regulation of gene expression. It also facilitates replication and faithful transmission of hereditary information to

daughter cells during mitosis, and the production of functional gametes in meiosis, which are intricate, highly dynamic and strictly controlled processes. At the beginning of mitosis and meiosis, the interphase chromatin undergoes a series of structural changes that lead to the formation of condensed chromosomes (Antonin and Neumann, 2016).

The organization of condensed chromosomes and their function is determined by a variety of proteins. Structural maintenance of chromosome (SMC) family complexes, including condensin, cohesin, and SMC5/6, modulate the chromosome structure and impact their function during mitosis (Skibbens, 2019). Replicated sister chromatids are tethered together by cohesins. In prophase, condensin II binds DNA and extrudes large initial scaffolding loops (Ganji et al., 2018). In prometaphase, after nuclear envelope breakdown, condensin I binds to chromatin and forms smaller loops for a further compaction, which are nested within the large loops produced by condensin II. Additional proteins were described as condensation factors including topoisomerase II and in mammals also chromosome-associated kinesin KIF4. Moreover, the condensation of chromosomes is facilitated by histone modifications, including phosphorylation and deacetylation (Antonin and Neumann, 2016).

Chromosome condensation was expected to be accompanied by the eviction of proteins involved in the regulation of gene expression, chromatin state, and accessibility (Martínez-Balbás et al., 1995). This was confirmed in the case of epigenetic modifiers that promote transcription (Ginno et al., 2018) and for a majority of polymerase II transcription elongation complexes (Parsons and Spencer, 1997; Ginno et al., 2018). However, repressive modifiers, some polymerase II ternary complexes, and a majority of transcription factors are retained, including core promoter-binding proteins (Parsons and Spencer, 1997; Ginno et al., 2018; Djeghloul et al., 2020). These proteins, collectively called mitotic bookmarking factors, ensure the transfer of gene regulatory information to daughter cells (Festuccia et al., 2016; Raccaud and Suter, 2018; Zaidi et al., 2018). As the accessibility of chromatin to regulatory proteins is not dramatically changed during chromosome condensation (Hsiung et al., 2015; Blythe and Wieschaus, 2016), many genes can be expressed during mitosis (Palozola et al., 2017), implying the association of various proteins and RNAs with the chromatin of condensed chromosomes.

In mammalian models, it has been shown that a perichromosomal layer covering the whole chromosome is

established simultaneously with the chromosome condensation except for the centromeric region where the kinetochore complex is formed. This layer represents at least 33% of the protein mass of mitotic chromosomes (Booth et al., 2016) and consists of pre-rRNA and proteins originating mostly from nucleoli, which disassemble during prophase. Stenström et al. (2020) identified 65 nucleolar proteins at the chromosome periphery. This recruitment was temporary as some of the proteins relocated during prometaphase, and the remaining ones were recruited only after metaphase. The proteins transferred during prometaphase included the Ki-67 protein, which has been shown the main organizer of the perichromosomal layer in human and animals (Booth et al., 2014). A series of studies revealed multiple roles of the layer, which include the formation and maintenance of chromosome architecture (Takagi et al., 2016), prevention of chromosome clumping (Cuylen et al., 2016), displacement of cytoplasmic components before nuclear envelope assembly (Cuylen-Haering et al., 2020), and transport of proteins and RNAs and their distribution to daughter nuclei (Sirri et al., 2016). The key role of the perichromosomal layer in chromosome function is reflected by its highly ordered structure (Hayashi et al., 2017), which excludes the formation of this domain by a random attachment of nuclear and cytoplasmic components.

Centromeric regions are the sites for the assembly of kinetochores – large protein complexes that attach chromosomes to spindle microtubules during cell division (Cheeseman, 2014). In vertebrates, the kinetochore consists of over a 100 proteins and comprises two major interaction networks (Pesenti et al., 2018). The constitutive centromere-associated network (CCAN) has 16 subunits and remains associated with centromeric chromatin throughout the cell cycle. The Knl1, Mis12, and Ndc80 network with 10 subunit super-complexes binds to CCAN at early prophase and remains attached during the whole mitosis (Hara and Fukagawa, 2020). Interestingly, the correct function of kinetochore depends on the translocation of the NOL11, WDR43, and Cirhin complex from the nucleoli to the perichromosomal layer. This is required for the centromeric enrichment of Aurora B and the subsequent phosphorylation of histone H3 (Fujimura et al., 2020) and underlines the key role of nucleolar proteins in the function of mitotic chromosomes.

Despite the great progress achieved during the past two decades in identifying and cataloging chromosomal proteins and unraveling their function, many proteins have an unknown function and many may remain to be discovered. The pioneering studies on human cell lines reported a relatively low number of chromosomal proteins, ranging from 60 to 250 (Morrison et al., 2002; Gassmann et al., 2005; Uchiyama et al., 2005; Takata et al., 2007). The first detailed survey by Ohta et al. (2010) revealed approximately 4,000 individual proteins and introduced a bioinformatics approach for statistical analysis to prove the authenticity of protein localization. A combination of six different classifiers by machine learning turned out to be crucial because only 19% of the total identified proteins could be annotated as truly chromosomal. This approach was further developed to detect protein complexes and their relation to chromosome structure and segregation (Ohta et al., 2016a;

Abbreviations: ACN, acetonitrile; ARATH, *Arabidopsis thaliana*; CCAN, centromere-associated network; DAPI, 4',6-diamidino-2'-phenylindole; DTT, dithiothreitol; ESI, electrospray ionization; EYFP, enhanced yellow fluorescent protein; FDR, false discovery rate; FoA, formic acid; GFP, green fluorescent protein; GO, gene ontology; HMG, high mobility group; HORVU, *Hordeum vulgare*; HyD, hybrid detectors; ID, identification; KMN, Knl1, Mis12, and Ndc80 network; nLC, nanoflow liquid chromatography; MALDI, matrix-assisted laser desorption/ionization; MCM, minichromosome maintenance; MG, microgradient; MGF, Mascot generic format; MS, mass spectrometry; MS/MS, tandem mass spectrometry; NSAF, normalized spectral abundance factor; NWC, NOL11, WDR43, and Cirhin complex; PMSE, phenylmethylsulfonyl fluoride; RAF-BT, raffinose-modified bovine trypsin; SDS-PAGE, sodium dodecyl sulfate–polyacrylamide gel electrophoresis; SCX, strong cation exchange; SMC, Structural maintenance of chromosome; TCEP, tris(2-carboxyethyl)phosphine; TFA, trifluoroacetic acid; WT, wild type.

Montaño-Gutierrez et al., 2017), mitosis-specific chromosome phosphorylation events (Ohta et al., 2016b), and components of the chromosomal scaffold (Ohta et al., 2019).

Most of the advances were made by analyzing human and animal chromosomes and very little is known about chromosomal proteins in plants. To date, proteomics studies in plants focused on interphase nuclei (Tan et al., 2007; Bigeard et al., 2014; Petrovská et al., 2014; Zeng and Jiang, 2016; Blavet et al., 2017). One of the reasons for the absence of studies on plant mitotic chromosomes may be a difficulty to obtain highly synchronized plant cell populations in mitosis. Ideally, the studies should be done on purified mitotic chromosomes as this helps to discriminate the “genuine” and functionally significant chromosomal proteins from those isolated from interphase nuclei, which escaped synchronization, and cytoplasmic proteins. However, any preparation of pure fractions of mitotic chromosomes is challenging in plants (Doležel et al., 2012; Zwyrková et al., 2020).

Here, we report on identification of a large number of proteins from condensed plant mitotic chromosomes. Our interdisciplinary approach comprised the induction of high degree of mitotic synchrony in meristem root-tip cells, purification of chromosomes by flow cytometric sorting, in-solution DNA and protein digestion, liquid chromatography of peptides, high-resolution MS/MS, and adapted multi-classifier data analysis.

MATERIALS AND METHODS

Chemicals

Benzonase[®] (Cat. No. E1014), DNase I (Cat. No. AMPD1), SOLu-trypsin (Cat. No. EMS0004), dithiothreitol (DTT), iodoacetamide, and tris(2-carboxyethyl)phosphine (TCEP) were from Sigma-Aldrich (Steinheim, Germany), and NEBNext[®] dsDNA Fragmentase[®] was from New England Biolabs (Ipswich, MA, United States). Raffinose-modified bovine trypsin (RAF-BT) was prepared as described (Šebela et al., 2006). Chromatography solvents were of LC-MS grade. All other chemicals were from commercial sources and were of analytical purity grade if not stated otherwise.

Flow Cytometric Chromosome Sorting for Proteomic Analysis

Suspensions of intact mitotic metaphase chromosomes were prepared as described by Lysák et al. (1999) with modifications. Briefly, root-tip meristem cells of young seedlings of barley [*Hordeum vulgare* (HORVU) L.] cv. Morex were accumulated in metaphase after treatments with 2 mM hydroxyurea for 18 h, 2.5 μ M amiprofos-methyl for 2 h, and ice water (overnight). Synchronized root tips were fixed in 2% (v/v) formaldehyde at 5°C for 15 min and homogenized using a Polytron PT1300D (Kinematica AG, Littau, Switzerland) at 15,000 rpm for 13 s in LB01-P buffer (Petrovská et al., 2014). The resulting chromosome suspension was stained with 2 μ g mL⁻¹ 4',6-diamidino-2-phenylindole (DAPI) and analyzed

at a rate of ~5,000 particles per second using a FACSaria SORP flow cytometer (Becton Dickinson, San José, United States). Sort windows were set on a dot plot of fluorescence pulse area versus fluorescence pulse width to select all seven chromosomes of barley. For proteomic analyses, samples were prepared by sorting a total of 10–11 $\times 10^6$ chromosomes into 15-mL Falcon tubes containing 1 mL LB01-P buffer supplemented with 5 mM phenylmethylsulfonyl fluoride. Flow-sorted chromosomes were pelleted at 2,500 rpm and 4°C for 30 min, and resuspended in ddH₂O.

Protein Extraction Procedure No. 1

The pellets of flow-sorted barley chromosomes were decrosslinked by incubation in 50 μ L of 50 mM Tris-HCl, pH 8.0, containing 2 mM MgCl₂, at 70°C for 9 h. This was followed by adding 50 μ L of the same buffer supplemented with 8 M urea and 10 mM DTT. After adding Benzonase (250 units), DNA was digested at 25°C for 24 h. Similarly, DNase I (20 units) was applied for DNA digestion. In parallel, Fragmentase alone (20 μ L) or in a combination with Benzonase (as above) was used. The digestion buffer for Fragmentase was 50 mM Tris-HCl, pH 8.0, containing 15 mM MgCl₂, and 50 mM NaCl (pipetted in an amount of 50 μ L to the chromosomal pellet). The DNA digestion with Fragmentase proceeded at 37°C for 24 h. The released proteins were recovered by precipitation with chilled acetone (1:4, v/v) at –20°C for 24 h.

Gel Electrophoresis

Protein precipitate from the extraction step (procedure no. 1) was dissolved in 25 μ L of Laemmli sample buffer and kept at 60°C for 30 min. Sodium dodecylsulfate polyacrylamide gel electrophoresis (SDS-PAGE) was performed with 10% T/3.3% C resolving and 4% T/3.3% C stacking 1-mm thick vertical gels following a standard protocol (Laemmli, 1970) and using a Mini-Protean II apparatus (Bio-Rad, Hercules, CA, United States). %T stands for the total monomer concentration (in g per 100 mL) and %C stands for weight percentage of crosslinker (*N,N*-methylenebisacrylamide). The whole protein sample (25 μ L) was applied to a sample well at the top of the stacking gel. Electrophoresis was run at 110 V until the marker dye reached the bottom of the resolving gel. Gel staining employed a standard protocol with 0.025% w/v Coomassie Brilliant Blue G-250 in 40% v/v methanol–10% v/v acetic acid (background destaining by 5% v/v methanol–7% v/v acetic acid). Gel images were obtained using an ImageScanner device and Lab Scan 5.0 software (Amersham Biosciences, Uppsala, Sweden).

In-Gel Digestion of Proteins

The sample lane was cut horizontally into 17 sections representing protein fractions (12 stained bands and 5 less stained larger areas) of a different molecular mass. After destaining using 50 mM NH₄HCO₃ in 50% v/v acetonitrile (ACN) for 45 min, proteins were in-gel reduced by 10 mM DTT in 100 mM NH₄HCO₃, and then alkylated by 55 mM iodoacetamide in 100 mM NH₄HCO₃ (Shevchenko et al., 2006). In-gel digestion was performed using RAF-BT (Šebela et al., 2006). Peptides were

extracted from the digests with 5% v/v formic acid (FoA)/ACN, 1:2, v/v (Shevchenko et al., 2006), recovered in test tubes after solvent evaporation in a vacuum centrifuge, and finally purified using C18-StageTips (Rappsilber et al., 2007).

In-Solution Digestion of Proteins No. 1

The entire precipitate from extraction procedure no. 1 was dissolved in 40 μ L of 100 mM triethylammonium bicarbonate, pH 8.0, containing 6 M urea and 2 M thiourea. The protein content was then assayed by the bicinchoninic acid method (Smith et al., 1985) after a sample aliquot dilution to decrease the urea concentration to 3 M. Proteins were reduced by TCEP (5 mM, 23°C, 45 min) and alkylated using iodoacetamide (50 mM, 23°C, 30 min). In-solution digestion with RAF-BT was subsequently done using a protein-to-trypsin molar ratio of 20:1.

In-solution digests were fractionated using the StageTips (Rappsilber et al., 2007) containing Empore™ Cation Exchange-SR extraction disks 2251 (3 M Bioanalytical Technologies, St. Paul, MN, United States) or by reversed-phase chromatography in a microgradient (MG) device (Franc et al., 2013a,b). The cation-exchange separation was performed using a stepwise concentration gradient of ammonium acetate (25 mM, 50 mM, 75 mM, 125 mM, and 200 mM) when the total elution was achieved by 5% v/v NH_4OH in 80% v/v ACN. The separate peptide fractions were then recovered in test tubes after solvent evaporation in a vacuum centrifuge and purified using the StageTips with Empore™ C18 extraction disks 2215 (3 M Technologies).

Protein Extraction and In-Solution Digestion Procedure No. 2

A suspension containing 10×10^6 flow-sorted barley chromosomes was repeatedly mixed with 150 μ L of mass spectrometry (MS)-quality water for washings. The solid material was collected by a brief centrifugation. Next, the pellet was suspended in 40 μ L of 50 mM Tris-HCl, pH 8.0, containing 2 mM MgCl_2 and kept at 70°C and 850 rpm for 5 h. Proteins were denatured by the addition of 20 μ L of the same buffer containing 8 M urea and 10 mM DTT. The mixture was incubated at 23°C for 1 h before adding 1 μ L (250 units) of Benzonase and kept at 23°C without shaking for 18 h. Disulfide reduction was achieved by the addition of 15 μ L of 5 mM TCEP and incubation at 23°C for 45 min. This was followed by alkylation of cysteine thiols by adding 15 μ L of 50 mM iodoacetamide in 50 mM Tris-HCl, pH 8.0, and incubating at 23°C for 30 min. Protein digestion was performed using 1 μ g of SOLu-trypsin in an overall volume of 240 μ L of the 50 mM Tris-HCl buffer, pH 8.0, containing MgCl_2 at 37°C and 350 rpm for 18 h. The digestion was stopped by adding 2 μ L of 50% v/v FoA.

The second sample was the original root-tip homogenate containing chromosomes as used for chromosome flow sorting, and the third sample was a chromosome-depleted fraction (i.e., a homogenate from which chromosomes were removed by flow cytometric sorting). Cell lysate proteins were obtained from 1 mL of the extract in a 5-mL tube using acetone

precipitation (1:4, v/v) at –20°C for 24 h and centrifugation at 20,000 g and 4°C for 15 min. The pellet was then suspended in 1 mL of fresh acetone, transferred into a 1.5-mL tube, and collected by centrifugation as above. Further processing of the additional samples followed the protocol for chromosomes with the initial washing step omitted in case of the original root-tip homogenate.

Peptide Quantification Assay

The acidified peptide mixture from procedure no. 2 was spun down at 10,000 g for 15 min and the supernatant was transferred into a new tube. Then, the tryptophan content in the peptides was determined using a microarray fluorescence reader Synergy MX (BioTek Instruments, United States) as published by Wisniewski and Gaugaz (2015). Samples of 200 μ L were loaded into microtitration plate wells. The instrument parameters were as follows: excitation wavelength of 295 nm and bandwidth of 9.0 nm; emission wavelength of 350 nm and bandwidth of 20.0 nm; gain of 75 units, 10 reads; 20°C; and integration time of 50 μ s. The calibration solutions contained 0.01–5.0 μ g μL^{-1} tryptophan in the sample buffer with urea. Peptide amounts in the assayed samples were calculated using the assumption that HORVU proteins contain on average 1.95% tryptophan by mass (derived from the UniProt barley protein database, see below for details).

Microgradient Separation of Peptides

Tryptic peptides from the digests were first chromatographed using a MG device (Franc et al., 2013a,b). The peptides in an amount of 4 μ g were loaded into an equilibrated microcolumn (250 μ m i.d. \times 30 mM) made of Kinetex EVO C18 2.6 μ m core-shell particles (Phenomenex, 00G-4,725-E0) and desalted by washing with 25 μ L of 0.1% v/v TFA. Then, the retained peptides were eluted by a stepwise gradient of 8, 12, 16, 20, 24, 28, 36, and 48% v/v ACN in 20 mM NH_4HCO_3 aspirated into the gas-tight syringe. The eluate was collected in seven consecutive 4- μ L fractions. Each fraction was then diluted by 21 μ L of 5% v/v FoA for the subsequent MS analysis.

Mass Spectrometry of Peptides

Nanoflow liquid chromatography-tandem mass spectrometry (nLC-MS/MS) analyses were performed on a maXis UHR-Q-TOF mass spectrometer equipped with a nanoelectrospray ion source (Bruker Daltonik) and connected to a Dionex UltiMate3000 RSLCnano liquid chromatograph (Thermo Fisher Scientific, Germering, Germany). Each sample was measured in two runs and the data were pooled. The experimental setup including the reversed-phase analytical column, pre-column, composition of mobile phases, flow rates, gradient programming, and other automated MS and MS/MS data acquisition parameters was the same as described previously (Chamrád et al., 2014).

Data Analysis and Annotation

Raw data were converted into Mascot generic format-formatted files and processed for database searches using PEAKS Studio 10 (Bioinformatics Solutions, Waterloo, ON, Canada). The search

parameters were as follows: mass tolerance for precursor ions and fragments – 50 ppm and 0.05 Da, respectively; enzyme – trypsin (semispecific); the number of missed cleavages – 2; allowed modifications per peptide – up to 3; variable peptide modifications – Met oxidation, Asn/Gln deamidation, protein N-terminal acetylation; and fixed peptide modification – Cys carbamidomethylation. The sequence databases used were barley (HORVU) proteome database downloaded from the UniProtKB (<https://www.uniprot.org>, 11/10/2020, Proteome ID UP000011116, 189,799 entries; International Barley Genome Sequencing Consortium et al., 2012) and cRAP contaminant database (downloaded from <https://www.thegpm.org/crap/> on 11/10/2020). The false discovery rate was set at 1% as a positivity threshold for the peptide-spectrum match plus peptide and protein sequence matches. At least one unique peptide was required for positive protein identification and only the first identification (ID) with the highest $-\log P$ score for each protein group was used for the subsequent data evaluation.

The obtained list of IDs matching the set of barley protein sequences was then searched against the UniProtKB/Swiss-Prot database to find *Arabidopsis thaliana* (ARATH) homologs by blastp (protein-protein BLAST; Altschul et al., 2005). Then, the available information on the cellular localization, related gene ontology (GO) terms, molecular mass, and sequence length for each *Arabidopsis* protein accession was acquired via UniProtKB Retrieve/ID mapping tool. A limit of 70% sequence homology was set up for the further search on UniProtKB protein localization information for *Arabidopsis* homologs. The whole protein FASTA-formatted file was reduced into partial files of 400 IDs for the application of other bioinformatics tools, such as NucPred (Brameier et al., 2007), Localizer (Sperschneider et al., 2017), CELLO2GO (Yu et al., 2014), and WegoLoc (Chi and Nam, 2012). In Localizer, the input was specified as “full plant sequences.” The plant BaCellO dataset and default settings were used in WegoLoc. In CELLO2GO search parameters, the eukaryotic organism option was selected. Also, matching GO terms and other information were obtained by searches using DAVID Functional Annotation Tool (Huang et al., 2009).

Evaluation of Nuclear or Chromosomal Localization

All data obtained from the databases and bioinformatics tools were merged using Perseus v.1.6.10.45 (Tyanova et al., 2016) and further processed in Microsoft Excel 2016. Six groups reflecting the prediction results and UniProtKB information were established to categorize the identified proteins (Search S1). Protein IDs yielding information on a nuclear/chromosomal localization in more than two prediction tools, which possessed a positive record on their nuclear origin in UniProtKB, were marked as “NUCLEAR.” Those IDs with more than two nuclear prediction hits and lacking any UniProtKB information on nuclear localization were grouped as “PREDICTED NUCLEAR.” Proteins labeled as nuclear/chromosomal by two prediction tools with a reliable record in UniProtKB were classified as “POSSIBLY NUCLEAR.” The group “DISCREPANCY UNIPROT” contained IDs with non-nuclear UniProtKB localization information and

more than two positive nuclear/chromosomal localization hits from the prediction tools. The group “DISCREPANCY PREDICTION” refers to protein IDs labeled as nuclear in UniProtKB and yielding less than two positive hits from the prediction tools. Finally, proteins classified in the “CYTOSOLIC” group were assigned according to information available on their subcellular localization in UniProtKB for HORVU or the corresponding ARATH protein accessions by searching with tags “cytos,” “cytop,” “mitoch,” “memb,” and “recept.” One positive hit for nuclear localization was a maximum for this group. The following criteria were used to filter out positive nuclear/chromosomal localizations: Localizer – predicted nuclear localization; NucPred – prediction score ≥ 0.50 ; WegoLoc – predicted localization contains the tag “nucl”; and CELLO2GO – the predicted localization (CP) result contains the tag “nucl” or “chromo.” The UniProtKB HORVU IDs and their ARATH homologs were searched for the tags “chromos,” “chromat,” and “nucl” in the “Subcellular location (CC)” information provided in the database entry. Information on protein domains was obtained using CD-Search (Marchler-Bauer and Bryant, 2004; default settings) and barley FASTA sequences.

Each protein containing at least one functional domain was scored using an in-house made database of domains (inspired by Ohta et al., 2010) based on experiments following the in-solution digestion procedure 2 and MG peptide separation. Finally, it contained 869 domains. Those domains bound to the protein ID groups “NUCLEAR,” “PREDICTED NUCLEAR,” and “POSSIBLY NUCLEAR” were attributed as nuclear. Domains related to “CYTOSOLIC” proteins were considered false. Each domain for a protein ID was then scored for these attributes. Domains not included in the database were marked as unknown. Comprehensive data combining nuclear prediction hits, information on protein localization in the UniProtKB, and the domain score were re-evaluated (Search S2). Protein IDs with more than three nuclear prediction hits plus the existing nuclear localization information in UniProtKB (barley accessions) and true domain attribute were “NUCLEAR.” The same score but the existing nuclear localization information in UniProtKB for ARATH homolog only resulted in “NUCLEAR (BLAST)” classification. Proteins lacking any domain information were classified in the group “UNINSUFFICIENT CD INFO.” Those with less than three nuclear prediction hits were denoted as “POSSIBLY NUCLEAR.” Missing or non-nuclear localizations found for barley and ARATH accessions in the corresponding UniProtKB/Swiss-Prot entries were evaluated as “DISCREPANCY UNIPROT.”

Generating Barley EYFP-FIB1 Reporter Line

The CDS sequence of barley *FIBRILLARIN 1* (*FIB1*; HORVU6Hr1G091860), cultivar Golden Promise, was amplified to generate the *ZmUBI1::EYFP-FIBRILLARIN1::T35S* fusion construct. The amplification was achieved with cDNA obtained by a reverse transcription (Transcriptor High Fidelity cDNA Synthesis Kit; Roche) using total RNA isolated from roots (RNeasy kit; Qiagen) with the following primer pair: 5'-ATGAGGGCTCCCATGAGAGG-3' and 5'-CTTTTGCTTC

TTGGGCATCCTGT-3', including the stop codon. *FIB1* CDS was then reamplified with another primer pair 5'-GGGGACA ACTTTGTATAATAAAGTTGTTCACTTTTGCTTCTTGGGC ATCC-3' and 5'-GGGGACAGCTTTCTTGACAAAGTGGT AATGAGGGCTCCCATGAGAGG-3' containing the attB sites and cloned *via* BP reaction into a *pDONR-P2r-P3* vector by Gateway cloning strategy (Gateway™). The final expression cassette, including *ZmUBI1* promoter, *EYFP-FIB1*, and *T35S* terminator, was subcloned by multisite LR reaction combining three entry vectors *pEN-L4-UBIL-R1*, *pEN-L1-Y-L2*, and *pDONR-P2r-P3* with *FIB1* CDS into the *pH7m34GW* destination vector. All constructs assemblies were verified by Sanger sequencing.

The full construct in *pH7m34GW* vector was transformed into *Agrobacterium tumefaciens* strain AGL1. For barley transformation, immature embryos of the cultivar Golden Promise were dissected and transformed according to the previously described protocol (Marthe et al., 2015). Regenerated plants were genotyped for the presence of *hptII* gene, conferring resistance to hygromycin, by PCR with primer pair 5'-GACGTCTGTCTCGAGAAGTTTCTG-3' and 5'-CGAGTACTT CTACACAGCCATC-3'. The presence of EYFP-FIB1 fusion protein *in planta* was confirmed by the confocal microscopy using a Leica TCS SP8 STED3X microscope (Leica Microsystems, Wetzlar, Germany), equipped with an HC PL APO CS2 20 ×/0.75 DRY objective, hybrid detectors (HyD), and the Leica Application Suite X (LAS-X) software version 3.5.5 with the Leica Lightning module (Leica, Buffalo Grove, IL, United States).

Isolation of Mitotic Chromosomes for Microscopic Analyses

Preparation of suspensions of mitotic metaphase chromosomes and flow cytometric chromosome sorting was done as described above for the proteomic analyses. However, chromosome suspensions were prepared in LB01 buffer (Doležel et al., 1989) from barley cv. Golden Promise and EYFP-FIB1 transgenic plants, and 10⁵ chromosomes were flow sorted into 25 μL of LB01 buffer. 10 μL of the flow-sorted chromosome suspension was pipetted into a 10-μL drop of P5 buffer (Kubaláková et al., 1997) on poly-lysine coated microscopic slides (Thermo Scientific™), air dried for up to 15 min, and stored at -20°C until use. To evaluate the effect of RNA removal, RNase A (Sigma Aldrich) was added to 100 μL aliquots of the flow-sorted chromosome suspensions in LB01 to a final concentration of 0.01 ng μL⁻¹ and incubated for 30 min at 16°C prior to pipetting into microscopic slides.

Isolation of Interphase Nuclei for Microscopic Analyses

For the isolation of root-tip meristem cell nuclei, both Golden Promise and EYFP-FIB1 transgenic seeds were surface sterilized as described (Marthe et al., 2015), cold stratified for 2 days at 4°C on a wet paper towel, and germinated for 2 days at 24°C in dark. Suspensions of cell nuclei were prepared following a previous protocol (Doležel et al., 1992) with modifications. Briefly, roots of the young seedlings were fixed in 3% (v/v)

formaldehyde in 10 mM Tris buffer with additives (pH 7.5; Doležel et al., 2011) for 15 min on ice plus 5 min on ice/vacuum (500 mBa). Then, they were washed twice in the same buffer for 10 min on ice. About 30 root tips were cut with a razor blade and homogenized in 500 μL P5 buffer (Kubaláková et al., 1997) using Polytron PT1300D homogenizer (Kinematica AG) at 15,000 rpm for 13 s. The homogenate was filtered through a 30 μm nylon mesh and centrifuged at 2,000 g and 4°C for 10 min. The supernatant was removed and the pellet containing nuclei was resuspended in 100 μL of the P5 buffer. About 10 μL of the suspension was pipetted into poly-lysine coated slides (Thermo Scientific™), air dried for up to 15 min, and stored at -20°C.

Immunostaining and Microscopy

The immunostaining was performed as described (Jasenčáková et al., 2001). EYFP-FIB1 was detected with primary mouse antisera against FIB1 (1:100; ab4566; Abcam) and secondary antibodies goat anti-mouse-Cy5 (Alexa Fluor® 647; 1:300; A21235; Invitrogen) or with a goat anti-mouse-Cy3 (Alexa Fluor® 546; 1:300; A-11003; Invitrogen) for nuclei or metaphase chromosomes, respectively. Alternatively, EYFP-FIB1 on metaphase chromosomes was detected with rabbit antisera against GFP (1,100; ab290; Abcam) recognizing also EYFP and secondary antibodies goat anti-rabbit-Cy3 (Alexa Fluor® 647; 1:300; A-11010; Invitrogen) for metaphase chromosomes. Nuclei and chromosomes were counterstained with DAPI dihydrochloride (1 μg mL⁻¹) in a Vectashield medium (Vector Laboratories).

Microscopic images were acquired using a Leica TCS SP8 STED3X confocal microscope (Leica Microsystems, Wetzlar, Germany), equipped with an HC PL APO CS2 63 ×/1.40 Oil objective, hybrid detectors, and the LAS-X software version 3.5.5 with the Leica Lightning module (Leica, Buffalo Grove, IL, United States). Confocal images were captured separately in sequential scans, to avoid spectral mixing, using 405 nm (DAPI), 508 nm (EYFP), 557 nm (Alexa Fluor® 546), and 594 nm (Alexa Fluor® 647) laser lines for excitation and appropriate emission spectrum. Pictures were processed in Adobe Photoshop version 12.0 (Adobe Systems).

RESULTS

Gel-Based Identification of Barley Chromosomal Proteins

Our initial experiments followed the protocol used by Petrovská et al. (2014) and Chamrád et al. (2018) to characterize the proteome of barley interphase nuclei. Their procedure included a heat-treatment, nuclease-assisted protein extraction, SDS-PAGE, in-gel proteolytic digestion, and MS/MS-based protein identification. The protein extraction step was facilitated by heat-induced disruption of formaldehyde cross-links to dissociate nuclear/chromosomal proteins from their complexes with DNA. The protocol yielded only 63 barley protein IDs (**Supplementary Table S1**) using 11 million chromosomes. Even though this number was much lower than expected, the

electrophoretic pattern (**Figure 1**) was typical for chromosomal/nuclear preparations with distinct histone bands (Ohta et al., 2010; Petrovská et al., 2014). A majority of the identified proteins had a nuclear/chromosomal localization and related functions. This group included histones and also ribosomal proteins (assigned mostly as non-classified as well as cytosolic proteins according to their localization) and a few DNA/RNA-binding proteins. Other protein IDs included, e.g., abundant enzymes representing components of energy metabolism pathways (glycolysis and oxidative phosphorylation).

Gel-Free Approaches Including Fractionations of Peptide Mixtures

We suspected that the low yield of protein IDs was related to a low protein input (10 million barley chromosomes provided an average protein mass of 4.4 μ g). Therefore, the gel-based procedure was replaced by a gel-free protocol. Moreover, DNA digestion was performed differently using a set of nucleases comprising DNase I, Benzonase, and Fragmentase, the latter two were also combined in a single reaction mixture. The recovered proteins were then subjected to tryptic proteolysis and the resulting peptides were fractionated on a strong cation exchanger prior to nanoflow liquid chromatography (nLC)-electrospray ionization (ESI)-MS/MS. **Table 1** shows an overview of all experiments, which are documented in **Supplementary Table S2**. The best results with regard to the number of protein IDs in a single experiment were obtained with the protocol using Benzonase (1169–1531 proteins). This enzyme was employed in all subsequent experiments.

Figure 2 shows the predicted nuclear or non-nuclear localization of all identified proteins attributed in the two-round search approach referred to as S1 and S2 here. Database searches provided an overall number of 4139 protein IDs by combining individual datasets (**Supplementary Table S3**). A total of 674 proteins might be considered nuclear/chromosomal utilizing predictors based on data from gene ontology prediction tools, UniProtKB database annotations, and conserved domain searches. The more stringent search approach S2, which additionally considered information on the presence of a verified nuclear domain in the sequence of each identified protein, clearly confirmed 228 nuclear/chromosomal hits (143 + 62 + 23) and additional 485 entries (428 + 18 + 39) were found less plausible for classification in this category. Some of the latter IDs could not be verified by nuclear domain in S2 search (18 items) or consistent results in both S1 and S2 search (39 items). The reason resides, namely, in a discrepancy found for their localization in the UniProtKB database (i.e., they are not denoted as nuclear – 428 items).

The Panther GO (gene ontology) classification tool was applied to evaluate the identified 674 nuclear/chromosomal barley proteins (including those with the localization annotation discrepancy in UniProtKB) as regards to the attributed protein class name. Arabidopsis homologs (636 in total) were reduced to 293 unique Arabidopsis database entries for the GO classification search referring to 405 original barley proteins IDs (**Supplementary Table S3**). Almost two-thirds of the evaluated IDs belonged to nucleic acids-binding proteins including histones, replication factors, and various DNA/RNA processing enzymes, such as helicases, ligases, methyltransferases,

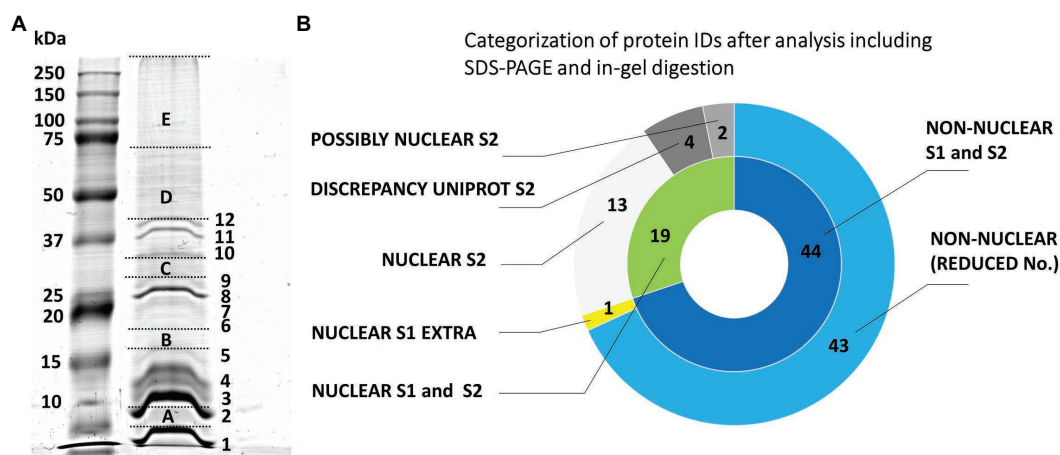


FIGURE 1 | Evaluation of the origin of proteins from mitotic chromosomes identified by GeLC-ESI-Q-TOF MS/MS. **(A)** SDS-PAGE of extracted barley chromosomal proteins (Coomassie Brilliant Blue staining). The separation was achieved in a 10% T/3.3% C resolving polyacrylamide gel. Left lane, protein marker 10–250 kDa (Kaleidoscope Standards, Bio-Rad); right lane, chromosomal proteins. The excised gel fractions and bands are labeled by capital letters A–E and numbers 1–12, respectively; this labeling is used in **Supplementary Table S1** for reference. **(B)** The nested pie chart shows information on the possible nuclear or non-nuclear localization of all identified proteins and their distribution into categories reflecting results of a two-round search approach (S1 and S2) utilizing predictors based on data from gene ontology prediction tools, UniProtKB database annotations and conserved domain searches (NCBI CDD database). The principle of S1 and S2 sorting is elucidated in Materials and Methods. The inner ring shows combined results of the two data search and evaluation procedures. The area labeled “NUCLEAR S1 and S2” refers to the consistently obtained attributes NUCLEAR, PREDICTED NUCLEAR/DISCREPANCY UNIPROT, and POSSIBLY NUCLEAR. The outer ring shows a protein distribution based on the procedure S2 plus an additional non-overlapping hit obtained using S1 (“NUCLEAR S1 EXTRA”). The label “NON-NUCLEAR (REDUCED No.)” refers to subtraction of the non-overlapping hit from the total number of non-nuclear identification.

TABLE 1 | A summary of the results of nLC-ESI-MS/MS analyses yielding protein identification after previous peptide fractionation using strong cation exchanger.

Sample processing prior to before SCX	Matched peptide MS/MS spectra	Mean sequence coverage	Matched peptides	Unique matched peptides	Protein IDs	Possibly nuclear proteins ^a		Nuclear proteins (BLAST) ^a		Nuclear proteins ^a	
						#	%	#	%	#	%
Benzonase and in-sol digestion	60360	20.2	7491	4810	1169	17	1.5	17	1.5	47	4.0
Fragmentase and in-sol digestion	23705	17.8	4364	2943	815	5	0.6	13	1.6	25	3.1
Fragmentase+Benzonase and in-sol digestion	13232	17.1	1981	1,346	435	6	1.4	9	2.1	22	5.1
DNase I and in-sol digestion	67819	18.9	6764	4210	1090	15	1.4	17	1.6	57	5.2
Benzonase and in-sol digestion	37137	15.2	6047	4243	1216	11	0.9	22	1.8	35	2.9
Benzonase and in-sol digestion ^b	50659	19.8	7577	5029	1209	10	0.8	19	1.6	47	3.9
Benzonase and in-sol digestion (no precipitation)	24609	13.2	6873	4885	1436	13	0.9	18	1.3	46	3.2
Benzonase and in-sol digestion (no precipitation) ^b	58019	15	7186	5387	1531	13	0.8	18	1.2	42	2.7
Overall	135009	14.2	18795	13237	4139	31	0.7	62	1.5	143	3.5

^aNuclear localization in data search S2 as attributed to protein IDs using predictors (see Materials and Methods and Supplementary Table S2).

^bExtraction of chromosomes was performed at pH 9 otherwise it was pH 7.

topoisomerases, chromatin-remodeling complex ATPase, DNA-directed RNA polymerase subunits, and others. SMC proteins (including cohesins and condensins) were represented by 13 items. Approximately 15% of the IDs were ribosomal proteins, ribosome biogenesis regulators, and translation factors. Chromatin proteins and gene-specific transcription regulators represented roughly 5%. Other attributed nuclear/chromosomal proteins were, e.g., kinetochore proteins, nucleosome assembly proteins, importin, ubiquitin, and ubiquitin-related enzymes.

Another set of experiments involved peptide fractionation using a C18 reversed-phase MG device (Moravcová et al., 2009). This approach has repeatedly been shown very helpful and efficient for a pre-separation of peptides from digests prior to nanoLC-matrix-assisted laser desorption/ionization-MS/MS or nanoLC-ESI-MS/MS analysis (Franc et al., 2013a,b). In that case, each analyzed peptide sample was first separated into seven fractions that were individually subjected to nanoLC-ESI-MS/MS. The obtained results are summarized in **Figure 3**. The total number of unique barley protein IDs was 2941 (**Supplementary Table S4**), from which 398 might be considered nuclear/chromosomal based on the bioinformatics data processing S1 + S2 as already mentioned above using UniProtKB database and prediction tools referring to the appropriate conserved protein domains and attributed gene ontology terms. The search approach S2 confirmed 155 nuclear/chromosomal hits (92 + 43 + 20). Additional 299 entries (243 + 56) were found less plausible for classification in this category, from which the number 56 were inconsistently retrieved results in both S1 and S2 search. A repeated application of the MG separation showed 1193 reproducible protein IDs. They were present in at least two biological replicates, see below, from which 144 were classified as nuclear/chromosomal.

The consensual number of 398 barley protein IDs provided 371 Arabidopsis homologs, which were reduced to 263 unique Arabidopsis database entries for the GO classification search referring to 252 original barley protein IDs (**Supplementary Table S4**). Again, a majority of the evaluated IDs (54%) belonged to nucleic acids-binding proteins including histones, replication/transcription/splicing factors, and various DNA/RNA processing enzymes, such as helicases, ligases, methyltransferases, topoisomerases, chromatin-remodeling complex ATPase, DNA-directed RNA polymerase subunits, and others. SMC proteins were represented by six items. About 16% were ribosomal proteins and translation factors. Chromatin proteins and gene-specific transcription regulators represented roughly 4%. Other attributed nuclear/chromosomal proteins included nucleosome assembly proteins, a kinetochore protein, transporters, and ubiquitin-related enzymes.

Enrichment of Nuclear/Chromosomal Proteins

The experimental workflow with MG pre-separation of peptides was applied to three different sample types: (1) flow-sorted barley chromosomes, (2) original root-tip homogenate as a control, and (3) chromosome-depleted homogenate (chromosomes were removed by flow cytometric sorting).

Categorization of protein IDs after analysis including SCX-based peptide fractionation

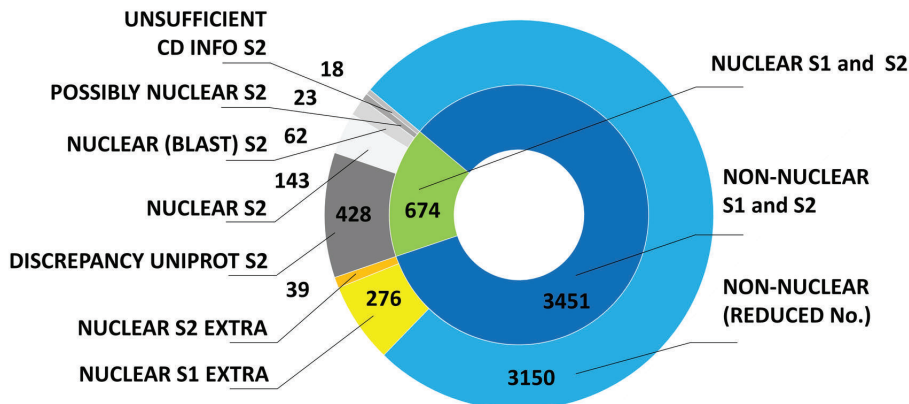


FIGURE 2 | Evaluation of the origin of proteins from mitotic chromosomes identified by nLC-ESI-Q-TOF MS/MS with SCX fractionation of tryptic peptides. The nested pie chart shows information on the possible nuclear or non-nuclear localization of all identified proteins and their distribution into categories reflecting results of a two-round search approach (S1 and S2). The principle of S1 and S2 sorting is provided in Materials and Methods. See the legend to **Figure 1** for elucidation of the attributed categories.

Every sample type was analyzed in three biological replicates and each of them in two technical replicates. The results are summarized in **Figure 4**. Our analyses considered only proteins which were identified in at least two biological replicates. Normalized spectral abundance factor values were chosen as a quantitative measure (Zybailov et al., 2006) for comparison. Proteins verified in S1 + S2 search and categorized as nuclear (and accordingly considered chromosomal) represented 30% of all repetitive IDs for the flow-sorted chromosomes. This was significantly more than ~10% obtained for the control (i.e., the original root-tip homogenate) and the chromosome-depleted fraction. Data analysis confirmed the expected enrichment of nuclear/chromosomal proteins in chromosomes as the percentages for individual search categories were rather similar for all three sample types when comparing the numbers of protein IDs (**Figure 4**). Non-nuclear proteins always represented more than 80% of IDs, and almost 90% were identified in the chromosome-depleted fraction. The category NUCLEAR S2 was the most enriched one and contained histones categorized according to Arabidopsis homology as histones and their variants: H2 (13 IDs), H1 (six IDs), and H3 (three IDs). Next, four DNA helicases were found although three of them are classified as DNA replication licensing factor or minichromosome maintenance (MCM) proteins. Single SMC protein and DNA (cytosine-5)-methyltransferase CHROMOMETHYLASE 3 (CMT3; EC 2.1.1.37) were found in this category, which may reflect the under-representation of characterized barley representatives in the database. Additionally, three chromatin handling proteins, chromatin-remodeling ATPase (2 IDs) and facilitates chromatin transcription complex subunit SSRP1 protein, confirm the presence of predominantly well-characterized DNA-binding proteins or enzymes in this group.

Altogether, a combination of the strong cation exchange (SCX) and MG-related analyses provided a list of 837 unique IDs, which may be considered nuclear/chromosomal based on the applied bioinformatics processing (**Supplementary Table S5**). This group of identified proteins was compared with the content of the UNcleProt barley nuclear protein database (Blavet et al., 2017). Only 311 out of the 837 proteins had matches in the database. **Table 2** shows that a majority of them, categorized by searches according to their names and functional annotations, were DNA-associated proteins (including histones) and RNA-associated proteins as well as proteins attributed to ribosomes. Numerous matched IDs were uncharacterized proteins in the barley proteome but could be assigned by homology to their Arabidopsis counterparts. Many novel protein IDs outside the UNcleProt belonged to the same categories but above that the others were typically chromosomal (e.g., condensin, cohesin, and kinetochore components) or mitosis-related (kinesins).

Localization of FIB1 on Mitotic Chromosomes

Besides the known chromatin proteins, the SCX and MG identified a high number of chromosomal proteins that are not associated with chromatin. A prominent group was represented by nucleolar proteins, including abundant peptides from FIB1. FIB1 is a marker of nucleoli that forms foci of various densities. We have confirmed the localization of FIB1 in nucleoli of barley interphase nuclei by immunostaining and also by constructing a barley reporter line constitutively expressing a translational fusion of EYFP-FIB1 (**Figures 5A,B**). To confirm FIB1 localization on mitotic chromosomes as suggested by the proteomic analysis, we flow-sorted metaphase chromosomes of wild-type and EYFP-FIB1 reporter line into microscopic slides and observed them either directly (EYFP-FIB1) or after immunodetection with the antibodies against FIB1 and/or GFP

Categorization of protein IDs after analysis including MG-based peptide fractionation

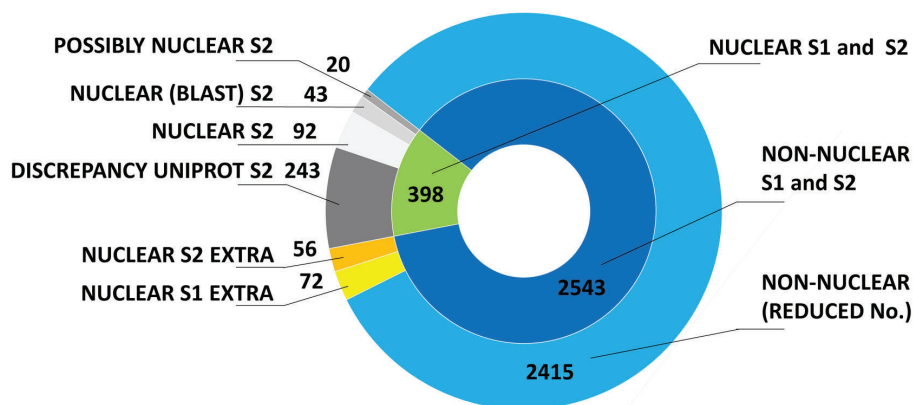


FIGURE 3 | Evaluation of the origin of proteins from mitotic chromosomes identified by nLC-ESI-Q-TOF MS/MS with MG fractionation of tryptic peptides. The nested pie chart shows information on the possible nuclear or non-nuclear localization of all identified proteins and their distribution into categories reflecting results of a two-round search approach (S1 and S2). The principle of S1 and S2 sorting is provided in Materials and Methods. See the legend to **Figure 1** for elucidation of the attributed categories.

(recognizes also EYFP). In all cases, a signal was observed confirming the presence of FIB1 (native or fusion) protein, which was not the case for negative controls when chromosomes were incubated only with a secondary antibody (**Figures 5C–F**). The chromosomes were covered entirely with foci of higher signal intensity. On some chromosomes, we observed even FIB1 localization in the kinetochore-binding region (**Figure 5D**). This observation confirmed that nucleolar protein FIB1 is associated with plant mitotic chromosomes during cell division.

FIB1 is an RNA methyltransferase that functions in complex with other proteins and RNA molecules. Therefore, we asked whether FIB1 is localized on chromosomes as an isolated protein or in complex with RNA. To test this, we treated flow-sorted chromosomes by RNase (**Figure 6**). In both cases, immunolocalized native FIB1 and EYFP-FIB1 fusion protein, RNase A treatment led to the loss of FIB1 signals, suggesting that the entire FIB1 complex including RNA molecules is associated with barley mitotic chromosomes.

DISCUSSION

Flow Cytometry as a Critical Step in Plant Chromosomal Proteomics

We have identified the largest set to date of proteins associated with plant mitotic chromosomes. Barley was chosen as a model plant because its reference genome is available (Mascher et al., 2017) as well as a plethora of transcriptome data (Kintlová et al., 2017; Rapazote-Flores et al., 2019). Its nuclear proteome has been characterized as well (Petrovská et al., 2014; Blavet et al., 2017). Importantly, a well-established method is available for the preparation of suspensions of intact mitotic metaphase chromosomes and their purification by flow cytometric sorting (Lysák et al., 1999). This allowed us to prepare samples enriched for proteins from mitotic metaphase chromosomes.

Vertebrate chromosomes, on the other hand, are commonly prepared by a density gradient centrifugation, for example, by applying sucrose and Percoll gradients (Samejima and Earnshaw, 2018). While highly synchronized mitotic cell populations have been used to characterize the proteome of human and animal chromosomes, such a synchrony is hardly reachable with plant tissues.

As chromosomes are released into the cytoplasm during mitosis, it is critical to ensure that the chromosomal protein content is not contaminated by cytoplasmic proteins. As such a contamination cannot be *a priori* avoided, we have identified chromosomal proteins by comparing the results of protein identification in: (1) the original homogenate containing chromosomes plus cellular and tissue debris, (2) chromosomes purified by flow sorting, and (3) chromosome-depleted homogenate containing only cellular and tissue debris. Given that the protocol for preparation of chromosome suspensions (Lysák et al., 1999) includes mild formaldehyde fixation, there is a risk of crosslinking cytoplasmic proteins with those forming the perichromosomal layer. As this should be a random process, it should result in protein clusters of varying size irregularly associated with the chromosome surface. However, only highly regular structures were observed on the surface of flow-sorted barley chromosomes using environmental scanning electron microscopy (V. Neděla, personal communication). Based on this observation and our experimental design, we consider the results obtained in this work as well supported. We categorized all proteins identified in flow-sorted chromosomes using the information obtained from the relevant UniProtKB database records and related DAVID search data, and compared with a previous proteomics analysis of avian chromosomes (Ohta et al., 2010). The comparison showed a good overall agreement as the majority of proteins was classified as nuclear or chromosomal, while uncharacterized proteins represented consistently about 20–25% (**Figure 7**).

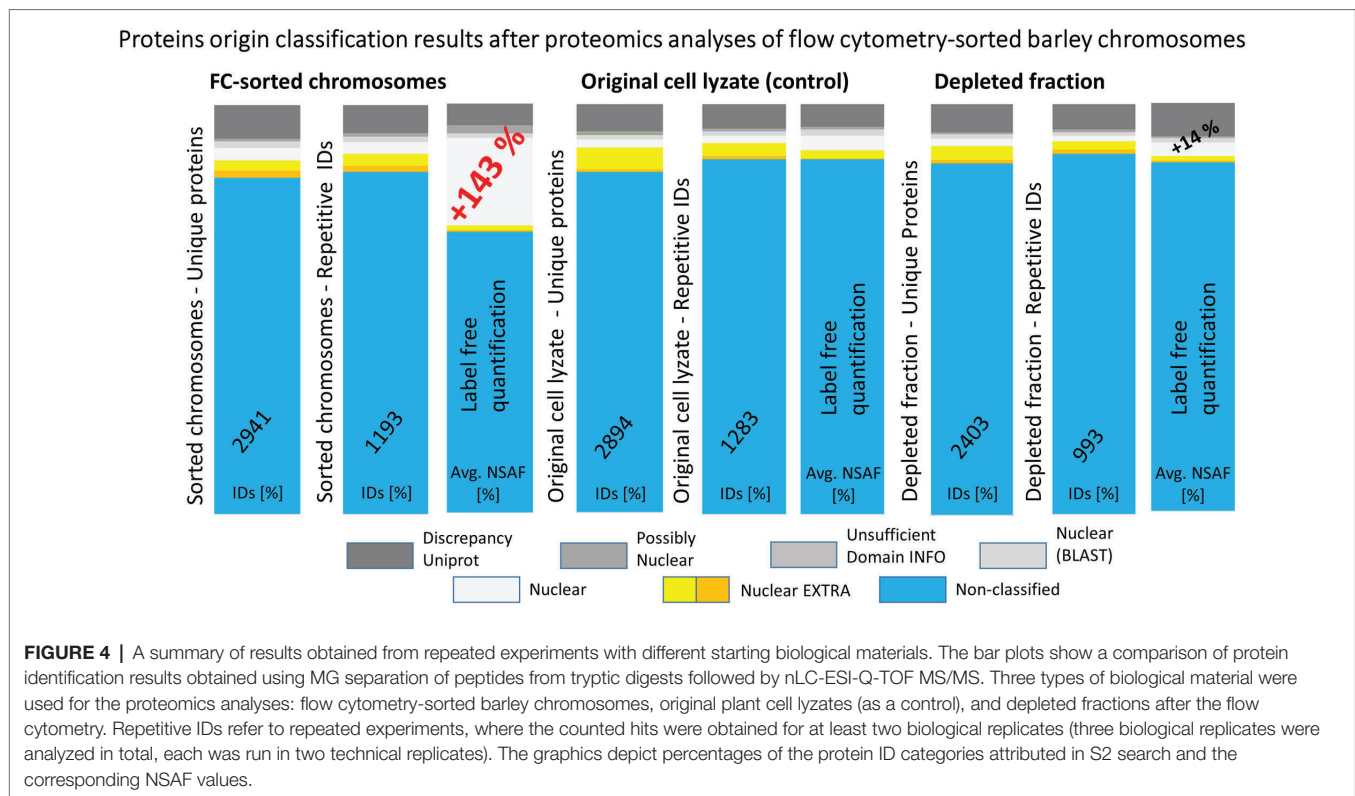


TABLE 2 | Attributes assigned to the 837 identified barley chromosomal proteins (NUCLEAR S1 + S2).

Searched text string	Novel IDs in chromosomes		Matched nuclear IDs	
	HORVU ^a	ARATH ^b	HORVU ^a	ARATH ^b
Chromosome	11	20	3	13
Chromatin	2	22	2	8
DNA	17	41	17	35
Kinetochor	0	3	0	1
Histon	52	61	62	76
Replicat	6	11	2	11
Mitotic	0	1	0	2
Kinesin	10	12	0	0
Condensin	5	4	0	0
Cohesin	0	4	0	2
Transcript	0	18	3	13
RNA	11	54	7	36
Ribosome	16	35	19	34
Uncharacterized	185	1	88	2

The text strings provided in the first column were applied as "keywords" for searching in the names of barley or homologous Arabidopsis proteins (see **Supplementary Table S5**). Only 311 out of the 837 proteins matched the original dataset of the barley nuclear protein database UNcleProt (Blavet et al., 2017). The others were thus considered novel IDs.

^aHORVU, *Hordeum vulgare*.

^bARATH, *Arabidopsis thaliana*.

To assess barley chromosomal proteome from a biological point of view, we considered a semi-quantitative nature of our methods and looked at the most relevant proteins and complexes identified. These proteins were classified as nuclear/chromosomal

and were ordered decreasingly according to the number of unique identified peptides and analyzed as regards to their biological role based on the existing annotation and homology to Arabidopsis.

Pre-separations of Peptides Prior to nLC-MS/MS to Increase the Protein Identification Rate

In-gel digestion yielded only 63 proteins with 16 classified as nuclear/chromosomal. These proteins comprised almost exclusively histone proteins (H1 to H4) specific to both euchromatin (H3.3, H2A.XB, and H2A.Z) and heterochromatin (H3.1, H2A.W, and H1.2). The heterochromatic variants were generally more frequent, which may correspond to the high proportion of repetitive DNA in the barley genome (Baker et al., 2015). The GTP-binding protein RAN3 (Hv: M0UF14; At: Q8H156/AT5G55190) was the only non-histone case likely responsible for nucleocytoplasmic protein transport. However, RAN3 most likely does not have a direct DNA-binding activity and the analysis in Arabidopsis identified it as interactor of METHYL-BINDING PROTEIN 5, which is one of four Arabidopsis MBDs binding to 5-methyl cytosine (Yano et al., 2006). In summary, the in-gel digestion method revealed practically only nucleosomal subunits, suggesting a loss of a majority of chromosomal proteins and/or a failure to detect them when using this approach.

The other two methods used, i.e., the SCX and C18 reversed-phase MG, were based on the in-solution isolated chromosomal proteins and differed in the principle of pre-separation of peptide

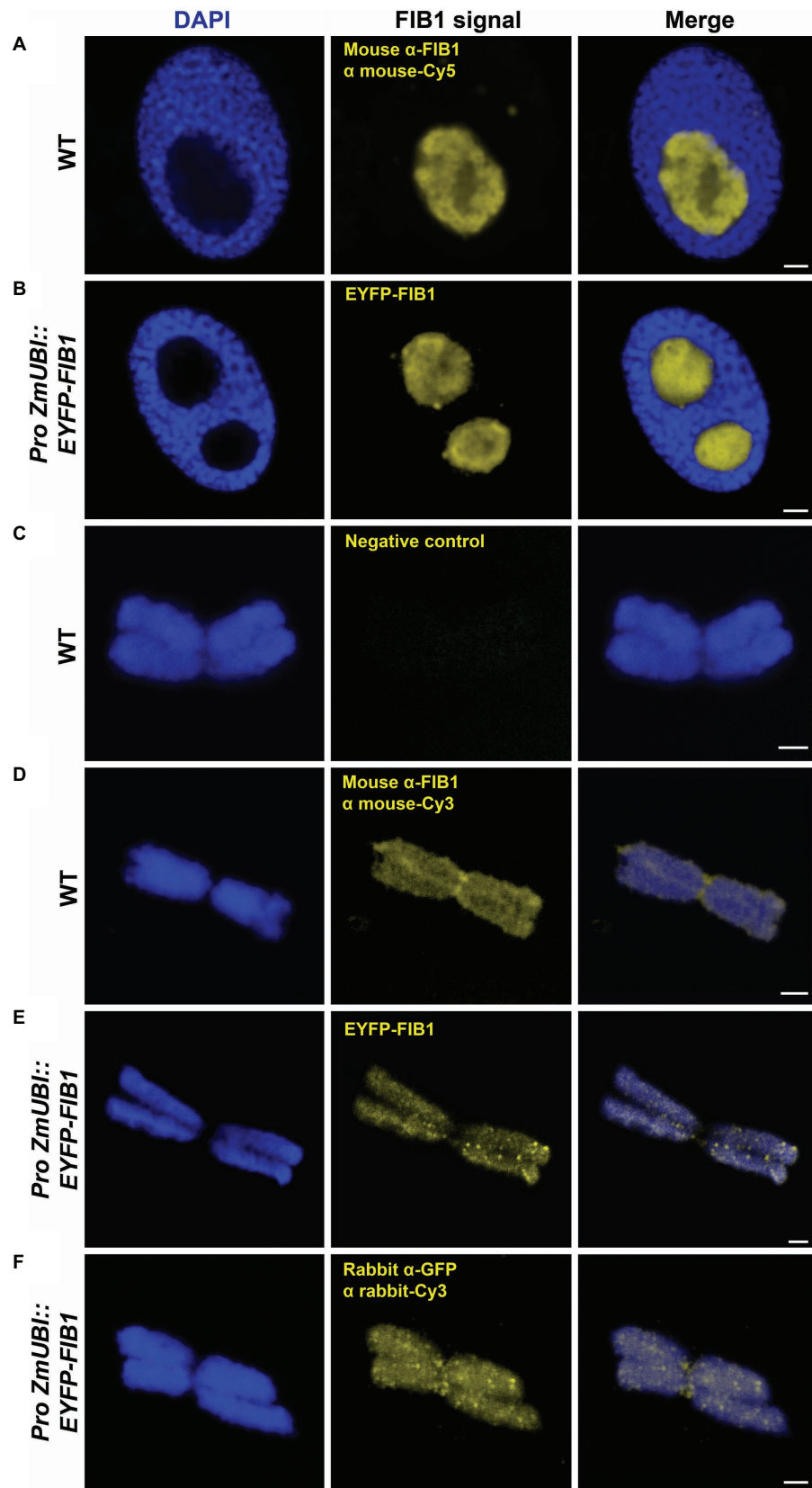


FIGURE 5 | (Continued)

FIGURE 5 | Detection of barley FIB1 in interphase nuclei and on metaphase chromosomes. All nuclei and chromosomes were counterstained with DAPI. Unstained regions within interphase nuclei correspond to nucleoli. **(A)** Wild-type (WT) interphase nucleus with FIB1 detected via immunolocalization with a specific antibody against FIB1 and secondary fluorochrome-coupled antibody. **(B)** The interphase nucleus of the barley reporter line expressing a translational fusion of the EYFP-FIB1. **(C)** Metaphase chromosome without immunostaining serving as a negative control for autofluorescence in Cy3 channel. **(D)** WT metaphase chromosome with FIB1 detected as described in **(A)**. **(E)** Reporter line metaphase chromosome with direct EYFP-FIB1 signal. **(F)** Reporter line chromosome with EYFP-FIB1 signal enhanced via immunolocalization with anti-GFP-Cy3 antibody (recognizing also EYFP). Scale bars = 2 μ m.

mixtures. Consistently, around 15% of the obtained protein IDs were classified as nuclear/chromosomal. The lists of the most abundant proteins were very similar for both methods (**Supplementary Tables 3 and 4**). The four most common proteins/complexes (Group 1) were TOPOISOMERASE 2 (TOP2), POLY(ADP-RIBOSE) POLYMERASE 2 (PARP2), various histone proteins, and condensin complex subunits. At the fifth to the seventh position (Group 2), we found inner nuclear envelope protein CROWDED NUCLEI 1 (CRWN1), nucleolar proteins (e.g., FIB1), and subunits of the replication licensing complex MCM MCM2 to MCM7. The remaining positions (Group 3) were more variable between the methods and represented a mix of proteins with various chromatin-related functions. They included chromatin-remodeling ISWI complex factor (CHR11); FACT complex factors (SPT16 and SSRP1 subunits); high mobility group proteins; histone chaperone NAP1,2; DNA repair proteins ZINC 4 FINGER DNA 3'-PHOSPHOESTERASE (ZDP), LIGASE 1 (LIG1) and KU80; and transcriptional gene silencing factors CHG DNA methyltransferase CMT3, CG DNA METHYLTRANSFERASE 1 (MET1), or ARGONAUTE 4.

Based on the spectra of the most abundant chromosomal proteins, we can draw a picture of barley metaphase mitotic chromosome proteins. Using all three methods, we obtained abundant histone proteins, which are the expected component of the highly compact metaphase chromosomes. The frequent presence of histone H1.2 agrees with the transcriptionally inactive chromatin of condensed chromosomes. From the condensin complex, we found mainly the core subunits STRUCTURAL MAINTENANCE OF CHROMOSOMES 2 and 4 (SMC2 and SMC4) and there was only one hit for the cohesin complex, suggesting that the latter is less abundant. To our surprise, the most abundant peptides in both SXC and MG methods originated from TOP2. Although the TOP1 was present, it was less abundant. This indicates frequent sister chromatid interwindings and/or supercoils that need to be mitigated primarily by the TOP2 and to a lesser extent by the TOP1 activities. The candidates from the Group 2 are intriguing as they represent typical interphase nuclear proteins. CRWN1 is an inner nuclear envelope (NE) protein that interacts with other chromatin-binding proteins and thus mediates chromatin and chromosome organization (Meier et al., 2016; Mikulski et al., 2019). It is tempting to speculate that the complex remains bound to the surface of the chromosome also during mitosis, helping to anchor the centromeric region to the NE. This could, on the one hand, accelerate the kinetics of the division and, on the other hand, help maintaining Rab1 chromosome organization found in barley nuclei (Tiang et al., 2012).

A surprising observation concerned the numerous peptides derived from the maintenance complex 2 to 7 (MCM2-7). This complex is typical for DNA replication initiation and elongation

during the S-phase of the cell cycle (Tuteja et al., 2011). Currently, no data support a direct role of the MCM2-7 complex during mitosis. Therefore, the MCM2-7 proteins may represent a contamination from the cytoplasm. However, the presence of some other (Group 3) proteins, such as DNA replication coupled maintenance DNA methyltransferases MET1 and CMT3, indicates that some replication-related processes appear during mitosis, possibly at specific DNA repair sites. Furthermore, there is a specific report of MCM function in late mitosis. Other members of Group 3 indicate active transcription (FACT and ISWI complex subunits) and DNA repair. From the DNA repair enzymes, we detected KU80, which acts as a heterodimer with KU70 and stabilizes free DNA ends. In addition, we found ZDP and LIG1, both acting in the excision repair pathways. This indicates a repair of DNA double and single-strand breaks that could arise from the tension during chromosome condensation and/or topoisomerase activity.

Validation of Perichromosomal Location of FIB1

Abundant nucleolar proteins bind to chromosomes after nucleoli disassemble at the onset of mitosis. Several studies have demonstrated the presence of nucleolar proteins over the entire mitosis and their important role in reconstituting a new nucleolus after the mitosis is completed (reviewed in Kalinina et al., 2018). Our proteomic data confirm the idea that at least part of these nucleolar proteins is physically attached to plant mitotic chromosomes, where they presumably contribute to the formation of a perichromosomal layer. We have experimentally validated this localization for the large nucleolar protein FIB1 using multiple approaches. FIB1 is a part of small nuclear ribonucleoprotein complexes involved in the first steps of RNA splicing and processing pre-ribosomal (r)RNAs (Reichow et al., 2007). Sirri et al. (2016) demonstrated that precursor rRNAs associate with the perichromosomal layer of human chromosomes where they serve as binding sites for various nucleolar proteins. In our work, the treatment of barley chromosomes with RNase A resulted in a strong reduction of FIB1 signal. This observation supports the critical role of RNAs in the assembly of perichromosomal layer also in plants and confirms the specific binding of FIB1. The marker of proliferation Ki67 is another nucleolar protein associating with perichromosomal layer in human (Takagi et al., 1999). According to Hayashi et al. (2017), Ki67 functions as a binding scaffold for pre-RNAs to which nucleolar proteins bind. Given the critical role of Ki67 in human, it is surprising that our analyses did not identify Ki67 in the proteome of barley chromosomes. Given the large evolutionary distance between animals and plants, it is possible that a similar role is played by a different and not yet described protein.

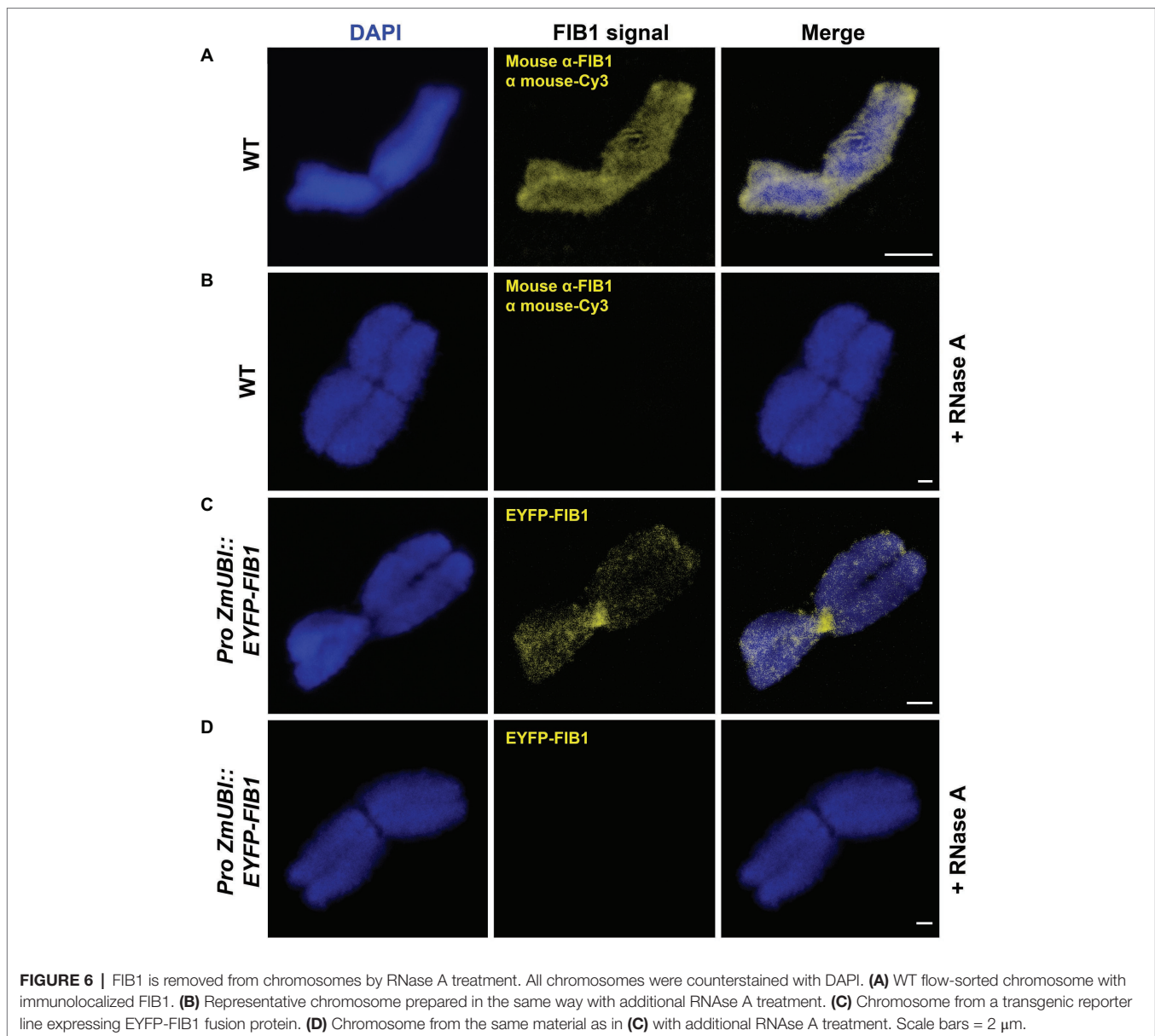
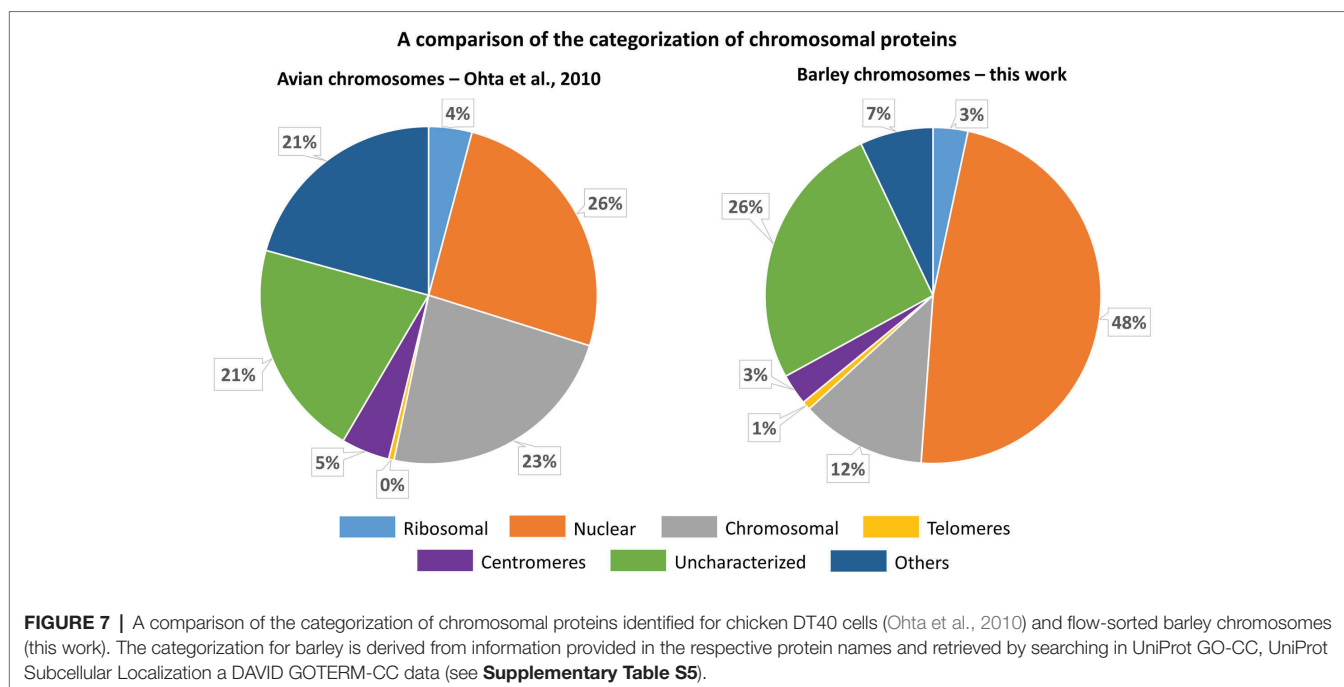


FIGURE 6 | FIB1 is removed from chromosomes by RNase A treatment. All chromosomes were counterstained with DAPI. **(A)** WT flow-sorted chromosome with immunolocalized FIB1. **(B)** Representative chromosome prepared in the same way with additional RNase A treatment. **(C)** Chromosome from a transgenic reporter line expressing EYFP-FIB1 fusion protein. **(D)** Chromosome from the same material as in **(C)** with additional RNase A treatment. Scale bars = 2 μ m.

CONCLUSION

Our results provide valuable insights into the protein composition of condensed barley chromosomes and support a multi-layer model suggested for human mitotic chromosome (Uchiyama et al., 2005; Takata et al., 2007). This model categorized the identified proteins into separate groups: (1) coating cytoplasmic proteins on chromosome surfaces, (2) a perichromosomal layer comprising RNAs and nucleolar proteins, and (3) chromosome structural and fibrous proteins deeper in the chromosome core. Indeed, we detected the presence of many cytoplasmic proteins in the sorted mitotic barley chromosomes. However, these were excluded by our multi-classifier data analysis as random cellular hitchhikers with no essential functions during mitosis. On the other hand, a large group of nucleolar proteins was assigned as truly chromosomal and this finding, together with an important organizational role

of RNA, was further confirmed by immunolocalization experiments. Finally, we included into the list a variety of proteins contributing to the processes of chromosome organization and maintenance. Generally, there were attempts to assign the identified barley proteins to their counterparts in Arabidopsis. In some cases, we could find a high homology for relevant hits supported by experimental data in the literature. Examples are SWITCH/SUCROSE NONFERMENTING (SWI/SNF) chromatin-remodeling complex proteins. Barley SNF protein, UniProtKB access. no. A0A287IBE5, shows 75% sequence similarity to its ARATH homolog Q9FMT4. Barley SWI3C subunit (access. no. A0A287QVR1) is identical at 46%. The possible regulatory function of Arabidopsis SWI3C resides in affecting plant development as its mutations led to lower fertility (Sarnowski et al., 2005). Barley PROLIFERATING CELL NUCLEAR ANTIGEN 2 (PCNA2), access. no. A0A287FZQ3, is largely homologous (sequence similarities



above 80%) to Arabidopsis (Q9ZW35) and human PCNAs (Q6FHF5). This protein is an auxiliary component for DNA polymerase delta and is involved in the replication control. Its interaction partner REPLICATION FACTOR C PROTEIN SUBUNIT 1, which participates in meiotic recombination and crossover formation process (Liu et al., 2013), was identified in several forms in the present proteomics dataset. As exemplified by the missing counterpart of human Ki67, many chromosome-associated proteins that play key roles in plant mitotic pathways remain elusive. Thus, our dataset may serve as a valuable resource for functional characterization of plant chromosomal proteins, their comparative phylogenetic analyses, and ultimately, the development of the next-generation models for the hierarchical organization of plant chromosomes.

DATA AVAILABILITY STATEMENT

The datasets presented in this study can be found in the PRIDE Archive (<https://www.ebi.ac.uk/pride/archive/>; Perez-Riverol et al., 2019). The accession number is PXD024689.

AUTHOR CONTRIBUTIONS

BP and JV maintained barley plants and purified mitotic chromosomes by flow cytometric sorting. ZP performed all experiments comprising microgradient pre-separation of peptides, he also processed, analyzed, and curated the data, created all figures, and contributed to the original manuscript draft writing. JB carried out all experiments that included in-gel digestion and in-solution digestion followed by SCX pre-separation of peptides. IC partly designed the study and employed the methodologies,

he also created the tables and contributed to data processing and writing of the original manuscript draft. RL was responsible for all MS analyses. KK prepared barley transgenic line and performed immunostaining and microscopy. VB coordinated barley transformation. AP evaluated and discussed the biological meaning of the obtained results. JD, MŠ, and AP conceived, conducted, and supervised the study and secured funding. MŠ wrote the original manuscript draft. All authors read, edited, and approved the final manuscript.

FUNDING

This work was supported by the ERDF project “Plants as a tool for sustainable global development” (No. CZ.02.1.01/0.0/0.0/16_019/0000827), MEYS INTER-COST grant LTC18026, and stimulated by the COST action CA16212 “Impact of nuclear domains on gene expression and plant traits.”

ACKNOWLEDGMENTS

We thank Petr Cápál, Zdeňka Dubská, Romana Šperková, and Jitka Weiserová for the assistance with flow cytometric sorting of chromosomes and cell nuclei, and Vendula Svobodová and Iva Hradilová with barley transformation and plant regeneration.

SUPPLEMENTARY MATERIAL

The Supplementary material for this article can be found online at <https://www.frontiersin.org/articles/10.3389/fpls.2021.723674/full#supplementary-material>

REFERENCES

- Altschul, S. F., Wootton, J. C., Gertz, E. M., Agarwala, R., Morgulis, A., Schäffer, A. A., et al. (2005). Protein database searches using compositionally adjusted substitution matrices. *FEBS J.* 272, 5101–5109. doi: 10.1111/j.1742-4658.2005.04945.x
- Antonin, W., and Neumann, H. (2016). Chromosome condensation and decondensation during mitosis. *Curr. Opin. Cell Biol.* 40, 15–22. doi: 10.1016/j.ceb.2016.01.013
- Baker, K., Dhillon, T., Colas, L., Cook, N., Milne, I., Milne, L., et al. (2015). Chromatin state analysis of the barley epigenome reveals a higher-order structure defined by H3K27me1 and H3K27me3 abundance. *Plant J.* 84, 111–124. doi: 10.1111/tpj.12963
- Bigear, J., Rayapuram, N., Bonhomme, L., Hirt, H., and Pflieger, D. (2014). Proteomic and phosphoproteomic analyses of chromatin-associated proteins from *Arabidopsis thaliana*. *Proteomics* 14, 2141–2155. doi: 10.1002/pmic.201400072
- Blavet, N., Uřinová, J., Jeřábková, H., Chamrád, I., Vrána, J., Lenobel, R., et al. (2017). UNcleProt (universal nuclear protein database of barley): The first nuclear protein database that distinguishes proteins from different phases of the cell cycle. *Nucleus* 8, 70–80. doi: 10.1080/19491034.2016.1255391
- Blythe, S. A., and Wieschaus, E. F. (2016). Establishment and maintenance of heritable chromatin structure during early *Drosophila* embryogenesis. *eLife* 5:e20148. doi: 10.7554/eLife.20148
- Booth, D. G., Beckett, A. J., Molina, O., Samejima, I., Masumoto, H., Kouprina, N., et al. (2016). 3D-CLEM reveals that a major portion of mitotic chromosomes is not chromatin. *Mol. Cell* 64, 790–802. doi: 10.1016/j.molcel.2016.10.009
- Booth, D. G., Takagi, M., Sanchez-Pulido, L., Petfalski, E., Vargiu, G., Samejima, K., et al. (2014). Ki-67 is a PP1-interacting protein that organises the mitotic chromosome periphery. *eLife* 3:e01641. doi: 10.7554/eLife.01641
- Brameier, M., Krings, A., and MacCallum, R. M. (2007). NucPred—predicting nuclear localization of proteins. *Bioinformatics* 23, 1159–1160. doi: 10.1093/bioinformatics/btm066
- Chamrád, I., Simerský, R., Běsešová, L., Strnad, M., Šebela, M., and Lenobel, R. (2014). Proteomic identification of a candidate sequence of wheat cytokinin-binding protein 1. *J. Plant Growth Regul.* 33, 896–902. doi: 10.1007/s00344-014-9419-z
- Chamrád, I., Uřinová, J., Petrovská, B., Jeřábková, H., Lenobel, R., Vrána, J., et al. (2018). Identification of plant nuclear proteins based on a combination of flow sorting, SDS-PAGE, and LC-MS/MS analysis. *Methods Mol. Biol.* 1696, 57–79. doi: 10.1007/978-1-4939-7411-5_4
- Cheeseman, I. M. (2014). The kinetochore. *Cold Spring Harb. Perspect. Biol.* 6:a015826. doi: 10.1101/cshperspect.a015826
- Chi, S. M., and Nam, D. (2012). WegoLoc: accurate prediction of protein subcellular localization using weighted gene ontology terms. *Bioinformatics* 28, 1028–1030. doi: 10.1093/bioinformatics/bts062
- Cuylen, S., Blaukopf, C., Politi, A. Z., Müller-Reichert, T., Neumann, B., Poser, I., et al. (2016). Ki-67 acts as a biological surfactant to disperse mitotic chromosomes. *Nature* 535, 308–312. doi: 10.1038/nature18610
- Cuylen-Haering, S., Petrovic, M., Hernandez-Armendariz, A., Schneider, M. W., Samwer, M., Blaukopf, C., et al. (2020). Chromosome clustering by Ki-67 excludes cytoplasm during nuclear assembly. *Nature* 587, 285–290. doi: 10.1038/s41586-020-2672-3
- Djeghloul, D., Patel, B., Kramer, H., Dimond, A., Whilding, C., Brown, K., et al. (2020). Identifying proteins bound to native mitotic ESC chromosomes reveals chromatin repressors are important for compaction. *Nat. Commun.* 11, 1–15. doi: 10.1038/s41467-020-17823-z
- Doležel, J., Binarová, P., and Lucretti, S. (1989). Analysis of nuclear DNA content in plant cells by flow cytometry. *Biol. Plant.* 31, 113–120. doi: 10.1007/BF02907241
- Doležel, J., Kubaláková, M., Číhalíková, J., Suchánková, P., and Šimková, H. (2011). Chromosome analysis and sorting using flow cytometry. *Methods Mol. Biol.* 701, 221–238. doi: 10.1007/978-1-61737-957-4_12
- Doležel, J., Sgorbati, S., and Lucretti, S. (1992). Comparison of three DNA fluorochromes for flow cytometric estimation of nuclear DNA content in plants. *Physiol. Plant.* 85, 625–631. doi: 10.1111/j.1399-3054.1992.tb04764.x
- Doležel, J., Vrána, J., Šafář, J., Bartoš, J., Kubaláková, M., and Šimková, H. (2012). Chromosomes in the flow to simplify genome analysis. *Funct. Integr. Genomics* 12, 397–416. doi: 10.1007/s10142-012-0293-0
- Festuccia, N., Dubois, A., Vandormael-Pournin, S., Tejada, E. G., Mouren, A., and Bessonard, S. (2016). Mitotic binding of Esrrb marks key regulatory regions of the pluripotency network. *Nat. Cell Biol.* 18, 1139–1148. doi: 10.1038/ncb3418
- Fierz, B., and Poirer, M. G. (2019). Biophysics of chromatin dynamics. *Annu. Rev. Biophys.* 48, 321–345. doi: 10.1146/annurev-biophys-070317-032847
- Franc, V., Řehulka, P., Medda, R., Padiglia, A., Floris, G., and Šebela, M. (2013a). Analysis of the glycosylation pattern of plant copper amine oxidases by MALDI-TOF/TOF MS coupled to a manual chromatographic separation of glycans and glycopeptides. *Electrophoresis* 34, 2357–2367. doi: 10.1002/elps.201200622
- Franc, V., Řehulka, P., Raus, M., Stulík, J., Novak, J., Renfrow, M. B., et al. (2013b). Elucidating heterogeneity of IgA1 hinge-region O-glycosylation by use of MALDI-TOF/TOF mass spectrometry: role of cysteine alkylation during sample processing. *J. Proteomics* 92, 299–312. doi: 10.1016/j.jprot.2013.07.013
- Fujimura, A., Hayashi, Y., Kato, K., Kogure, Y., Kameyama, M., Shimamoto, H., et al. (2020). Identification of a novel nucleolar protein complex required for mitotic chromosome segregation through centromeric accumulation of Aurora B. *Nucleic Acids Res.* 48, 6583–6596. doi: 10.1093/nar/gkaa449
- Ganji, M., Shaltiel, I. A., Bisht, S., Kim, E., Kalichava, A., Haering, C. H., et al. (2018). Real-time imaging of DNA loop extrusion by condensin. *Science* 360, 102–105. doi: 10.1126/science.aar7831
- Gassmann, R., Henzing, A. J., and Earnshaw, W. C. (2005). Novel components of human mitotic chromosomes identified by proteomic analysis of the chromosome scaffold fraction. *Chromosoma* 113, 385–397. doi: 10.1007/s00412-004-0326-0
- Ginno, P. A., Burger, L., Seebacher, J., Iesmantavicius, V., and Schübeler, D. (2018). Cell cycle-resolved chromatin proteomics reveals the extent of mitotic preservation of the genomic regulatory landscape. *Nat. Commun.* 9, 1–12. doi: 10.1038/s41467-018-06007-5
- Hara, M., and Fukagawa, T. (2020). Dynamics of kinetochore structure and its regulations during mitotic progression. *Cell. Mol. Life Sci.* 77, 1–15. doi: 10.1007/s00018-020-03472-4
- Hayashi, Y., Kato, K., and Kimura, K. (2017). The hierarchical structure of the perichromosomal layer comprises Ki67, ribosomal RNAs, and nucleolar proteins. *Biochem. Biophys. Res. Commun.* 493, 1043–1049. doi: 10.1016/j.bbrc.2017.09.092
- Hsiung, C. C. S., Morrissey, C. S., Udugama, M., Frank, C. L., Keller, C. A., Baek, S., et al. (2015). Genome accessibility is widely preserved and locally modulated during mitosis. *Genome Res.* 25, 213–225. doi: 10.1101/gr.180646.114
- Huang, D. W., Sherman, B. T., and Lempicki, R. A. (2009). Bioinformatics enrichment tools: paths toward the comprehensive functional analysis of large gene lists. *Nucleic Acids Res.* 37, 1–13. doi: 10.1093/nar/gkn923
- International Barley Genome Sequencing Consortium, Mayer, K. F. X., Waugh, R., Brown, J. W. S., Schulman, A., Langridge, P., et al. (2012). A physical, genetic and functional sequence assembly of the barley genome. *Nature* 491, 711–716. doi: 10.1038/nature11543
- Jasenčáková, Z., Meister, A., and Schubert, I. (2001). Chromatin organization and its relation to replication and histone acetylation during the cell cycle in barley. *Chromosoma* 110, 83–92. doi: 10.1007/s004120100132
- Kalinina, N. O., Makarova, S., Makhotenko, A., Love, A. J., and Taliensky, M. (2018). The multiple functions of the nucleolus in plant development, disease and stress responses. *Front. Plant Sci.* 9:132. doi: 10.3389/fpls.2018.00132
- Kintlová, M., Blavet, N., Cegan, R., and Hobza, R. (2017). Transcriptome of barley under three different heavy metal stress reaction. *Genom. Data* 13, 15–17. doi: 10.1016/j.gdata.2017.05.016
- Kubaláková, M., Macas, J., and Doležel, J. (1997). Mapping of repeated DNA sequences in plant chromosomes by PRINS and C-PRINS. *Theor. Appl. Genet.* 94, 758–763. doi: 10.1007/s001220050475
- Laemmli, U. K. (1970). Cleavage of structural proteins during the assembly of the head of bacteriophage T4. *Nature* 227, 680–685. doi: 10.1038/227680a0
- Liu, Y., Deng, Y., Li, G., and Zhao, J. (2013). Replication factor C1 (RFC1) is required for double-strand break repair during meiotic homologous recombination in *Arabidopsis*. *Plant J.* 73, 154–165. doi: 10.1111/tpj.12024
- Lysák, M. A., Číhalíková, J., Kubaláková, M., Šimková, H., Künzel, G., and Doležel, J. (1999). Flow karyotyping and sorting of mitotic chromosomes of barley (*Hordeum vulgare* L.). *Chromosom. Res.* 7, 431–444. doi: 10.1023/A:1009293628638

- Marchler-Bauer, A., and Bryant, S. H. (2004). CD-search: protein domain annotations on the fly. *Nucleic Acids Res.* 32, W327–W331. doi: 10.1093/nar/gkh454
- Marthe, C., Kumlehn, J., and Hensel, G. (2015). Barley (*Hordeum vulgare* L.) transformation using immature embryos. *Methods Mol. Biol.* 1223, 71–83. doi: 10.1007/978-1-4939-1695-5_6
- Martínez-Balbás, M. A., Dey, A., Rabindran, S. K., Ozato, K., and Wu, C. (1995). Displacement of sequence-specific transcription factors from mitotic chromatin. *Cell* 83, 29–38. doi: 10.1016/0092-8674(95)90231-7
- Mascher, M., Gundlach, H., Himmelbach, A., Beier, S., Twardziok, S. O., Wicker, T., et al. (2017). A chromosome conformation capture ordered sequence of the barley genome. *Nature* 544, 427–433. doi: 10.1038/nature22043
- Meier, I., Griffis, A. H., Groves, N. R., and Wagner, A. (2016). Regulation of nuclear shape and size in plants. *Curr. Opin. Cell Biol.* 40, 114–123. doi: 10.1016/j.ceb.2016.03.005
- Mikulski, P., Hohenstatt, M. L., Farrona, S., Smaczniak, C., Stahl, Y., Kaufmann, K., et al. (2019). The chromatin-associated protein PWO1 interacts with plant nuclear Lamin-like components to regulate nuclear size. *Plant Cell* 31, 1141–1154. doi: 10.1105/tpc.18.00663
- Montaño-Gutierrez, L. F., Ohta, S., Kustatscher, G., Earnshaw, W. C., and Rappsilber, J. (2017). Nano random forests to mine protein complexes and their relationships in quantitative proteomics data. *Mol. Biol. Cell* 28, 673–680. doi: 10.1091/mbc.E16-06-0370
- Moravcová, D., Kahle, V., Řehulková, H., Chmelík, J., and Řehulka, P. (2009). Short monolithic columns for purification and fractionation of peptide samples for matrix-assisted laser desorption/ionization time-of-flight/time-of-flight mass spectrometry analysis in proteomics. *J. Chromatogr. A* 1216, 3629–3636. doi: 10.1016/j.chroma.2009.01.075
- Morrison, C., Henzing, A. J., Jensen, O. N., Osheroff, N., Dodson, H., Kandels-Lewis, S. E., et al. (2002). Proteomic analysis of human metaphase chromosomes reveals topoisomerase II alpha as an Aurora B substrate. *Nucleic Acids Res.* 30, 5318–5327. doi: 10.1093/nar/gkf665
- Ohta, S., Bukowski-Wills, J. C., Sanchez-Pulido, L., de Lima Alves, F., Wood, L., Chen, Z., et al. (2010). The protein composition of mitotic chromosomes determined using multiclassifier combinatorial proteomics. *Cell* 142, 810–821. doi: 10.1016/j.cell.2010.07.047
- Ohta, S., Kimura, M., Takagi, S., Toramoto, I., and Ishihama, Y. (2016b). Identification of mitosis-specific phosphorylation in mitotic chromosome-associated proteins. *J. Proteome Res.* 15, 3331–3341. doi: 10.1021/acs.jproteome.6b00512
- Ohta, S., Montaño-Gutierrez, L. F., de Lima Alves, F., Ogawa, H., Toramoto, I., Sato, N., et al. (2016a). Proteomics analysis with a nano random Forest approach reveals novel functional interactions regulated by SMC complexes on mitotic chromosomes. *Mol. Cell. Proteomics* 15, 2802–2818. doi: 10.1074/mcp.m116.057885
- Ohta, S., Taniguchi, T., Sato, N., Hamada, M., Taniguchi, H., and Rappsilber, J. (2019). Quantitative proteomics of the mitotic chromosome scaffold reveals the association of BAZ1B with chromosomal axes. *Mol. Cell. Proteomics* 18, 169–181. doi: 10.1074/mcp.RA118.000923
- Palozola, K. C., Donahue, G., Liu, H., Grant, G. R., Becker, J. S., Cote, A., et al. (2017). Mitotic transcription and waves of gene reactivation during mitotic exit. *Science* 358, 119–122. doi: 10.1126/science.aal4671
- Parsons, G. G., and Spencer, C. A. (1997). Mitotic repression of RNA polymerase II transcription is accompanied by release of transcription elongation complexes. *Mol. Cell. Biol.* 17, 5791–5802. doi: 10.1128/MCB.17.10.5791
- Perez-Riverol, Y., Csordas, A., Bai, J., Bernal-Llinares, M., Hewapathirana, S., Kundu, D. J., et al. (2019). The PRIDE database and related tools and resources in 2019: improving support for quantification data. *Nucleic Acids Res.* 47, D442–D450. doi: 10.1093/nar/gky1106
- Pesenti, M. E., Prumbaum, D., Auckland, P., Smith, C. M., Faesen, A. C., Petrovic, A., et al. (2018). Reconstitution of a 26-subunit human kinetochore reveals cooperative microtubule binding by CENP-OPQUR and NDC80. *Mol. Cell* 71, 923–939. doi: 10.1016/j.molcel.2018.07.038
- Petrovská, B., Jeřábková, H., Chamrád, I., Vrána, J., Lenobel, R., Ufinovská, J., et al. (2014). Proteomic analysis of barley cell nuclei purified by flow sorting. *Cytogenet. Genome Res.* 143, 78–86. doi: 10.1159/000365311
- Raccuda, M., and Suter, D. M. (2018). Transcription factor retention on mitotic chromosomes: regulatory mechanisms and impact on cell fate decisions. *FEBS Lett.* 592, 878–887. doi: 10.1002/1873-3468.12828
- Rapazote-Flores, P., Bayer, M., Milne, L., Mayer, C. D., Fuller, J., Guo, W., et al. (2019). BaRTv1.0: an improved barley reference transcript dataset to determine accurate changes in the barley transcriptome using RNA-seq. *BMC Genomics* 20:968. doi: 10.1186/s12864-019-6243-7
- Rappsilber, J., Mann, M., and Ishihama, Y. (2007). Protocol for micro-purification, enrichment, pre-fractionation and storage of peptides for proteomics using stagetips. *Nat. Protoc.* 2, 1896–1906. doi: 10.1038/nprot.2007.261
- Reichow, S. L., Hamma, T., Ferré-D'Amaré, A. R., and Varani, G. (2007). The structure and function of small nucleolar ribonucleoproteins. *Nucleic Acids Res.* 35, 1452–1464. doi: 10.1093/nar/gkl1172
- Samejima, I., and Earnshaw, W. C. (2018). Isolation of mitotic chromosomes from vertebrate cells and characterization of their proteome by mass spectrometry. *Methods Cell Biol.* 144, 329–348. doi: 10.1016/bs.mcb.2018.03.021
- Sarnowski, T. J., Ríos, G., Jásik, J., Świeżewski, S., Kaczanowski, S., Li, Y., et al. (2005). SWI3 subunits of putative SWI/SNF chromatin-remodeling complexes play distinct roles during Arabidopsis development. *Plant Cell* 17, 2454–2472. doi: 10.1105/tpc.105.031203
- Šebela, M., Štosová, T., Havliš, J., Wielsch, N., Thomas, H., Zdráhal, Z., et al. (2006). Thermostable trypsin conjugates for high-throughput proteomics: synthesis and performance evaluation. *Proteomics* 6, 2959–2963. doi: 10.1002/pmic.200500576
- Shevchenko, A., Tomas, H., Havliš, J., Olsen, J. V., and Mann, M. (2006). In-gel digestion for mass spectrometric characterization of proteins and proteomes. *Nat. Protoc.* 1, 2856–2860. doi: 10.1038/nprot.2006.468
- Sirri, V., Jourdan, N., Hernandez-Verdun, D., and Roussel, P. (2016). Sharing of mitotic pre-ribosomal particles between daughter cells. *J. Cell Sci.* 129, 1592–1604. doi: 10.1242/jcs.180521
- Skibbens, R. V. (2019). Condensins and cohesins – one of these things is not like the other! *J. Cell Sci.* 132:jcs.220491. doi: 10.1242/jcs.220491
- Smith, P. K., Krohn, R. I., Hermanson, G. T., Mallia, A. K., Gartner, F. H., Provenzano, M. D., et al. (1985). Measurement of protein using bicinchoninic acid. *Anal. Biochem.* 150, 76–85. doi: 10.1016/0003-2697(85)90442-7
- Sperschneider, J., Catanzariti, A. M., DeBoer, K., Petre, B., Gardiner, D. M., Singh, K. B., et al. (2017). LOCALIZER: subcellular localization prediction of both plant and effector proteins in the plant cell. *Sci. Rep.* 7:44598. doi: 10.1038/srep44598
- Stenström, L., Mahdessian, D., Gnann, C., Cesnik, A. J., Ouyang, W., Leonetti, M. D., et al. (2020). Mapping the nucleolar proteome reveals a spatiotemporal organization related to intrinsic protein disorder. *Mol. Syst. Biol.* 16:e9469. doi: 10.15252/msb.20209469
- Takagi, M., Matsuoka, Y., Kurihara, T., and Yoneda, Y. (1999). Chmadrin: a novel Ki-67 antigen-related perichromosomal protein possibly implicated in higher order chromatin structure. *J. Cell Sci.* 112, 2463–2472. doi: 10.1242/jcs.112.15.2463
- Takagi, M., Natsume, T., Kanemaki, M. T., and Imamoto, N. (2016). Perichromosomal protein Ki67 supports mitotic chromosome architecture. *Genes Cells* 21, 1113–1124. doi: 10.1111/gtc.12420
- Takata, H., Uchiyama, S., Nakamura, N., Nakashima, S., Kobayashi, S., Sone, T., et al. (2007). A comparative proteome analysis of human metaphase chromosomes isolated from two different cell lines reveals a set of conserved chromosome-associated proteins. *Genes Cells* 12, 269–284. doi: 10.1111/j.1365-2443.2007.01051.x
- Tan, F., Li, G., Chitteti, B. R., and Peng, Z. (2007). Proteome and phosphoproteome analysis of chromatin associated proteins in rice (*Oryza sativa*). *Proteomics* 7, 4511–4527. doi: 10.1002/pmic.200700580
- Tiang, C. L., He, Y., and Pawlowski, W. P. (2012). Chromosome organization and dynamics during interphase, mitosis, and meiosis in plants. *Plant Physiol.* 158, 26–34. doi: 10.1104/pp.111.187161
- Tuteja, N., Tran, N. Q., Dang, H. Q., and Tuteja, R. (2011). Plant MCM proteins: role in DNA replication and beyond. *Plant Mol. Biol.* 77, 537–545. doi: 10.1007/s11103-011-9836-3
- Tyanova, S., Temu, T., Sinitcyn, P., Carlson, A., Hein, M. Y., Geiger, T., et al. (2016). The Perseus computational platform for comprehensive analysis of (prote)omics data. *Nat. Methods* 13, 731–740. doi: 10.1038/nmeth.3901
- Uchiyama, S., Kobayashi, S., Takata, H., Ishihara, T., Hori, N., Higashi, T., et al. (2005). Proteome analysis of human metaphase chromosomes. *J. Biol. Chem.* 280, 16994–17004. doi: 10.1074/jbc.M412774200
- Wisniewski, J. R., and Gaugaz, F. Z. (2015). Fast and sensitive total protein and peptide assays for proteomic analysis. *Anal. Chem.* 87, 4110–4116. doi: 10.1021/ac504689z

- Yano, A., Kodama, Y., Koike, A., Shinya, T., Kim, H. J., and Matsumoto, M. (2006). Interaction between methyl CpG-binding protein and ran GTPase during cell division in tobacco cultured cells. *Ann. Bot.* 98, 1179–1187. doi: 10.1093/aob/mcl211
- Yu, C. S., Cheng, C. W., Su, W. C., Chang, K. C., Huang, S. W., Hwang, J. K., et al. (2014). CELLO2GO: a web server for protein subCELLular LOcalization prediction with functional gene ontology annotation. *PLoS One* 9:e99368. doi: 10.1371/journal.pone.0099368
- Zaidi, S. S. E. A., Mukhtar, M. S., and Mansoor, S. (2018). Genome editing: targeting susceptibility genes for plant disease resistance. *Trends Biotechnol.* 36, 898–906. doi: 10.1016/j.tibtech.2018.04.005
- Zeng, Z., and Jiang, J. (2016). Isolation and proteomics analysis of barley centromeric chromatin using PICH. *J. Proteome Res.* 15, 1875–1882. doi: 10.1021/acs.jproteome.6b00063
- Zwyrtková, J., Šimková, H., and Doležel, J. (2020). Chromosome genomics uncovers plant genome organization and function. *Biotechnol. Adv.* 46:107659. doi: 10.1016/j.biotechadv.2020.107659
- Zybailov, B., Mosley, A. L., Sardi, M. E., Coleman, M. K., Florens, L., and Washburn, M. P. (2006). Statistical analysis of membrane proteome expression changes in *Saccharomyces cerevisiae*. *J. Proteome Res.* 5, 2339–2347. doi: 10.1021/pr060161n
- Conflict of Interest:** The authors declare that the research was conducted in the absence of any commercial or financial relationships that could be construed as a potential conflict of interest.
- Publisher's Note:** All claims expressed in this article are solely those of the authors and do not necessarily represent those of their affiliated organizations, or those of the publisher, the editors and the reviewers. Any product that may be evaluated in this article, or claim that may be made by its manufacturer, is not guaranteed or endorsed by the publisher.

Copyright © 2021 Perutka, Kaduchová, Chamrád, Beinhauer, Lenobel, Petrovská, Bergougnoux, Vrána, Pecinka, Doležel and Šebela. This is an open-access article distributed under the terms of the Creative Commons Attribution License (CC BY). The use, distribution or reproduction in other forums is permitted, provided the original author(s) and the copyright owner(s) are credited and that the original publication in this journal is cited, in accordance with accepted academic practice. No use, distribution or reproduction is permitted which does not comply with these terms.

Appendix V

Towards *in vivo* analysis of chromatin dynamics in barley

Lahnerová, K., Stromšíková, H., Střelcová, K., Doležel, J., Bergounoux-Fojtík, V,
and Pecinka, A.

In: Abstract of 4th INDEPTH meeting ,“Impact of chromatin domains on plant
phenotypes“

Madrid, Spain, 2019

Towards *in vivo* analysis of chromatin dynamics in barley



Kateřina Lahnerová¹, Hana Stromšíková¹, Kateřina Střelcová², Jaroslav Doležel¹, Véronique Bergougnoux-Fojtík², Aleš Pečina¹



¹Institute of Experimental Botany of the Czech Academy of Sciences, Centre of the Region Haná for Biotechnological and Agricultural Research, Olomouc, Czech Republic

²Department of Cell Biology, Faculty of Science, Centre of the Region Haná for Biotechnological and Agricultural Research, Palacký University, Olomouc, Czech Republic

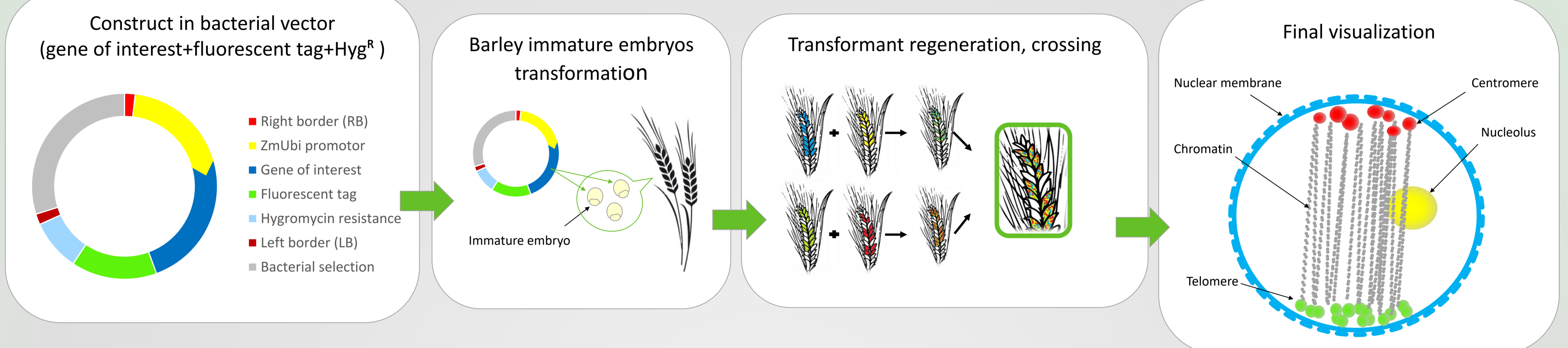
Introduction

The organization of chromatin in cell nuclei is dynamic and undergoes changes during cell cycle and cell tissue differentiation. This is necessary for correct segregation of genetic information, regulation of gene expression or DNA replication. While there is growing information about *in vivo* dynamics of nuclear domains in plant species with small genomes, such data are limited in plants with large and complex genomes.

We are presenting our efforts in developing a series of cultivated barley *Hordeum vulgare* ($2n = 2x = 14$; 5 Gbp/1C) marker lines carrying fluorescently labelled fusion proteins indicative of specific chromosome and nuclear domains such as centromere, telomere and nucleolus. Production of multi-marker lines will enable comprehensive analysis of chromatin dynamics in both wild type and mutant plants under various conditions.

The principle

Fluorescent marker lines



CRISPR/Cas9 mutants

CRISPR/Cas9 mutagenesis of barley SMC complexes

Protein complex	Function	Mutated protein	Transformants
Cohesin	kleisin	SYN1	4x T1
		SYN2	8xT1
	destabilizer	WAPL1	transformation
Condensin	regulatory subunits	CAP-G2	transformation
SMC5/6	SUMO ligase	NSE2	T3 plants

Cohesin complex

CTF7, SMC1, SMC3, WAPL, PDS5, SYN1, SYN2, SCC3

HvSYN2 genomic sequence (7072 bp) targeted by CRISPR/Cas9

5' 3'

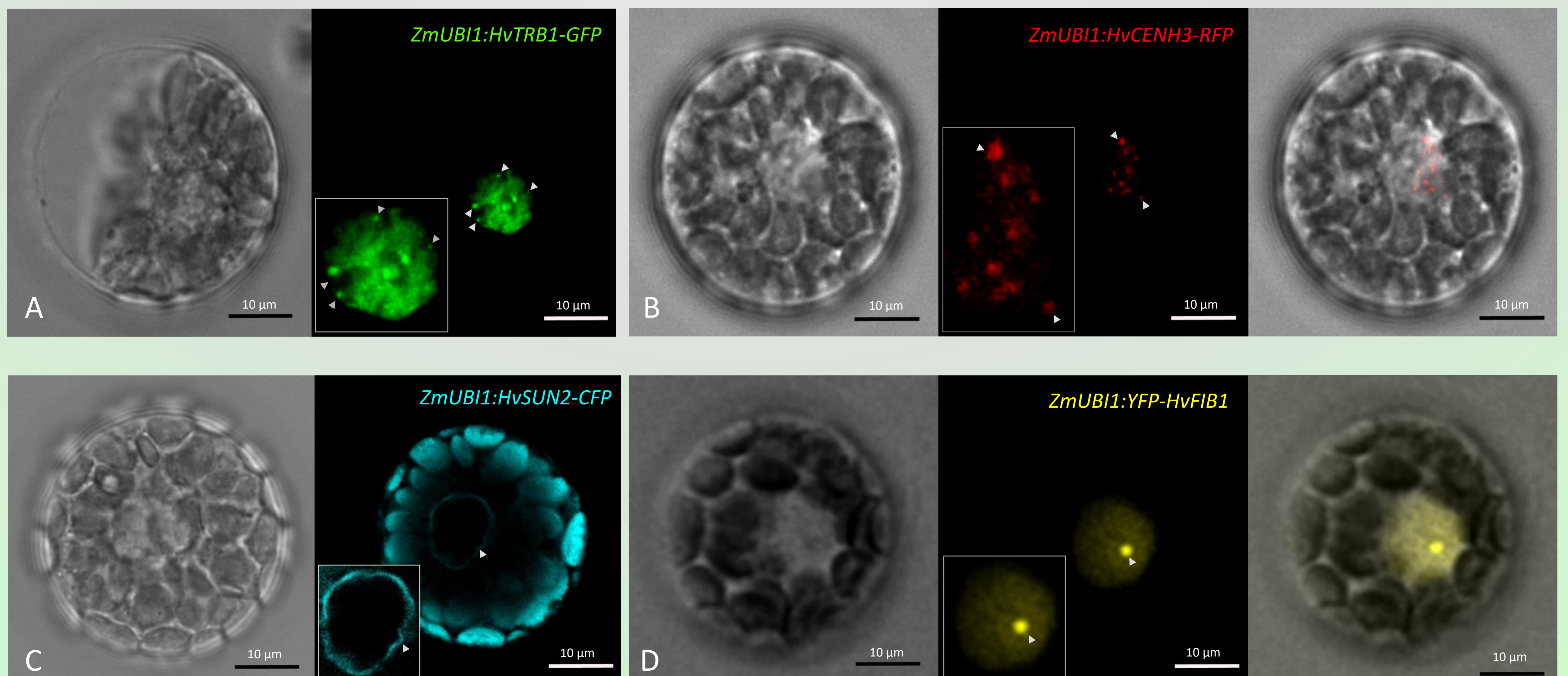
CGTGCTGTCCTCCGACGCGG, CTGCCGCCCTCGCCCCCTCGG

LB, 35S ter, PvUbi2 pro, ZmUbi1 pro, Cyt4, P2A, TaCas9, HSPter, PvUbi1 pro, G, gRNArep, CytK, gRNArep, CytK, 35S ter, RB

The results

Fluorescently tagged marker proteins designed for visualization of telomere (TRB1-GFP, A), centromere (CENH3-RFP, B), nucleus (SUN2-CFP, C) and nucleolus (YFP-FIB1, D). Arrows pointing out characteristic localization pattern.

Barley leaf protoplasts



Appendix VI

Developing system for tracking *in planta* chromatin dynamics in barley

(*Hordeum vulgare*)

Lahnerová, K., Stromšíková, H., Střelcová, K., Mičúchová, A., Bergougnoux-Fojtík, V, Šamaj, J., and Pecinka, A.

In: Abstract of „1st Czech Plant Nucleus Workshop 2021 (CPNW2021)“

Olomouc, Czech Republic, 2021

and

Kaduchová, K., Stromšíková, H., Střelcová, K., Mičúchová, A., Křižňanská, H. Bergougnoux-Fojtík, V, Galuszka, P., Šamaj, J., and Pecinka, A.

In: Abstract book of ‘Cytogenetics meeting 2021’

Görlitz, Germany, 2021.

Developing system for *in planta* tracking of chromatin dynamics in barley (*Hordeum vulgare*)



Kaduchová Kateřina¹, Střelcová Kateřina², Mičúchová Alžběta², Křižňanská¹ Hana, Stromšíková Hana¹, Bergougnoux-Fojtík Véronique², Galuszka Petr², Šamaj Jozef³ and Pečinka Aleš¹

¹Institute of Experimental Botany (IEB) of the Czech Academy of Sciences, Centre of the Region Haná for Biotechnological and Agricultural Research, Šlechtitelů 31, Olomouc, 77900, CZE
²Department of Plant Genetics and Engineering, Faculty of Science, Centre of the Region Haná for Biotechnological and Agricultural Research, CATRIN, Palacký University, Olomouc, 77900, CZE
³Department of Cell and Developmental Biology, Faculty of Science, Centre of the Region Haná for Biotechnological and Agricultural Research, Palacký University, Olomouc, 77900, CZE

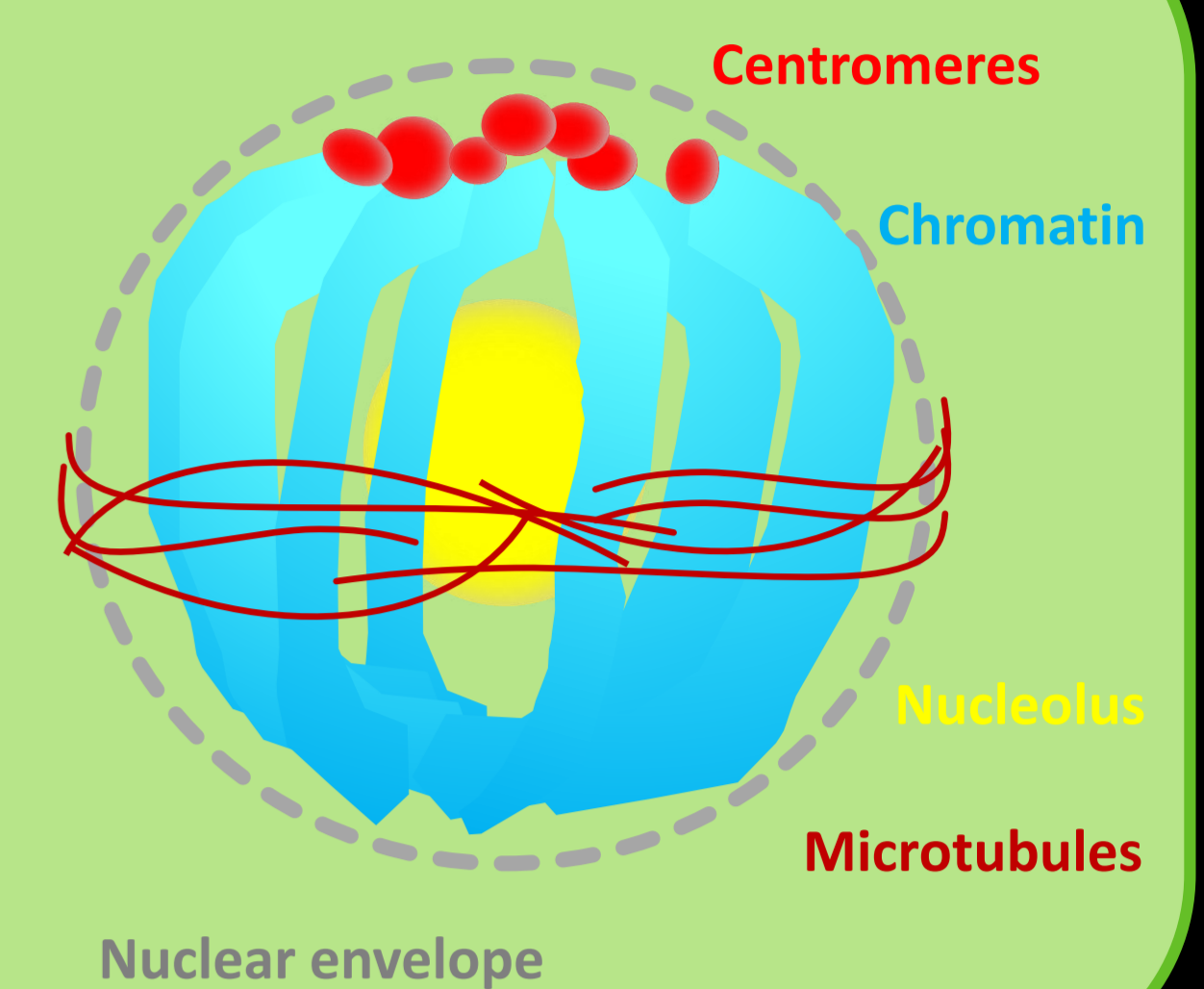
Introduction

The structure of the chromosome and chromatin organization in cell nuclei may change rapidly during cell cycle, in different cell tissues or in response to environmental stimuli. Due to the limited experimental resources, it is important to develop tools for investigating chromatin dynamics in plants with large genomes.

We developed a series of stable barley (*Hordeum vulgare*, $2n = 2x = 14$; 5,1 Gbp/1C) transgenic lines carrying translational fusions of fluorescent and nuclear proteins. **Fluorescent marker lines (FMLs)** are indicative of specific chromosome and nuclear domains. Single as well as multi-marker lines are subjected to confocal microscopy to study 3D *in vivo* dynamics of nuclear domains.

This set of FMLs will help in better understanding of chromatin organization and dynamics in cereals with large genomes in tissue specific manner.

Preprophase nucleus of multi-marker FML

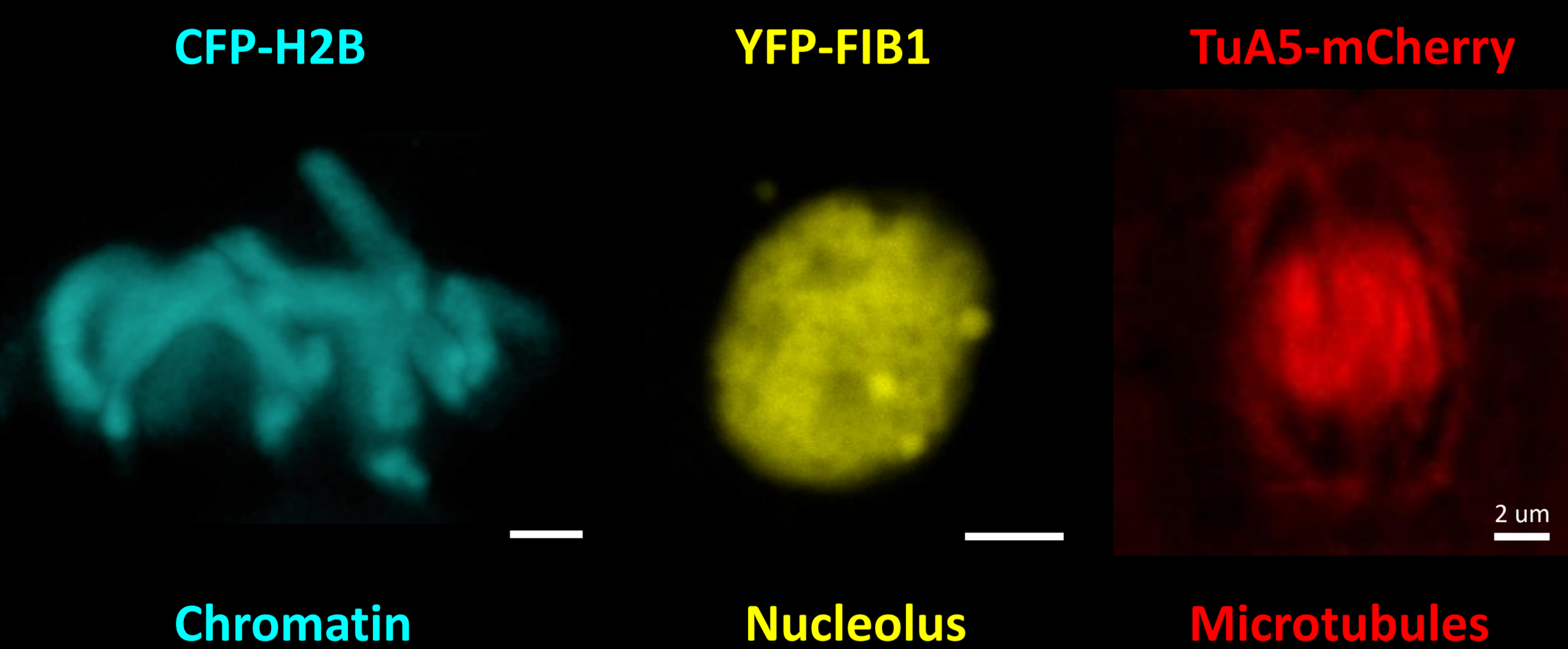


The principle



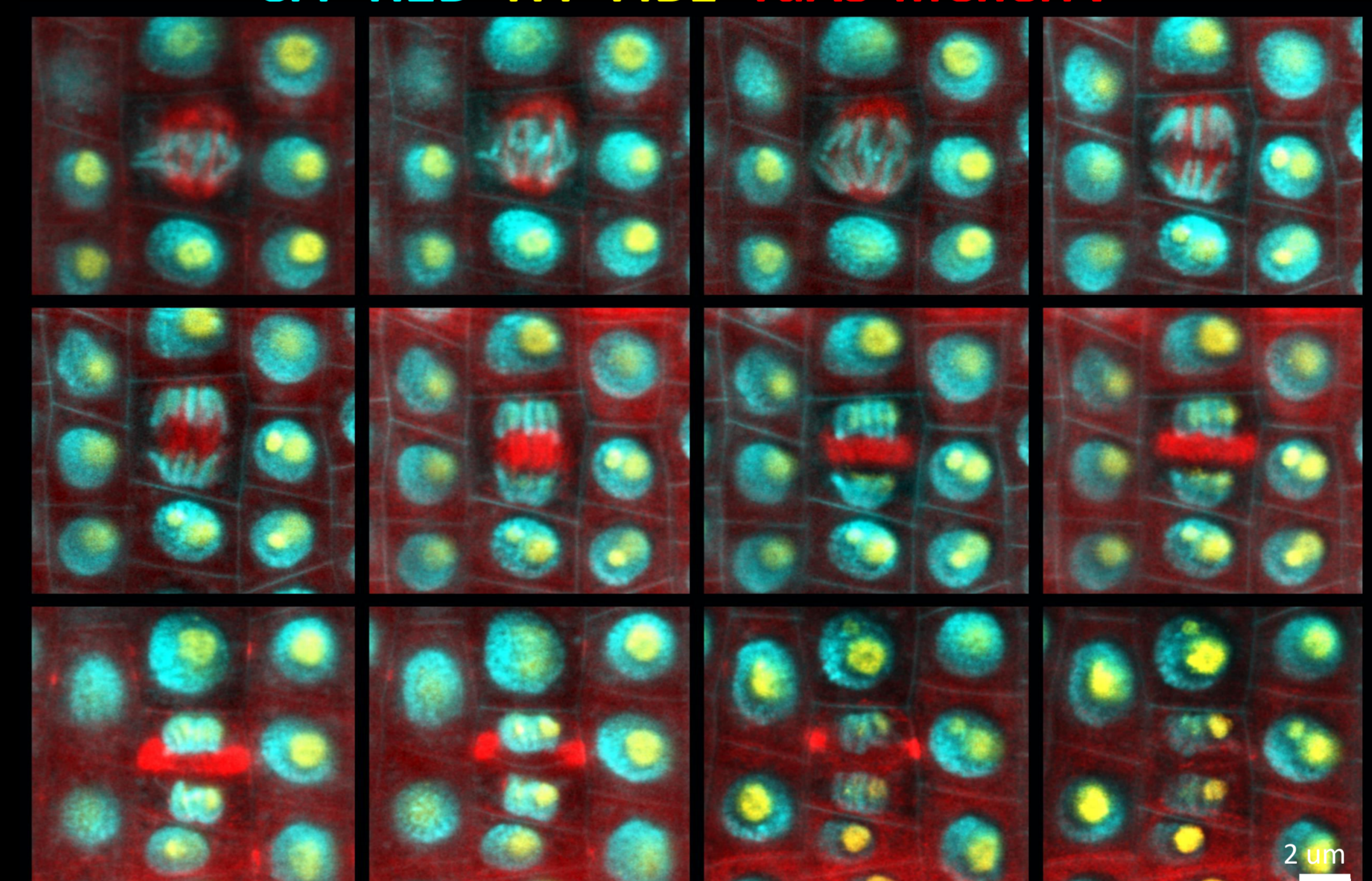
Results

Native structure and localization of FMLs proteins in living cells



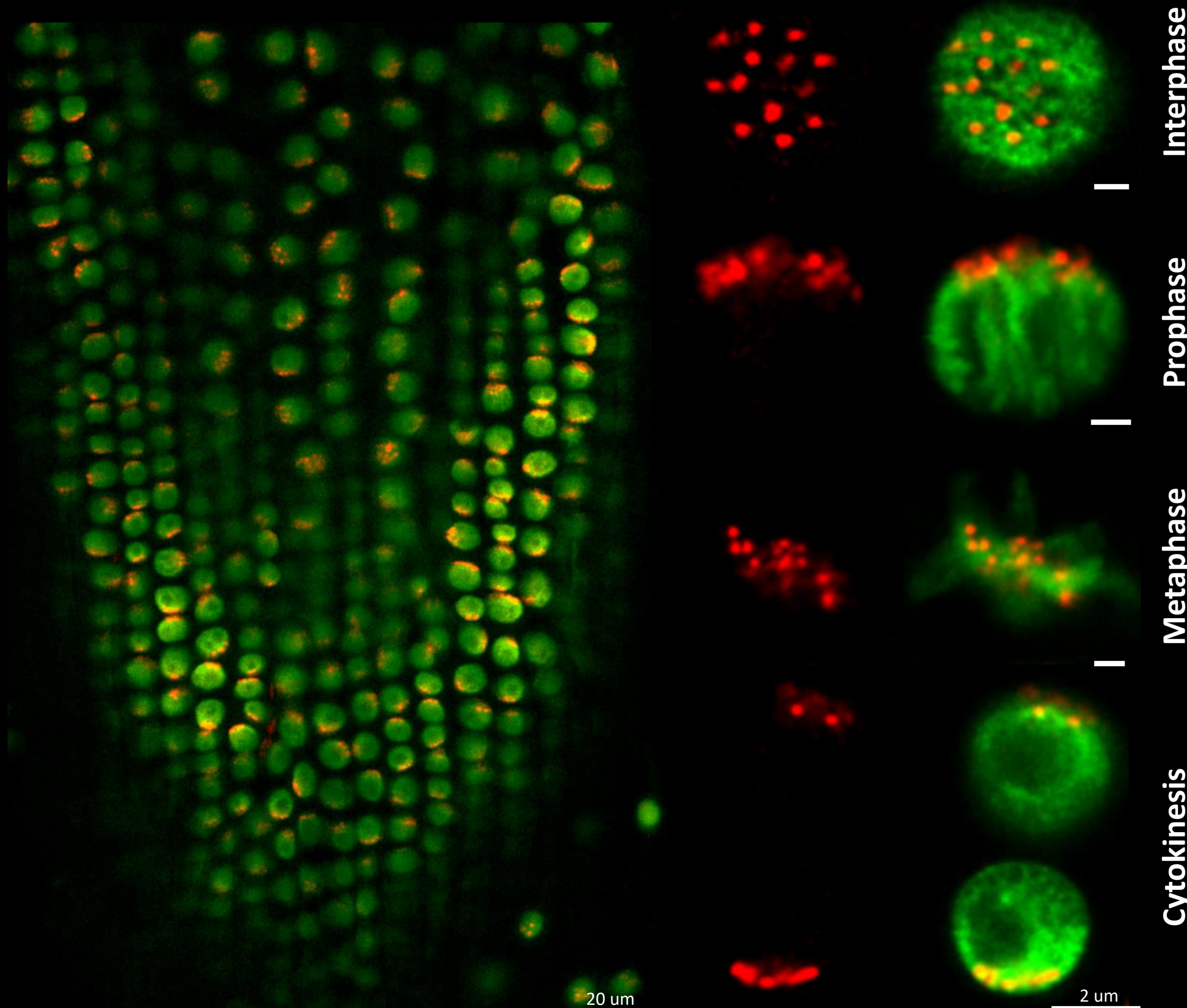
Analysis of mitosis in time

CFP-H2B YFP-FIB1 TuA5-mCherry

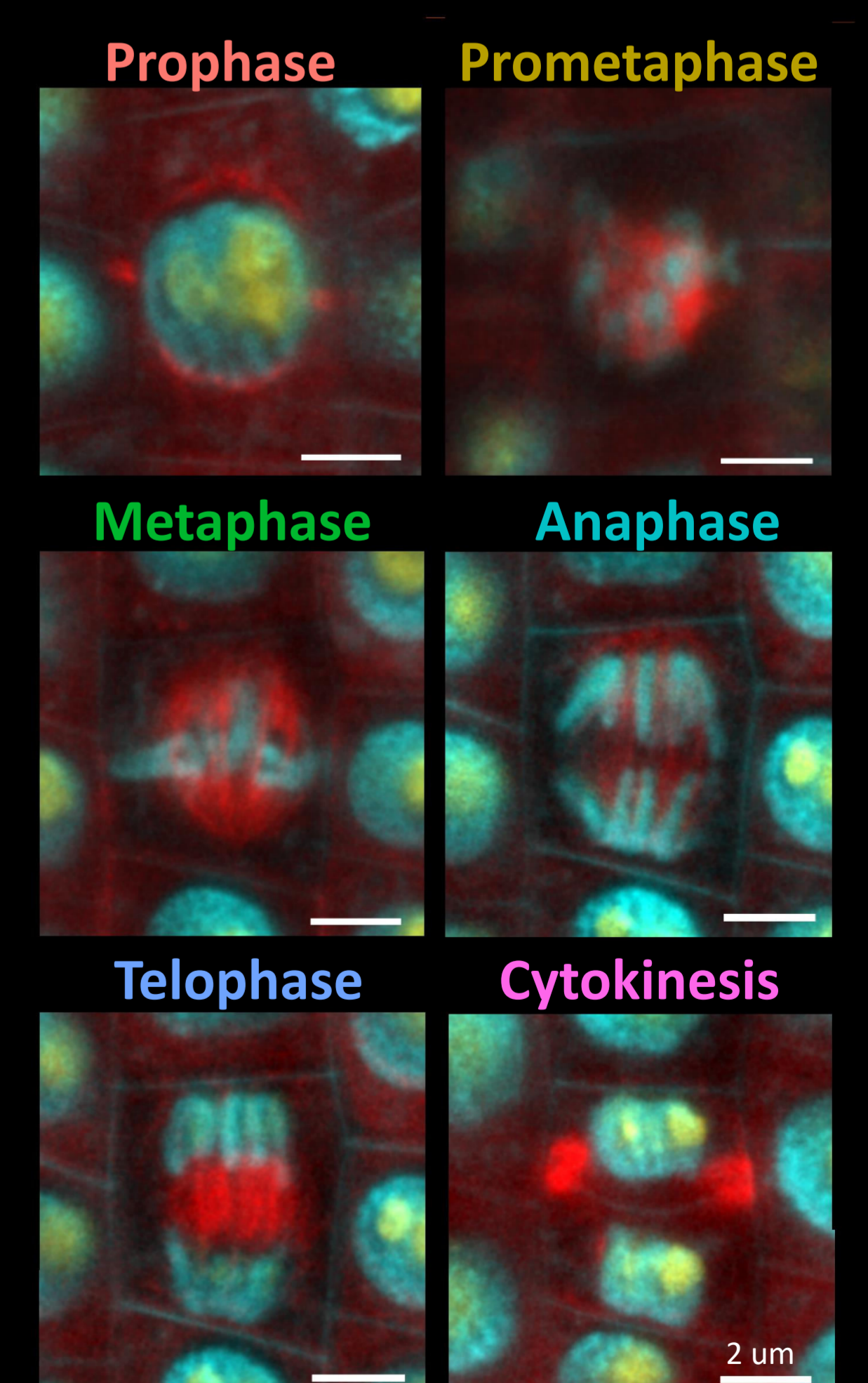
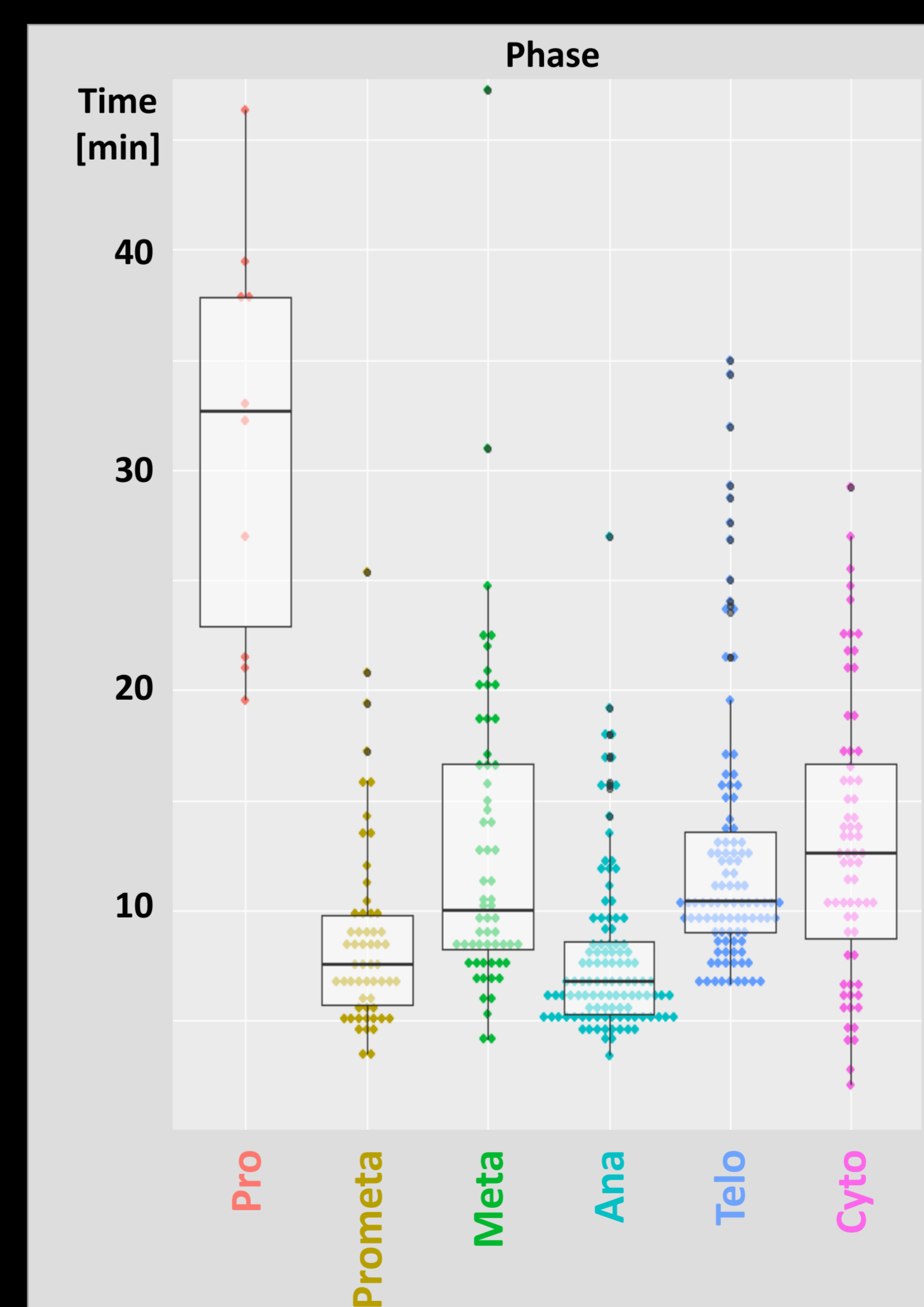


Analysis of centromere dynamics

RFP-CENH3 (centromeres) GFP-H2B (chromatin)



Mitosis length measurement and its dynamics



Conclusion

Average mitosis in barley takes about 70 min (prophase to telophase) and 80 min with cytokinesis included.

Ph.D. thesis was carried out at the Department of Cell Biology and Genetics, Faculty of Science, Palacký University Olomouc, between the years 2019-2023.

Ph.D. candidate: **Mgr. Kateřina Kaduchová**

Supervisor: **Assoc. Prof. Aleš Pečinka, Ph.D.**

Reviewers:

.....
.....

.....
.....

.....
.....

.....
.....

The evaluation of this Ph.D. thesis was written by

.....
.....
.....

The summary of the Ph.D. thesis was sent for distribution on
.....

The oral defense will take place on
.....in front of the commission for
the Ph.D. study of the study program Molecular and Cell Biology in
.....
.....

The Ph.D. thesis is available in the Library of the Biological Departments of
the Faculty of Science at Palacký University Olomouc, Šlechtitelů 11,
Olomouc-Holice.

Prof. RNDr. Zdeněk Dvořák, DrSc. et Ph.D.

Chairman of the Commission for the Ph.D.

Thesis of the Study Program Molecular and Cell Biology

Department of Cell Biology and Genetics, Faculty of Science

Palacký University Olomouc

Content

1	Introduction	5
2	Aims of the thesis	7
3	Materials and methods	8
4	Summary of results	12
5	Summary	14
6	References.....	16
7	List of author’s publications	18
7.1	First author publications.....	18
7.2	Co-authorship publications.....	18
7.3	Published abstracts – poster presentation	19
7.4	Published abstracts – oral presentation.....	19
8	Souhrn (Summary in Czech)	21

1 Introduction

The organization of the nuclear genome undergoes dynamic changes during the cell cycle. Primarily, it is determined by the cell and tissue type and the developmental requirements of the organism. In response to environmental conditions and stress stimuli, cells modify the organization of the genome to adjust gene transcription levels, facilitate repair processes, or modify accessibility for DNA binding proteins (reviewed in Schubert and Shaw, 2011, Rosa and Shaw, 2013, Dogan and Liu, 2018). The most notable alterations in the nuclear and cellular organization occur during mitotic division, a dynamical process that ensures even distribution of genetic information into emerging daughter cells (reviewed in Tiang *et al.*, 2012, Liu and Lee, 2022).

Despite the commonalities in the nuclear organization among higher plants, significant differences have been observed between individual plant species with varying genome composition. These observations have led to the presumption that their nuclear and cellular dynamics may also differ. Currently, most knowledge in this field is based on the relatively small and repeat-poor genome of the model plant *Arabidopsis thaliana* ($2n = 2x = 10$; 119 Mbp/1C). However, our understanding of the dynamics of large plant genomes, found in certain agriculturally significant species such as cereal crops, remains limited. Expanding the knowledge about how genome organization changes in these plants could aid in selecting cultivars adapted to changing climatic conditions.

Barley (*Hordeum vulgare*) is a temperate cereal crop with a diploid genome ($2n = 2x = 14$; 4.88 Gbp/1C) organized in a Rab1 conformation with centromeres and telomeres positioned at opposite nuclear poles (Rabl, 1885). Thanks to its low number of large chromosomes, barley has become a favorable model for cytogenetic and molecular studies, enabling detailed exploration of

its organization at a high-resolution level (Kwasniewska *et al.*, 2018, Kubalova *et al.*, 2023). However, the dynamics of barley chromosomes within a cell has yet to be investigated due to the absence of available *in vivo* tools, such as fluorescent marker lines frequently used for dynamical studies in *Arabidopsis*. The development of such tools would not only help the plant research community in expanding the knowledge of cereal crops' genome organization dynamics but also provide valuable resources for future studies in this field.

2 Aims of the thesis

I Development of translational fusion fluorescent marker lines for *in vivo* nuclear and cellular dynamics studies in barley

The first aim of the thesis was to develop a collection of translational fusion fluorescent marker lines (FMLs) of barley for *in vivo* study of nuclear and cellular processes in living plants with large genomes.

II Optimization of the time-lapse *in planta* microscopy analysis of fluorescent marker lines

The second aim of the thesis was to improve and optimize the *in planta* time-lapse analysis of cell dynamics in growing barley roots. The microscopy and the mounting of the growing root samples were simplified by designing the microscopy holder for the *in vivo* analysis of cereal crops' roots.

III Understanding the spatial organization and dynamics of chromosomes and microtubules during barley mitosis

The third aim of the thesis was to analyze the mitotic division in barley roots using the developed FMLs.

3 Materials and methods

Plant material, crossing, and embryo dissection

Two cultivars of two-row spring-type *H. vulgare* L. cv. Golden Promise (GP) and cv. Morex were used. A barley GP cultivar was used for the *Agrobacterium tumefaciens* mediated embryo transformation.

Crosses between the FMLs were done according to (Thomas *et al.*, 2019). The mature F1 hybrid seeds were surface sterilized as described (Marthe *et al.*, 2015), soaked in sterile water, and cold stratified. Embryos were manually extracted under a binocular microscope and germinated on sterile plates with ½ Murashige-Skoog agar media.

Molecular cloning of reporter constructs

For cloning, Gateway™ vector cloning set was used. For all constructs, the CDS of the marker gene was amplified from synthesized cDNA with primers prolonged by corresponding attb sites (on 5' primer end) and then subcloned into a selected donor vector. For C'-ter translational fusion constructs, CDS of the marker gene and fluorescent tag sequence were amplified with primers overlapping gene and fluorescent tag gene fusion site. Afterward, these PCR products were hybridized, used as a template for amplification with attb-containing primers, and then subcloned into donor vector as previously. All final constructs were verified by Sanger sequencing. Verified entry vectors were subcloned into binary vectors optimized for transformation on Monocotyledonous species.

***Agrobacterium tumefaciens* mediated transformation of immature barley embryos**

Preparation of *Agrobacterium tumefaciens* inoculums and immature embryos transformation was done according to the previously described protocols (Harwood, 2009, Marthe *et al.*, 2015).

Genotyping of transgenic plants, ploidy measurement, copy number determination

Regenerated plants were genotyped for the presence of a *HYGROMYCIN* selection gene by PCR amplification and the specific fluorescent signal presence under the microscope.

Ploidy measurement was done according to the previously described protocol (Dolezel *et al.*, 1994) with modifications. The ploidy was analyzed on a Partec PAS I flow cytometer using GP as a diploid standard. DNA was stained with the 4',6-diamidin-2-fenylindol (DAPI).

The estimation of *HYGROMYCIN PHOSPHATASE* copies was performed by segregation analysis and digital droplet PCR (ddPCR) using ddPCR™ Supermix for Probes (no dUTP) (Bio-Rad, Hercules, CA, USA) according to the manufacturer's instructions with a 60 °C annealing/extension phase and 40 ng of *Hind*III-HF digested DNA for each sample. Primers and TaqMan® probes for *HYGROMYCIN PHOSPHATASE* (VIC fluorescent dye) and reference gene *CONSTANCE-LIKE CO2* (FAM fluorescent dye) were used accordingly to (Strejčková *et al.*, 2024; unpublished).

Isolation of interphase nuclei and chromosome sorting, RNAase treatment

Preparation of samples for chromosome sorting from root-tip meristem cell nuclei was done as described previously (Dolezel *et al.*, 1992)

with modifications. Root tips were homogenized using Polytron PT1300D homogenizer (Kinematica AG).

Suspensions of intact mitotic metaphase chromosomes were prepared as described by (Lysak *et al.*, 1999). The resulting chromosome suspension was analyzed at a rate of ~5,000 particles per second using a FACS Aria SORP flow cytometer (Becton Dickinson, San José, United States). Sort windows were set on a dot plot of fluorescence pulse area versus fluorescence pulse width to select all seven barley chromosomes.

RNase A was done in the flow-sorted chromosome suspensions before pipetting onto microscopic slides.

Immunostaining of sorted nuclei and metaphase chromosomes

The immunostaining was performed as described (Jasencakova *et al.*, 2001). EYFP-FIB1 was detected with primary mouse antisera against FIB1 (ab4566; Abcam) and secondary antibodies goat anti-mouse-Cy5 (Alexa Fluor® 647; A21235; Invitrogen) or with a goat anti-mouse-Cy3 (Alexa Fluor® 546; A-11003; Invitrogen) for nuclei or metaphase chromosomes, respectively. Alternatively, EYFP-FIB1 on metaphase chromosomes was detected with rabbit antisera against GFP (ab290; Abcam), recognizing also EYFP and secondary antibodies goat anti-rabbit-Cy3 (Alexa Fluor® 647; A-11010; Invitrogen) for metaphase chromosomes.

Microscopy

All confocal microscopic images were acquired using a Leica TCS SP8 STED3X confocal microscope (Leica Microsystems, Wetzlar, Germany) equipped with an HC PL APO CS2 20x/0,75 DRY objective, HC PL APO CS2

63×/1.40 Oil objective, hybrid detectors (HyD), and the Leica Application Suite X (LAS-X) software version 3.5.5 with the Leica Lightning module (Leica, Buffalo Grove, IL, USA).

Microscopic images were captured separately in sequential scans for immunologically stained nuclei and chromosomes to avoid spectral mixing in fluorophore-fitting excitation and emission spectra.

For the time-lapse analysis, 2 days after germination FML plantlets were used. Root samples were mounted on the microscopy slide with home-made microscopy chamber or in the EasyClick microscopy sample holder. During the time-lapse analysis of mitosis, confocal Z-stack images of approximately 20-30 μm width were captured in 1 min scanning windows.

Microscopy data post-processing

Images were processed in Adobe Photoshop version 12.0 (Adobe Systems), ImageJ Fiji version 1.53c (Schindelin et al., 2012), Inkscape (Inkscape project), and Imaris version 9.7.2 (Oxford Instruments).

4 Summary of results

I Development of translational fusion fluorescent marker lines for *in vivo* nuclear and cellular dynamics studies in barley

Different FML variants for chromatin, nucleolus, and centromeres were developed and crossed together with the microtubular FML to create multi-FMLs. These lines became a valuable material for *in vivo* studies of nuclear and cellular dynamics of barley and large cereal crops' genomes.

II Optimization of the time-lapse *in planta* microscopy analysis of fluorescent marker lines

The *in planta* time-lapse analysis of nuclear and cellular dynamics in growing barley roots was optimized and subsequently improved by designing and implementing the EasyClick microscopy holder optimized for *in vivo* analysis of cereal crop roots on the cellular level.

III Understanding the spatial organization and dynamics of chromosomes and microtubules during barley mitosis

In vivo analysis of multi-FMLs uncovered both conserved and unique features of the barley root cells' mitosis. It revealed that mitotic chromosome spiralization starts before the prometaphase and continues until the telophase. They showed that barley mitotic chromosomes are coated by the layer of RNAs a protein molecules. Moreover, they revealed that anaphase chromosomes are pulled to the opposite cell corners instead of the opposite cell wall's centers.

Finally, they helped to measure durations of individual mitotic phases in barley root cells and mitosis itself. These findings will enable the detailed study of *in vivo* cellular and nuclear dynamics under different growth conditions.

5 Summary

This thesis focuses on developing tools for analyzing the nuclear genome dynamics and organization in agronomically important cereal crop barley (*Hordeum vulgare*). Investigating these processes in living cells significantly helps to understand their cellular regulation and complete information obtained by studies done on fixed samples.

The thesis describes the procedure of developing translational fusion fluorescent marker (FMLs) lines for the analysis of living cells in barley. Individual lines for chromatin, nucleolus, centromeres, and microtubules were crossed to originate multi-marker lines, which were used to study mitotic division in barley root cells. They enabled identifying and characterizing individual mitotic phases and measuring their durations using time-lapse *in vivo* microscopy. Medians of particular phase's durations were used to set the average mitosis duration in barley root cells.

Developed FMLs also helped to bring new insights into barley mitosis. It was proved that in some cells, chromosome spiralization is initiated before the prophase and reaches the maximum not in metaphase but in telophase in all cells. Moreover, it was observed that in anaphase, chromosome pulling axis is tilted from the cell division axis orientation more into the cell walls corners. For measurement of the tilting angle in the 3D nuclear space, the detailed workflow was created in Imaris bitplane software. Furthermore, obtained indicated that metaphase chromosomes are covered by the layer of RNAs protein molecules, which resembles features of the perichromosomal layer found on human chromosomes. Using developed FMLs, durations of mitosis and its individual phases in barley root cells were estimated.

In the scope of this thesis, the microscopy sample holder for time-lapse microscopy of the nuclear dynamics in root cells was designed and optimized. It significantly simplifies detailed microscopy of growing roots of wider diameter, as found in most cereal crops.

Developed barley FMLs will enable us to better understand mechanisms influencing large genomes dynamics, facilitating the agronomical breeding of cereal crops cultivars adapted to the changing environmental conditions.

6 References

- Dogan, E.S. and Liu, C.** (2018) Three-dimensional chromatin packing and positioning of plant genomes. *Nature Plants*, **4**, 521-529.
- Dolezel, J., Lucretti, S. and Schubert, I.** (1994) Plant chromosome analysis and sorting by flow cytometry. *Critical Reviews in Plant Sciences*, **13**, 275-309.
- Dolezel, J., Sgorbati, S. and Lucretti, S.** (1992) Comparison of 3 fluorophores for flow cytometric estimation of nuclear-DNA content in plants. *Physiologia Plantarum*, **85**, 625-631.
- Harwood, W.A., Bartlett, J.G., Alves, S.C., Perry, M., Smedley, M.A., Leyland, N., Snape, J.W.** (2009) Barley transformation using *Agrobacterium*-mediated techniques, pp. 137-147.
- Jasencakova, Z., Meister, A. and Schubert, I.** (2001) Chromatin organization and its relation to replication and histone acetylation during the cell cycle in barley. *Chromosoma*, **110**, 83-92.
- Kubalova, I., Camara, A.S., Capal, P., Beseda, T., Rouillard, J.M., Krause, G.M., Holusova, K., Toegelova, H., Himmelbach, A., Stein, N., Houben, A., Dolezel, J., Mascher, M., Simkova, H. and Schubert, V.** (2023) Helical coiling of metaphase chromatids. *Nucleic Acids Research*, **51**, 2641-2654.
- Kwasniewska, J., Zubrzycka, K. and Kus, A.** (2018) Impact of mutagens on DNA replication in barley chromosomes. *International Journal of Molecular Sciences*, **19**.
- Liu, B. and Lee, Y.R.J.** (2022) Spindle assembly and mitosis in plants. *Annual Review of Plant Biology*, **73**, 227-254.
- Lysak, M.A., Cihalikova, J., Kubalakova, M., Simkova, H., Kunzel, G. and Dolezel, J.** (1999) Flow karyotyping and sorting of mitotic chromosomes of barley (*Hordeum vulgare* L.). *Chromosome Research*, **7**, 431-444.
- Marthe, C., Kumlehn, J. and Hensel, G.** (2015) Barley (*Hordeum vulgare* L.) transformation using immature embryos. *Agrobacterium Protocols, Vol 1, 3rd Edition*, **1223**, 71-83.
- Rabl, C.** (1885) Über Zelltheilung: Morphologisches Jahrbuch, pp. 214-330.
- Rosa, S. and Shaw, P.** (2013) Insights into chromatin structure and dynamics in plants: Biology, pp. 1378-1410.
- Schubert, I. and Shaw, P.** (2011) Organization and dynamics of plant interphase chromosomes. *Trends in Plant Science*, **16**, 273-281.

- Thomas, W.T.B., Bull, H., Booth, A., Hamilton, R., Forster, B.P. and Franckowiak, J.D.** (2019) A practical guide to barley crossing. *BARLEY: Methods and Protocols*, **1900**, 21-36.
- Tiang, C.L., He, Y. and Pawlowski, W.P.** (2012) Chromosome organization and dynamics during interphase, mitosis, and meiosis in plants. *Plant Physiology*, **158**, 26-34.

7 List of author's publications

7.1 First author publications

Randall, R.S.†, Jourdain, C.†, Nowicka, A.†, **Kaduchová, K.**†, Kubová, M.†, Ayoub, M.A.†, Schubert, V.†, Tatout, Ch.†, Colas, I.†, Kalyanikrishna, Desset, S., Mermet, S., Stevens, A., Kubalova, I., Mandáková, T., Heckmann, S., Lysak, M.A., Panatta, M., Santoro, R., Schubert, D., Pecinka, A., Routh, D., and Baroux, C., (2022). Image analysis workflows to reveal the spatial organization of cell nuclei and chromosomes. *Nucleus*, 13, 277-299. doi: 10.1080/19491034.2022.2144013.

Kaduchová, K., Marchetti, C., Ovečka, M., Galuszka, M., Bergougnoux, V., Šamaj, J., and Pecinka, A. (2023). Spatial organization and dynamics of chromosomes during barley mitosis. *The Plant Journal*, 115, 602-613. doi: 10.1111/tpj.16355.

Kaduchová, K., Čmiel, V., Koláčková, V., and Pecinka, A. (2023). EasyClick: An improved system for confocal microscopy of live roots with a user-optimized sample holder. *Planta*, *in press*.

7.2 Co-authorship publications

Perutka, Z., **Kaduchová, K.**, Chamrád, I., Beinhauer, J., Lenobel, R., Petrovská, B., Bergougnoux, V., Vrána, J., Pecinka, A., Doležel, J., and Šebela, M. (2021). Proteome analysis of condensed barley mitotic chromosomes. *Frontiers in Plant Science*, 12, 723674. doi: 10.3389/fpls.2021.723674.

7.3 Published abstracts – poster presentation

Lahnerová, K., Stromšíková, H., Střelcová, K., Doležel, J., Bergougnoux-Fojtík, V, and Pecinka, A. (2019). Towards *in vivo* analysis of chromatin dynamics in barley. In: Abstract book of the 4th INDEPTH meeting ‘Impact of chromatin domains on plant phenotypes’, p. 44. Madrid, Spain, 2019.

Lahnerová, K., Stromšíková, H., Střelcová, K., Mičúchová, A., Bergougnoux-Fojtík, V, Šamaj, J., and Pecinka, A. (2021). Developing system for tracking *in planta* chromatin dynamics in barley (*Hordeum vulgare*). In: Abstract book of the ‘1st Czech Plant Nucleus Workshop 2021 (CPNW2021)’, p. 48. Olomouc, Czech Republic, 2021.

This poster won “The best poster prize of the 1st Czech Plant Nucleus Workshop 2021”.

Kaduchová, K., Stromšíková, H., Střelcová, K., Mičúchová, A., Křižňanská, H. Bergougnoux-Fojtík, V, Galuszka, P., Šamaj, J., and Pecinka, A. (2021). Developing system for *in planta* tracking of chromatin dynamics in barley (*Hordeum vulgare*). In: Abstract book of the ‘Cytogenetics meeting 2021’, p. 51. Görlitz, Germany, 2021.

7.4 Published abstracts – oral presentation

Lahnerová, K., Stromšíková, H., Střelcová, K., Mičúchová, A., Bergougnoux-Fojtík, V, Šamaj, J., and Pecinka, A. (2020). *In planta* microscopy of barley fluorescent marker lines. Online INDEPTH Imaris Training School, Zürich, Switzerland, 2020.

Kaduchová, K., Střelcová, K., Mičúchová, A., Galuszka, P., Bergougnoux-Fojtík, V, Šamaj, J., and Pecinka, A. (2022). Analysis of *in vivo* chromatin dynamics during mitotic division in barley (*Hordeum vulgare*). In: Abstract book of the ‘7th European Workshop on Plant Chromatin 2022 (EWPC2022)’, p. 66. Průhonice, Praha, 2022.

This oral presentation won “The best flash-talk of the the 7th European Workshop on Plant Chromatin 2022 prize”.

Kaduchová, K., Galuszka, P., Bergougnoux-Fojtík, V, Šamaj, J., and Pecinka, A. (2022). Live analysis of barley nuclei and chromosomes using fluorescent marker lines. In: Abstract book of the ‘2nd EPI-CATCH Conference’, p. 56. Crete, Greece, 2022.

Kaduchová, K., Marchetti, C., Ovečka, M., Galuszka, P., Bergougnoux, V, Šamaj, J., and Pecinka, A. (2023). Towards understanding of spatial *in vivo* dynamics of mitotic division in barley (*Hordeum vulgare*). In: Abstract book of the ‘3rd EPI-CATCH Conference’ p. 43. Sofia, Bulgaria, 2023.

Kaduchová, K., Marchetti, C., Ovečka, M., Galuszka, P., Bergougnoux, V, Šamaj, J., and Pecinka, A. (2023). Towards understanding of spatial *in vivo* dynamics of mitotic division in barley (*Hordeum vulgare*). In: Abstract book of the ‘2nd Czech Plant Nucleus Workshop’ (CPNW2023), p. 15. Brno, Czech Republic, 2023.

This oral presentation won “The best talk of the 2nd Czech Plant Nucleus Workshop 2023 prize.”

8 Souhrn (Summary in Czech)

Název práce: Analýza dynamiky a 3D organizace jaderného genomu u ječmene setého (*Hordeum vulgare*)

Předkládaná práce se zaměřuje na vývoj nástrojů pro studium analýzy dynamiky a organizace jaderného genomu u hospodářsky významné plodiny ječmene setého (*Hordeum vulgare*). Sledování zmíněných procesů v žijících rostlinách umožňuje lépe porozumět jejich regulaci a napomáhá doplnit informace získané ze studia fixovaných vzorků.

Dizertační práce obsahuje postup vývoje translačně fúzních fluorescenčních markerových linií ječmene, pomocí kterých je možné charakterizovat dynamické změny odehrávající se v živých buňkách. Jednotlivé markerové linie vytvořené pro studium organizace chromatinu, jádérka, centromer a mikrotubulů byly postupně vzájemně skříženy za vzniku multi-markerových linií, a použity pro studium mitotického dělení v buňkách kořene. Pomocí těchto linií se podařilo identifikovat a charakterizovat jednotlivá stadia mitózy ječmene, a změřit délku jejich trvání za použití time-lapse *in vivo* mikroskopie. Z mediánů jednotlivých mitotických fází byla následně stanovena průměrná délka mitózy v kořenových buňkách ječmene.

Vytvořené linie rovněž napomohly odhalit nové poznatky rozšiřující známá fakta týkající se mitózy ječmene. Bylo prokázáno, že spiralizace chromatinu je u části buněk iniciována již před mitotickou profází, a u všech buněk dosahuje maxima ne v metafázi, ale během telofáze. Dále bylo pozorováno, že během anafáze je osa dělení chromozomů vychýlena od osy buněčného dělení směrem do rohů buněčných stěn. Pro stanovení úhlu odchylky v 3D buněčném prostoru byl vytvořen návodný postup pro rendrovací platformu Imaris bitplane. Data získaná z analýzy mitotických chromozomů

rovněž naznačují jejich pokrytí vrstvou RNA molekul a proteinů, podobající se perichromozomální vrstvě detekované u lidských chromozomů.

V rámci práce byl rovněž navržen a zoptimalizován držák vzorků pro time-lapse mikroskopii jaderné dynamiky v kořenových buňkách, který významně zjednodušuje detailní mikroskopii u rychle rostoucích kořenů většího průměru, mezi něž patří většina obilovin.

Vytvořené markerové linie ječmene umožní lépe porozumět mechanismům ovlivňujícím dynamiku velkých rostlinných genomů, což v budoucnu usnadní šlechtění odrůd obilovin lépe adaptovaných na měnící se klimatické podmínky.